Synthesis and Evaluation of Photoactivatable D-Amino Acid Probes of Bacterial Peptidoglycan Biosynthesis

By

Rafid Taj Aldeen

A thesis submitted in partial fulfilment of the requirements for the degree of

Doctor of Philosophy

March 2021

Acknowledgment

First and foremost, I would like to express my sincere gratitude to my supervisor Dr Michael Hall for guiding and supporting me during the course of my four year PhD journey, as my scientific knowledge and academic experience has been greatly enhanced under his supervision. During my research, he inspired me on how to manage different issues raised through the work and he taught me that there is always a logical reason behind any positive or negative experimental result. He was always a good role model, showing patience and understanding, and making me feel more confident and empowered. Furthermore, if I was feeling down he would always encourage me to keep moving forward. He was outstanding as both a supervisor and a friend.

Additionally, I would like to relay a great thank you for all the members of MJH group who had supported me throughout my PhD study, both in the present and the past. Whenever I was confused or stuck on my synthesis they would be there to help and give advice. Moreover, a special thank you for my colleagues Dr. Kin Lok Ho and Dr. Lina Mardiana for their support in providing notes during the period of research and editing this work. I would also like to take the opportunity to extend my thanks to all other work fellows in Johnson lab for the positive work atmosphere. At this moment of writing my acknowledgment note I cannot move on without mentioning my good friend Ronnie Ragbirsingh who was always there to listen and help.

I would like to express my appreciation for the assistance of NMR facility group (Prof. William McFarlane, Dr Corinne Wills, and Dr Casey Dixon) and the X-ray centre (Dr Paul Waddell) for their help in obtaining the analytical data for my research.

I wish to thank my collaborators in CBCB (Prof. Waldemar Vollmer and Dr Matthias Winkle) for the opportunity to collaborate with them.

Finally, I would like to thank my family, my wife (Rasha Kafali) and my daughters for their understanding, love and their continuous encouragement during the course of my PhD.

Abstract

The bacterial cell wall contains peptidoglycan (PG), a mesh-like polymer of glycan strands crosslinked by short peptide chains. PG is essential for bacterial cell viability and as such PG biosynthesis is an important antibiotic target. Despite considerable study, there remain many PG associated enzymes with unknown function, identification of which will allow us to develop the antibiotics of the future.

This project is focused on the development of D-amino acid based photoaffinity probes, for the covalent capture of PG associated proteins. Following the evaluation of a number of strategies, a photoactivatable fluorescent D-amino acid probe was successfully synthesised, methoxy coumarin trifluoromethyl diazirine D-alanine or MCTDA.Addionally it can be shown by LCMS that MCTDA is accepted as a substrate by the bacterial transpeptidase enzyme LdtD and that, through the action of LdtD, MCTDA can be successfully incorporated into both isolated muropeptide and whole PG of *E. coli*. Evaluation of photoactivated capture of PG associated proteins by incorporated MCTDA is ongoing in the laboratory (Figure **1**).

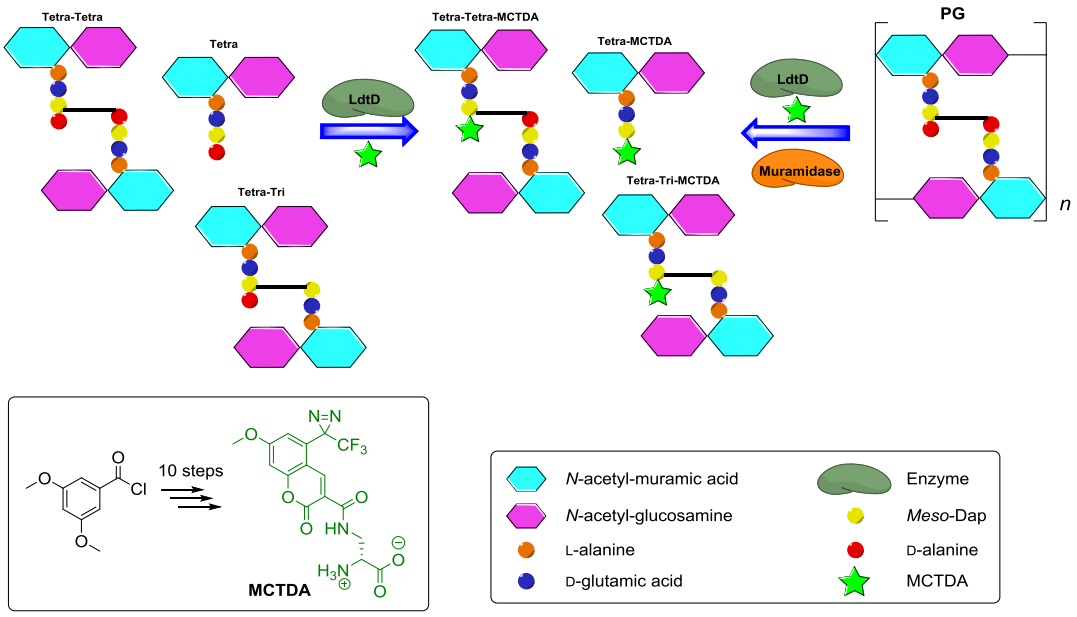

Figure 1: Synthesis of photoactivatable amino acid probe MCTDA and incorporation into PG and muropeptide (*E. coli*) by LdtD.

Abbreviation

Ar	Aromatic
Boc	tert-Butyloxycarbonyl
Bu	Butyl
cat.	Catalyst
CBCB	Centre for Bacterial Cell Biology
CDI	Carbonyldiimidazole
COSY	Correlated spectroscopy
DCM	Dichloromethane
DMSO	Dimethylsulfoxide
DMF	Dimethylformamide
DIPEA	Diisopropyl ethyl amine
d	Doublet
ee	Enantiomeric excess
eq	Equivalence
Et	Ethyl
ESI	Electron spray ionisation
FA	Formic acid
FDAA	Fluorescent D-amino acids
HMBC	Heteronuclear multiple bond coherence
HRMS	High resolution mass spectrometry
HSQC	Heteronuclear single quantum coherence
HPLC	High performance liquid chromatography

h	hour
HEPES	(4-(2-hydroxyethyl)-1-piperazineethanesulfonic acid
IR	Infrared
J	Coupling constant
Mp	Melting point
m	Multiplet
Me	Methyl
MeCN	Acetonitrile
MeOH	Methanol
min	Minute
mM	Millimolar
NMR	Nuclear magnetic resonance
NBS	*N*-Bromosuccinimide
o	ortho
p	para
Pr	Propyl
Ph	Phenyl
PG	Peptidoglycan
q	Quartet
rt	Room temperature
RP	Reverse phase
s	Singlet
SPB	Sodium phosphate buffer

t	Triplet
TLC	Thin layer chromatography
TBAF	Tetra-*n*-butylammonium fluoride
TFA	Trifluoroacetic acid
THF	Tetrahydrofuran
TBAH	Tetra-*n*-butylammonium hydroxide
TEA	Triethylamine
TBAI	Tetra-*n*-butylammonium iodide
$TMSCF_3$	Trifluoromethyl trimethylsilane
Tris	Tris(hydroxymethyl)aminomethane
TX-100	Triton X-100
WHO	World Health Organization

Contents

Chapter 1. Introduction

This thesis will examine the synthesis of unnatural amino acids as molecular probes for bacterial peptidoglycan (PG) biosynthesis to better understand bacterial cell wall biology.

Therefore, in this chapter key concepts behind this thesis will be introduced. Starting with a general overview of the bacterial cell wall, the focal point will be on the peptidoglycan (PG) layer including PG biosynthesis and the PG as an antibiotic target. Next, recent advances in the enzymatic incorporation of unnatural amino acids into bacterial PG as molecular probes will be highlited. Finally, the use of molecular probes containing diazirines, capable of photoaffinity labelling, as a method for the pull-down and identification of proteins will be discussed.

1.1 The Bacterial Cell Wall

The bacterial cell wall is a complex multilayer scaffold that surrounds the cytoplasmic material of a bacteria. The bacterial cell wall shields the bacteria from the external environment, facilitates the selective transport of macromolecules into the cytoplasm and aids the removal of toxins and waste.[1]

Bacteria can be classified into two groups based on the architecture of their cell wall. The first group, known as Gram-positive bacteria, have a cell wall containing two layers, a plasma membrane layer composed of phospholipids and a thick layer (30-100 nm) of a heteropolymer called peptidoglycan (PG), made up from glycan strands cross-linked by short peptides (Figure **1.1**).[1,2, 4,5]

The cell wall of the second group of bacteria, known as the Gram-negatives, contains three layers, the inner plasma membrane composed of a phospholipid bilayer, a thin layer of PG (5-10 nm) and an outer plasma membrane layer composed of glycolipids, called lipopolysaccharides (LPS), and phospholipids (Figure **1.1**).[2, 3, 4,6]

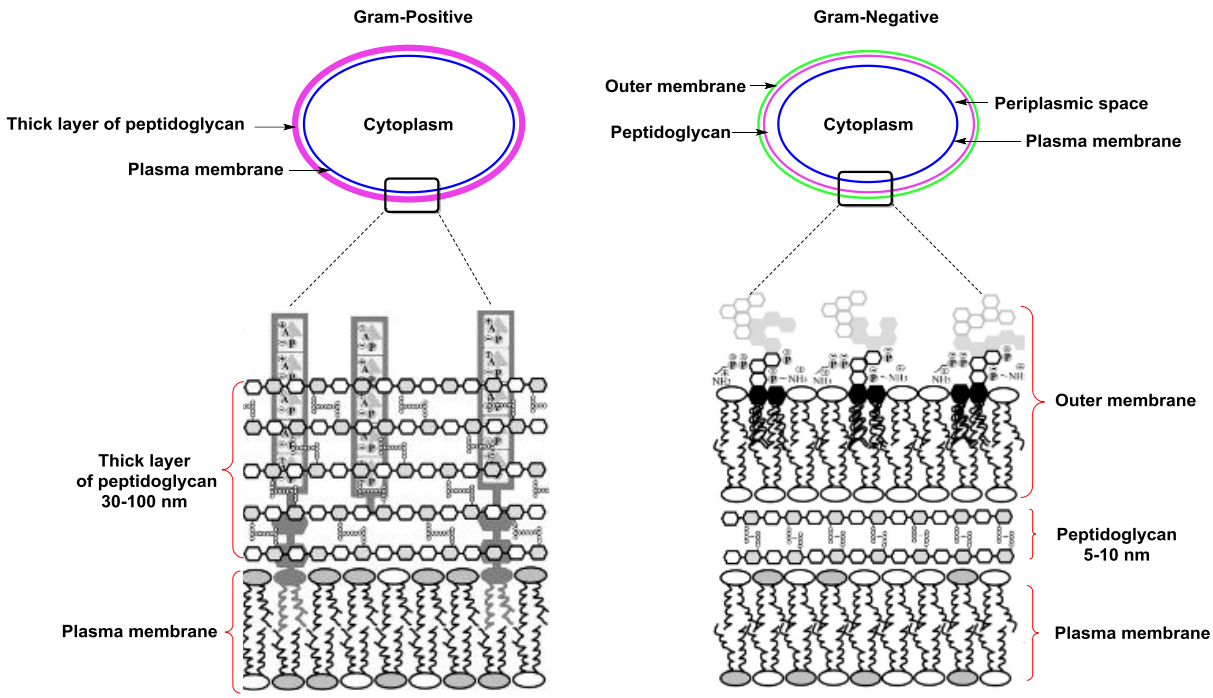

Figure 1.1: The cell wall of both Gram positive and Gram-negative bacteria. (picture adapted from ref. [12,5]).

1.2 The Structure of Bacterial Peptidoglycan (PG)

Peptidoglycan (PG) is an essential component in all bacterial cell walls. PG is a rigid mesh-like heteropolymer that encases the bacterial cytoplasmic membrane and provides mechanical support to maintain the bacterial shape.[3,7-9]

The PG of the Gram-negative bacteria *E. coli* is made up of oligomeric linear glycan strands cross-linked by short peptide chains. The glycan strands are composed of the two saccharides *N*-acetylglucosamine (NAG) and *N*-acetylmuramic acid (NAM), whilst the short peptide chains contain both L-amino and D-amino acids (Figure **1.2**).[10-12]

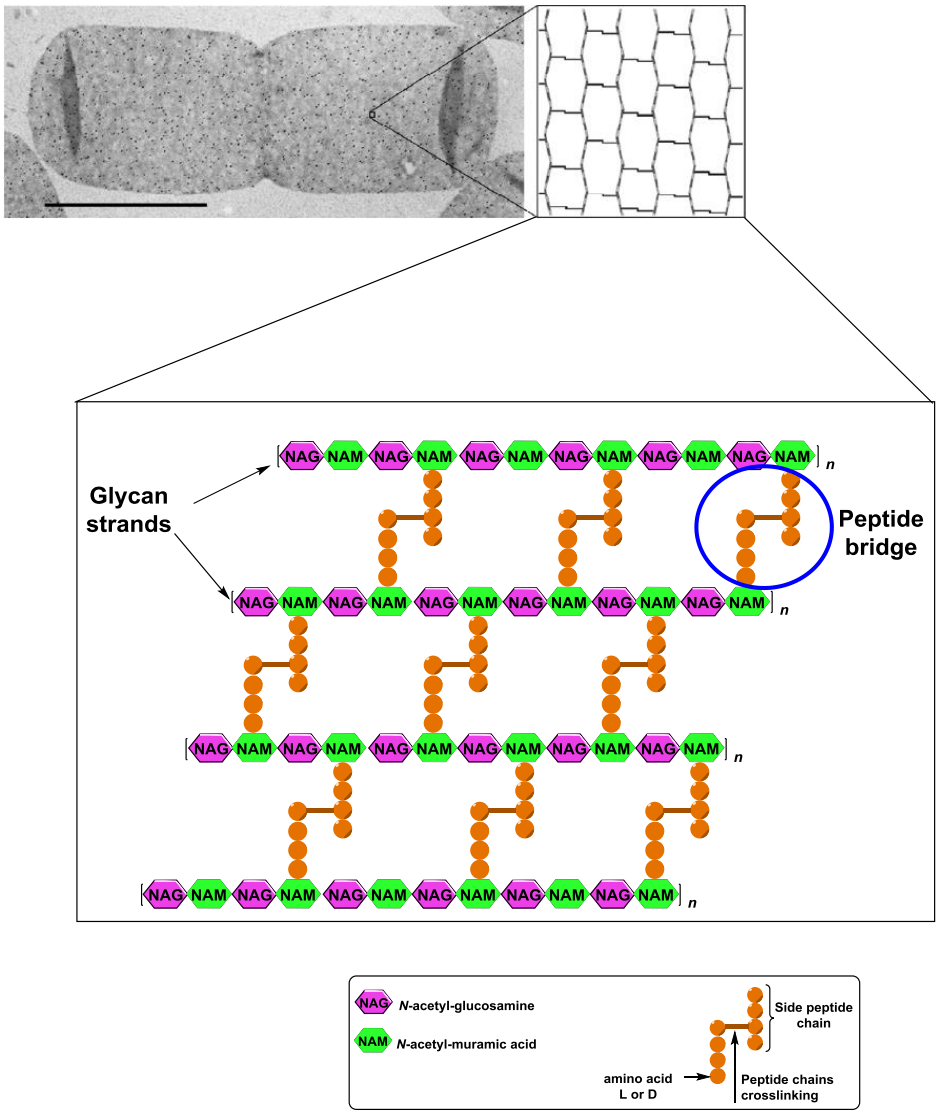

Figure 1.2: *E. coli* bacteria cell wall peptidoglycan composition (picture adapted from ref. [13, 14].

The glycan saccharide *N*-acetylglucosamine (NAG), is formed from the amino sugar glucosamine following *N*-acetylation. *N*-acetylmuramic acid (NAM) is also based on *N*-acetylated glucosamine but including a C3 D-lactyl ether, to which is connected the short peptide chains via an amide bond. Within the PG glycan the NAM and NAG subunits are linked to each other by β-1→4 glycosidic bonds (Figure **1.3**).[8,15,16]

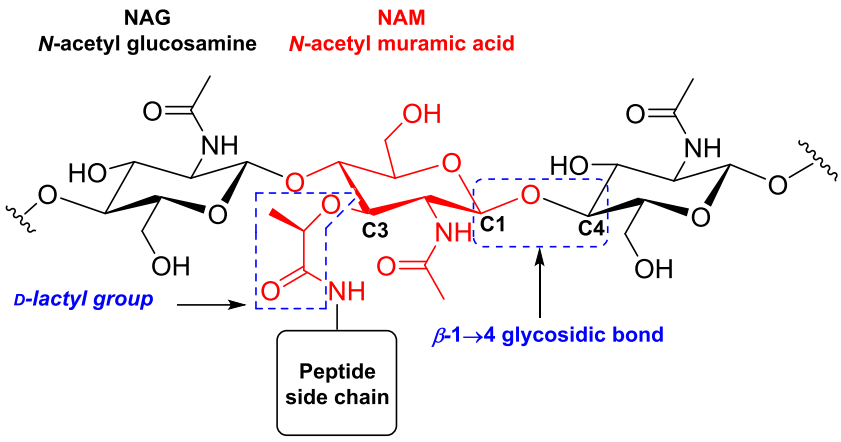

Figure 1.3: Molecular composition of the PG glycan polysaccharide backbone.

In *E. coli*, the most abundant short peptide chains in the PG contain four amino acids known, L-alanine (L-Ala), D-glutamic acid (D-Glu), *meso*-2,6-diaminopimelic acid (*m*-DAP), and D-alanine (D-Ala),[17] with the L-alanine (L-Ala) attached to the C3 D-lactyl group of NAM. The D-glutamic acid residue connects to the amine at the L-centre of *meso*-2,6-diaminopimelic acid via the γ-carboxyl group, with the remaining unit of D-alanine (D-Ala) being connected via *m*-DAP (Figure **1.4**).[13,18]

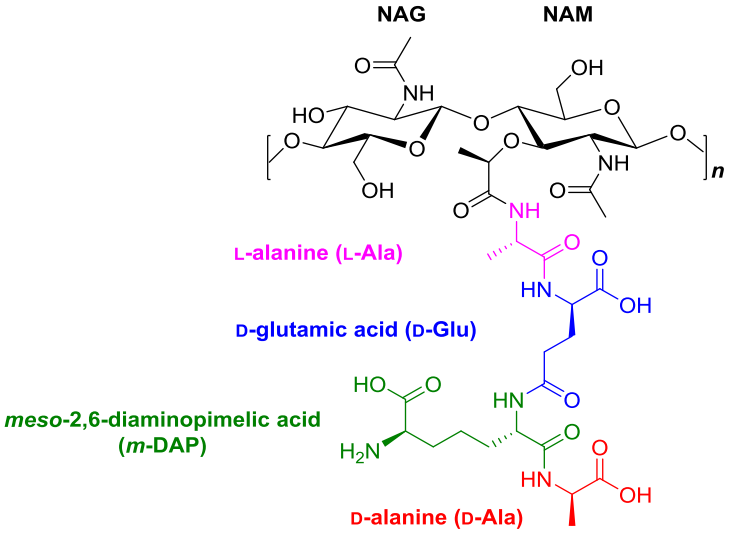

Figure 1.4: Section of *E. coli* PG, showing the most commonly occurring tetrapeptide disaccharide unit.

1.3 Biosynthesis of Peptidoglycan (PG) in *E. coli*

The biosynthesis of PG in *E. coli* consists of a complex pathway containing approximately 20 biosynthetic steps occurring in both the cytosol and the periplasmic compartment of Gram-negative bacteria.[1] These biosynthetic steps can be summarised into three main groups: the biosynthesis of lipid II, the polymerisation of the NAG-NAM disaccharides, and the cross-linking of the peptide chains.[13,19,20]

1.3.1 Biosynthesis of Lipid II in *E. coli*

Lipid II is a key biosynthetic intermediate in the formation of PG in *E. coli*, and other bacteria, consisting of two saccharide units (NAG and NAM), a short peptide chain and a lipophilic tail. Lipid II biosynthesis (Figure **1.5**) occurs in the bacterial cytoplasm, starting from fructose-6-phosphate (**1.1**). Fructose-6-phosphate (**1.1**) is first aminated to form glucoseamine-6-phosphate (**1.3**) (GlmS), isomerised to glucoseamine-1-phosphate (**1.4**) (GlmM), the *N*-acetyl group is introduced (GlmU) and finally uridyldiphosphate group is added to the 1-position (GlmU), to form the nucleotide substituted NAG unit, uridine diphosphate-*N*-acetylglucosamine (**1.6**) (UDP-NAG) (Figure **1.5**).[13,20,21]

The UDP-NAG (**1.6**) is later used in the final steps of lipid II biosynthesis, but is also the precursor for the biosynthetic of the NAM unit. Thus UDP-NAG (**1.6)** is transformed into the nucleotide substituted NAM unit, uridine diphosphate-*N*-acetylmuramic acid (**1.9**) (UDP-NAM), via enol ether formation at C-3 (phosphoenolpyruvate **1.7** and MurA) followed by reduction to the corresponding D-lactyl ether (NADPH and MurB). Following the biosynthesis of UDP-NAM (**1.9**), five amino acid units are sequentially added at the UDP-NAM D-lactyl position, via four ATP dependant ligases: L-Ala, MurC; D-Glu, MurD; *m*-DAP, MurE; and D-Ala-D-Ala, MurF.[20,22] The resulting UDP-NAM-L-Ala-γ-D-Glu-*m*-DAP-D-Ala-D-Ala (**1.13**) is converted to lipid I (**1.14**), through the attachment of the lipophilic side chain, undecaprenyl phosphate (C_{55}-P (**1.16**), MraY). Lipid I (**1.16**) is finally converted to lipid II (**1.15**) via the addition of NAG sugar unit at the C-4 hydroxyl of NAM (UDP-NAG (**1.6**), MurG). The undecaprenyl side chain is highly lipophilic and allows lipid II (**1.15**) to pass through the plasma membrane, into the periplasmic space where it undergoes further reactions to be incorporated into the PG (Figure **1.5**).[19,23-25]

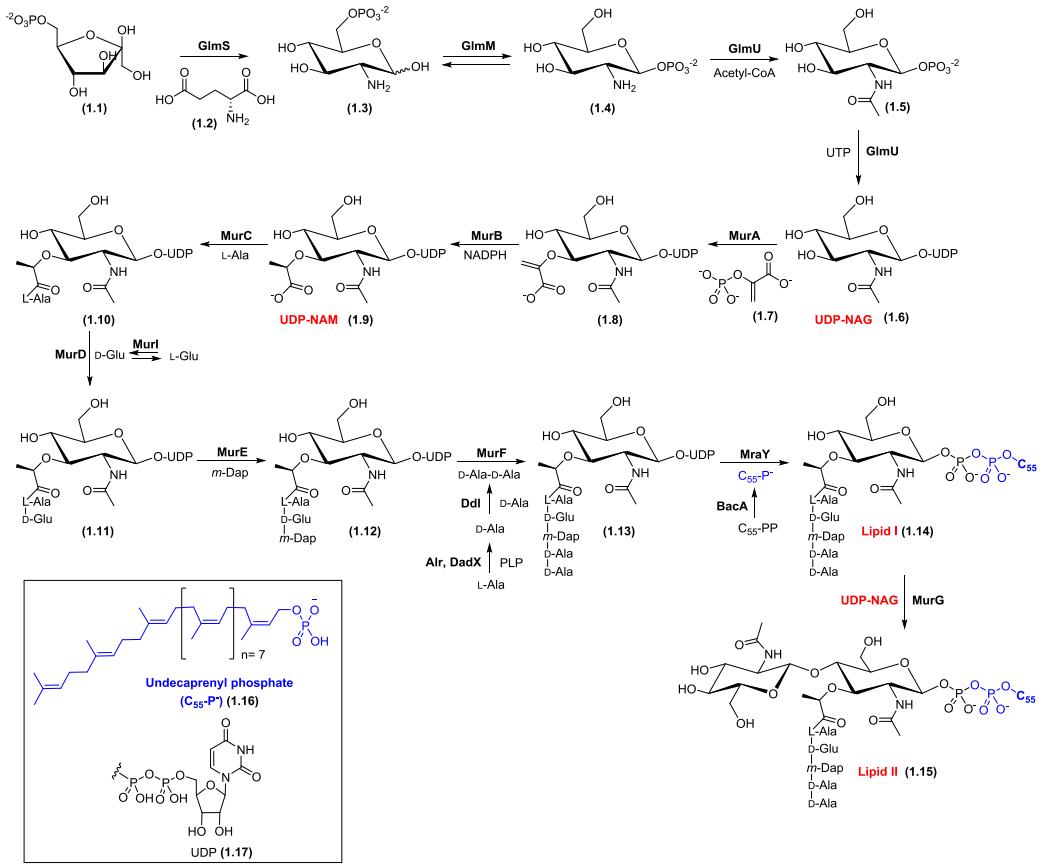

Figure 1.5: Biosynthesis of lipid II in *E. coli*.

1.3.2 Polymerization of Lipid II to form Polyglycan

Once lipid II is translocated to the periplasm compartment, it undergoes a glycan elongation process catalysed by a subgroup of penicillin binding proteins (PBP) transglycosylases (GTases) to form linear polyglycan strands.[19]

The formation of polyglycan strands occurs (Figure **1.6**) when the NAG residue at lipid II is attached to a neighbouring NAM residue of PG donor strand via β,1-4 glycosidic bond. The formation of β,1-4 glycosidic bond between NAM and NAG takes place through activation by GTase (via Glu233) of the phosphorylated C-1 position of the NAM residue of the glycan donor strand. The activated C-1 position of the glycan donor is then attacked by the C-4 hydroxyl group of the terminal NAG residue of lipid II, with release of undecaprenyl pyrophosphate (C_{55}-PP) which is recycled to form further lipid II (Figure **1.6**).[26-31]

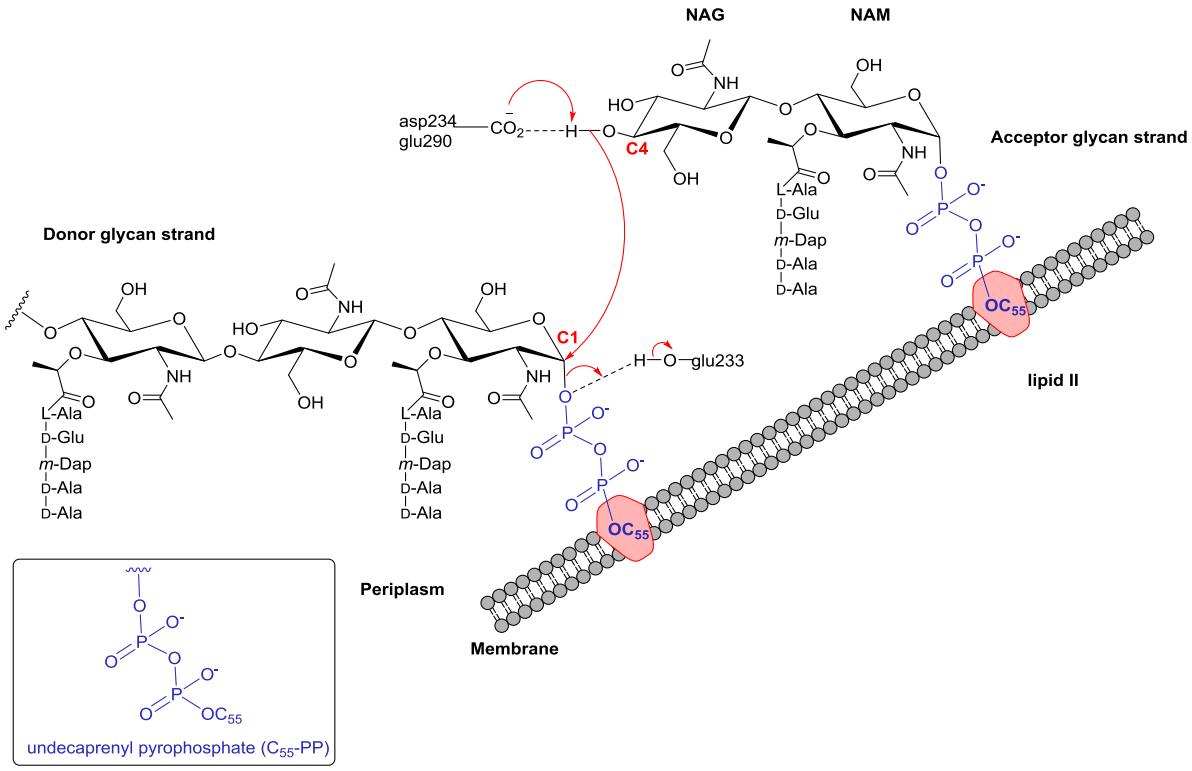

Figure 1.6: Schematic showing glycan elongation in *E. coli* via GTase (picture adapted from ref. [27].

1.3.3 PG Transpeptidation

The final step of peptidoglycan (PG) biosynthesis is the cross-linking of the polyglycan strands via an amide bond (Gram-negative) or short interpeptide bridge (Gram-positive).[8] The formation of this amide linkages between the peptide chains of PG occurs through an enzymatic reaction called transpeptidation. There are two known types of PG transpeptidation, DD-transpeptidation and LD-transpeptidation.[19]

In DD-transpeptidation the fourth amino acid residue D-alanine (D-Ala) of an acyl donor tetrapeptide glycan strand is cross-linked to the third amino acid residue *meso*-2,6-diaminopimelic acid (*m*-DAP) of an acyl acceptor tetrapeptide glycan strand. This DD-transpeptidation is mediated by a subgroup of penicillin binding proteins (PBP) called the DD-transpeptidases (DD-TPase), which contain a key serine residue in the active site which hydrolyses the D-ala-D-ala amide bond to form a covalently bound acyl intermediate.[32,33] DD-CPase, another PBP, then hydrolyses the terminal D-alanine residue of another pentapeptide glycan strand to give a tetrapeptide glycan strand. The DD-TPase acyl bound intermediate is then attacked by the free amine of the third residue, *m*-DAP, of the tetrapeptide glycan strand leading to a new amide cross-link between the D-Ala residue and *m*-DAP residue. This type of PG cross-link is called a Tetra-Tetra (4-3) and accounts for 90-98% of all cross-links in the PG of *E. coli* (Figure **1.7**).[30,34-37]

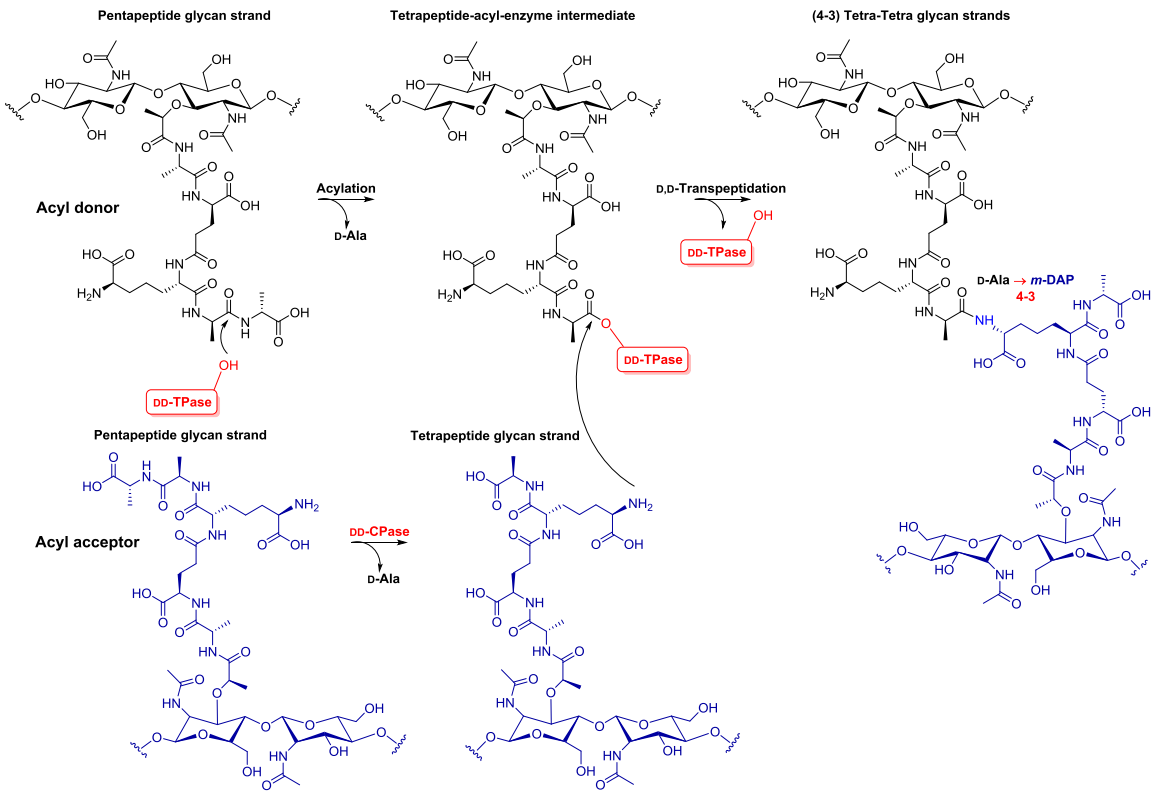

Figure 1.7: Tetra-Tetra (4-3) cross-link formation via DD-TPase in *E. coli*. (picture adapted from ref. [37]).

Beside the major DD-transpeptidation pathway, there is also minor class of PG cross-linking reactions called LD-transpeptidation, in which two adjacent tetrapeptide chains from neighbouring glycan strands are crosslinked by the formation of amide bond between two *m*-DAP units at positions 3 of each peptide chain. The resulting DAP-DAP bridge between these two peptide chains called a Tetra-Tri (3-3) which form 2-10% of *E. coli* PG cross-links.[38-41]

In *E. coli*, the LD-transpeptidation pathway is typically a minor pathway. However when the cell wall integrity is compromised by exposure to PG active antibiotic such as ampicillin, LD-transpeptidation becomes more important.

LD-Transpeptidation is mediated by LD-transpeptidases (LD-TPase).[38,42] In *E. coli* one of the main LD-TPases is LdtD. LdtD forms Tetra-Tri (3-3) and Tri-Tri (3-3) cross links in the PG, via an *m*-DAP-*m*-DAP bridge. LdtD can also hydrolyse the terminal D-Ala residue of a tetrapeptide glycan strand, called a LD-carboxypeptidation, to give the corresponding tripeptide. Finally, LdtD can also exchange of the terminal D-Ala residue of a tetrapeptide

glycan strand with other D-amino acids, both endogenous and exogeneous. Since LD-transpeptidases operate through a different mechanism to the PBPs, and use a key cystine residue in place of serine for the activation of amino acids, they are not effected by the β-lactams. Therefore they can allow a bacteria to evade successful treatment with a penicillin, through the maintenance of the PG biosynthesis (Figure **1.8**).[42,43]

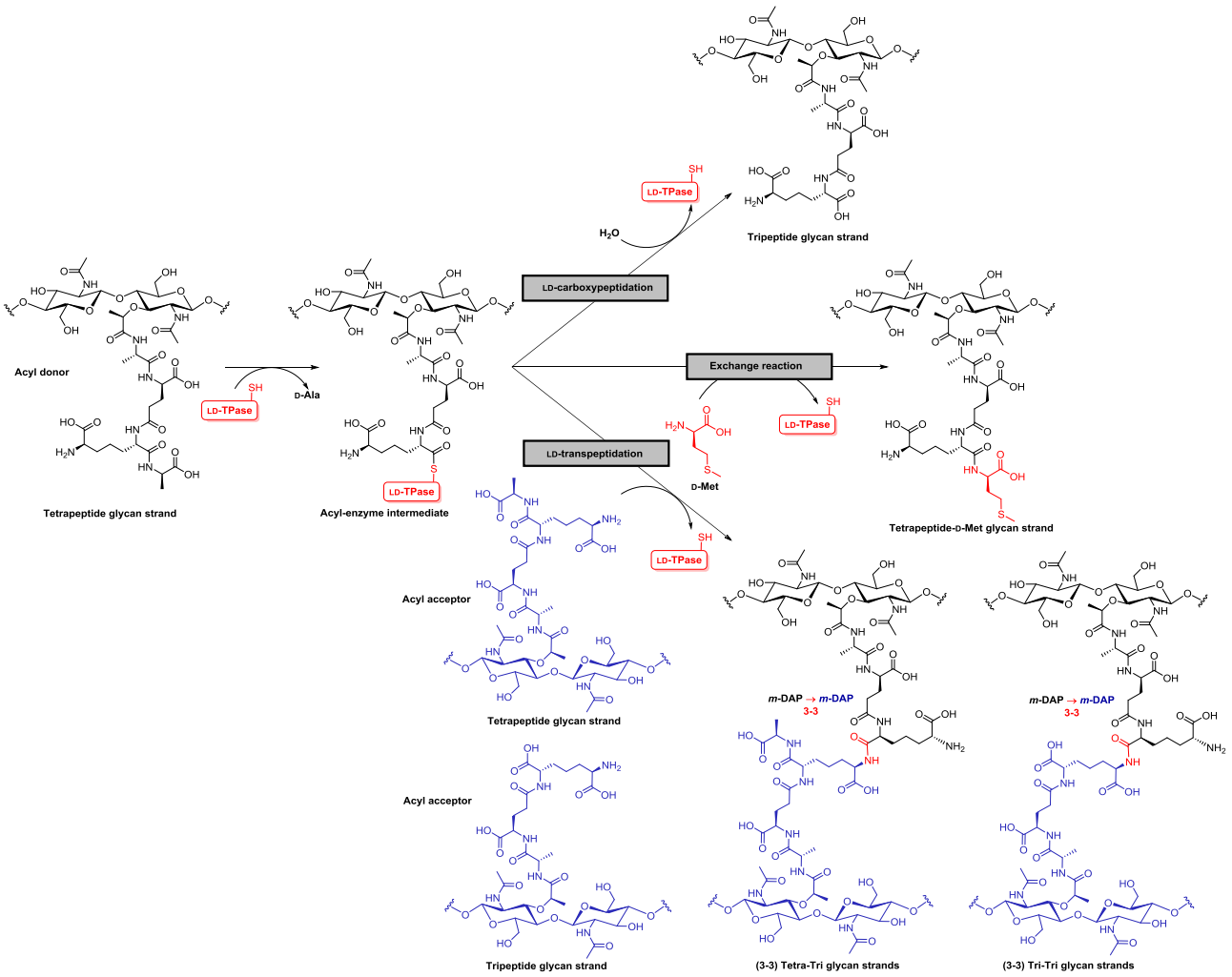

Figure 1.8: Formation of Tetra-Tri (3-3) and Tri-Tri (3-3) cross-links via LD-TPase in *E. coli*. (picture adapted from ref. [40,41]).

1.4 PG Biosynthesis and Antibiotics

Our project is focused on the development of probes for PG biosynthesis, which is an essential biosynthetic pathway in bacteria. The disruption of PG biosynthesis leads to the formation of a defective PG layer that is unable to withstand the internal cytoplasmic osmotic pressure leading to cell lysis. Therefore, the inhibition of PG biosynthesis is an important target in the development of antibiotics. Thus greater understanding of PG biosynthesis, through the identification of the essential enzymes involved and their functions, should allow us to develop the new antibiotics in the future.[30]

The occurrence of D-amino acids in PG is thought to provide the bacteria protection from protolytic action of external enzymes, yet this also represents a potential antibiotic target as the presence D-amino acids is highly specific to bacteria reducing the chances of mammalian toxicity.[45] The glycopeptide and the β-Lactam antibiotics both inhibit the late polymerisation steps in PG biosynthesis (glycosylation and transpeptidation) making them useful antibiotics. The glycopeptide vancomycin binds the D-Ala-D-Ala terminal of PG precursor lipid II and prevents glycosylation. β-lactams, such as penicillin, are structurally related to the terminal D-Ala-D-Ala residue of PG pentapeptide and inhibit enzymes involved in PG cross-linking (e.g. transpeptidation) through covalent modification of the active site. There are many other antibiotics that interfere with PG biosynthesis, including such as D-cycloserine (seromycin) which prevents the formation of the essential PG precursor D-Ala-D-Ala via the inhibition both D-alanine racemase and D-alanyl-D-alanine ligase (Figure **1.9**).[45-47]

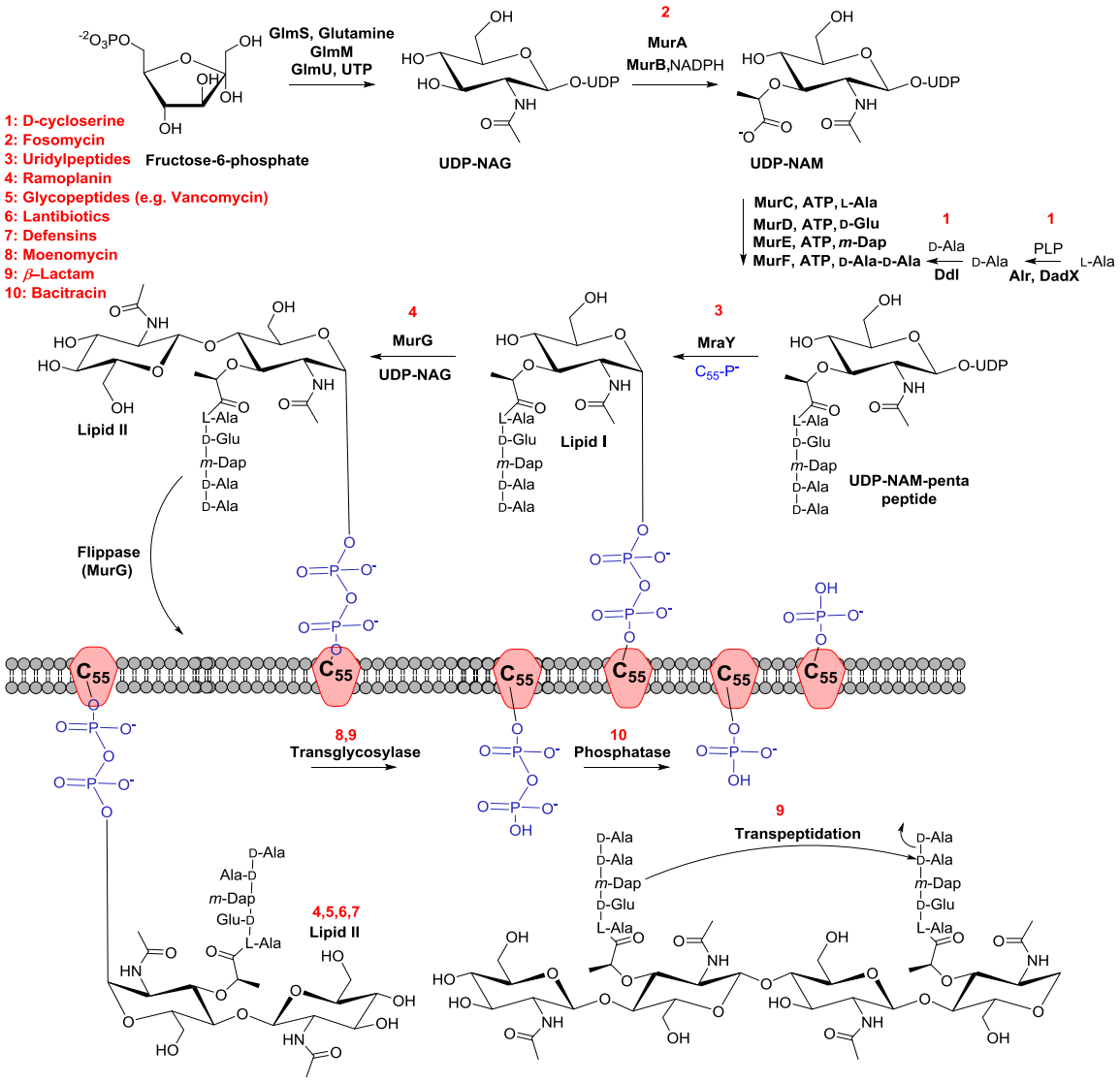

Figure 1.9: Antibiotic targets within the PG biosynthesis pathway (picture adopted from ref. [47]).

Due to the increase in drug-resistant pathogenic bacteria (e.g. *Acinetobacter baumannii*, *Pseudomonas aeruginosa* and *Enterobacteriaceae*) which have developed resistance to many common antibiotics such as the *β*-lactams, there is a growing interest in the development of new mode of action antibiotics. Thus improving the understanding of PG biosynthesis, through the identification of essential biosynthetic enzymes, is hoped to aid in the future development of new antibiotics.[48,49]

1.5 Enzymatic Incorporation of Unnatural D-amino Acids into Bacterial PG

The PG biosynthesis machinery does not only create new PG but it also remodels the existing PG layer. This remodelling can also include the incorporation of endogenous and exogenous D-amino acids, such as D-Met, D-Leu, D-Phe or D-Tyr via LD-transpeptidation.[50,51] In *E. coli* the L,D-TPase enzymes (e.g. LdtD) remodel PG through D-amino acid exchange of the fourth residue (D-Ala) of a tetrapeptide glycan stand.[39, 50,51,52] L,D-TPase enzymes are promiscuous and can incorporate a wide range of natural and unnatural D-amino acids into the PG. Several groups have reported the incorporation of D-amino acids in to the PG of live *E. coli* via an L,D-TPase pathway, including D-Met, D-Tyr, D-Phe, D-Cys and D-Met.[39,50,53]

1.6 Analysis of Amino Acid Composition of Bacterial PG through Enzymatic Digestion and LC-MS

In order to monitor the incorporation of new D-amino acids into bacterial PG a number of specialist analytic approached have been developed, most important of these is the enzymatic cleavage and LC-MS analysis of the resulting modified muropeptides.[53,54] Thus PG from *E. coli* can be cleaved with a lysozyme, muramidase, isolated from the fungus *Chalaropsis*. Muramidase hydrolyses the glycan strand of PG at the β-1,4 glycosidic bonds between the NAM and NAG units. This releases the small water soluble PG fragments called muropeptides, comprising of the disaccharide NAG and NAM connected to a short peptide chain (Figure **1.10**). Theses muropeptides, including modified muropeptides, can then be separated by HPLC and their compositions determined by mass spectrometry.[55-62]

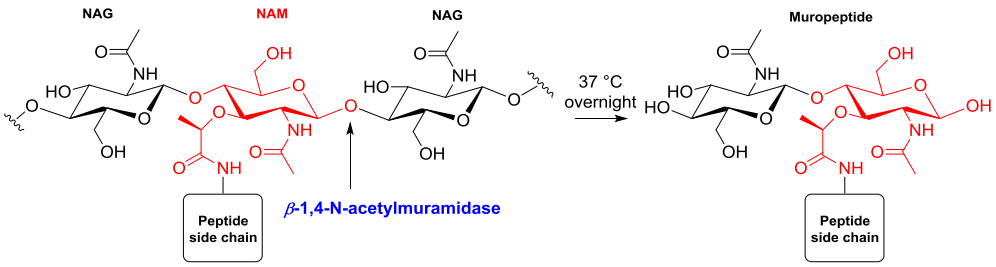

Figure 1.10: PG digestion with muramidase.

1.7 Enzymatic Incorporation of Fluorescent D-Amino Acids into Bacterial PG

Recently VanNieuwenhze and Vollmer have used the promiscuous L,D-TPase enzyme, LdtD, in order to introduce a range of fluorescent D-amino acids (FDL, TDL, HADA and NADA) into bacterial PG, including that of *E. coli* (Figure **1.11**).[63-68]

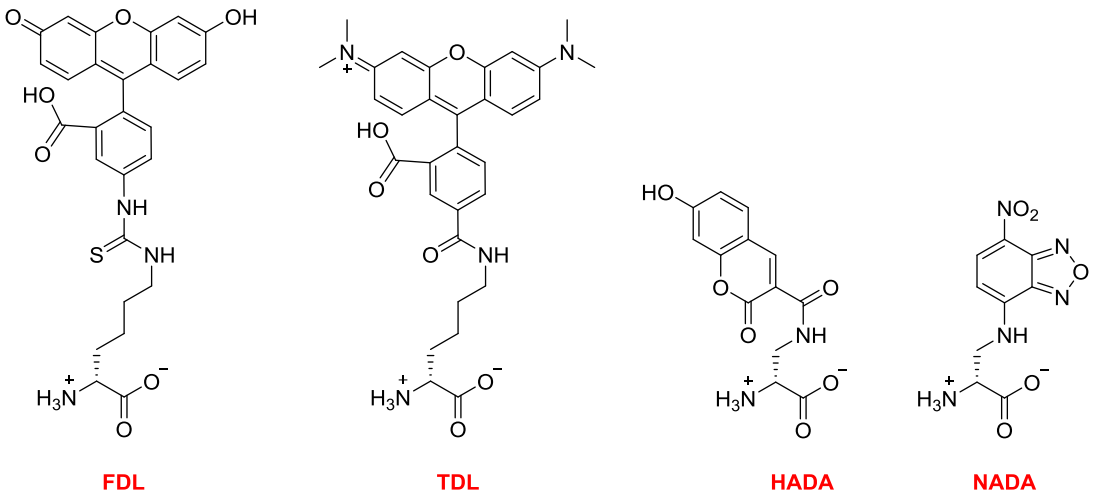

Figure 1.11: Fluorescent D-amino acids incorporated into diverse bacteria species (*in vivo* study). Fluorescent D-amino acids (FDAA) can be used visualize the sites of active PG biosynthesis and remodeling within the bacterial cell. For example, VanNieuwenhze *et al*. have shown that following short labelling times with HADA (e.g. exposure to HADA for 2-8% of the bacterial doubling time (Note: bacterial doubling time for common lab strains of *E. coli* is approximately 20 min)), *E. coli* was shown to uptake HADA preferentially at the septum, showing that this is the site of growth of new cell wall PG (Figure **1.12, a**). This was supported by a further experiment in which a longer labelling time with HADA was followed by fluorescence imaging overtime, which showed that the growth of new PG after labelling occurred in the middle of the bacteria with the remaining HADA migrating to the ends of the bacteria (Figure **1.12**, **b**).

A

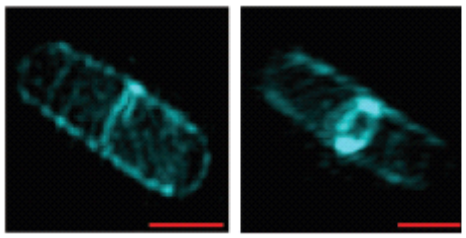

B

Figure 1.12: (**A**) High resolution microscopy of *E. coli* after short labelling pulses with HADA; (**B**) Time-lapse fluorescence microscopy of HADA-labelled *E. coli* (picture adapted from ref. [63]).

1.8 Photoactivatable Amino Acids

Photoactivatable amino acids are synthetic structural homologues of the naturally occurring amino acids with photoactivatable groups, such as diazirine, as part of their side chains (example: photomethionine, photoleucine, photoisoleucine, photothyptophan, photophenylalanine, photolysine) (Figure **1.13**).[69]

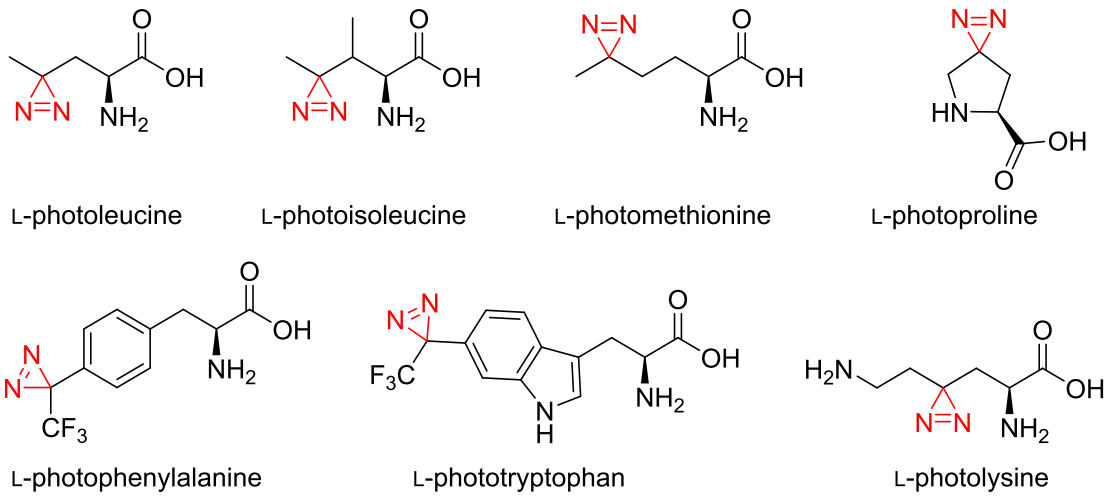

Figure 1.13: Photoactivatable amino acids.

The photolysis of photoactivable amino acids containing a diazirine ring requires UV irradiation (360 nm) which cleaves the diazirine to a carbene (Figure **1.14**) which can insert into a neighbouring bond (e.g. NH, OH, or CH) covalently crosslinking any nearby molecules such as proteins.[70]

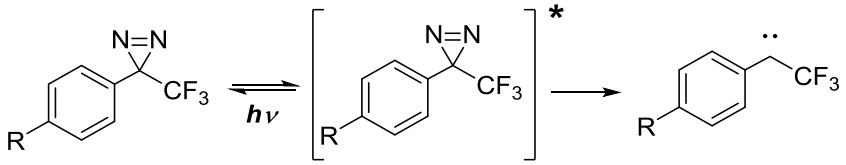

Figure 1.14: Formation of carbenes from diazirines (picture adapted from ref. [70]).

Therefore, diazirine-containing photoactivatable amino acids have been used widely to investigate cell biology at a molecular level, using the covalent cross-linking of near-by biological structures in the identification of protein-protein interactions and novel binding sites in target enzymes.[71] Current work on diazirine-containing photoactivatable amino

acids has focused on the synthesis and applications of L-amino acid systems, whilst little has been done in the area of diazirine containing photoactivatable D-amino acids.

1.9 Research Aim

Although much is known about the biosynthesis of PG in *E. coli*, there are many cell wall associated enzymes for which the function is unknown. For example, *E. coli* contains over 100 outer membrane lipoproteins with unknown function.[72] Thereforenew approaches will be developed to explore the function of PG associated proteins, particularly those involved in PG remodelling and biosynthesis. This work is hoped to provide valuable enzyme targets for future antibiotic development.

Since unnatural D-amino acids can be incorporated into bacterial PG by native PG biosynthesis machinery a plan to synthesize unnatural D-amino acids which include a photoactivatable cross-linking group (diazirine) on their side chains will be created. These photoactivatable D-amino acids will be covalently incorporated into the PG of *E. coli* by L,D-Tpase (LdtD), and on irradiation with UV light will form a carbene capable of covalently crosslinking any nearby PG-associated proteins. Following isolation of the PG and digestion with muramidase, the resulting muropeptide-D-amino acid-protein complex will be isolated and identified by LC-MS/MS, allowing the discovery of new PG-associated proteins (Figure **1.15**).[73,74]

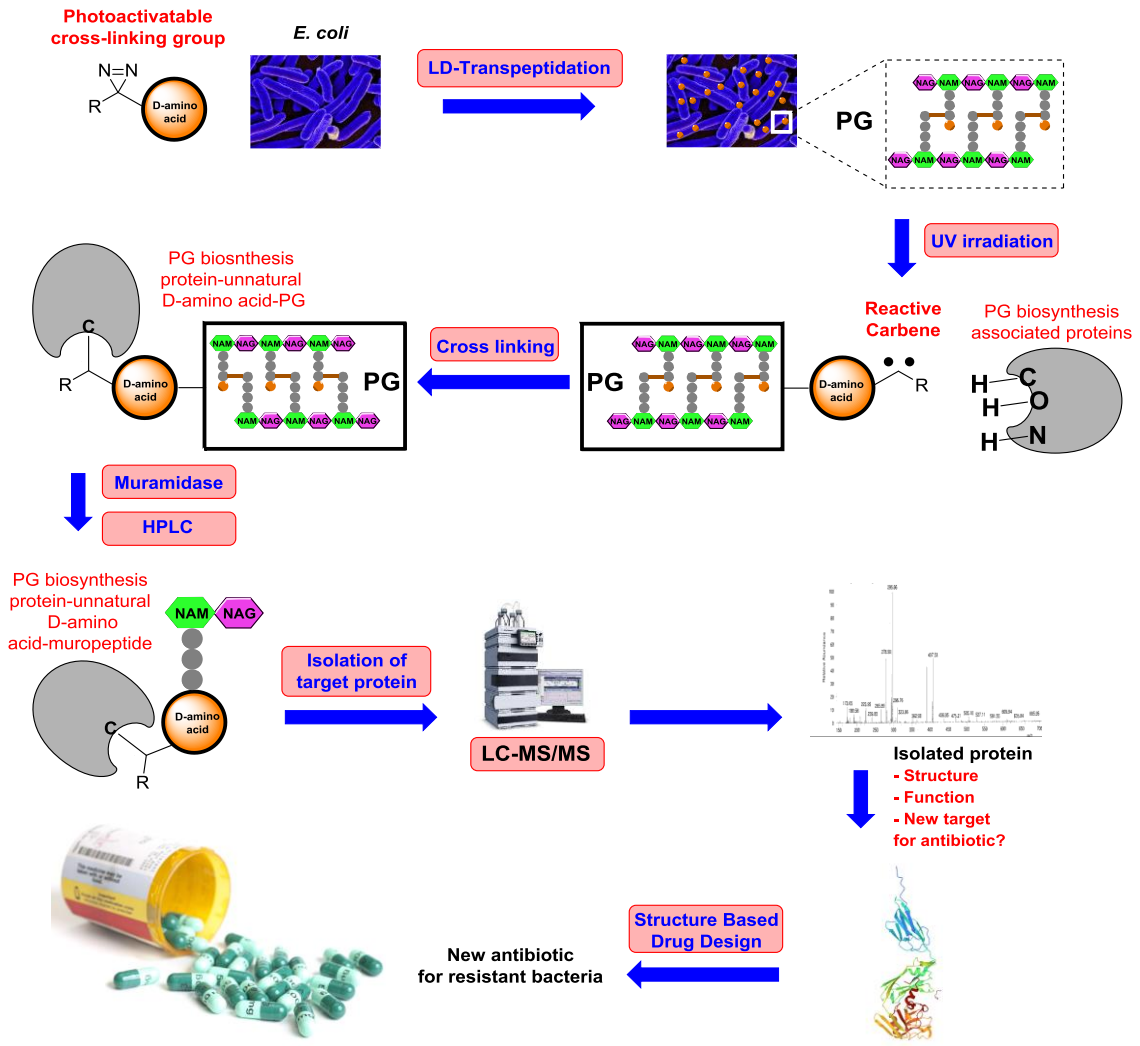

Figure 1.15: Project plan for capture and identification of PG associated proteins with photoactivatable D-amino acids.

1.10 References

1- T. Silhavy, D. Kahne and S. Walker, *Cold Spring Harb Perspect Biol*., 2012, **2**, 1-16**.**

2- A. Glauert, M. Thornley, *Annu. Rev. Microbiol*., 1969, **23**, 98-159.

3- F. Neuhaus and J. Baddiley, *Microbiol. Mol. Biol. Rev*., 2003, **67**, 686-723.

4- R. Milton and K. Kim, *Medical Microbiology*, ed. S. Baron, UTMB, Texas, 4th edn., 1996, ch. 2.

5- N. Malanovic, K. Lohner, *Biochim. Biophys. Acta*., 2016, **1858**, 936-946.

6- A. Asmar and J. Collet, *FEMS Microbiol. Lett*., 2018, **365**, 1-8.

7- W. Vollmer and J. V. Höltje, *J. Bacteriol*., 2004, **186**, 5978-5987.

8- W. Vollmer, D. Blanot and M. De Pedro, *FEMS Microbiol. Rev.*, 2008, **32**, 149-167.

9- S. Dramsi, S. Magnet, S. Davison, and M. Arthur, *FEMS Microbiol. Rev*., 2008, **32**, 307-320.

10- F. Cava, H. Lam, M. Pedro and M. Waldor, *Cell. Mol. Life Sci.*, 2011, **68**, 817-831.

11- N. Bui, A. Eberhardt, D. Vollmer, T. Kern, C. Bougault, A. Tomasz, J. Simone and W. Vollmer, *Anal. Biochem.*, 2012, **421**, 657-66.

12- W. Weidel, and H. Pelzer, *Adv. Enzymol*., 1964, **26**, 193-232.

13- W. Vollmer, and U. Bertsche, *Biochim. Biophys. Acta*., 2008, **1778**, 1714-1734.

14- L. Malinicova, M. Piknova, P. Pristas, and P.Javorsky, in *Current Research, Technology and Education Topics in Applied Microbiology and Microbial Biotechnology*, ed. A. Mendez-Vilas, Formatex Research Center, Badajoz, 2010, vol. 1, pp. 463-472.

15- J. Höltje, D Mirelman, N Sharon, and U. Schwarz, *J. Bacteriol*., 1975, **124**, 1067-1076.

16- W. Vollmer and S. Seligman *Trends Microbiol*, 2010, **18**, 59-66.]

17- K. Schleifer and O. Kandler, *Bacteriol. Rev*., 1972, **36**, 407-477.

18- U. Jurgens, G. Drews, and J. Weckesser, *J. Bectriol*.,1983, **154**, 471-478.

19- A. Egan, J. Errington and W. Vollmer, *Nat. Rev. Microbiol*., 2020, **18**, 446-460.

20- H. Barreteau, A. Kovac, A. Boniface, M. Sova, S. Gobec, and D. Blanot, *FEMS Microbiol. Rev*., 2008, **32**, 168–207.

21- D. Mengin-Lecreulx, and J. van Heijenoort, *J. Bacteriol*., 1994, **176**, 5788-5795.

22- A. Bouhss S. Dementin, J. van Heijenoort, C. Parquet, and D. Blanot, *Methods. Enzymol*., 2002, **354**, 189-196.

23- K. Ehlert, and J. Höltje, *J. Bacteriol*. 1996, **178**, 6766-6771.

24- T. Mohammadi, V. van Dam, R. Sijbrandi, T. Vernet, A. Zapun, A. Bouhss, M. Bruin, M. Nguyen-Disteche, B. Kruijff1 and E. Breukink, *EMBO*, 2011, **30**, 1425-1432.

25- T. Sham, K. Butler, D. Lebar, D. Kahne, G. Bernhardt, and N. Ruiz, *Science*, 2014, **345**, 220-222.

26- C. Goffin, and J-M. Ghuysen, *Microbiol. Mol. Biol. Rev*., 1998, **62**, 1079-1093.

27- J. van Heijenoort, *Glycobiology*, 2001, **11**, 25-36.

28- M Terrak , T. Ghosh, J. van Heijenoort, J. Beeumen, M. Lampilas, J. Aszodi, J. Ayala, J. Ghuysen, and M. Nguyen-Distèche, *Mol. Microbiol*., 1999, **34**, 350-364.

29- D. King, G. Wasney, M. Nosella, A. Fong, N. Strynadka, *J. Biol. Chem*., 2017, **292**, 979-993.

30- N. Caveney, F. Li and N. Strynadka, *Curr. Opin. Struct. Biol*., 2018, **53**, 45-58.

31- M. El Ghachi, N. Howe, CY. Huang, *Nat. Commun*., 2018, **9**, 1-13.

32- C. Goffin, and J-M. Ghuysen, *Microbiol. Mol. Biol. Rev*., 1998, **62**, 1079-1093.

33- C. Ealand, R. Asmal, L. Mashigo, L. Campbell, and B. Kana, *Sci. Rep*., 2019, **9**, 5194.

34- J. Holtje, *Microbiol. Mol. Biol. Rev*., 1998, **62**, 181-203.

35- E. Sauvage, F. Kerff, M. Terrak, J. Ayala and P. Charlier, *FEMS, Microbiol. Rev*., 2008, **32**, 234-258.

36- R. Tripathi and N. Nair, *J. Am. Chem. Soc*., 2013, **135**, 14679−14690.

37- T. Lupoli, H. Tsukamoto, E. Doud, T. Wang, S. Walker, and D. Kahne, *J. Am. Chem. Soc*., 2011, **133**, 10748–10751.

38- N. Mora, A Martorana, J. Biboy, C. Otten, M. Winkle, C. Serrano, A. Silva, L. Atkinson, H. Yau, E. Breukink, T. Blaauwen, W. Vollmer, and A. Polissi, *mBio*., 2019, DOI: 10.1128/mBio.02729-18.

39- M. Caparros, A. Pisabarro, and M. De Pedro, *J. Bacteriol*., 1992, **174**, 5549-5559.

40- J. Mainardi, M. Fourgeaud, J. Hugonnet, L. Dubost, J. Brouard, J. Ouazzani, L. Rice, L. Gutmann, and M. Arthur, *J. Biol. Chem*., 2005, **280**, 38146-38152.

41- J. Mainardi, R. Villet, T. Bugg, C. Mayer and M. Arthur, *FEMS. Microbiol. Rev*., 2008, **32**, 386-408.

42- S. Magnet, L. Dubost, A. Marie, M. Arthur, and L. Gutmann, *J. Bacteriol*., 2008, **190**, 4782-4785.

43- J. Hugonnet, D. Mengin-Lecreulx, Alejandro Monton, T. Blaauwen, E. Carbonnelle, C. Veckerle, Y. Brun, M. Nieuwenhze, C. Bouchier, K. Tu, L. Rice, and M. Arthur, *Elife*., 2016, DOI: 10.7554/eLife.19469.

44- L. Sütterlin, Z. Edoo, J. Hugonnet, J. Mainardi, and M. Arthur, *Antimicrob. Agents Chemother*., 2018, DOI: 10.1128/AAC.01607-17.

45- T. Bugg, and C. Walsh, *Nat. Prod. Rep*., 1992, **9**, 199-215.

46- J. Coyette, and A. Ende, *FEMS, Microbiol. Rev*., 2008, **32**, 147-148.

47- P. Sarkar, V. Yarlagadda, C. Ghosh and J. Haldar, *Med. Chem. Commun*., 2017, **8**, 516-533.

48- P. Hawkey and D. Livermore, *BMJ*., 2012, **344**, 2-7.

49- C. Willyard, *Nature*., 2017, **543**, 15.

50- A. Typas, M. Banzhaf, C. Gross, and W. Vollmer, *Nat. Rev. Microbiol*., 2012, **10**, 123-136.

51- H. Lam, D. Oh, F. Cava, C. Takacs, J. Clardy, M. de Pedro and M. Waldor, *Science*, 2009, **325**, 1552-1555.

52- F. Cava, M. Pedro, H. Lam, B. Davis and M. Waldor, *EMBO*, 2011, **30**, 3442-3453.

53- M. De Pedro, J. Quintela, J. Holtje, and H. Schwarz, *J. Bacteriol*., 1997, **179**, 2823-2834.

54- M. Bern R. Beniston and S. Mesnage, *Anal Bioanal Chem*., 2017, **409**,551-560.

55- O. Krokhin, R. Craig, V. Spicer, W. Ens, K. Standin, R. Beavis, and J. Wilkins, *Mol Cell Proteomics*., 2004, **9**, 908-919.

56- B. Glauner, J. Holtje, and U. Schwarz, *J. Biol. Chem*., 1988, **263**, 10088-10095.

57- J. Lyne, D. Carters, X. HelI, G. Stubbsll, and J. Hash, *J. Biol. Chem*., 1990, **265**, 6928-6930.

58- W. Vollmer, B. Joris, P. Charlier, and S. Foster, *FEMS. Microbiol. Rev*., 2008, **32**, 259-286.

59- J. Gmeiner, P. Essig, and H. Martin, *FEBS. Lett*., 1982, **138**, 109-112.

60- W. Vollmer, B. Joris, P. Charlier, and S. Foster, *FEMS Microbiol. Rev*., 2008, **32**, 259-286.

61- B. Glauner, J. Höltje, and U. Schwarz, *J. Biol. Chem*., 1988, **263**, 10088-10095.

62- B. Glauner, *Anal. Biochem*., 1988, **172**, 451-464.

63- E. Kuru, H. Hughes, P. Brown, E. Hall, S. Tekkam, F. Cava, M. de Pedro, V Brun, and M. VanNieuwenhze, *Angew. Chem., Int. Ed*., 2012, **51**, 12519-12523.

64- Y. Hsu, J. Rittichier, E. Kuru, J. Yablonowski, E. Pasciak, S. Tekkam, E. Hall, B. Murphy, T. Lee, E. Garner, K. Huang,Y. Brun and M. VanNieuwenhze, *Chem. Sci*., 2017, **8**, 6313-6321.

65- E. Kuru, A. Radkov, X. Meng, A. Egan, L. Alvarez, A. Dowson, G. Booher, E. Breukink, D. Roper, F. Cava, W. Vollmer, Y. Brun, and M. VanNieuwenhze, *ACS Chem. Bio*., 2019, **14**, 2745-2756.

66-Y. Hsu, G. Booher, A. Egan, W. Vollmer, and M. VanNieuwenhze, *Acc. Chem. Res*., 2019, **52**, 2713−2722.

67- F. Cava, W. Vollmer, Y. Brun, and M. VanNieuwenhze, *ACS Chem. Biol*., 2019, **14**, 2745−2756.

68-A. Radkove, Y. Hsu, G. Booher, and M. VanNieuwenhze, *Ann Rev Biochem*., 2018, **87**, 991-1014.

69- S. Ge, B. Chen, Y. Wu, Q. Long, Y. Zhao, P. Wanga and S. Yang, *RSC Adv*., 2018, **8**, 29428-29454.

70- J. Brunner, H. Serin, and F. Richards, *J. Biol. Chem*., 1980, **255**, 3313-3318.

71- M. Suchanek, A. Radzikowska and C. Thiel, *Nat. Meth*., 2005, **2**, 261-268.

72- H. Miyadai, K. Masuda, S. Matsuyama and H. Tokuda, *J. Biol. Chem*., 2004, **279**, 39807–39813.

73- Y. Tangpo, Z. Liu and D. L. Xiang, *Chem. Sci.*, 2015, **6**, 1011-1017.

74- Y. Ikeda and E. J. Behrman, *Synth. Commun*., 2008, **38**, 2276–2284.

Chapter 2. Synthesis of Photoactivatable D-Amino Acids

2.1 Introduction

One of the key aims of this project will be to synthesise a number of photoactivatable D-amino acids that can later be incorporated into PG via native biosynthesis machinery. Therefore, in this chapter, I planned to examine the synthesis of both D-photoleucine (**2.1**) and D-photomethionine (**2.2**), containing a key diazirine as the photoactivatable group, which are structural analogues to the naturally occurring D-methionine (**2.3**) and D-leucine (**2.4**) respectively (Figure **2.1**). [1,2]

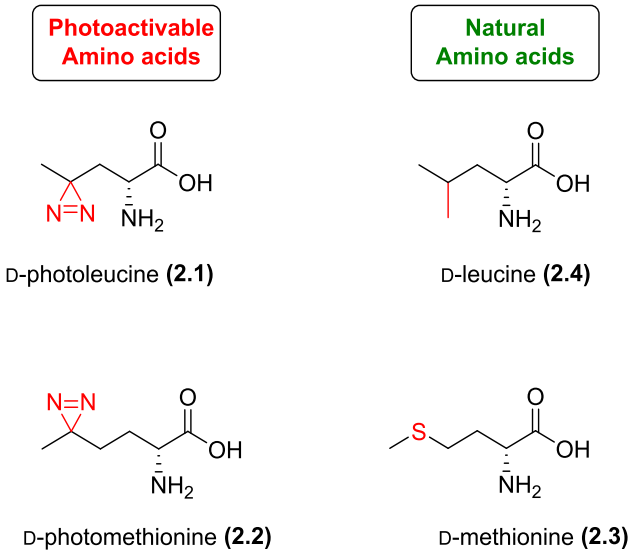

Figure 2.1: Comparison between our target D-photoleucine (**2.1**) and D-photomethionine (**2.2**) to the corresponding natural D-leucine (**2.4**) and D-methionine (**2.3**).

2.2 Results and Discussion

2.2.1 Racemic Synthesis of Photoleucine

Firstly, a racemic synthesis of photoactivatable amino acids will be examined, as I propose that if a racemic mixture of amino acids were given to bacteria it will selectively incorporate only D-amino acids into the PG. As such, it might not be needed to synthesise an enantiopure amino acid but could use racemic material. Therefore, I plan to use a synthetic route to make the racemic mixture of the desired photo cross-linking amino acid.Subsequently the resulting racemic amino acid will be fed to the bacteria and the incorporation into the PG will be examined. Then the bacteria will be irradiated to induce

the generation of reactive carbene from PG incorporated photo cross-linking amin acid, these carbenes should be able to cross-linking any nearby PG associated protein.

In 2008, Behrman *et al*., reported a racemic synthesis of a diazirine containing photoleucine (**2.1**) in 3 steps starting from levulinic acid (**2.5**) (Figure **2.2**). First, Behrman incorporated the diazirine group into levulinic acid (**2.5**) to give the corresponding photolevulinic acid (**2.6**), followed by a bromination at the α-position and a subsequent aminolysis to incorporate the required α-amino group.[3] Therefore, the Behrman's synthesis to access our target photoleucine will be tested (**2.1**).

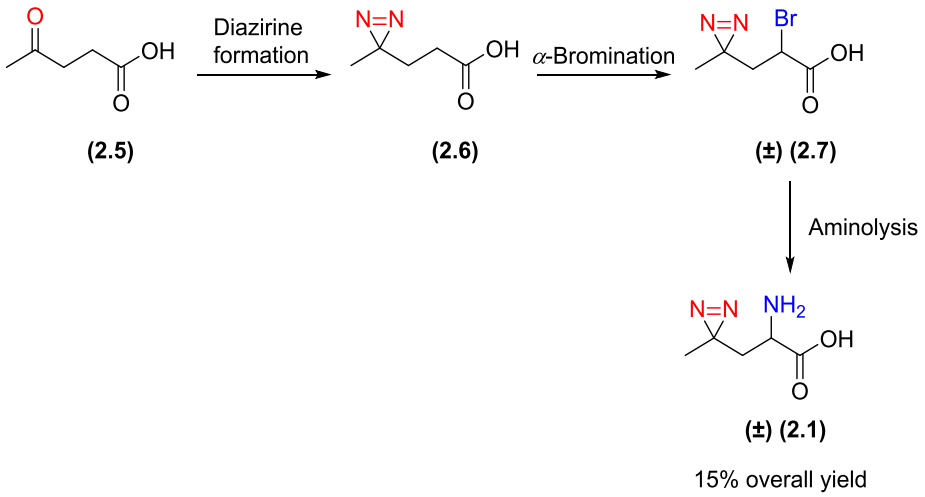

Figure 2.2: Behrman's racemic synthesis of photoleucine (**2.1**).

2.2.1.1 Synthesis of Photolevulinic Acid (2.6)

The first synthetic step towards the production of racemic photoleucine (**2.1**) (Figure **2.2**) was the synthesis of photolevulinic acid (**2.6**), through the installation of a diazirine at the 4-position of levulinic acid (**2.5**). Based on the work of Behrman *et al*., I proposed to form the desired photolevulinic acid (**2.6**) via the conversion of levulinic acid (**2.5**) into the corresponding imine (**2.8**) followed by the reaction with hydroxylamine-*O*-sulfonic acid (HOSA) to give aminal sulfate (**2.9**). Aminal sulfate (**2.9**) will then undergo intramolecular ring closure to form diaziridine levulinic acid (**2.10**). A plan was put in place to isolate diaziridine levulinic acid (**2.10**), which will be subsequently oxidised to give our target photolevulinic acid (**2.6**) (Figure **2.3**)[1,3,4].

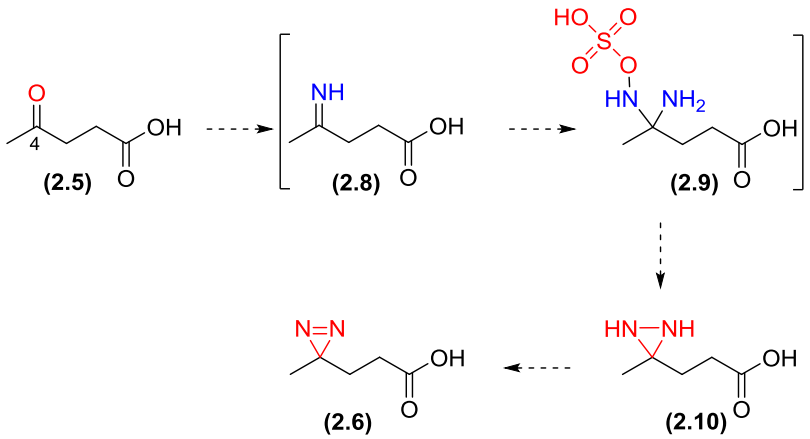

Figure 2.3: Planned synthetic route towards photolevulinic acid (**2.6**).

Thus, a methanolic solution of levulinic acid (**2.5**) was treated with liquid ammonia at -78 °C, followed by the addition of methanolic solution of hydroxylamine-*O*-sulfonic acid (HOSA). After a reaction time of 23 h, the diaziridine (**2.10**) was obtained after filtering the reaction mixture. The crude diaziridine (**2.10**) was then oxidised with iodine and triethylamine at 5 °C for 30 minutes. Following acid-base extraction into DCM the desired photolevulinic acid (**2.6**) was isolated in a 34% yield over two steps with no further purification required (Figure **2.4**).

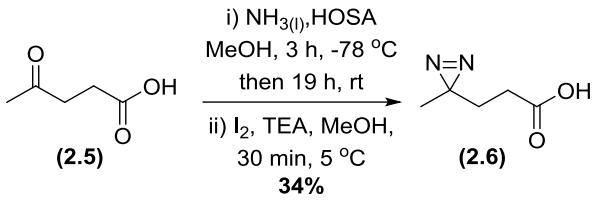

Figure 2.4: Synthesis of photolevulinic acid (**2.6**) from levulinic acid (**2.5**).

The structure of photolevulinic acid (**2.6**) was confirmed by ^{13}C NMR spectroscopy. The shift of the ^{13}C NMR signal corresponding to an aliphatic diazirine carbon atom typically occurs between 24.8 and 28.2 ppm (mean = 26.1 ppm, S.D. = 1.6, over 8 compounds), pleasingly the C-4 atom of photolevulinic acid (**2.6**) showed a ^{13}C NMR shift of 25.2 ppm, thus falling within this range.[3,4,5,6]

With sufficient quantities of photolevulinic acid (**2.6**) in hand I decided to move on to the next synthetic step.

2.2.1.2 Bromination of Photolevulinic Acid (2.6) to give *α*-Bromo Photolevulinic Acid (2.7)

In order to access our target molecule photoleucine (**2.1**) an amine function group into the *α*-position of photolevulinic acid would need to be introduced (**2.6**). This would be done through the introduction of a good leaving group at the *α*-position of photolevulinic acid (**2.6**) followed by substitution with ammonia. Thus, our next synthetic step was to examine the *α*-bromination of photolevulinic acid (**2.6**) (Figure **2.5**).

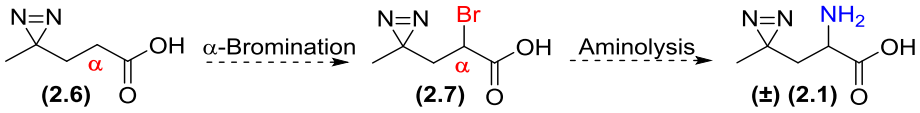

Figure 2.5: Planned synthesis racemic photoleucine (**2.1**) via *α* -bromination of photolevulinic acid (**2.6**), followed by aminolysis.

Therefore, a Hell-Volhard-Zelinsky (HVZ) reaction was employed based on a modified procedure by Dolbier *et al*., in order to *α*-brominate photolevulinic acid (**2.6**).[7]

In our first attempt to *α*-brominate photolevulinic acid (**2.6**) under HVZ conditions, a solution of photolevulinic acid (**2.6**) in acetic acid with 1 eq. of NBS in presence of a catalytic amount of H_2SO_4 was heated at 85 °C for 16 h. Unfortunately, following removal of the solvent under reduced pressure, ^{1}H NMR analysis of the crude reaction products indicated the formation of a complex mixture of compounds (Table **2.1,** entry **1**). Next the replacment of the solvent (acetic acid) in our HVZ reaction with THF was examined, in an attempt to remove the strongly acidic conditions perhaps responsible for the previous poor reaction outcome. Therefore, photolevulinic acid (**2.6**) was reacted with 1.5 eq. of NBS in the presence of catalytic H_2SO_4 in refluxing THF for 4 h. The reaction mixture was then evaporated under reduced pressure to remove solvent and the obtained crude residue was submitted to ^{1}H NMR which showed signals corresponding to the starting material photolevulinic acid (**2.6**) and a number of other unidentified compounds. TLC of the crude reaction mixture (ethyl acetate : hexane : methanol, 8:1:1) confirmed the presence of photolevulinic acid x (UV, R*f* = 0.79) and one major new compound (R*f* = 0.34). Unfortunately attempts to isolate this new compound was unsuccessful via silica gel column chromatography (Table **2.1,** entry **2**).

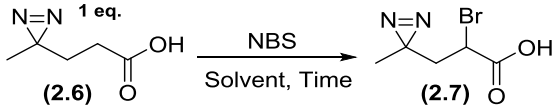

Entry	Reagents	Eq.	Solvent	Temperature °C	Reaction time	Reaction outcome
1	NBS H_2SO_4	1 0.1 mL	CH_3COOH	85	overnight	Complex product mixture
2	NBS H_2SO_4	1.5 0.01 mL	Dry THF	85	4 h	Starting material observed along with complex product mixture

Table 2.1: Attempted HVZ *α*-bromination of photolevulinic acid (**2.6**).

As attempts to use HVZ conditions for the *α*-bromination of photolevulinic acid (**2.6**) had proven unsuccessful, an investigation into an alternative *α*-bromination approach was decided on.

Smith *et al.*, has reported the *α*-halogenation of a diverse set of acyl chlorides, made *in situ* through the reaction of the corresponding carboxylic acids with thionyl chloride, under mild reaction conditions (Figure **2.6**).[8]

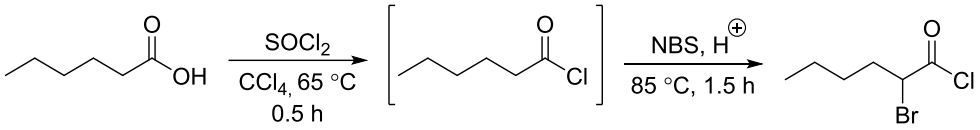

Figure 2.6: Smith's *α*-bromination of hexanoic acid with thionyl chloride and NBS.

Therefore this approach to the synthesis *α*-bromo photolevulinic acid was adapted (**2.7**). In our first reaction, photolevulinic acid (**2.6**) in DCM with thionyl chloride were both reacted for 30 min at 30 °C with the reaction vessel open to air. Subsequently, NBS was added along with a catalytic amount of aqueous HBr (48%) and the reaction mixture refluxed for 1.5 h. The reaction mixture was then worked up and the obtained reaction crude material was submitted to NMR analysis.^{1}H NMR spectroscopic analysis showed the presence of starting material (**2.6**) (photolevulinic acid) and the formation of succinimide, however none of the desired products could be observed (Table **2.2,** entry **1**).

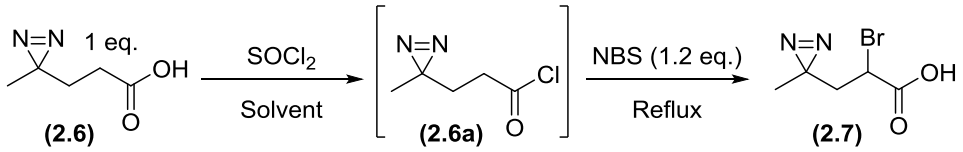

Entry	Reagent	Solvent	Reaction time	Reaction outcome
1	3.9 eq. $SOCl_2$ 48% HBr (2 drops)	DCM	2 h	No reaction, starting material recovered
2	3.9 eq. $SOCl_2$ 48% HBr (2 drops)	Dry DCM	2 h	No reaction, starting material recovered
3	3.9 eq. $SOCl_2$ 48% HBr (1 drops)	Dry DCM	overnight	No reaction, starting material recovered
4	4 eq. $SOCl_2$	Dry THF	3.2 h	2:1 ratio of photolevulinic acid : unidentified product (^{1}H NMR)

Table 2.2: Attempted α-bromination reactions of photolevulinic acid (**2.6**) with $SOCl_2$ and NBS.

Next, it was decided to repeat the bromination reaction but whilst minimising the water present, to aid in the formation of desired acyl chloride intermediate (**2.6a**). Therefore, the α-bromination of photolevulinic acid was repeated (**2.6**) but with anhydrous DCM and a decreased volume of aqueous HBr (48%). However, analysis of the crude ^{1}H NMR spectrum still showed only starting material (**2.6**) (photolevulinic acid) (Table **2.2**, entry **2**). Whilst extended reaction times also failed to show production of the desired product (Table **2.2,** entry.**3**).

Finally, removal of the aqueous HBr (48%) and a solvent swap to dry THF was attempted to remove any sources of water in this reaction. Thus, following thionyl chloride addition, the reaction was refluxed for 50 min, following which a solution of NBS solution in dry THF was added and the reaction refluxed for a further 2.5 h. Following work up, the solvent was removed under reduced pressure to give the crude product mixture. Analysis by ^{1}H NMR spectroscopy showed the presence of a 2:1 ratio of starting material (**2.6**) (photolevulinic acid) and a new unidentified product (Table **2.2,** entry **4**).

Analysis of the ^{1}H NMR spectra of the unidentified product showed one triplet at 4.12 ppm (J = 6.0 Hz, 1H), and two further triplets at 3.57 ppm (J = 6.4 Hz, 1H), and 3.44 ppm (J = 6.4 Hz, 1H) corresponding to the new molecule. Unfortunately, these signals did not match ^{1}H NMR data reported in literature for our desired product, α-bromo photolevulinic acid (**2.7**) (Figure **2.7**).[4]

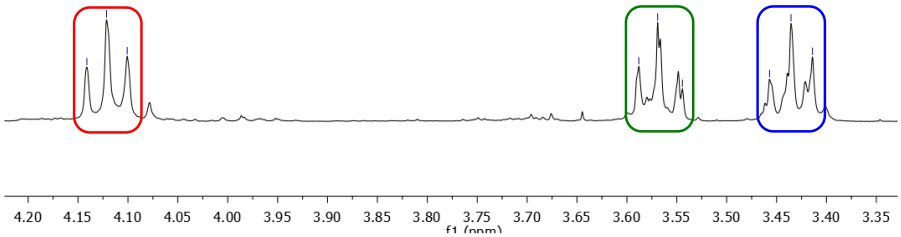

Figure 2.7: Expansion of the ^{1}H NMR spectrum of unidentified product obtained after Smith's α-bromination of photolevulinic acid (**2.6**).

Due to the time constraints and the difficulty to achieve the bromination reaction to produce α-bromo photolevulinic acid (**2.7**), an alternative route towards our target molecules D-photoleucine (**2.1**) and D-photomethionine (**2.2**) was examined.

2.2.2 One-Pot Organocatalytic Stereoinversion and Deuteration of L-Amino Acids to *α*-Deuterated D-Amino Acids

As an alternative route, a convertion of commercially available L-photo photoleucine (**2.11**) and L- photomethionine (**2.12**) to our target D-photoleucine (**2.1**) and D-photomethionine was planned (**2.2**). Recently, in 2015, Chin *et al*., have demonstrated that L-amino acids (eg. L-alanine **2.13**) can be converted to the corresponding *α*-deuterated D-amino acids (eg. D-alanine **2.14**) using a chiral phase transfer guanidine organocatalyst (**2.15**), an aryl aldehyde (**2.16**) in the presence of D_2O (Figure **2.8,** A).[9,10]

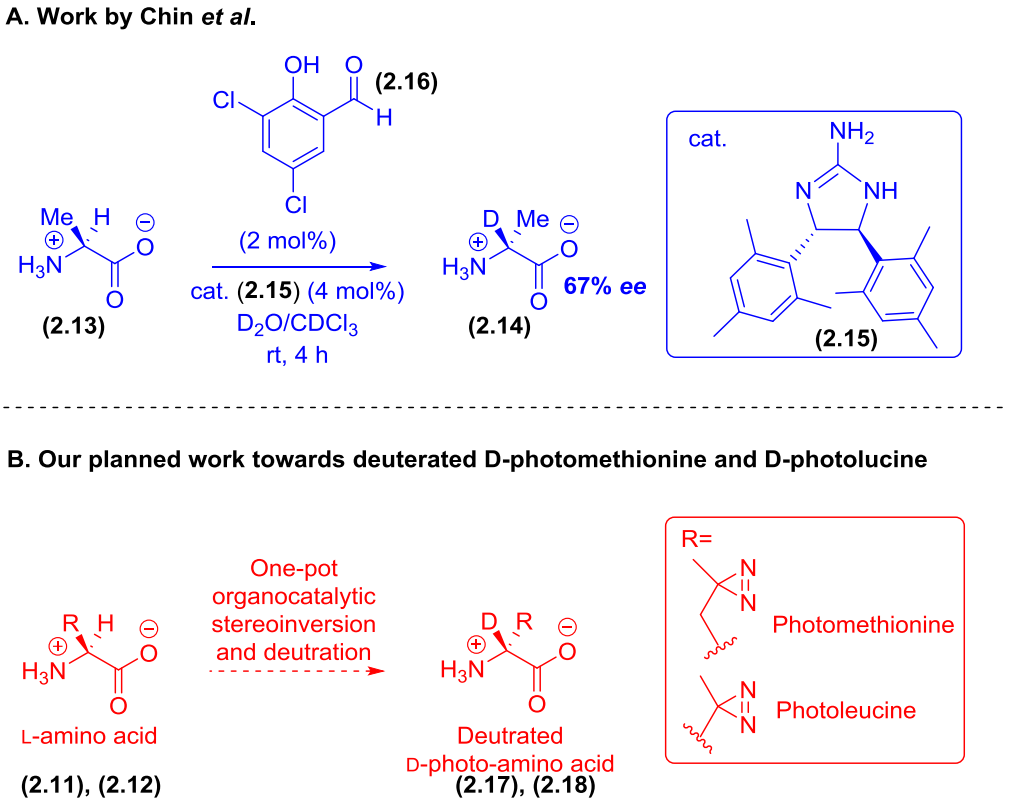

Figure 2.8: (**A**) Chin's one-pot organocatalytic stereoinversion and deuteration of L-alanine (**2.13**) to α-deuterated D-alanine (**2.14**). (**B**) Proposed one-pot organocatalytic stereoinversion and deuteration of both L-photoleucine (**2.11**) and L-photomethionine (**2.12**).

So, it was planned to test this chemistry with a simple L-amino acid (**2.13**) (L-alanine), then subsequently to extend this approach to convert L-photoleucine (**2.11**) and L-photomethionine (**2.12**) into the corresponding *α*-deuterated D-photoleucine (**2.17**) and *α*-deuterated D-photomethionine (**2.18**) (Figure **2.8, B**).

2.2.3 Preparation of the Phase Transfer Catalyst (*S*,*S*)-mesityl-guanidine (2.15)

To examine the catalytic stereoinversion and deuteration of L-amino acids to *α*-deuterated D-amino acids, first the synthesis of the phase transfer catalyst (*S*,*S*)-mesityl guanidine (**2.15**) was required. It was proposed that (*S*,*S*)-mesityl guanidine (**2.15**) could be synthesised in 4 steps based on the work of Chin *et al.*, [9] starting with a condensation between (*R*,*R*)-bis-hydroxy-phenyl diamine (**2.19**) with mesitaldehyde (**2.20**) to give the (*R*,*R*)-bis-hydroxy-phenyl diimine (**2.21**). This (*R*,*R*)-bis-hydroxy-phenyl diimine (**2.21**) will be converted to the corresponding (*S*,*S*)-bis-hydroxy-phenyl diimine (**2.22**) via a diaza Cope rearrangement. Finally, (*S*,*S*)-mesityl-guanidine (**2.15**) will be formed via an imine hydrolysis of (*S*,*S*)-bis-hydroxy-phenyl diimine (**2.22**), followed by a condensation of the resulting (*S*,*S*)-bis-mesityl diamine (**2.23**) with cyanogen bromide (Figure **2.9**).

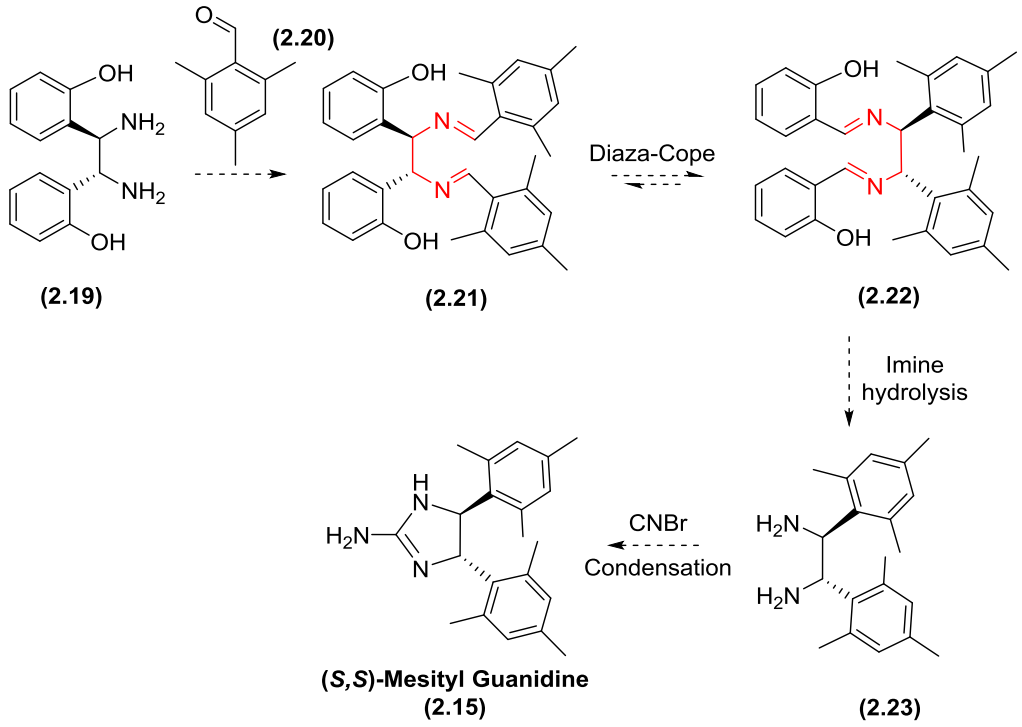

Figure 2.9: Planned synthetic route towards phase transfer organocatalyst, mesityl guanidine (**2.15**).

2.2.3.1 Synthesis of (*R,R*)-bis-hydroxy-phenyl diimine (2.21)

Therefore, our first step towards the catalyst mesityl guanidine (**2.15**) was the synthesis of (*R,R*)-bis-hydroxy-phenyl diimine (**2.21**). Thus, (*R,R*)-bis-hydroxy-phenyl diamine (**2.19**) was condensed with mesitaldehyde (**2.20**) in ethanol at 0 ^{o}C to form the desired (*R,R*)-bis-hydroxy-phenyl diimine (**2.21**) which was isolated by a simple filtration to give a 77 % yield (Figure **2.10**).

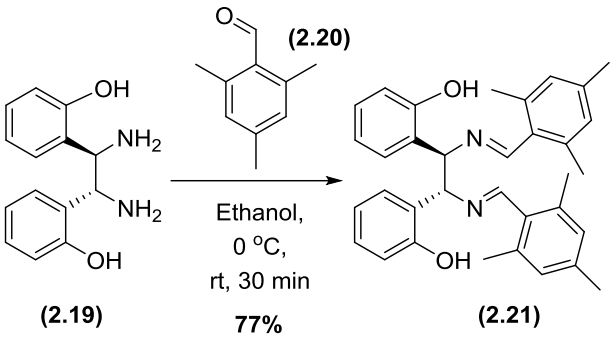

Figure 2.10: Condensation between bis-hydroxy-phenyl diamine (**2.19**) and mesitaldehyde (**2.20**).

The structure of the obtained (*R,R*)-bis-hydroxy-phenyl diimine (**2.21**) was confirmed by ^{1}H NMR spectrum which showed a set of signals at 8.55 ppm (s, 2H) and 4.91 ppm (s, 2H) corresponding to the imine protons and the benzylic protons respectively. In addition, a signal was observed at 10.30 ppm (s, 2H) corresponding to the two phenolic OH groups (Figure **2.11**).

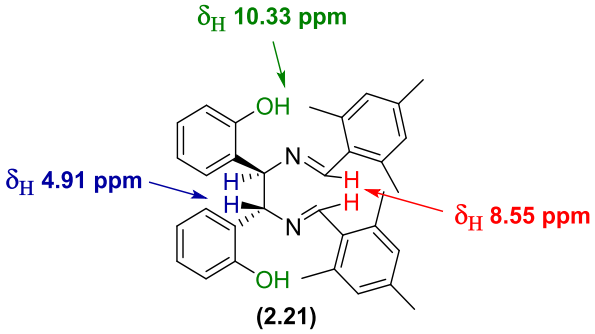

Figure 2.11: ^{1}H NMR spectroscopic analysis of (*R,R*)-bis-hydroxy-phenyl diimine (**2.21**).

With the desired (*R,R*)-bis-hydroxy-phenyl diimine (**2.21**) in hand, I proceeded to the next step in the synthesis of mesityl guanidine (**2.15**).

2.2.3.2 Synthesis of (*S*,*S*)-bis-hydroxy-phenyl diimine (2.22) via Diaza-Cope Rearrangement.

The next step in our planned route was the synthesis of (*S*,*S*)-bis-hydroxy-phenyl diimine (**2.22**) via the diaza-Cope rearrangement of (*R*,*R*)-bis-hydroxy-phenyl diimine (**2.21**). Therefore, (*R*,*R*)-bis-hydroxy-phenyl diimine (**2.21**) was stirred in chloroform for one week at room temperature to give the desired (*S*,*S*)-bis-hydroxy-phenyl diimine (**2.22**) in quantitative yield following a simple evaporation (Figure **2.12**).

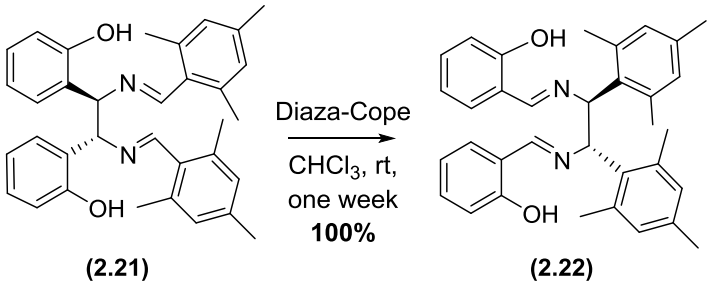

Figure 2.12: Diaza-Cope rearrangement of (*R*,*R*)-bis-hydroxy-phenyl diimine (**2.21**).

The ^{1}H NMR spectrum gave us confidence that (*S*,*S*)-bis-hydroxy-phenyl diimine (**2.22**) was formed, which showed a downfield shift of the enolic OH from 10.30 ppm (**2.21**) to 13.22 ppm (**2.22**), this change may be due to the formation of a new intramolecular H-bond.[14] In addition,a downfield shift of the benzylic protons was observed from 4.91 ppm (**2.21**) to 5.68 ppm (**2.22**) which might be attributed to the resonance stabilization effect of an intramolecular H-bond.[9,10] (Figure **2.13**).

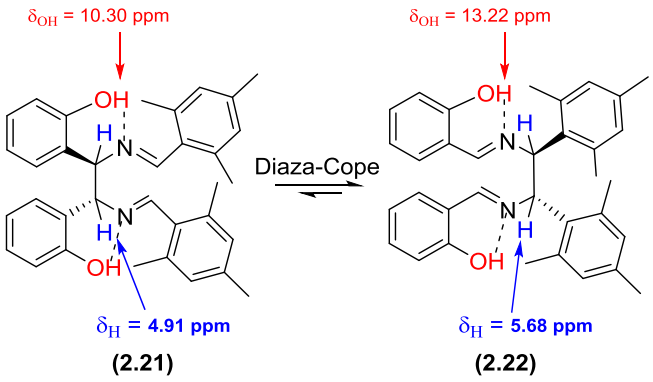

Figure 2.13: ^{1}H NMR shifts comparison between (*R*,*R*)-bis-hydroxy-phenyl diimine (**2.21**) and (*S*,*S*)-bis-hydroxy-phenyl diimine (**2.22**).

Once the desired (*S*,*S*)-bis-hydroxy-phenyl diimine was successfully synthesised (**2.22**) via a key diaza-Cope rearrangement, I decided to proceed to the next step.

2.2.3.3 Synthesis of (*S*,*S*)-bis-mesityl diamine (2.23)

The next step in the synthesis of our desired (*S*,*S*)-mesityl guanidine catalyst (**2.15**) was the hydrolysis of (*S*,*S*)-bis-hydroxy-phenyl diimine (**2.22**) to the corresponding mesityl diamine (**2.23**). Thus, (*S*,*S*)-bis-hydroxy-phenyl diimine (**2.22**) was dissolved in methanol, followed by the addition of HCl and the resulting reaction mixture stirred overnight at room temperature. Following acid base extraction in diethyl ether, the desired mesityl diamine (**2.23**) was obtained in a 59% yield with no further purification required (Figure **2.14**).

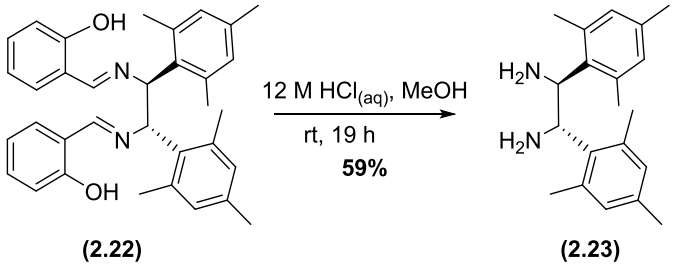

Figure 2.14: Hydrolysis of (***S,S***)-bis-hydroxy-phenyl diimine (**2.22**) to give (***S,S***)-bis-mesityl diamine (**2.23**).

The hydrolysis of (*S*,*S*)-bis-hydroxy-phenyl diimine (**2.22**) was confirmed by analysis of the ^{1}H NMR spectrum, which showed the loss of a set of signals at 8.44 ppm (s, 2H) and 7.19 – 7.30 (m, 8H), corresponding to the imine proton and the phenolic aromatic protons. Thus, this data supports the loss of the hydroxy benzylidene imine moiety.

With a sufficient amount of (*S*,*S*)-bis-mesityl diamine (**2.23**) in hand, I will proceed to the final step in the synthesis of the desired phase transfer catalyst, (*S*,*S*) mesityl-guanidine (**2.15**).

2.2.3.4 Synthesis of (*S*,*S*) mesityl-guanidine (2.15)

Finally for the preparation of the desired (*S*,*S*)-mesityl guanidine (**2.15**) the construction of the required aminoimidazole ring from our previously synthesised (*S*,*S*)-bis-mesityl diamine (**2.23**) will be needed via a condensation with cyanogen bromide. Thus, a chloroform solution of (*S*,*S*)-bis-mesityl diamine (**2.23**) was treated with cyanogen bromide

at 0 °C and the resulting reaction mixture was allowed warmed to room temperature overnight. The resulted guanidinium salt was concentrated under reduced pressure then partitioned between chloroform and water. The resulted residue was basified with NaOH and stirred at room temperature for 1 h, thenthe chloroform was removed by evaporation and the remained aqueous layer was filtered. The obtained precipitate was washed with water and dried under gravity to give the (*S*,*S*)-mesityl-guanidine (**2.15**) in 62 % yield with no further purification required (Figure **2.15**).

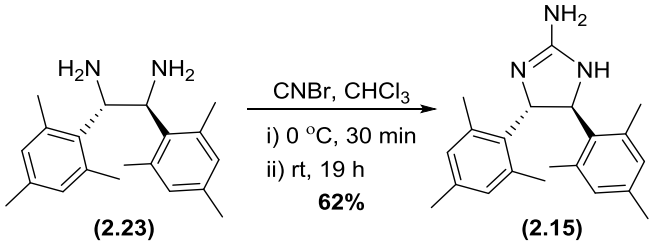

Figure 2.15: Synthesis of (*S*,*S*)-mesityl guanidine (**2.15**) via condensation between(*S*,*S*)-bis-mesityl diamine (**2.23**) and cyanogen bromide.

The structure of our (*S*,*S*)-mesityl-guanidine (**2.15**) was confirmed by ^{13}C NMR spectroscopy which showed a key signal at 161.7 ppm, corresponding to the guanidine sp^2 carbon atom at the C1 position. This guanidine sp^2 carbon was further confirmed by HMBC experiments which showed a key ^{1}H-^{13}C coupling between the benzylic proton at C3 (5.41 ppm) and the C1 guanidine sp^2 carbon (161.7 ppm) (Figure **2.16**).

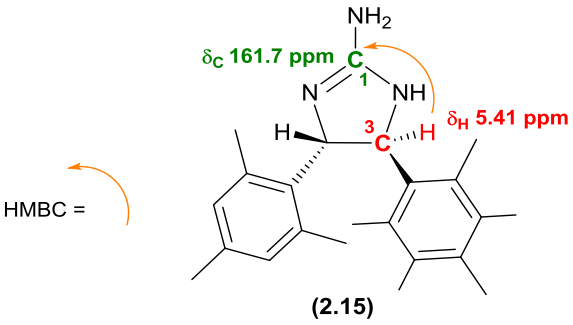

Figure 2.16: HMBC spectroscopic analysis of (*S*,*S*)-mesityl guanidine (**2.15**).

In conclusion,our desired phase transfer catalyst, (*S*,*S*)-mesityl guanidine (**2.15**) was successfully synthesised, in 4 steps with an overall yield of 28 % starting with a commercially available (*R*,*R*)-bis-hydroxy-phenyl diamine (**2.19**) and mesitaldehyde (**2.20**).

Therefore, with the desired (*S*,*S*)-mesityl guanidine (**2.15**) in hand, the next step was proceeded to, in order to test the stereoinversion and deuteration of a simple α-amino acid.

2.2.4 Catalytic Stereoinversion and Deuteration of L-Alanine

In the next step, I planned to examine the catalytic stereoinversion and deuteration of L-alanine (**2.13**) to *α*-deuterated D-alanine (**2.14**) with our previously isolated phase transfer catalyst, (*S*,*S*)-mesityl guanidine (**2.15**), as a test system.

Based on the work of Chin *et al.*, I proposed to conduct our test reaction by treating L-alanine (**2.13**) with (*S*,*S*)-mesityl guanidine (**2.15**) and aryl aldehyde (**2.16**) in a two solvent system (D_2O/H_2O) to give our desired *α*-deuterated D-alanine (**2.14**) (Figure **2.17**).

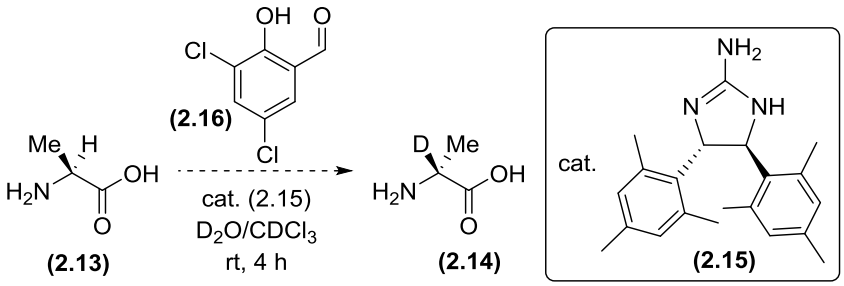

Figure 2.17: Planned test system for the catalytic stereoinversion and deuteration of L-alanine (**2.13**) to deuterated D-alanine (**2.14**).

Thus, enantiopure L-alanine (**2.13**) was dissolved in D_2O and stirred vigorously with $CDCl_3$ solution of aryl aldehyde (**2.16**) (2 mol %) and (*S*,*S*)-mesityl-guanidine (**2.15**) (4 mol %). The reaction mixture was stirred at room temperature for 4 h. The D_2O layer was separated from the organic layer and then extracted with a fresh $CDCl_3$ solution of (*S*,*S*)-mesityl-guanidine (**2.15**).

The obtained organic layer was analysed by ^1H NMR spectroscopy which showed six broad signals at 6.83 (s, 2H-Ar), 6.63 (s, 2H-Ar), 5.37 (s, 2H-benzylic), 2.47 (s, 6H-methyl), 2.20 (6H-methyl) and 1.68 ppm (6H-methyl) corresponding to the (*S*,*S*)-mesityl-guanidine catalyst (**2.15**). Also a low intensity peak at 3.23 ppm was obsereved which was assigned to the alpha proton of L-alanine. In addition, several peaks in the region (0.90-1.25 ppm) were observed, it had been postulated that these peaks could correspond to alanine related

methyl groups and thus they might be an indicator to the formation of several products and the presence of the starting material L-alanine (**2.13**) (Figure **2.18**)

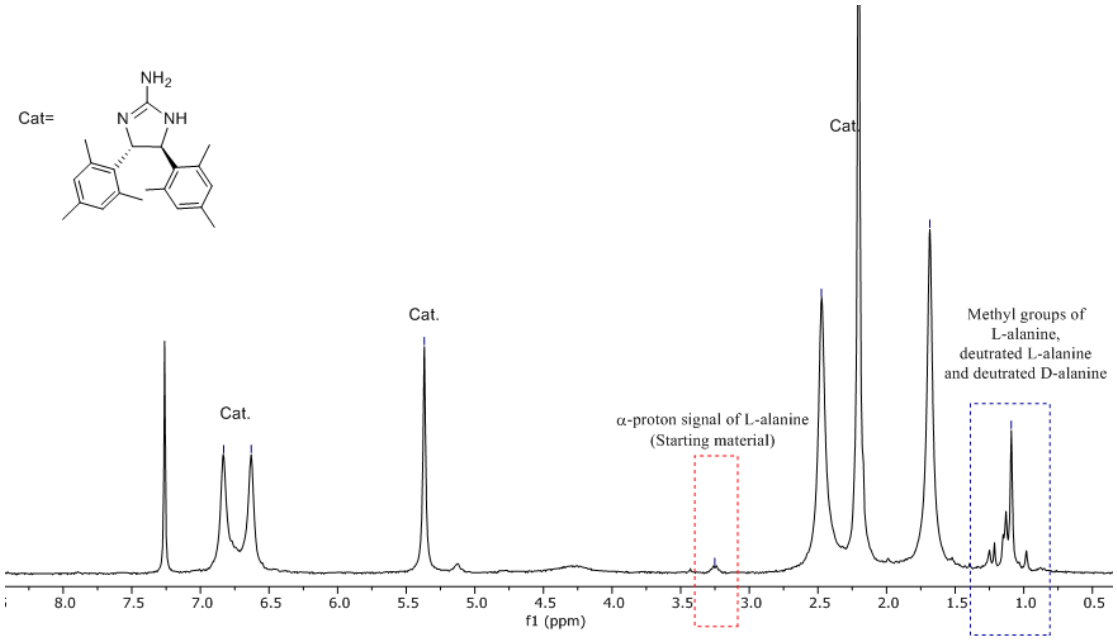

Figure 2.18: ^{1}H NMR spectrum of the $CDCl_3$ /(*S*,*S*)-mesityl-guanidine (Cat.) extract from the D_2O layer of a catalytic stereoinversion and deuteration of L-alanine (**2.13**) to deuterated D-alanine (**2.14**).

Since many products and starting material have been observed in the ^{1}H NMR spectrum of our first experiment (Table **2.3**, entry **1**), the reaction with a longer reaction time of 72 h was repeated to attempt to increase product formation. The reaction was repeated as previously, and after the 72 h, ^{1}H NMR spectrum showed another complicated spectrum containing multiple broad peaks again, and it was difficult to differentiate between starting material (L-alanine **2.13**), and the presence of the desired deuterated D-alanine (**2.14**) (Table **2.3**, entry **2**).

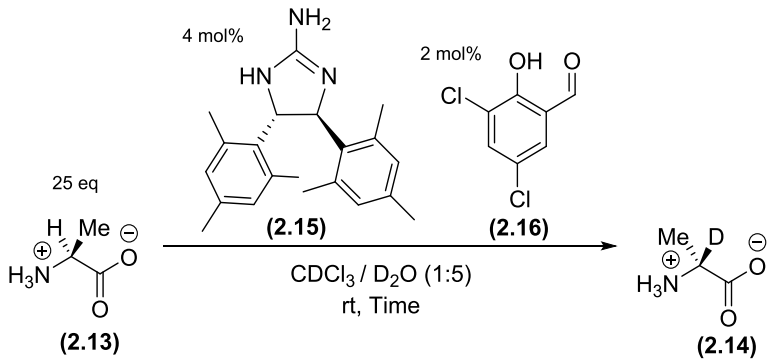

Entry	Reaction time	Reaction outcome
1	4 h	Staring material (L-alanine) and several unidentifiable products
2	72 h	Complex mixture

Table 2.3: Attempted synthesis of α-deuterated D-alanine (**2.14**) via catalytic stereoinversion and α-deuteration of L-alanine (**2.13**).

Therefore it was decided to make two standard solutions of enantiopure L-alanine (**2.13**) with (*S*,*S*)-mesityl guanidine (**2.15**) (Figure **2.19**, A) and enantiopure D-alanine (**2.24**) with (*S*,*S*)-mesityl guanidine (**2.15**) (Figure **2.19**, B) and use their ^{1}H NMR spectra as a reference to compare with the ^{1}H NMR spectrum obtained from the reactions of L-alanine (**2.13**) with aryl aldehyde (**2.16**) and mesityl guanidine (**2.15**).

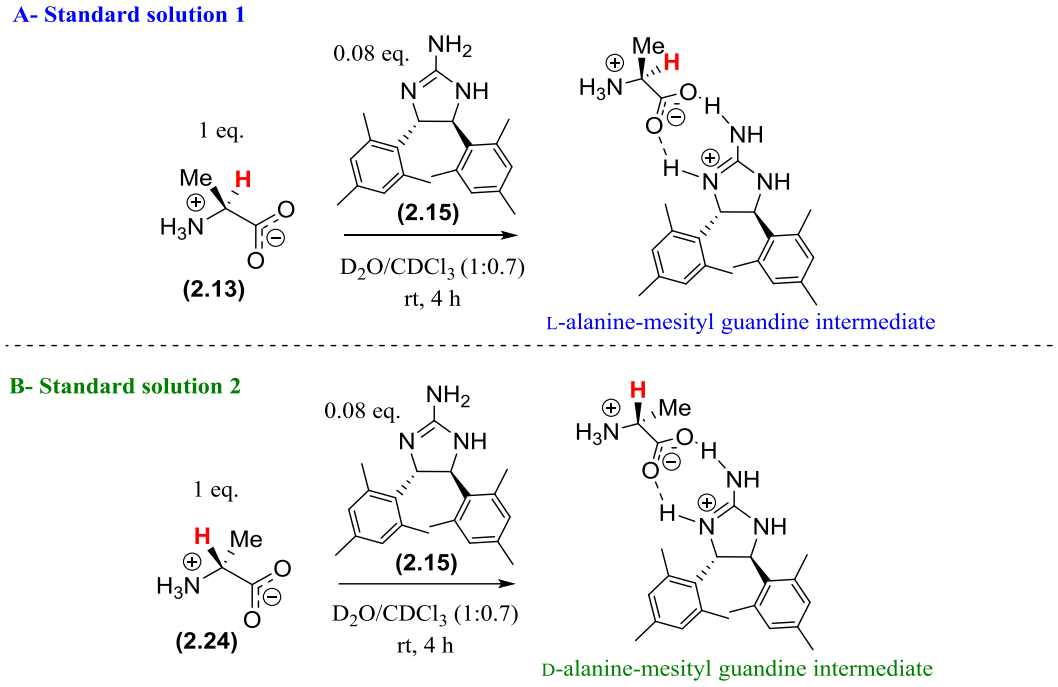

Figure 2.19: (**A**) Preparation of L-alanine and mesityl guanidine catalyst solution. (**B**) Preparation of D-alanine and mesityl guanidine catalyst solution.

The preparation of these standards involved stirring a D_2O solution of enantiopure (L-alanine and D-alanine) separately with $CDCl_3$ solutions of mesityl guanidine (**2.15**) for 4 h then extracting the aqueous layers with fresh $CDCl_3$ solutions of the catalyst (**2.15**). A comparison of the ^1H NMR spectrum obtained from the reaction of L-alanine (**2.13**) with aryl aldehyde (**2.16**) and mesityl guanidine (**2.15**), was done with the ^1H NMR spectra of our two standards (Figure **2.20**).

The ^1H NMR spectra of our standards were complex, however it was observed that the ^1H NMR signals obtained from the reaction of L-alanine (**2.13**) with aryl aldehyde (**2.16**) and mesityl guanidine (**2.15**) (Figure **2.20**, B) have similarity to that attributed to the methyl group (1.09 ppm) of the enantiopure D-alanine (**2.24**) mixed with (*S*,*S*)-mesityl guanidine (**2.15**) (Figure **2.20**, C). This indicates the formation of deuterated D-alanine (**2.14**) in the reaction.

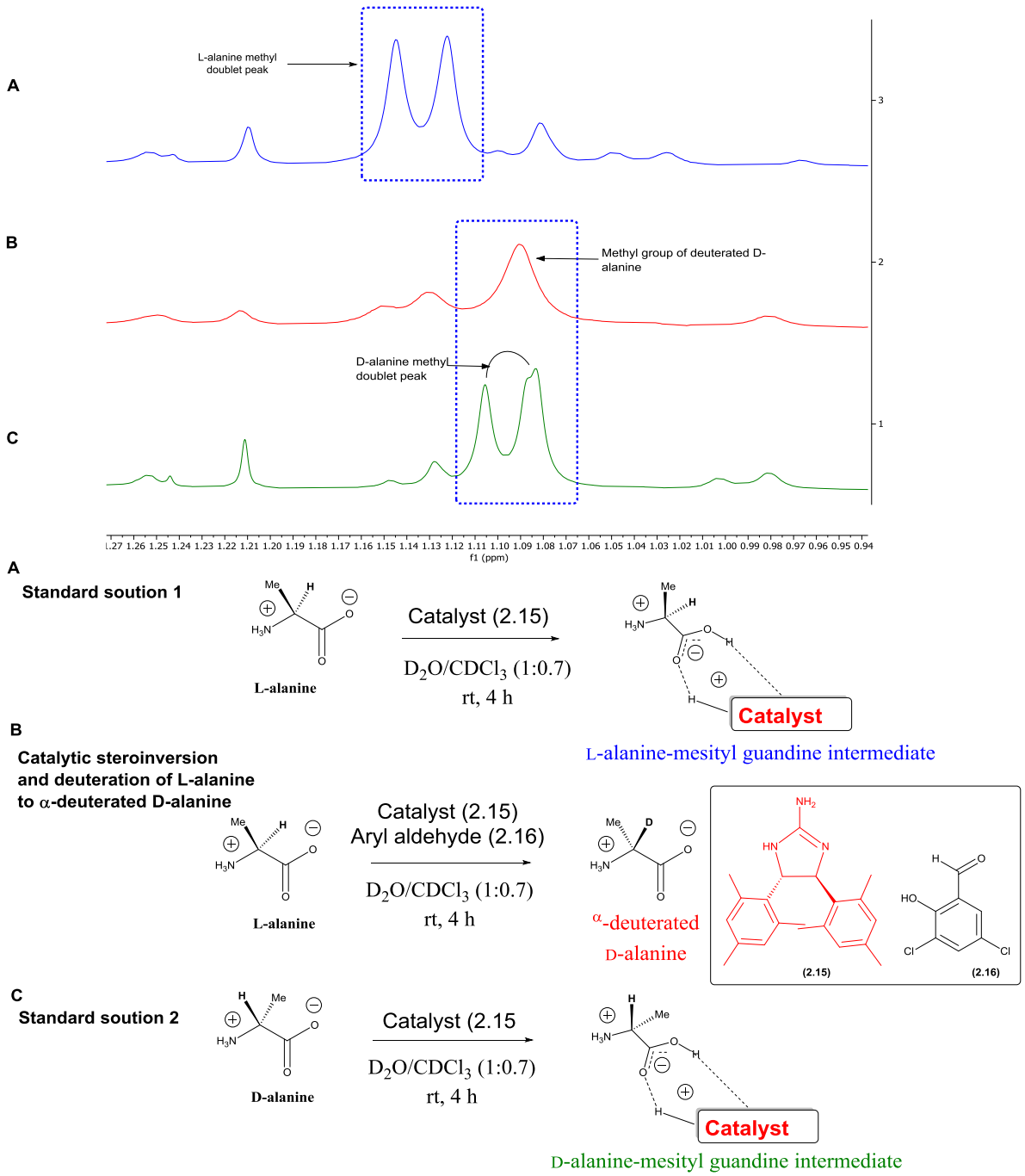

Figure 2.20: ^{1}H NMR spectra comparison between, (**B**) catalytic conversion and deuteration of L-alanine to D-alanine and two control reactions, (**A**) (L-ala + catalyst (**2.15**)) and (**C**) (D-ala + catalyst (**2.15**)).

Despite the potential for the formation of *α*-deuterated D-alanine (**2.14**), this test reaction gave a complex mixture of products which was not easy to interpret. As such, it was decided to move on to an alternative approach in which O'Donnell asymmetric phase

transfer catalysis method would be used to synthesise enantiopure D-photomethionine (**2.2**).

2.2.5 Towards the Synthesis of D-Photoactivatable Amino Acid via an Enantioselective Phase transfer Alkylation

In 1978, O'Donnell *et al*., first reported a racemic synthesis of both D and L α-amino acids via a key catalytic phase transfer alkylation of a prochiral glycine imine ester (**2.25**) (Figure **2.21**, **A**). This racemic route was then further developed by the same research group to an enantioselective route through replacing the achiral phase transfer reagent (TBAH) to chiral phase transfer catalyst (**2.26**) derived from cinchona alkaloids. O'Donnell enantioselective methodology to access D or L α- amino acids in a high level of enantiomeric excess starts with an enantioselective phase transfer alkylation at the α-position of glycine imine ester (**2.29**) with alkyl or allyl halide (R-X) in the presence of cinchona alkaloid derivative (**2.26**) (chiral quaternary ammonium salt) as the phase transfer catalyst, to give the corresponding α-alkyl imino ester (**2.30**). Finally, α-alkyl imino ester (**2.30**) was converted to the corresponding D or L amino acids via an acid catalysed hydrolysis in 75-81 % yield and 66-48 % *ee* (Figure **2.21**, **B**)[11,12].

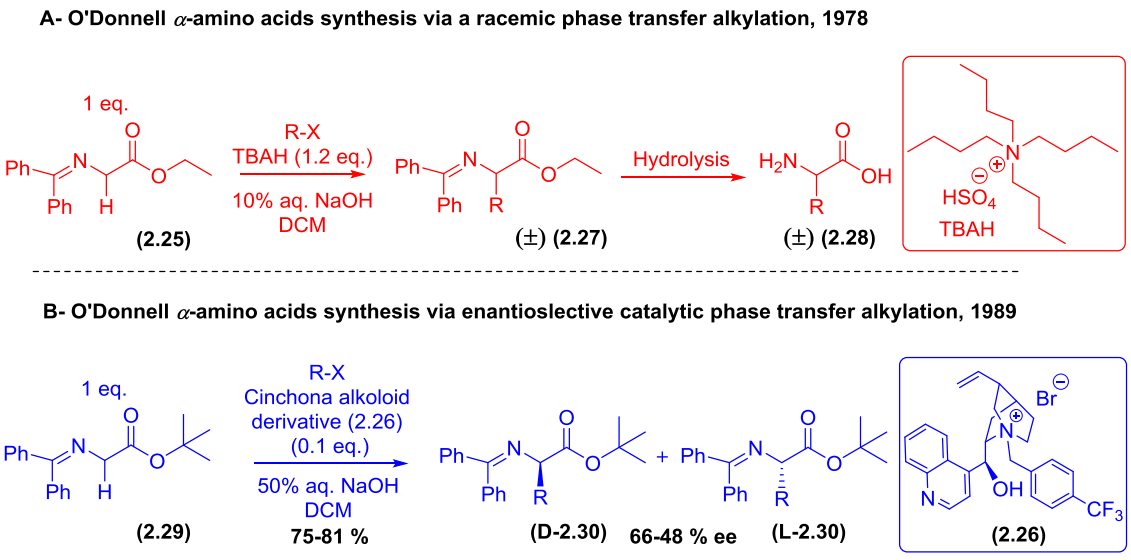

Figure 2.21: (**A**) O'Donnell's racemic synthesis of α-amino acids via phase transfer alkylation and, (**B**) O'Donnell's enantioselective synthesis of α-amino acids via catalytic phase transfer alkylation.

Therefore, the O'Donnell's enantioselective synthesis of D- and L-amino acids for the synthesis of our target D-photomethionine (**2.2**) would be adapted starting with commercially available glycine imine ester (**2.29**). In order to access D-photomethionine (**2.2**) first it was planned to introduce the required methionine side chain via an enantioselective phase transfer Michael-addition of a prochiral glycine imine ester (**2.29**) with methyl vinyl ketone (**2.31**) to give D-methionine imino ester (**2.32**). Finally, to incorporate the required diazirine functionality, the convertion of the imino group of D-methionine imino ester (**2.32**) to a more stable Boc-protected adduct (**2.34**) was decided upon, followed by diazirine formation chemistry described in our first route (aminolysis and oxidation of the ketone) and a subsequent hydrolysis to give our target D-photomethionine (**2.2**) (Figure **2.22**).[11-15]

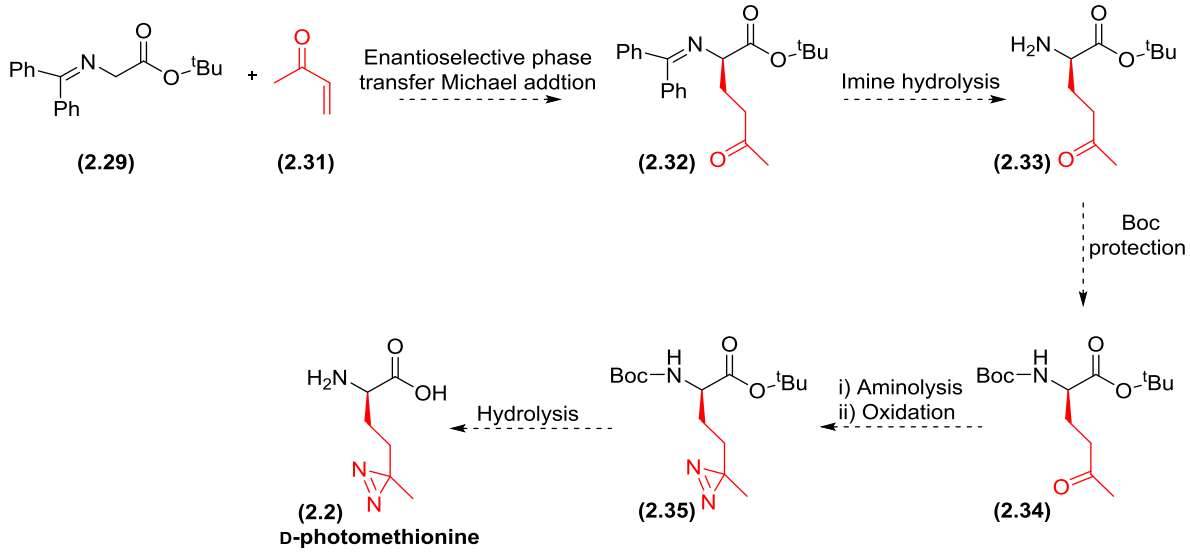

Figure 2.22: Planned asymmetric synthesis of D-photomethionine (**2.2**).

2.2.5.1 Non-Enantioselective *α*-Alkylation of Glycine Imine Ester with Benzyl Bromide

In order to test O'Donnell's catalytic phase transfer synthesis of *α*-amino acids, a plan to examine a racemic *α*-alkylation of glycine imine ester (**2.29**) using simple electrophilic partner (**2.36**) (benzyl bromide) as a test system (Figure **2.23**) was created.

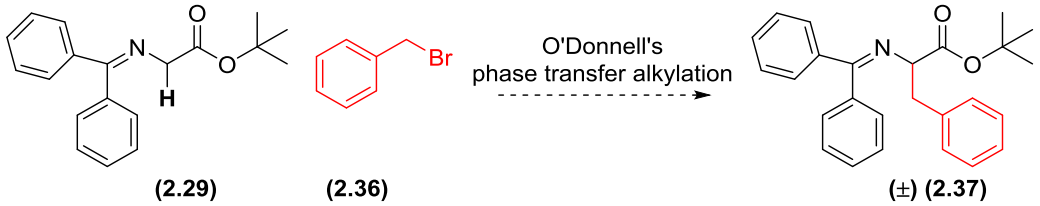

Figure 2.23: Planned *α*-alkylation of glycine imine ester (**2.29**) via O'Donnell's phase transfer alkylation.

Thus, glycine imine ester (**2.29**) was reacted with benzyl bromide (**2.36**) in a solution of DCM and NaOH $_{(aq)}$ in the presence of TBAI, as the phase transfer reagent, for 16 h at room temperature. Following an aqueous work-up and a subsequent column chromatography to give the desired *α*-benzyl imino ester (**2.37**) in 26 % yield, and 48 % recovered of the starting glycine imine ester (**2.29**) (Table **2.4**, entry **1**).

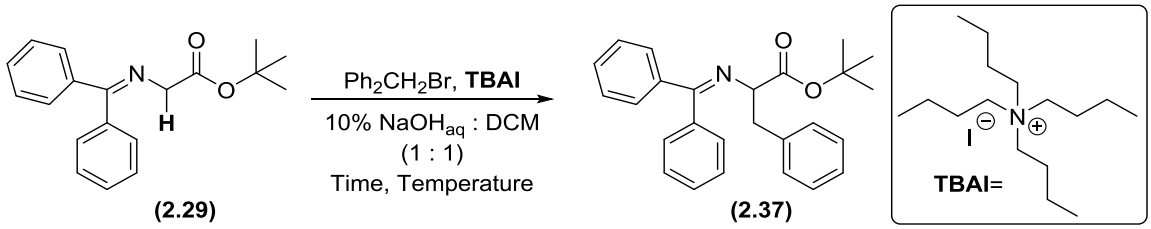

Entry	Temp. (C°)	Time (h)	Yield of (2.37) (%)
1	rt	16	26
2	30	48	63

Table 2.4: *α*-benzylation of glycine imine ester (2.29) via non-enantioselective phase transfer chemistry.

With a positive result on our initial *α*-benzylation of glycine imine ester (**2.29**) under non-enantioselective phase transfer conditions it was decided to improve our reaction productivity by increasing the reaction temperature and reaction time. Thus, repeating our

previous reaction at 30 °C with an extended reaction time (48 h), α-benzyl imino acid (**2.37**) was obtained with an improved isolated yield 63 % (Table **2.4**, entry **2**).

The ^{1}H NMR spectrum confirmed the structure of our α-benzyl imino ester (**2.37**) which showed two signals at 3.26 ppm (dd, *J* = 13.5, 4.5 Hz, 1H) and at 3.16 ppm (dd, *J* = 13.5, 9.0 Hz, 1H) corresponding to a pair of diastereotopic protons at the benzylic position. In addition, a key signal was observed at 4.11 ppm (dd, *J* = 9.0, 4.5 Hz, 1H) corresponding to the α-proton. Therefore, this data confirmed the presence of a new benzyl group at the α-position.

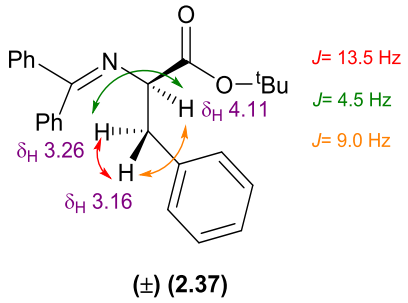

Figure 2 24: ^{1}H-^{1}H coupling analysis of α-benzyl imino ester (**2.37**).

With a satisfactory result from the non-enantioselective α-alkylation of glycine imine ester (**2.29**) with benzyl bromide, I decided to test the incorporation of the required methionine side chain carbon backbone to our starting glycine imine ester (**2.29**).

2.2.5.2 Non-Enantioselective α-Alkylation of Glycine Imine Ester with Methyl Vinyl Ketone (MVK)

In the next step, the plan to test the incorporation of the methionine side chain to the α-position of the prochiral glycine imine ester (**2.29**) was put in place via a non-enantioselective phase transfer Michael-addition with MVK (**2.31**) (Figure **2.25**).

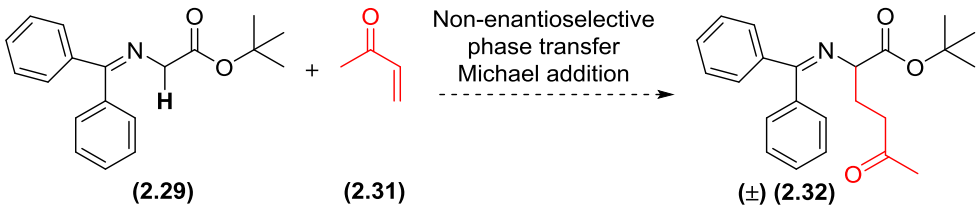

Figure 2.25: Planned non-enantioselective Michael addition of glycine imine ester (**2.29**) to methyl vinyl ketone (**2.31**) via O'Donnell's phase transfer alkylation.

Therefore, glycine imine ester (**2.29**) was stirred with methyl vinyl ketone (**2.31**) and the phase transfer reagent (TBAI) in a solution of DCM and $NaOH_{(aq)}$, for 16 h at room temperature. Following separation of the aqueous layer, the organic layer was then worked up and evaporated under reduced pressure to remove solvent (Figure **2.26**).

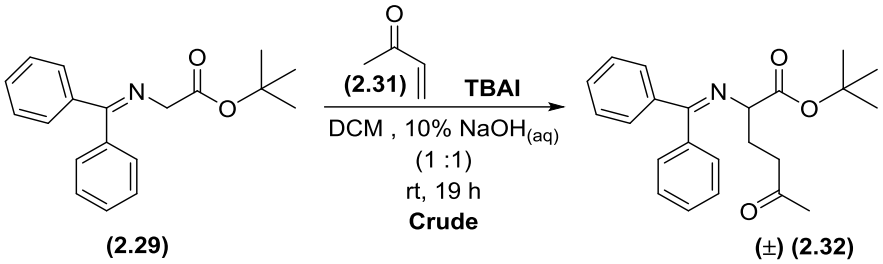

Figure 2.26: Racemic synthesis of methionine imino ester (**2.32**) via phase transfer α-alkylation of glycine imine ester (**2.29**) with methyl vinyl ketone (**2.31**).

TLC analysis of the crude reaction mixture against starting material (**2.29**), showed three active spots under UV, the first one with R*f* = 0.68 corresponding to starting material (**2.29**). In addition, another two spots with R*f* = 0.31 and R*f* = 0.37 possibly corresponds to the desired racemic methionine imino ester (**2.32**) and an unknown by product. As the two products with R*f* = 0.31 and R*f* = 0.37 have very similar retention time, it can be concluded that they will be difficult to separate and due to the concerns of undesired hydrolysis of racemic methionine imino ester (**2.32**) through silica gel, no further purification would be done.

The ^{1}H NMR spectroscopic analysis of the crude reaction mixture gave us confidence that racemic methionine imino ester (**2.32**) was formed, as it showed one singlet at 2.12 ppm corresponds to three protons of the methyl group of the ketone, and a key triplet signal at 3.99 ppm (*J* = 6 Hz, 1H) corresponding to the *α*-proton. In addition, there was an observation of a set of signals at 2.52 ppm (q, *J* = 7.4 Hz, 2H) and 2.12-2.17 ppm (m, 2H) (overlapping with the methyl protons) corresponding to two sets of methylene protons at C-3 and C-4 positions respectively (Figure **2.27**).

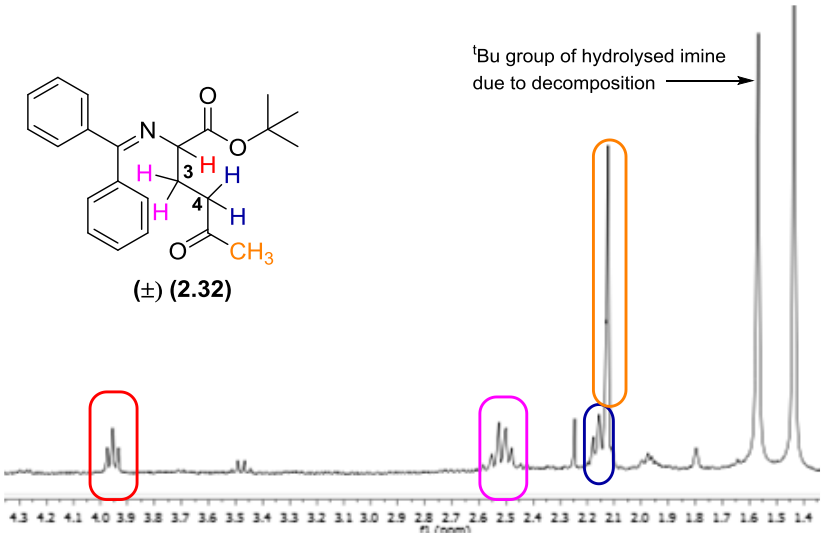

Figure 2.27: Expansion of ^{1}H NMR spectrum of compound (**2.32**).

In conclusion, it can be confirmed that the prochiral imine glycine ester (**2.29**) can succssfully *α*-alkylated with benzyl bromide and methyl vinyl ketone respectively using O'Donnell non-enantioselective phase transfer catalysis.

In our next step it was proposed that the synthesis of enantiopure D- photomethionine (**2.2**) via enantioselective Michael addition chemistry mediated by chiral phase transfer catalyst would be investigated.

2.2.5.3 Catalytic Enantioselective Michael Addition by Phase Transfer Catalyst towards D-Photomethionine (2.2)

In order to examine the enantioselective *α*-alkylation of glycine imine ester (**2.29**) with methyl vinyl ketone (**2.31**) via an enantioselective phase transfer Michael addition towards our target D-photomethionine (**2.2**), I planned to use chiral phase transfer catalyst derived from cinchona alkaloids to mediate our proposed reaction. Furthermore, Lygo *et al*., has reported that use of inorganic solid base (Cs_2CO_3) in enantioselective *α*-alkylation of glycine imine esters had dramatically enhanced the enantioselectivity of reaction. Therefore, the aqueous NaOH base will be replaced with Cs_2CO_3 solid base to minimise water in our reaction media and to improve the enantioselectivity (Figure **2.28**).[16,14]

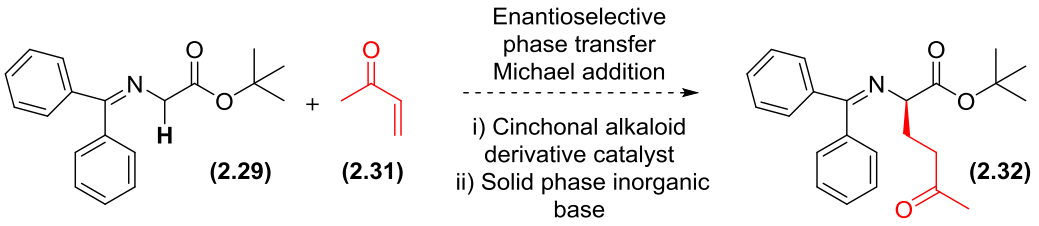

Figure 2.28: Planned enantioselective phase transfer Michael addition towards D-photomethionine (**2.2**).

Thus, a mixture of glycine imine ester (**2.29**) (1 eq.), Cs_2CO_3 (5 eq.), and organocatalyst (**2.38**) (2 mol %) was reacted with methyl vinyl ketone (**2.31**) (2 eq.) in dry DCM for 3 h at -20 °C, in an atmosphere of nitrogen. The reaction mixture was then warmed up and stirred at room temperature for 19 h. Following an aqueous work-up, the anticipated enantioenriched D-methionine imino ester (**2.32**) was afforded in 93 % yield with no further purification required (Figure **2.29**).

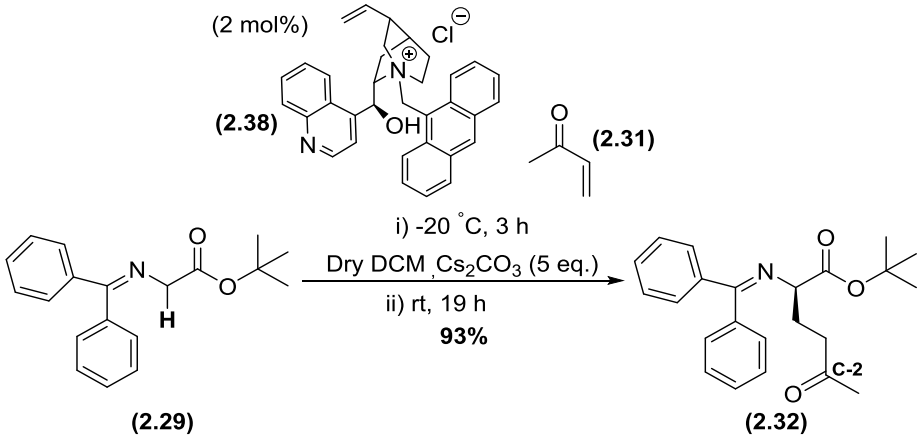

Figure 2.29: Synthesis of D-methionine imino ester (**2.32**) via enantioselective phase transfer Michael addition with cinchona alkaloid derivative (**2.38**).

The structure of D-methionine imino ester (**2.32**) was confirmed by both ^{1}H NMR spectroscopy, which was consistent to the previously isolated racemic methionine imino ester (± **2.32**), and ^{13}C NMR spectroscopy, which showed a key signal at 208.3 ppm corresponding to the ketone carbon atom at C2.

Pleasingly with desired D-methionine imino ester (**2.32**) in hand it could be confidently used in the next selective imine hydrolysis step.

2.2.5.4 Selective Imine Hydrolysis of D-Methionine Imino Ester (2.32)

To access the structure of our target molecule (**2.2**) (D-photomethionine), it was anticipated that the imine protection group at D-methionine imino ester (**2.32**) will require to be replaced with a more stable amine protection group such as Boc group. A Boc protection group is expected to tolerate the subsequent aminolysis and oxidation conditions to convert the resulted D-methionine Boc-amino ester (**2.34**) to D-photomethionine Boc-amino ester (**2.35**), moreover, the Boc group could be removed readily when necessary (Figure **2.30**).

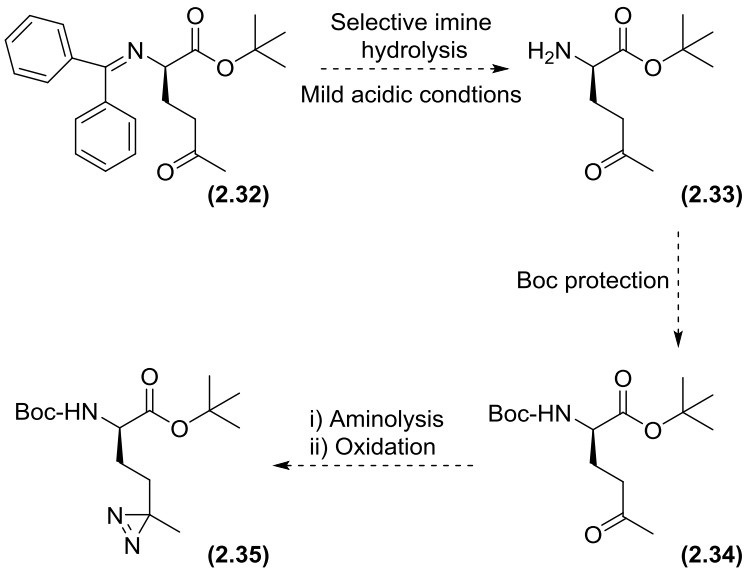

Figure 2.30: Selective imine hydrolysis plan of D-methionine imino ester (**2.32**) followed by Boc protection of D-methionine amino ester (**2.33**) and subsequent aminolysis and oxidation.

Thus, D-methionine imino ester (**2.32**) was hydrolysed in a solution of THF and aqueous citric acid (15 %) at room temperature for 16 h. Following work-up and extraction into CH_2Cl_2, the desired D-methionine amino ester (**2.33**) was isolated in 36 % yield with no further purification required (Figure **2.31**).

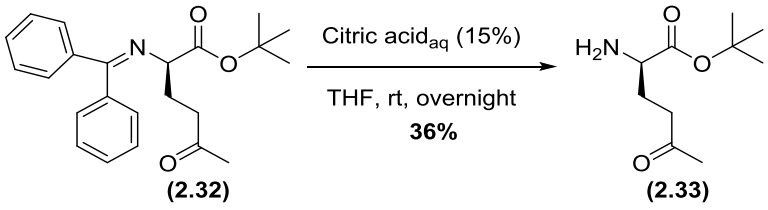

Figure 2.31: Selective imine hydrolysis of D-methionine imino ester (**2.32**).

The structure of D-methionine amino ester (**2.33**) was confirmed by ^{1}H NMR spectroscopy which showed the disappearance of the starting material (**2.32**) diphenyl protons signals at 7.68 – 7.59 ppm (m, 2H), 7.49 – 7.28 ppm (m, 6H), and 7.21 – 7.12 ppm (m, 2H). An additional coupling could be observed between the α-proton and the adjacent amine protons which appeared as a multiplets at 4.50-4.57 ppm (m, 1H) (Figure **2.32**).

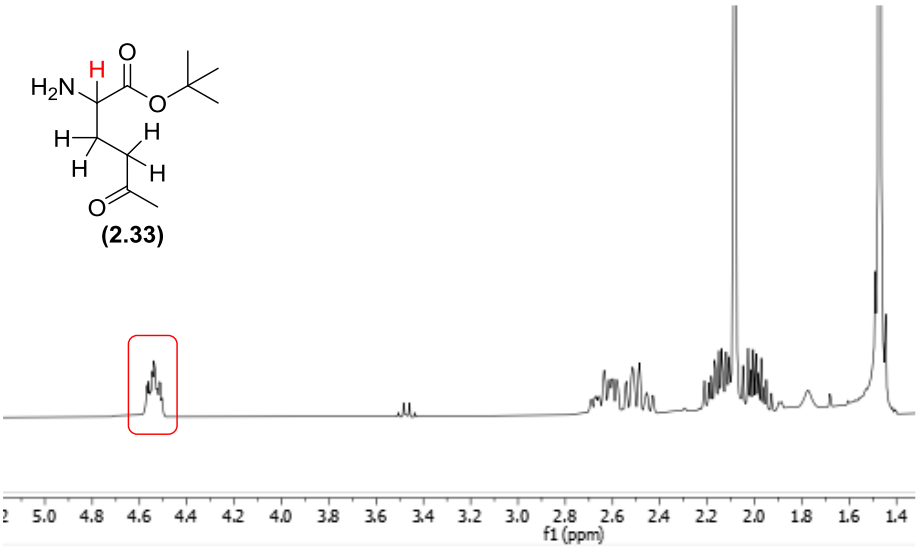

Figure 2.32: Expansion of the ^{1}H NMR spectrum of D-methionine amino ester (**2.33**).

After a successful selective imine hydrolysis of D-methionine imine ester (**2.32**), I planned to incorporate a Boc protection to our new amino group.

2.2.5.5 Boc Protection of D-Methionine Amino Ester (2.33)

Our next step was protecting the amine moiety of D-methionine amino ester (**2.33**) with a Boc protection group.

Thus, a THF solution of D-methionine amino ester (**2.33**) was treated with Boc anhydride under basic conditions at room temperature for 48 h. Following an extraction into ethyl acetate and subsequent column chromatography purification the desired D-methionine Boc-amino ester (**2.34**) was isolated in a 19 % yield (Figure **2.33**).

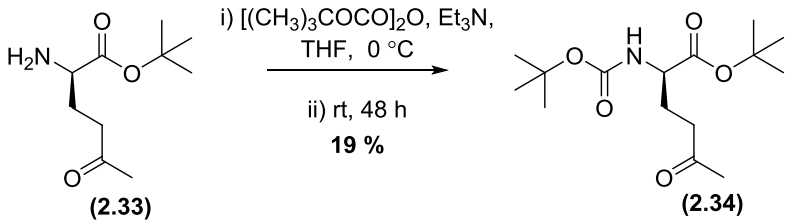

Figure 2.33: Boc protection of D-methionine amino ester (**2.3**) with Boc-anhydride.

The structure of our isolated Boc-protected product (**2.34**) was confirmed by ^{1}H NMR spectroscopy as the spectrum showed a key broad signal at 5.05 ppm (d, *J*= 7.0 Hz, 1H) corresponding to the amide proton, it also showed set of signals at 1.44 ppm (s, 9H) and 1.46 ppm (s, 9H) corresponding to the two tertiary butyl groups of the desired D-methionine Boc-amino ester (**2.34**). Furthermore, in the HRMS, *m/z* for D-methionine Boc-amino ester (**2.34**) ($C_{15}H_{27}NO_5$) showed 324.1781 which is fit with $C_{15}H_{27}NO_5Na$ and indicating that the desired molecule had been generated (**2.34**).

In summary, there has been a significant progress towards our target D-photomethionine (**2.2**) by using enantioselective phase transfer catalysis to achieve a successful alkylation of glycine imine ester (**2.29**) which gave 93 % yield of D-methionine imino ester (**2.32**). The unstable imino ester (**2.32**) was successfully converted to the amino ester (**2.33**) which is more stable and protected the resulted amine with a Boc group. However, due to the time constraint and the limited amount of starting material (**2.34**) in our hand, I have been unable to continue to the next aminolysis and then hydrolysis steps (Figure **2.34**).

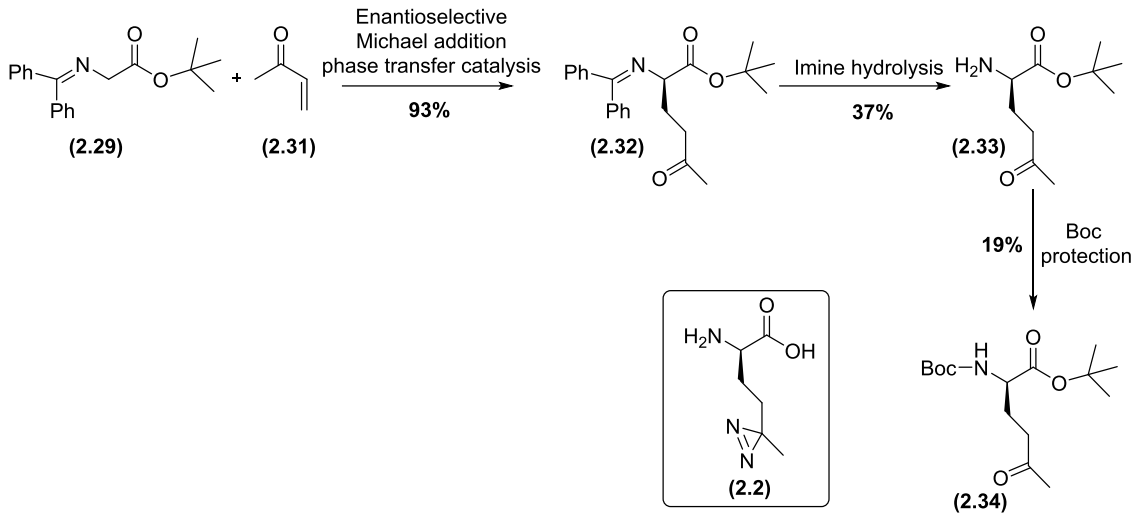

Figure 2.34: Enantioselective phase transfer catalysis route to synthesise D-photomethionine (**2.2**).

2.3 Conclusion and Future Work

In this chapter, I aimed to synthesise D-photoleucine (**2.1**) and D-photomethionine (**2.2**) which containing a photoactivatable group (diazirine) on their sidechains, these synthetic D-amino acids are structural analogues to the naturally occurring D-leucine (**2.3**) and D-methionine (**2.4**).

After investigating a number of synthetic strategies to access the molecular structure of both D-photoleucine (**2.1**) and D-photomethionine (**2.2**) our most successful approach to synthesise our desired D-photomethionine (**2.2**) was the enantioselective phase transfer catalysis. In this approach I have achieved a key enantioselective methionine side chain incorporation to the α-position of prochiral glycine imine ester (**2.29**) via asymmetrical Michael addition catalysed by cinchona derivative phase transfer catalyst at which the key intermediate (**2.32**) (D-methionine imino ester) was afforded in 93 % yield. However, starting our route with prochiral substrate might lead to low conversion to our desired D-enantiomer with high probability to form significant amount of the undesired L-methionine. Therefore, I decided to change our research focus and look on the synthesis of more promising photoactivatable fluorescent D-amino acid. Furthermore, to overcome the previous chirality issues an enantiopure D-amino acid can be used and its side chain can be functionalised with our proposed photoactivatable and fluorescent functionalities.

2.4 References

1- R. Church, and M. Weiss, *J. Org. Chem*., 1970, **35**, 2465-2471.

2- A. Mackinnon, L. Garrison, R. Hegde, and J. Taunton, *J. Am. Chem. Soc*., 2007, **129**, 14560-14561.

3- Y. Ikeda and E. Behrman, *Synth. Commun*., 2008, **38**, 2276–2284.

4- M. Suchanek, A. Radzikowska and C. Thiel, *Nat. Meth*., 2005, **2**, 261-268.

5- M. Al-Omari, K. Banert, and M. Hagedorn, *Chem. Int. Ed*., 2006, **45**, 309-311.

6- L. Wang, Z. Tachrim, N. Kurokawa, F. Ohashi, Y. Sakihama, Y. Hashidoko, M. Hashimoto, *Molecules*, 2017, **22**, 1389.

7- L. Zhang, J. Duan, Y. Xu, and W. Dolbier, *Tetrahedron lett*., 1998, **39**, 9621-9622.

8- D. Harpp, L. Bao, C. Black, J. Gleason, and R. Smith, *J. Org. Chem*., 1975, **40**, 3420-3427.

9- K. Moozeh, S. So, and J. Chin, *Angew. Chem., Int. Ed*., 2015, **127**, 9513-9517

10- R. Gora, M. Majza and S. Grabowski, *Chem. Phys*., 2013, **15**, 2514.

11- M. O'Donnell, J. Boniece and S. Earp, *Tetrahedron Lett*., 1978, **30**, 2641-2644.

12- M. O'Donnell; W. Bennett, and S. Wu, *J. Am. Chem. Soc*., 1989, **111**, 2353-2355.

13- E. Corey, F. Xu and M. Noe, *J. Am. Chem. Soc*., 1997, **119**, 12414-12415.

14- T. Ma, X. Fu, C. Kee, L. Zong, Y.Pan, K. Huang and C. Tan, *J. Am. Chem. Soc*., 2011, **133**, 2828-2831.

15- B. Lygo, B. Allbutt and E. Kirton, *Tetrahedron Lett*., 2005, **46**, 4461-4464.

16- E. Corey, and M. Noe, *Org. Synth*., 2003, **80**, 38.

Chapter 3. Synthesis of Methoxy Coumarin Trifluoromethyl Diazirine D-Alanine (MCTDA)

3.1 Introduction

Following our previous work examining a number of synthetic strategies to prepare D-amino acids capable of photo-crosslinking, in this chapter I continue to discuss the design and the synthesis of photo-crosslinking D-amino acids that can be used as tools to probe the bacteria peptidoglycan in our search for novel proteins involved in peptidoglycan biosynthesis.

As discussed in Chapter 1, the group of VanNieuwenhze have previously demonstrated[1] that the fluorescent D-amino acid (**3.1**) (HADA) can be incorporated into bacterial PG, in live bacteria, via the native PG biosynthetic machinery. They have subsequently used these, and related, fluorescent D-amino acids to probe bacterial cell wall biosynthesis. In independent work, the group of Tamahero and Hatanaka have reported[2] the synthesis of diazirine carboxycoumarin (**3.2**), a photoactivatable coumarin derivative containing a diazirine ring. In their paper, a photoactivatable carboxycoumarin (**3.2**) was attached, via an amide bond, to the natural product geldanamycin and subsequently used in the photo-cross-linking of the Hsp90 protein, the target of geldanamycin. Photoactivation of coumarin (**3.2**) resulted in the formation of a carbene, through loss of N_2 from the diazirine ring, and subsequent covalent cross-linking to Hsp90.

Therefore, due to the structural similarity of VanNieuwenhze's fluorescent D-amino acid (**3.1**) (HADA) and Tomohero's photoactivatable coumarin (**3.2**), I hypothesised that a molecule containing Tomohero's photoactivatable coumarin (**3.2**) linked to a suitable D-amino acid (e.g. 3-amino-D-alanine (**3.6**)) might be capable of enzymatic incorporation into bacterial PG. Furthermore, subsequent photolysis would allow such a probe to cross-link to nearby enzymes, providing a tool to investigate the enzymes involved in bacterial cell wall biosynthesis (Figure **3.1**).

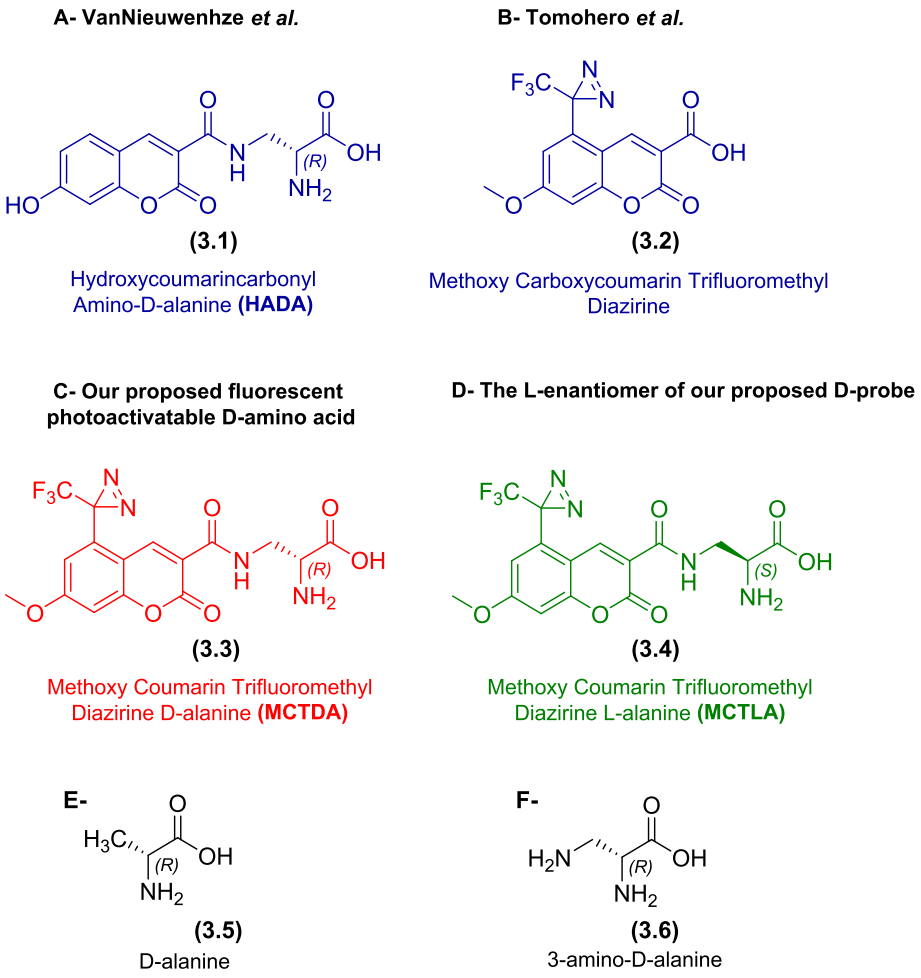

Figure 3.1: (**A**) Fluorescent D-amino acid HADA synthesised by VanNieuwenhze *et al.*, (**B**) photoactivatable coumarin synthesised by Tomohero *et al.*, (**C**) our proposed photoactivatable fluorescent D-amino acid (MCTDA **3.3**), (**D**) the L-enantiomer of MCTDA (MCTLA **3.4**), (**E**) D-alanine (**3.5**), (**F**) 3-amino-D-alanine (**3.6**).

Therefore, in this chapter the synthesis of methoxy-coumarin trifluoromethyl diazirine D-alanine (**3.3**) (MCTDA) will be discussed, consisting of a Tomohero-like fluorophore attached to D-amino acid (**3.6**) (3-amino-D-alanine). The enzymatic incorporation of MCTDA into bacterial PG will be examined, followed by UV irradiation to cross-link any nearby PG biosynthesis proteins (see Chapter 4). In this chapter the synthesis of methoxy-coumarin trifluoromethyl diazirine L-alanine (**3.4**) (MCTLA) will also be discussed, the corresponding L-enantiomer, as a negative control for later biological assays (Figure **3.1**).

3.1.1 Retrosynthetic Analysis of MCTDA

Our retrosynthetic analysis (Figure **3.2**) of our target molecule, MCTDA (**3.3**), begins with the disconnection of the amide bond, which can be formed via a conventional amide coupling between diazirine carboxycoumarin (**3.2**) and 3-amino-D-alanine (**3.6**). It was then planed to synthesise diazirine carboxycoumarin (**3.2**), following the work of Tomohero *et al.*,[2] by a Knoevenagel condensation and intramolecular ester formation between Meldrum's acid (**3.7**) (B ring) and C-5 hydroxy trifluoromethyl diazirine (**3.12**) (A ring). The formation of C-5 hydroxy trifluoromethyl diazirine (**3.12**) will require a selective *O*-demethylation, directed by the adjacent aldehyde. The formyl moiety of C-4 formyl trifluoromethyl diazirine (**3.11**) will be introduced via standard formylation approaches and the diazirine ring of compound (**3.10**) introduced from the corresponding ketone (**3.9**). Finally, a plan to prepare trifluoromethyl ketone (**3.9**) was proposed via the preparation of a suitable organometallic reagent and subsequent acylation.

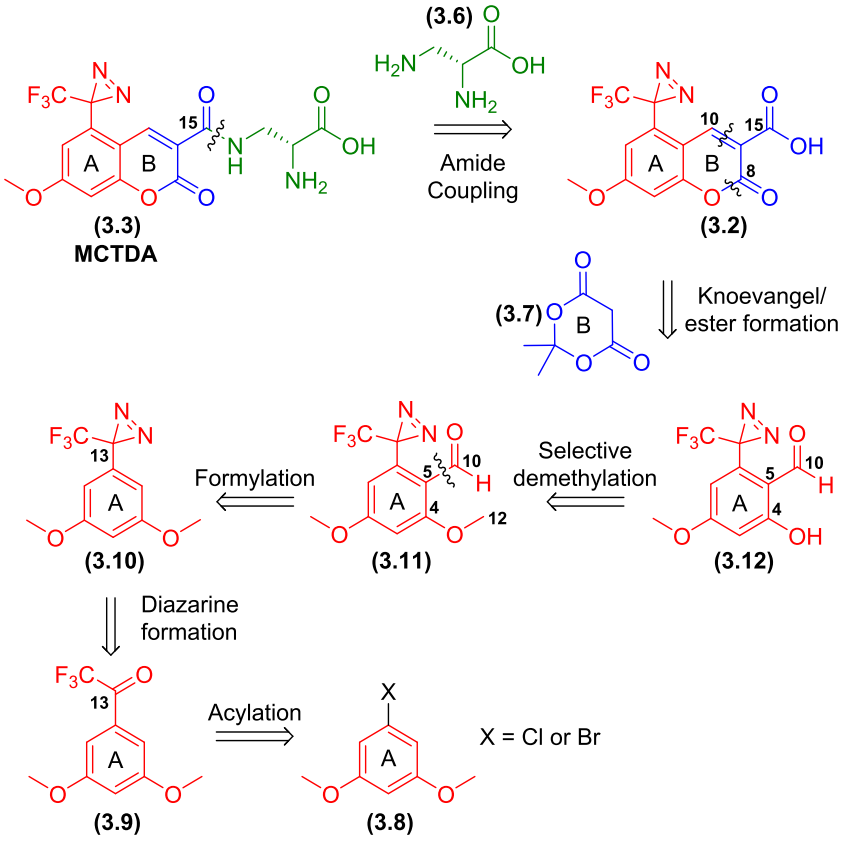

Figure 3.2: Proposed synthesis of MCTDA (**3.3**).

3.2 Results and Discussion

3.2.1 The Synthesis of Trifluoromethyl Ketone via Organometallic Chemistry

The first reaction was examining the preparation of trifluoromethyl ketone (**3.9**). Starting from the corresponding halogenated substrates a plan to convert these into suitable organometallic reagents and react them with appropriate acylating agents was devised.

3.2.1.1 Synthesis of Trifluoromethyl Ketone (3.9) through the Acylation of an Aryllithium

In our first attempted synthesis of the trifluoromethyl ketone (**3.9**), I planned to use a halogen-metal exchange reaction to form organolithium (**3.13**) followed by reaction with an amide (**3.14**) (Figure **3.3**).

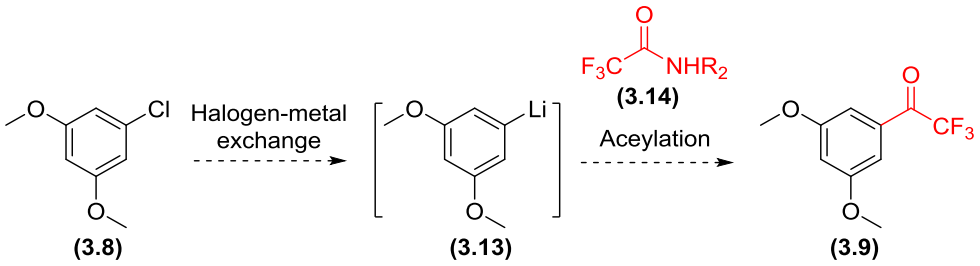

Figure 3.3: Halogen-metal exchange and amide reaction to give trifluoromethyl ketone (**3.9**).

Previous work by Saucier *et al.*,[3] has shown that bromopyridine (**3.15**) can undergo a halogen-metal exchange with *n*-BuLi to form lithiopyridine (**3.16**) *in situ*, followed by acylation with *N*,*N*-diethyl trifluoroacetamide (**3.17**), to incorporate a trifluoromethyl ketone moiety (**3.18**) (Figure **3.4**).

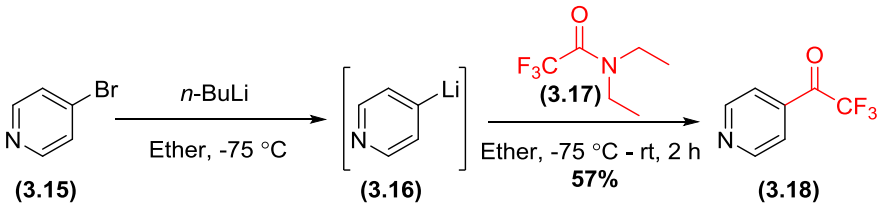

Figure 3.4: Saucier's synthesis of pyridyl trifluoromethyl ketone (**3.18**).

Thus, 1-chloro-3,5-dimethoxybenzene (**3.8**) was treated with 1 eq. *n*-BuLi at -78 °C for 30 h, followed by addition of 2 eq. trifluoromethyl amide (**3.14**) and further reaction at 0 °C for 2 h. Following work-up, ^{1}H NMR spectroscopic analysis of the crude reaction material showed the presence both unreacted 1-chloro-3,5-dimethoxybenzene (**3.8**) and trifluoromethyl amide (**3.14**), alongside a number of minor products. However, following column chromatography none of the desired trifluoromethyl ketone (**3.9**) was observed (Table **3.1**, entry **1**).

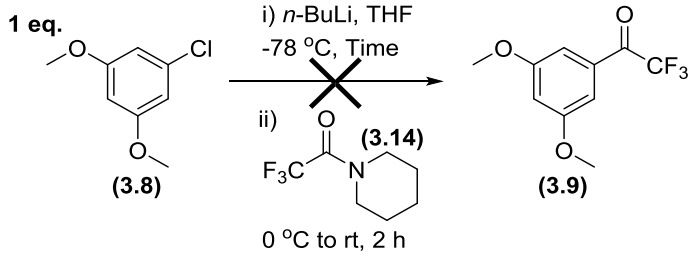

Entry	*n*-BuLi 1.6M in hexane (eq.)	Amide (3.14) (eq.)	Step (i) reaction time	Reaction outcome (as determined by ^{1}H NMR spectroscopic analysis)
1	1	2	30 min	Mainly unreacted starting materials
2	1.2	1	1 h	Mainly unreacted starting materials
3	1.5	1	1 h	Mainly unreacted starting materials

Table 3.1: Attempted halogen-metal exchange of 1-chloro-3,5-dimethoxybenzene (**3.8**) and reaction with trifluoromethyl amide (**3.14**).

The observation of unreacted 1-chloro-3,5-dimethoxybenzene (**3.8**) in the crude product suggested that the desired halogen-metal exchange reaction had not gone to completion under these conditions. Next, the reaction with 1.2 eq of *n*-BuLi equivalents was repeated and the time extended for the halogen-metal exchange to 1 h. However, the desired product was again not observed following work-up and purification (Table **3.1**, entry **2**). Further attempts to increase the equivalents of *n*-BuLi to 1.5 eq. also did not give access to our desired product (Table **3.1**, entry **3**). Thus, I decided to examine an alternative route.

3.2.1.2 Synthesis of Trifluoromethyl Ketone (3.9) via Acylation of an Organomagnesium

Next, an examination into an alternative approach towards our target trifluoromethyl ketone (**3.9**) was proposed. Based on the work of Tomohero *et al.*, we a plan was put in place to convert 1-chloro-3,5-dimethoxybenzene (**3.8**) to the corresponding organomagnesium reagent (**3.19**), followed by reaction with trifluoromethyl amide (**3.14**).

Therefore, in our first attempt 1-chloro-3,5-dimethoxybenzene (**3.8**) was refluxed overnight in dry THF in the presence of magnesium turnings (1.1 eq.) and 1,2-dibromoethane (0.2 eq.) as an initiator. The resulting reaction mixture was cooled to -20 ^{o}C, followed by the addition of a THF solution of trifluoromethyl amide (**3.14**) (1 eq.) and was allowed to warm to rt over 2 h. Following aqueous work-up, ^{1}H NMR spectroscopic analysis of the crude reaction mixture showed only the presence of unreacted 1-chloro-3,5-dimethoxybenzene (**3.8**) and the starting amide (**3.14**) (Table **3.2**, entry **1**).

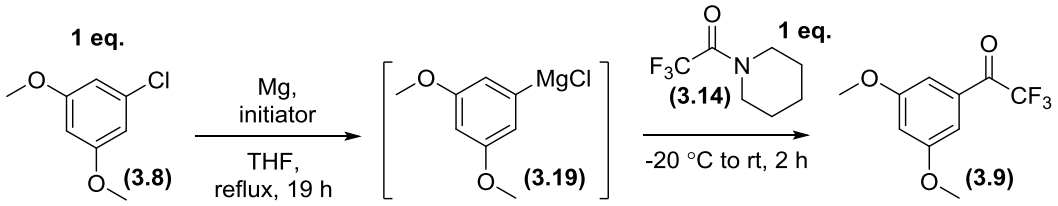

Entry	Mg (eq.)	Initiator	Initiator (eq.)	Reaction outcome (as determined by ^{1}H NMR spectroscopic analysis)
1	1.1	$BrCH_2CH_2Br$	1 drop	Unreacted arylchloride (**3.8**) and amide (**3.14**)
2	1.5	$BrCH_2CH_2Br$	0.2	Unreacted arylchloride (**3.8**) and amide (**3.14**)
3	1.1	I_2	Few crystals	Unreacted arylchloride (**3.8**) and amide (**3.14**)
4	1.5	I_2	Few crystals	Unreacted arylchloride (**3.8**) and amide (**3.14**)

Table 3.2: Attempted synthesis of trifluoromethyl ketone (**3.9**) via Grignard formation from arylchloride (**3.8**).

Increasing the number of equivalents of magnesium, had no impact on the reaction with starting materials observed unchanged. Changing the initiator to iodine, in an attempt to improve the activity of the magnesium, still resulted in no products being obtained (Table **3.2**, entries **2-4**).

Due to the lack of reactivity of 1-chloro-3,5-dimethoxybenzene (**3.8**), I next examined 1-bromo-3,5-dimethoxybenzene (**3.20**) as a starting material for the preparation of the desired intermediate Grignard reagent. Thus, magnesium turnings (1.1 eq.) were activated with 1,2-dibromoethane (0.2 eq.) in refluxing THF for 1 h, followed by the addition of 2.5 mmol of arylbromide (**3.20**), and the reaction was then refluxed overnight. The resulting reaction mixture was cooled to -20 ^{o}C, followed by the addition of a THF solution of 2.5 mmol trifluoromethyl amide (**3.14**) (1 eq.) and the reaction was allowed to warm to rt over 2 h. After acidic work-up, ^{1}H NMR spectroscopic analysis of the crude material showed the presence of both starting materials, arylbromide (**3.20**) and amide (**3.14**), alongside three aromatic by-products (**3.21**), (**3.22**), and (**3.23**) (Figure **3.7**). Through relative integration of their methoxy groups, it was determined that in comparison to arylbromide (**3.20**), the by-products had been formed in a 30:1:10:3 ratio. Unfortunately, after column chromatography neither the desired trifluoromethyl ketone (**3.9**) or the other aromatic by-products (**3.21**), (**3.22**), or (**3.23**) could be isolated (Figure **3.5**; Table **3.3**, entry **1**).

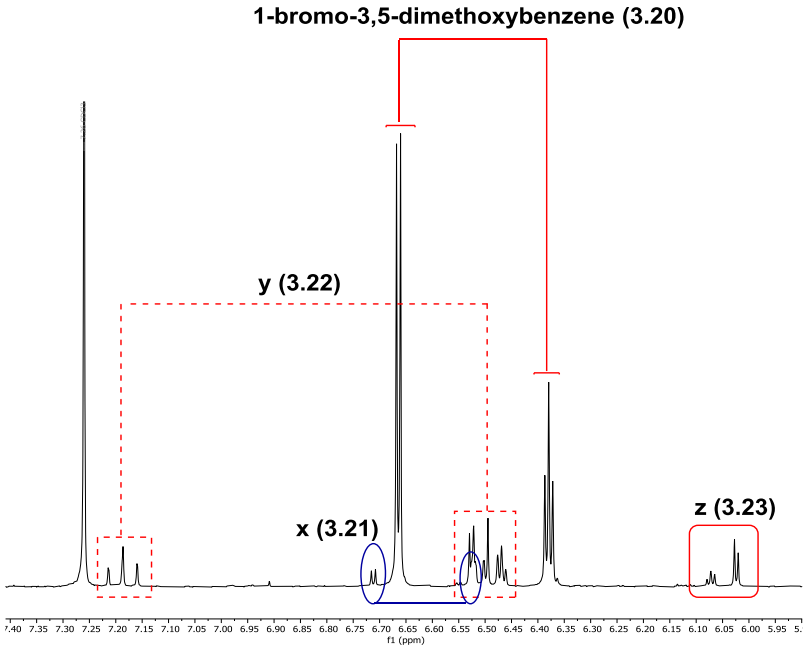

Figure 3.5: Partial ^{1}H NMR spectrum of crude reaction mixture, following attempted Grignard formation from arylbromide (**3.20**) and trapping with trifluoromethyl amide (**3.14**).

In an attempt to identify the by-products (**3.21**), (**3.22**), and (**3.23**), the previous reaction between arylbromide (**3.20**) and trifluoromethyl amide (**3.14**) was repeated on a 7.5 mmol scale. Again, ^{1}H NMR spectroscopic analysis of the crude reaction mixture showed

the formation of three aromatic by-products (**3.21**), (**3.22**), and (**3.23**) with a ratio of 1: 6 : 2 (recpectivly), to 1 (aryl bromide) based on relative integration of their methoxy groups. Despite the considerable increase in the formation of aromatic by-products (**3.21**), (**3.22**), and (**3.23**), none of the desired trifluoromethyl ketone (**3.9**) was observed (Table **3.3**, entry **2**).

In our next reaction, it was decided to increase the equivalents of Mg present to assist the formation of the intermediate Grignard reagent. Therefore, aryl bromide (**3.20**), 1,2-dibromoethane, and Mg (1.5 eq.) were stirred in refluxing THF overnight. As previously, the reaction was cooled to -20 °C, a THF solution of trifluoromethyl amide (**3.14**) was added, and the reaction mixture left to warm-up to rt over 2 h. ^{1}H NMR spectroscopic analysis of crude reaction mixture, showed the loss of aryl bromide (**3.20**) and the presence of trifluoromethyl amide (**3.14**). Again, none of the desired trifluoromethyl ketone (**3.9**) was identified, however two main aromatic by-products (**3.22**) and (**3.23**) were observed in a 2 : 1 ratio (Table **3.3**, entry **3**). Whilst repeating this reaction with activation of the Mg turnings with 1,2-dibromoethane in refluxing THF for 1h, gave similar results with (**3.22**) and (**3.23**) observed in a 2 : 1 ratio (Table **3.3**, entry **4**). Finally, scale up of the previous reaction to 7.5 mmol, gave very similar results with the three aromatic unidentifiable products (**3.21**), (**3.22**), and (**3.23**), present in a 1: 12: 5 ratio based on relative integration of their methoxy groups (Table **3.3**, entry **6**).

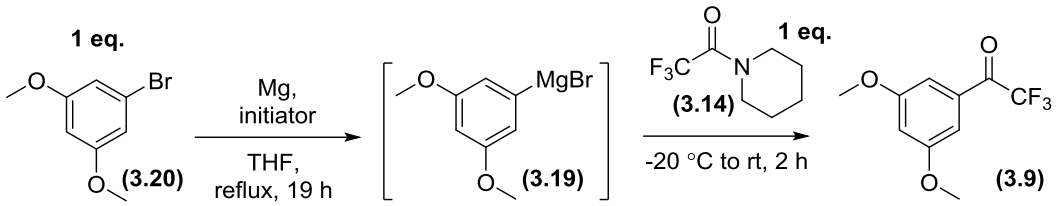

Entry	Mg (eq.)	Initiator	Initiator (eq.)	Notes	Reaction outcome[a]
1	1.1	$BrCH_2CH_2Br$	0.2	2.5 mmol scale Mg activated by 1h reflux with initiator	Unreacted aryl bromide (3.20) and by-products (3.21), (3.22) and (3.23) observed (30:10:3:1)
2	1.1	$BrCH_2CH_2Br$	0.2	7.5 mmol scale Mg activated by 1h reflux with initiator	Unreacted aryl bromide (3.20) and by-products (3.21), (3.22) and (3.23) observed (1:1:6:2)
3	1.5	$BrCH_2CH_2Br$	0.2	2.5 mmol scale	No aryl bromide observed, by-products (3.22) and (3.23) present (2:1)
4	1.5	$BrCH_2CH_2Br$	0.2	2.5 mmol scale Mg activated by 1h reflux with initiator	No aryl bromide observed, by-products (3.22) and (3.23) present (2:1)
6	1.5	$BrCH_2CH_2Br$	0.2	7.5 mmol scale Mg activated by 1h reflux with initiator	No aryl bromide observed, by-products (3.21), (3.22) and (3.23) present (1:12:5)

Table 3.3: Attempted synthesis of trifluoromethyl ketone (**3.9**) via Grignard formation from arylbromide (**3.20**). [**a**] ratio based on ^{1}HNMR integration.

Despite a number of attempts, our efforts to synthesise trifluoromethyl ketone (**3.9**) via the formation of a Grignard reagent from 1-bromo-3,5-dimethoxybenzene (**3.20**) and

subsequent trapping with trifluoromethyl amide (**3.14**) have not proven successful. Under our reaction conditions, it appears that the oxidative insertion of magnesium into 1-bromo-3,5-dimethoxybenzene (**3.20**) to form the corresponding Grignard reagent had occurred, however, no reaction with trifluoromethyl amide (**3.14**) was observed. Instead of the desired reaction, a number of as yet unidentifiable products (**3.21**, **3.22** and **3.23**) were observed, therefore in order to gain further understanding of the reaction it was decided to investigate the Grignard formation with 1-bromo-3,5-dimethoxybenzene (**3.20**) in more detail.

3.2.1.3 Deuteration of 1-bromo-3,5-dimethoxybenzene via Grignard Chemistry

In order to identify the by-products (**3.21**, **3.22** and **3.23**) and elucidate the pathways of their formation during our recent Grignard chemistry between arylbromide (**3.20**) and trifluoromethyl amide (**3.14**), a plan to test the oxidative insertion between magnesium metal and 1-bromo-3,5-dimethoxybenzene (**3.20**) was created via the deuteration of the magnesium 3,5-dimethoxybenzene intermediate (**3.19**) *in situ* with D_2O (Figure **3.6**).

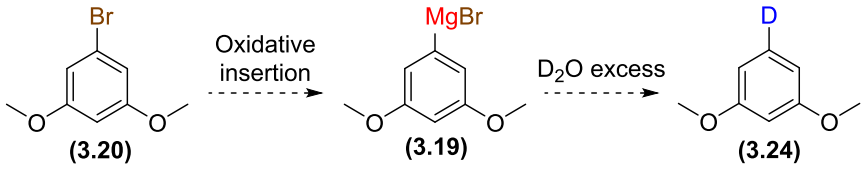

Figure 3.6: Planned test reaction for the deuterium trapping of the Grignard reagent formed from 1-bromo-3,5-dimethoxybenzene (**3.20**).

Thus, following our previous approach, 1-bromo-3,5-dimethoxybenzene (**3.20**) (1 eq.) was reacted magnesium metal (1.5 eq.) in refluxing THF for 19 h, in presence of catalytic amount of dibromoethane. The reaction mixture was then cooled to -20 °C, followed by the addition of a mixture of dry THF and D_2O, after which the resulting reaction mixture was allowed to warm up to rt over 2 h. Following workup, the ^1H NMR spectroscopic analysis of crude reaction mixture showed no deuterated product had been formed, however the same three aromatic by-products (**3.21**, **3.22** and **3.23**) were observed as previously, alongside unreacted aryl bromide (**3.20**) in a ratio (1: 5: 2: 2) (respectively) based on relative integration of their methoxy groups (Figure **3.7** and **3.8**).

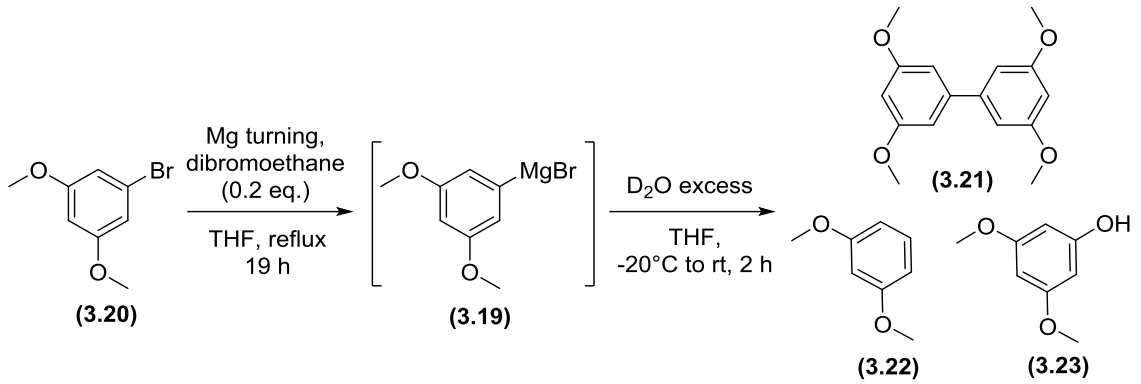

Figure 3.7: Attempted deuterium trapping of the Grignard reagent formed from 1-bromo-3,5-dimethoxybenzene (**3.20**).

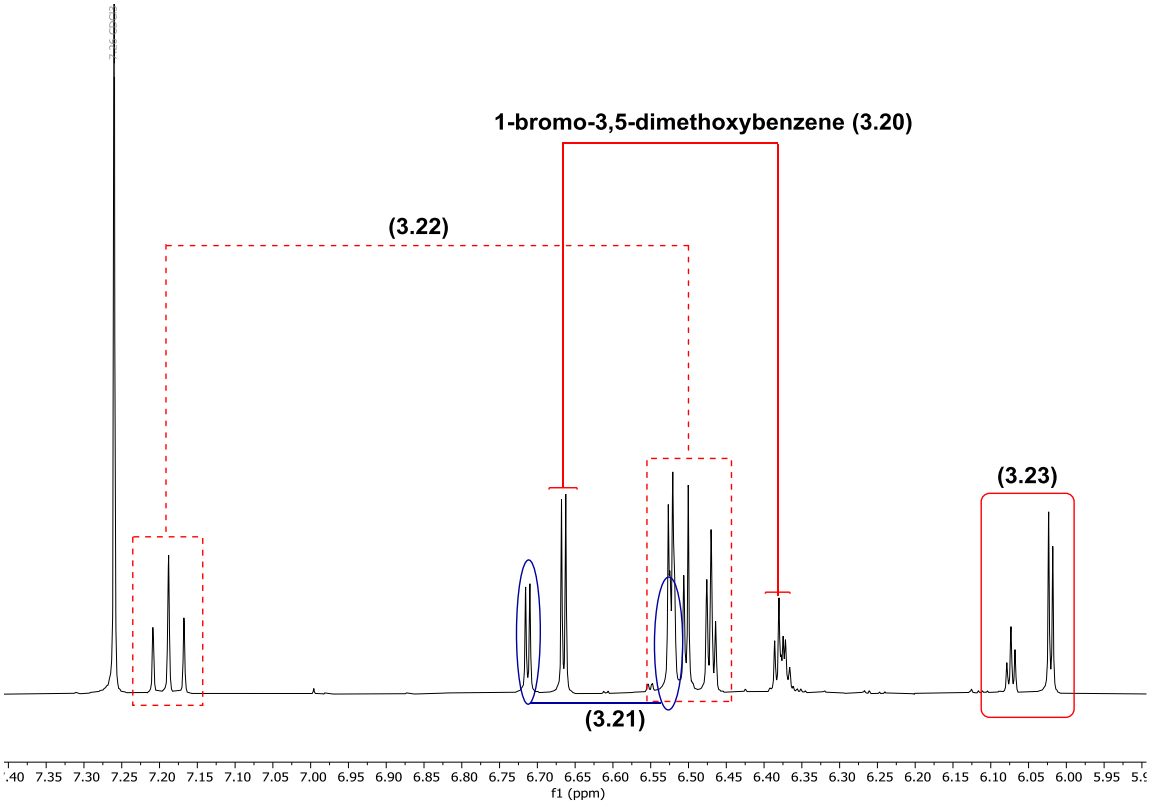

Figure 3.8: Partial ^{1}H NMR spectroscopic analysis of crude material resulting from the deuterium trapping experiment of the Grignard reagent formed from 1-bromo-3,5-dimethoxybenzene (**3.20**).

Following partial separation by column chromatography, the structure of the three by-products **3.21**, **3.22** and **3.23** have been determined. In the majority of our reactions the formation of (**3.22**) was observed as the major by-product. ^{1}H NMR spectroscopic analysis of by-product (**3.22**) showed a set of key signals at 7.20 (t, J = 8.2 Hz, 1H), 6.53 (dd, J = 8.2, 2.4 Hz, 1H) and 6.49 (t, J = 2.4 Hz, 1H) suggesting a symmetrical 1,3-disubsituted

benzene ring, along with a further signal at 3.79 (s, 6H) corresponding to two methoxy groups. Therefore the major by-product (**3.22**) is 1,3-dimethyoxy benzene, likely formed through the protonation of the intermediate Grignard reagent (Figure **3.9**).[4]

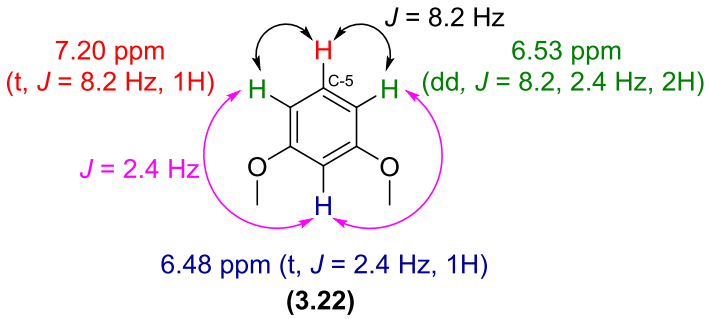

Figure 3.9: Structural assignment of the major by-product y as 1,3-dimethoxybenzene (**3.22**).

Next, analysis of the ^{1}H NMR spectrum of by-product (**3.21**) showed two aromatic proton environments at 6.71 (d, J = 2.2 Hz, 4H), and 6.47 (t, J = 2.2 Hz, 2H) suggesting a 1,3,5-trisubstituted aromatic ring with a plain of symmetry. Furthermore, the ^{1}H NMR spectrum showed a singlet at 3.84 (s, 12H) corresponding to the presence of four methoxy groups in identical environments. In addition, analysis of the ^{13}C NMR spectrum in combination with HSQC showed that the peak at 143.4 ppm is a quaternary carbon atom, thus aiding us in assigning by-product (**3.21**) as the corresponding Wurtz coupled dimer, 3,3',5,5'-tetramethoxy-1,1'-biphenyl (Figure **3.10**).[5,6]

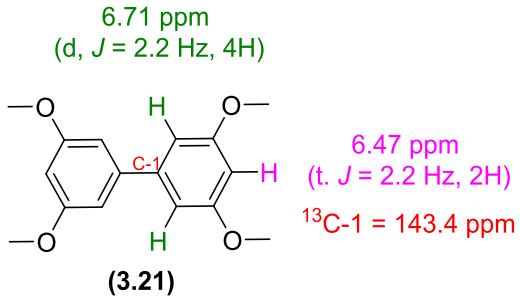

Figure 3.10: Structural elucidation of by-product (**3.21**) as 3,3',5,5'-tetramethoxy-1,1'-biphenyl.

Finally, the structure of by-product (**3.23**) was determined via ^{1}H NMR spectroscopic analysis, showing a set of signals at 6.07 (t, J = 2.1 Hz, 1H) and 6.02 (d, J = 2.1 Hz, 2H), corresponding to two aromatic proton environments and suggesting another 1,3,5-trisubstituted, symmetrical aromatic product. Moreover, the ^{1}H NMR spectrum showed a broad signal at 5.02 ppm (s, 1H) which might correspond to an OH group and ^{13}C NMR

spectrum showed a downfield signal at 157.5 ppm affirming the attachment of a group with high electronegativity such as OH. Therefore, the by-product (**3.23**) is 3,5-dimethoxyphenol (Figure **3.11**).[7]

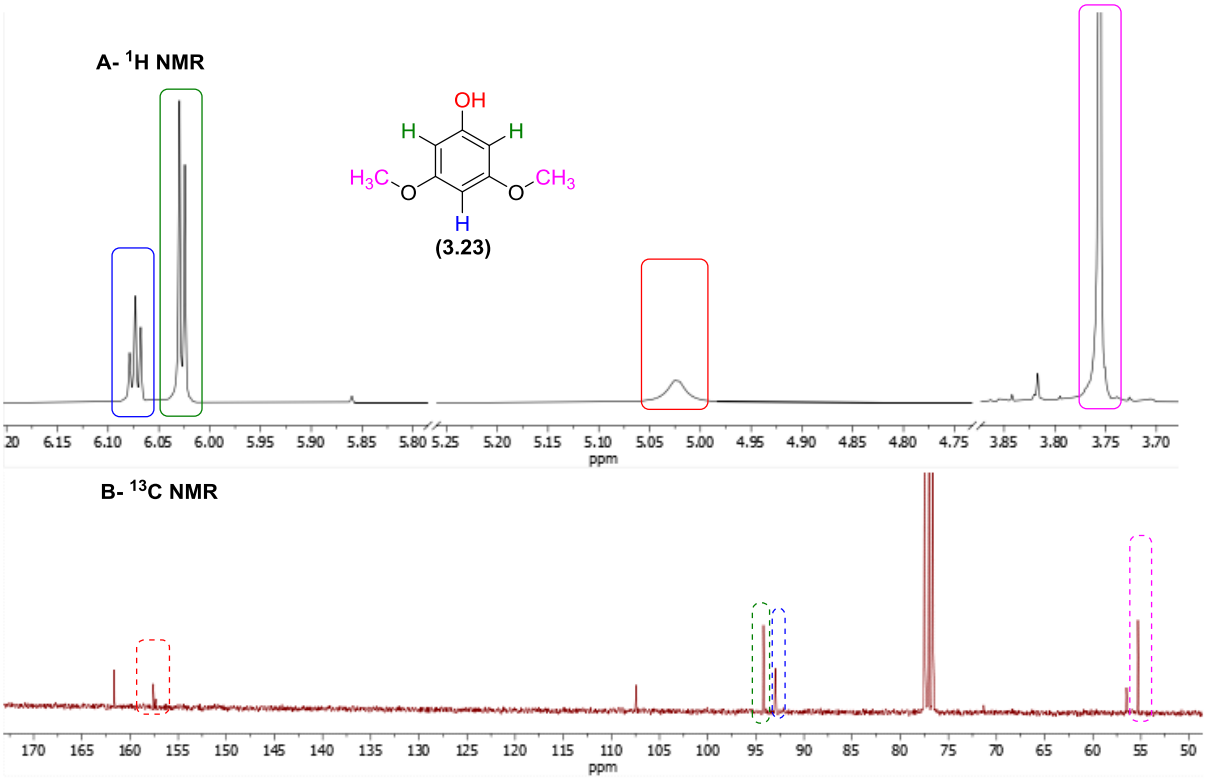

Figure 3.11: ^{1}H and ^{13}C NMR spectra of by-product 3,5-dimethoxyphenol (**3.23**).

It is likely that 3,5-dimethoxyphenol (**3.23**) was formed via the air oxidation of the intermediate Grignard reagent (**3.19**) (dimethoxyphenylmagnesium bromide), via the corresponding peroxide which was then reduced to 3,5-dimethoxyphenol (**3.23**) by either another equivalent of Grignard reagent or by unreacted magnesium.[8,9]

In conclusion, our attempts at the formation and trapping of the Grignard reagent derived from 1-bromo-3,5-dimethoxybenzene (**3.20**) consistently gave three main by-products, the Wurtz coupled dimer (**3.21**) (3,3',5,5'-tetramethoxy-1,1'-biphenyl), the protonated product 1,3-dimethoxybenzene (**3.22**) and the oxidised product 3,5-dimethoxyphenol (**3.23**). Therefore since this approach had not resulted in access to our desired target molecule, trifluoromethyl ketone (**3.9**), an alternative route was explored.

3.2.2 Weinreb Amide Approach Towards the Synthesis of Trifluoromethyl Ketone (3.9)

Recently, Leadbeater *et al.*[10] reported the synthesis of trifluoromethyl ketone via a trifluoromethylation of Weinreb amide[13] (**3.27**) with the Ruppert-Prakash reagent ($TMSCF_3$).[11,12] Therefore, I wished to examine this approach in the synthesis of our target trifluoromethyl ketone (**3.9**) (Figure **3.12**).

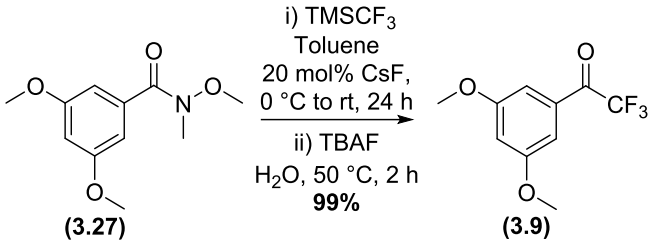

Figure 3.12: Leadbeater's synthesis of trifluoromethyl ketone (**3.9**) via Weinreb amide approach.

3.2.2.1 Synthesis of 3,5-dimethoxybenzamide (3.27) (Weinreb Amide)

Our first step to access trifluoromethyl ketone (**3.9**), was the synthesis of the corresponding Weinreb amide (**3.27**) via a condensation between 3,5-dimethoxybenzoyl chloride (**3.26**) and *N,O*-dimethyl hydroxylamine hydrochloride (**3.25**).

Therefore, 2 mmol of 3,5-dimethoxybenzoyl chloride (**3.26**) and 1.05 eq. of *N,O*-dimethyl hydroxylamine hydrochloride (**3.25**) was dissolved in CH_2Cl_2 at 0 °C. 2.1 eq. of pyridine was added over 10 min and the reaction mixture was then allowed to warm to rt overnight. After work-up and column chromatography, the desired Weinreb amide (**3.27**) was isolated in an 82 % yield (Figure **3.13**).

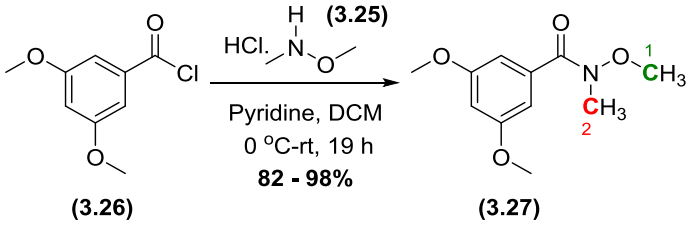

Figure 3.13: Synthesis of Weinreb amide (**3.27**) from the corresponding acid chloride (**3.26**) and *N,O*-dimethyl hydroxylamine hydrochloride (**3.25**).

The structure of Weinreb amide (**3.27**) was confirmed by the analysis of its ^{13}C NMR spectrum, showing two new signals at 61.2 and 34.1 ppm corresponding to the *O*-methyl (C1) and the *N*-methyl carbon atoms (C2) respectively of the newly formed amide.

To access large quantities of the Weinreb amide (**3.27**), the condensation reaction was sequentially scaled up from 2 to 125 mmol, using the same procedure as above. Yields remained high even at large scale, with an average yield of 92 % observed. In the case of high yielding large scale reactions, ^{1}H NMR spectroscopy showed high levels of purity and thus Weinreb amide (**3.27**) was taken forward without further purification. With significant quantities for the desired Weinreb amide (**3.27**) in hand the next synthetic step was examined.

3.2.2.2 Synthesis of Trifluoromethyl Ketone (3.9)

Our next step was to examine the trifluoromethylation of Weinreb amide (**3.27**), based on the work of Leadbeater *et al.*, [10] to form the corresponding trifluoromethyl ketone (**3.9**).

Therefore, an anhydrous toluene solution of 2.5 mmol of Weinreb amide (**3.27**) and CsF was treated with $TMSCF_3$ at 0 °C and the reaction mixture was then allowed to warm to rt overnight. After a total reaction time of 24 h, the intermediate silyl ether (**3.28**) was hydrolysed with TBAF in THF/H_2O (1:1) for 2 h at 50 °C. Following work-up and column chromatography, the desired trifluoromethyl ketone (**3.9**) was isolated in a 59 % yield (Figure **3.14**).

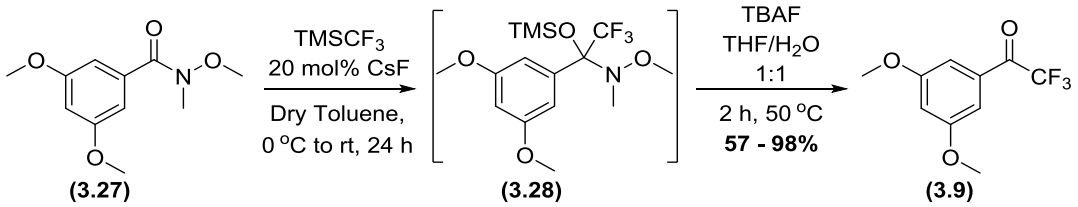

Figure 3.14: Synthesis of trifluoromethyl ketone (**3.9**) via reaction of Weinreb amide (**3.27**) with $TMSCF_3$.

The structure of trifluoromethyl ketone (**3.9**) was confirmed by the analysis of ^{19}F and ^{13}C and NMR spectra. The $^{19}F\{^{1}H\}$ NMR spectra showed a new singlet at -71.1 ppm corresponding to the fluorine atoms of the new trifluoromethyl moiety. In addition, the ^{13}C NMR spectra showed a two key signals, the first a ^{13}C-^{19}F coupled quartet at 180.2 ppm

(q, $^{3}J_{C\text{-}F}$ = 35.0 Hz) corresponding to the carbonyl carbon (C-2) of the ketone coupling to the CF_3 group, and the second another ^{13}C-^{19}F coupled quartet at 116.6 ppm (q, $^{2}J_{C\text{-}F}$ = 291.3 Hz) corresponding to the CF_3 carbon (C-3) (Figure **3.15**).[10]

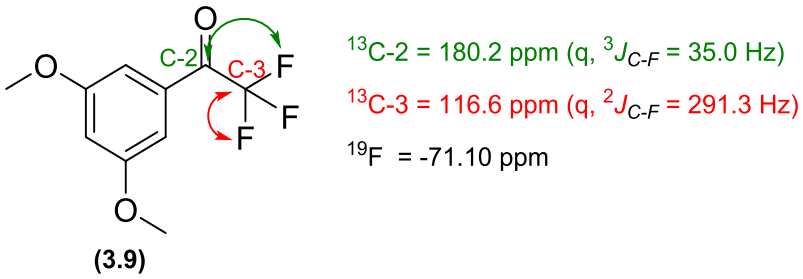

Figure 3.15: Key ^{19}F and ^{13}C NMR spectroscopic data for trifluoromethyl ketone (**3.9**).

Despite our initial success, attempts to repeat the trifluoromethylation reaction gave no further production of trifluoromethyl ketone (**3.9**), with only unreacted Weinreb amide (**3.27**) recovered. it was hypothesised that this may be due to the presence of unwanted water in the reaction, thus it was decided to dry Weinreb amide (**3.27**) prior to further reactions via a silica plug in EtOAc. Following drying of Weinreb amide (**3.27**) the trifluoromethylation reaction was repeated on a 1.8 mmol scale to give a 25 % isolated yield following column chromatography. Pleasingly, combining the pre-drying of Weinreb amide (**3.27**) with newly purchased $TMSCF_3$ gave a clean conversion to the desired trifluoromethyl ketone (**3.9**), resulting in improved yields of 80 % on a 2.3 mmol scale without the need for column chromatography. Following this success, the synthesis of trifluoromethyl ketone (**3.9**) was scaled up to a maximum scale of 80 mmol, with reproducibly good yields throughout and without the need for purification by column chromatography.

With gram quantities of trifluoromethyl ketone (**3.9**) in hand our next step was to examine the conversion of the ketone group into the corresponding diazirine (**3.10**).

3.2.3 Conversion of Trifluoromethyl Ketone (3.9) into Diazirine (3.10)

The next step in our synthesis was the incorporation of the required diazirine group at the C-2 position of trifluoromethyl ketone (**3.9**) (Figure **3.16**).

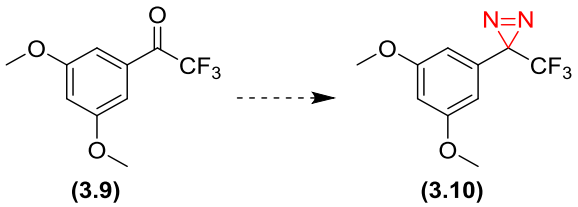

Figure 3.16: Planned conversion of trifluoromethyl ketone (**3.9**) into diazirine (**3.10**).

In 2007, Hayes *et al.*,[14,17] reported the synthesis of diazirine (**3.10**) in four steps starting from trifluoromethyl ketone (**3.9**), involving a condensation reaction with hydroxyl amine to afford the corresponding oxime (**3.29**), tosylation of the oxime, aminolysis with liquid ammonia and finally oxidation to the desired diazirine (**3.10**) (Figure **3.17**).[16]

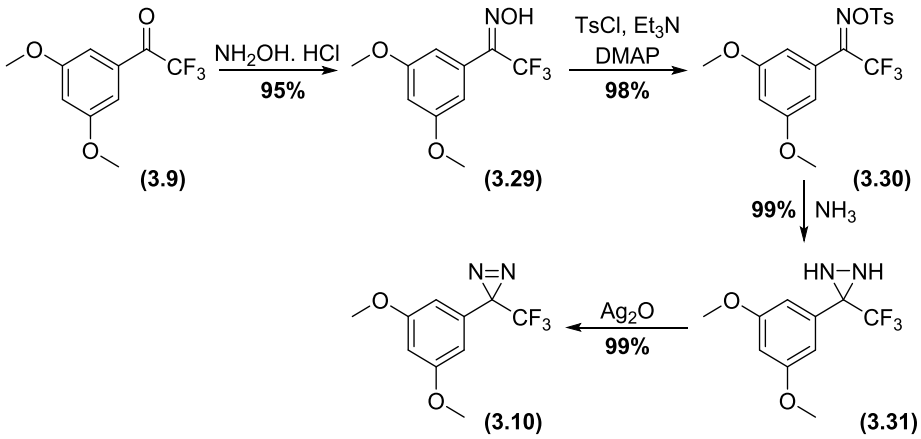

Figure 3.17: Hayes' synthesis of trifluoromethyl diazirine (**3.10**).

3.2.3.1 Synthesis of Trifluoromethyl Oxime (3.29)

Based on the Hayes' synthesis of trifluoromethyl oxime (**3.29**), trifluoromethyl ketone (**3.9**) (0.2 mmol) was reacted with hydroxylamine hydrochloride in pyridine : ethanol (2:1) at 60 °C for 19 h. Following work-up and column chromatography, the desired oxime (**3.29**) was isolated in a 68 % yield, with the structure confirmed by ^{13}C NMR spectroscopic analysis, which showed a new ^{13}C-^{19}F coupled quartet at 148.2 ppm (q, $^{2}J_{C\text{-}F}$ = 32.6 Hz) corresponding to the C-2 carbon atom of the oxime (Figure **3.18**, Table **3.6**: entry **1**).

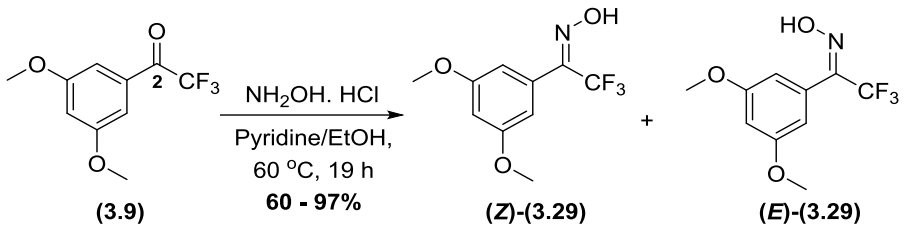

Figure 3.18: Condensation reaction of trifluoromethyl ketone (**3.9**) with hydroxylamine to give a mixture of *E*- and *Z*-trifluoromethyl oxime (**3.29**).

Interestingly, the crude ^{1}H NMR for this reaction showed two broad peaks at 9.05 and 8.84 ppm, in an approximate 1:1 ratio, which was assigned as the oxime OH. These two peaks have been attributed to the presence of two geometrical (*E*/*Z*) isomers of trifluoromethyl oxime (**3.29**) produced in the reaction. Following column chromatography, the isolated trifluoromethyl oxime (**3.29**) now appeared in a 3:1 ratio of geometrical isomers, with the signal at 8.84 ppm in the ^{1}H NMR spectrum corresponding to the major isomer. This observation suggests that isomerisation maybe occurring during purification.

In order to validate the molecular structure of trifluoromethyl oxime (**3.92**) and to further investigate the presence of geometrical isomers, high quality single crystals were grown by slow evaporation of a chloroform solution, allowing the crystal structure of trifluoromethyl oxime (**3.29**) to be obtained by X-ray diffraction analysis. The X-ray crystal structure confirmed the overall the structure of trifluoromethyl oxime (**3.29**). Interestingly, the crystal formed as a mixture of both the *E* and *Z* geometrical isomers, with the oxime group being disordered over two positions. The crystal was predominately composed of the *E*-isomer (95 %) with the *Z*-isomer present as a minor component (5 %). This suggests that the *E*-isomer is the most abundant following purification and may correspond to the observed ^{1}H NMR signal at 8.84 ppm (Figure **3.19**).

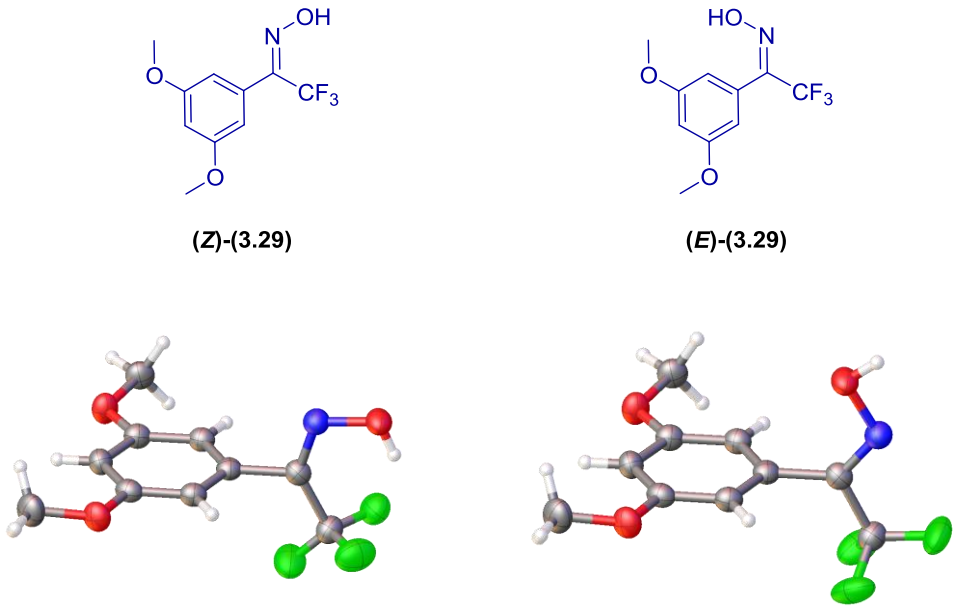

Figure **3.19:** X-ray crystal structure of trifluoromethyl oxime (**3.29**), showing the presences of both geometrical isomers.

Since it has been shown that the geometrical isomers can readily interconvert and the ratio of *E*:*Z* isomers would have little impact on the subsequent chemistry, next the scale up of the formation of trifluoromethyl oxime was examined (**3.29**) (Table **3.4**).

Entry	Reaction Scale/mmol	Yield/%	Entry	Reaction Scale/mmol	Yield/%
1	0.2[a]	68 %[c]	6	20.3[b]	75 %[d]
2	0.7[b]	65 %[c]	7	22.0[b]	97 %[d]
3	0.9[b]	60 %[d]	8	27.6[b]	92 %[d]
4	4.3[b]	99 %[d]	9	37.3[b]	70 %[d]
5	9.0[b]	83 %[c]	10	77.5[b]	90 %[d]

Table 3.4: Scale up of the synthesis of trifluoromethyl oxime (**3.29**). [**a**] concentration of trifluoromethyl ketone (**3.9**) in reaction = 0.13 M, [**b**] concentration of trifluoromethyl ketone (**3.9**) in reaction = 0.6 M, [**c**] isolated by column chromatography, [**d**] carried forward without further purification.

In our first attempt at scale up of the synthesis trifluoromethyl oxime (**3.29**) it showed that there was an increase in reaction concentration from 0.13 M to 0.6 M had little impact on the yield (65 %), thus future reactions were all carried out at around 0.6 M to assist in reducing reaction volume Table **3.6**: entry **2**). Next it showed that purification by column chromatography was unnecessary in most cases (Table **3.6**: entry **3**). It should be noted that the *E*/*Z* ratio of trifluoromethyl oxime (**3.29**) varied considerably (from 100%, across multiple scale up reactions, as measured by integration of the broad ^{1}H NMR signals corresponding to the oxime OH. Analysis was further complicated as these signals also varied in shift by up to 1 ppm. Finally, it was demonstrated that the synthesis of trifluoromethyl oxime (**3.29**) on a 77.5 mmol scale with an excellent yield of 90 %, providing sufficient material for the next synthetic step with no purification by column chromatography required (Table **3.6**: entry **10**). This reaction generated a 1.3 : 1 ratio of the *Z* to *E* isomers as confirmed by integration of both ^{1}H and ^{19}F NMR spectra (1.3 [^{1}H 8.45, ^{19}F -62.30 (ppm)] : 1 [^{1}H 8.21, ^{19}F -66.91 (ppm)]).

3.2.3.2 Synthesis of Trifluoromethyl *O*-tosyl Oxime (3.30)

In our next step a plan to examine the tosylation of trifluoromethyl oxime was devised, in order to convert the hydroxyl group into an improved leaving group as required later in the synthesis.

Therefore, trifluoromethyl oxime (**3.29**) in CH_2Cl_2 was reacted with *p*-toluene sulfonyl chloride, in the presence of DMAP and triethylamine at 0 °C for 1 h, after which the reaction mixture was allowed to warm to rt overnight. Following work-up, analysis of the crude reaction material by ^{1}H NMR spectroscopy showed the presence of two geometrical isomers in a 5:1 ratio (methoxy singlets at 3.79 and 3.78 ppm (5:1), methyl singlets at 2.48 and 2.46 ppm (5:1) (Figure **3.20**).

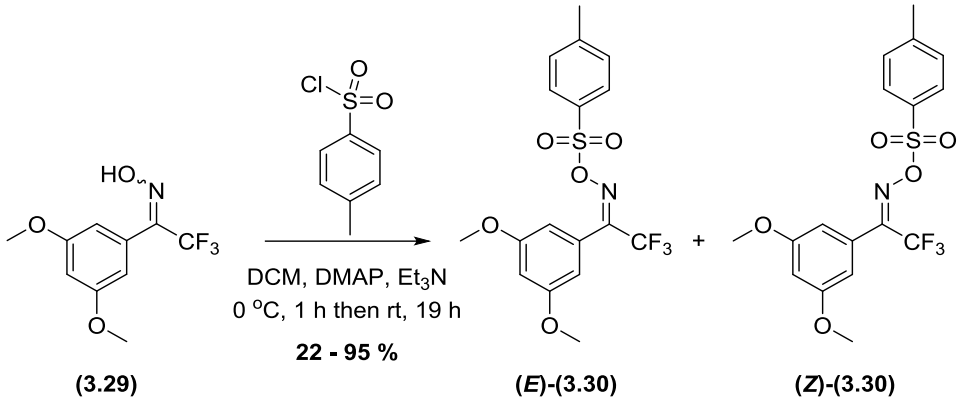

Figure 3.20: *O*-Tosylation of trifluoromethyl oxime (**3.29**).

In effort to purify the product, crystals were grown through slow evaporation of an EtOAc/hexane solution, resulting in a 22 % yield of *O*-tosyl trifluoromethyl oxime (**3.30**) with the structure confirmed by mass spectrometry (*m*/*z* = 426.0062 $[M+Na]^+$). Interestingly the ^{1}H NMR spectrum of crystalline *O*-tosyl trifluoromethyl oxime (**3.30**) showed that the ratio of geometrical isomers had significantly altered, from 5:1 to 1:9 (*Z*:*E*) based on the integration of the methoxy singlets at 3.79 and 3.78 ppm. The obtained crystals of *O*-tosyl trifluoromethyl oxime (**3.30**) were also analysed by single crystal X-ray diffraction. The crystal structure showed the presence of only the *E*-isomer, with eight molecules in the unit cell (Z = 8) packing in the monoclinic space group C2/c (Figure **3.21**). Through correlation of the X-ray and NMR results, this suggests that the methoxy group at 3.78 ppm in the ^{1}H NMR spectrum relates to the *E*-isomer of *O*-tosyl trifluoromethyl oxime (**3.30**).

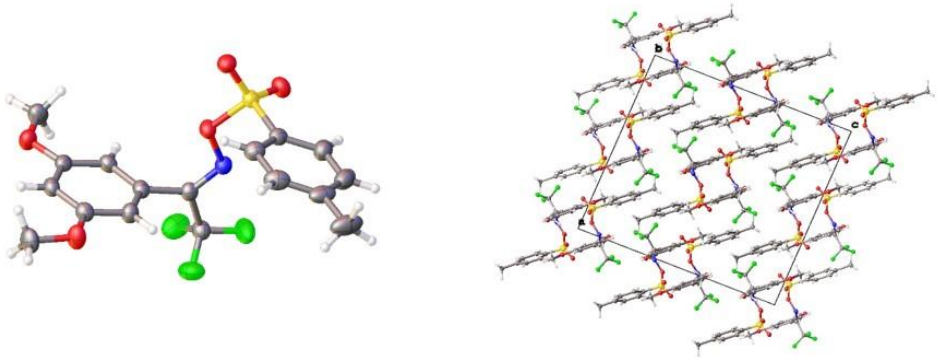

Figure 3.21: X-ray crystal structure of *O*-tosyl trifluoromethyl oxime (**3.30**) (Table **3.6**, entry **1**).

In the first attempt to prepare more *O*-tosyl trifluoromethyl oxime (**3.30**), the tosylation reaction was repeated on a 4.88 mmol scale. Analysis of the crude reaction material by ^{1}H NMR spectroscopy showed presence of two geometrical isomers in a 1:1 ratio, based on integration of the two methoxy singlets (3.79 and 3.78 ppm). Following poor separation on column chromatography and unsuccessful hot-to-cold crystallisation in EtOAc/hexane, the purification was attempted again through solvent evaporation from an EtOAc/hexane solution. After one week large colourless crystals were formed resulting in a 43 % isolated yield of *O*-tosyl trifluoromethyl oxime (**3.30**). NMR spectroscopy of the crystalline material showed two signals corresponding to the methoxy groups (^{1}H NMR, 3.79 and 3.78 ppm) and two signals corresponding to the CF_3 groups (^{19}F NMR, -67.12 and -61.55 ppm) in a 3:1 *Z*:*E* ratio. The crystals grown were suitable for X-ray diffraction analysis. Interestingly this showed that *O*-tosyl trifluoromethyl oxime (**3.30**) had formed a new crystal form, exhibiting a triclinic space group P-1 with 2 molecules in the unit cell (Z = 2), containing predominately the *Z*-isomer, disorder in the crystal structure arising from the presence of ~8% of the *E*-isomer (Figure **3.22**).

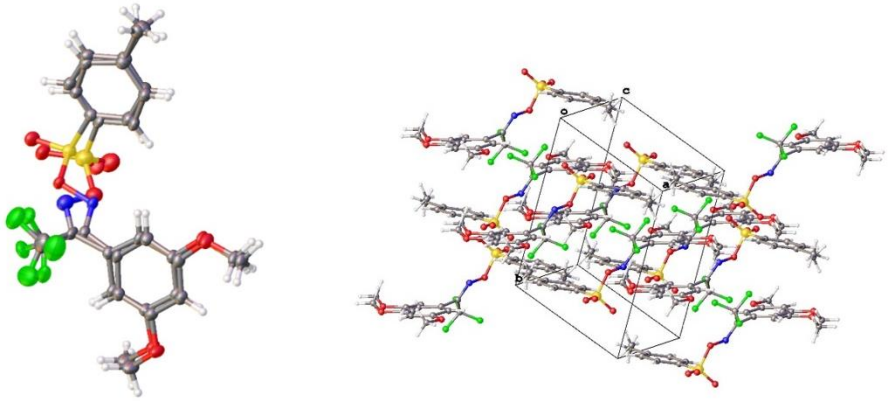

Figure 3.22: X-ray crystal structure of *O*-tosyl trifluoromethyl oxime (**3.30**) (Table **3.6**, entry **2**).

It is interesting to note that *O*-tosyl trifluoromethyl oxime (**3.30**) can create two different crystal forms, one contained entirely the *E*-isomer whilst the other contained predominately the *Z*-isomer. Since it is likely that the *E*- and *Z*-isomers can equilibrate in solution, the

observation of two different crystal forms each containing a major isomer may be a case of thermodynamic verses kinetic control in the crystal growth.

Next the reaction of *O*-tosyl trifluoromethyl oxime (**3.30**) formation was scaled up, whilst also looking to improve yields. Increasing the scale of the reaction to 7.4 mmol with crystallisation from EtOAc/hexane gave an improved yield of 63 %. Further stepwise scale up to 70.0 mmol gave a final yield of 95 % with no further purification required. During these reactions ^{1}H and ^{19}F NMR spectroscopy showed variable ratios of *Z* : *E* from 1.5:1 to 1:1.5 (Table **3.5**).

Entry	Reaction Scale/mmol	Yield/%	Entry	Reaction Scale/mmol	Yield/%
1	1.1	22 %[a]	5	21.2	88 %[b]
2	4.8	43 %[a]	6	26.0	95 %[b]
3	7.4	63 %[a]	7	25.5	88 %[b]
4	15.3	78 %[b]	8	70.0	95 %[b]

Table 3.5: Scale-up of the synthesis of *O*-tosyl trifluoromethyl oxime (**3.30**). [**a**] Isolated by crystallisation, [**b**] Taken forward without further purification.

It should be noted that our assignment of the ^{19}F NMR data for the *E*- and *Z*-isomers, based on the NMR of the crystal forms, does not agree with those predicted by Lindel *et al.*, and would require further investigation in the future.[18] However, following the successful synthesis of large quantities of *O*-tosyl trifluoromethyl oxime (**3.30**) I proceeded to the next step to examine the formation of the required diaziridine ring.

3.2.3.3 Synthesis of Trifluoromethyl diaziridine (3.31)

Next, the formation of a diaziridine at the C-2 position of *O*-tosyl trifluoromethyl oxime (**3.30**) was examined via reaction with ammonia, involving nucleophilic addition of ammonia to the oxime carbon, followed by substitution of the tosyl group in an intramolecular ring closure.

Therefore, *O*-tosyl trifluoromethyl oxime (**3.30**) (0.49 mmol) in CH_2Cl_2 was reacted with methanolic ammonia (7 M) for 1 h at -78 °C. The reaction mixture was then allowed to warm to rt overnight, following which the reaction vessel was opened to air to allow the loss of ammonia. Wet universal indicator paper was used to test for presence of ammonia gas. Once the ammonia had been removed, following work-up and column chromatography the desired trifluoromethyl diazirdine (**3.31**) was isolated in 88 % yield (Figure **3.23**).

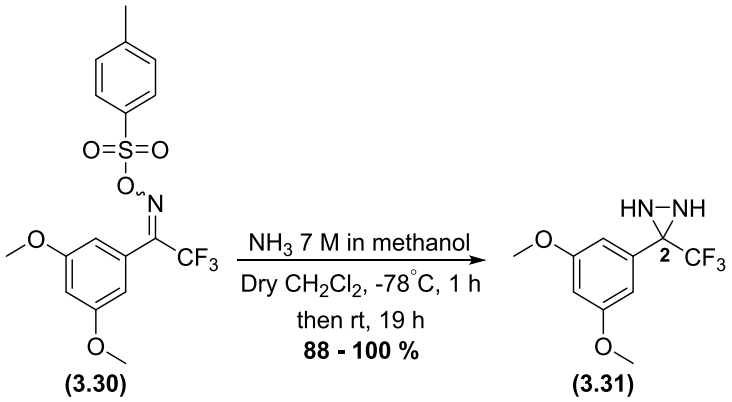

Figure 3.23: Synthesis of trifluoromethyl diaziridine (**3.31**) via reaction with methanolic ammonia.

The structure of our desired trifluoromethyl diaziridine (**3.31**) was confirmed by both ^{1}H and ^{13}C NMR spectroscopy. Analysis of the ^{1}H NMR spectrum showed two key signals at 2.68 (d, J = 8.8 Hz, 1H), and 2.16 ppm (d, J = 8.8 Hz, 1H) corresponding to the two N-H protons of the diaziridine moiety. In addition, the analysis of ^{13}C NMR spectra showed an upfield shift of the carbon atom at C-2 position from 154.3 ppm to 58.1 ppm (q, $^{2}J_{C\text{-}F}$ = 36 Hz) due to the change in the hybridization state from the starting material, *O*-tosyl trifluoromethyl oxime (**3.3**) (sp2), to the product, trifluoromethyl diaziridine (**3.31**) (sp3).

In order to further confirm the molecular structure of trifluoromethyl diaziridine (**3.31**), crystals were grown by slow evaporation of an ethyl acetate solution. X-ray diffraction analysis confirmed that trifluoromethyl diaziridine (**3.31**) had crystallised in a monoclinic space group P 21/c with 4 molecules in the unit cell (Z = 4) (Figure **3.24**).

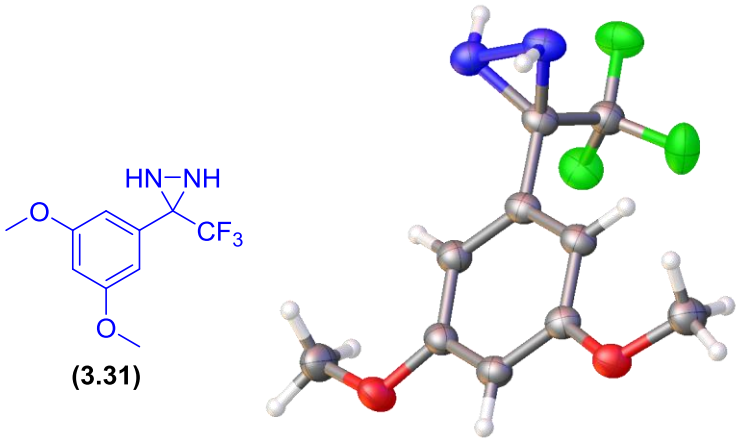

(3.31)

Figure 3.24: X-ray structure of trifluoromethyl diaziridine (**3.31**).

Next, the yield of trifluoromethyl diaziridine (**3.31**) was improved whilst also exploring the scale-up of the reaction. In our next attempt at the formation of trifluoromethyl diaziridine (**3.31**) on a 1.0 mmol scale, following column chromatography the desired product was isolated in 89 % yield alongside two minor by-products. Analysis of the by-products by ^{1}H and ^{19}F NMR spectroscopy allowed them to be assigned as the corresponding trifluoromethyl diazirine (**3.10**) and trifluoromethyl imine (**3.32**) (Figure **3.25**).

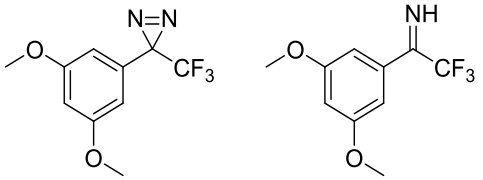

(3.10) (3.32)

Figure 3.25: By-products arising from the synthesis of trifluoromethyl diaziridine (**3.31**).

The formation of by-products trifluoromethyl diazirine (**3.10**) and trifluoromethyl imine (**3.32**) may occur through the reaction of *O*-tosyl trifluoromethyl oxime (**3.31**) with trifluoromethyl diaziridine (**3.31**) (Figure **3.25a**).

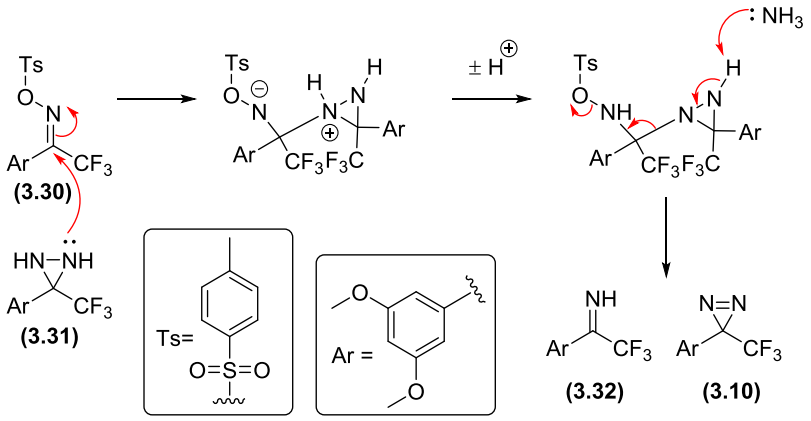

Figure 3.25a: Proposed mechanism for the formation of trifluoromethyl diazirine (**3.10**) and trifluoromethyl imine (**3.32**).

Since the main by-product being formed during purification was the trifluoromethyl diazirine (**3.10**), and that this molecule is the target of the next synthetic step it was decided to carry forward subsequent batches of trifluoromethyl diaziridine (**3.31**) without column chromatography. Thus, further scale-up reactions were shown to give reproducibly high yields (quantitative) up to 66.0 mmol scale.

With sufficient quantities of trifluoromethyl diaziridine (**3.31**) in hand I decided to carry on to examine the next synthetic step, the oxidation of the diaziridine ring.

3.2.3.4 Synthesis of Trifluoromethyl Diazirine (3.10)

After installing the diaziridine moiety at the C-2 position of trifluoromethyl ketone (**3.9**) over three steps, the next step for us was to examine the oxidation of the diaziridine moiety to form the required trifluoromethyl diazirine (**3.10**) (Figure **3.26**).

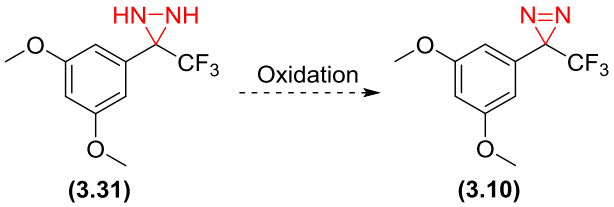

Figure 3.26: Planned oxidation of trifluoromethyl diaziridine (**3.31**) to form trifluoromethyl diazirine (**3.10**).

Based on the work of Hayes *et al.*, I decided to use iodine under basic conditions as our oxidising system.[14] Therefore, trifluoromethyl diaziridine (**3.31**) (0.4 mmol) was reacted with iodine (1.05 eq.) in methanol, in the presence of trimethylamine (2.0 eq.), at rt for 2

h. After which an additional portion of iodine (0.45 eq.) was added, the reaction was complete by TLC with a single new compound observed (R_f = 0.6). The reaction was partitioned between water and DCM, the organic extracts evaporated and then redissolved in hexane. The product was then washed with 1M HCl to remove Et_3N, and $Na_2S_2O_{3(sat)}$ to remove any iodine remaining. Following solvent evaporation, the desired trifluoromethyl diazirine (**3.10**) was obtained in 32 % yield without the need for column chromatography (Figure **3.27**).

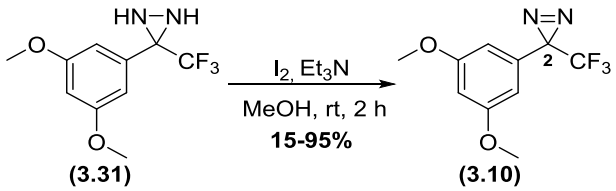

Figure 3.27: Trifluoromethyl diazirine (**3.10**) synthesis via I_2 oxidation of diaziridine (**3.31**).

The analysis of ^{13}C NMR and ^{1}H NMR spectra gave us confidence that our desired diazirine moiety have been formed. The ^{13}C NMR spectrum showed a signal at 28.9 (q, $^{2}J_{C\text{-}F}$ = 40 Hz) characteristic of the C-2 carbon atom of diazirine. In addition, the ^{1}H NMR spectrum showed the disappearance of the signals at 2.68 and 2.16 ppm, corresponding to the N-H protons of the starting material, trifluoromethyl diaziridine (**3.31**).

With initial success in the synthesis of the desired trifluoromethyl diazirine (**3.10**), I next looked to increase both the yield and the scale of the reaction. Therefore, the reaction was repeated on a 0.8 mmol scale. Unfortunately, following our standard work-up trifluoromethyl diazirine (**3.10**) was obtained in only a 15 % yield (Table **3.6**, entry **2**).

It was thought that the low yields might be due to loss of product during work-up, either through protonation by HCl or reduction by $Na_2S_2O_3$. Therefore, the reaction was repeated on a 2.6 mmol scale, omitting the HCl and $Na_2S_2O_3$ steps in the work up, and changing the extraction solvent to diethyl ether. This resulted in a much improved yield of 95 % of trifluoromethyl diazirine (**3.10**) (Table **3.6**, entry **3**). Further scale-up to 4.5 mmol resulted in good to moderate yields of the desired product (93, 50 and 68 %; Table **3.6**, entry **4**-**6**).

In the next synthetic step, the Lewis acid-catalysed formylation of trifluoromethyl diazirine (**3.10**) was examined. Following a number of poor reactions results it was thought that the

purity and water content of the starting material maybe effecting the results. Therefore, when the reaction was scaled up to 5.5 and 9.2 mmol I attempted to isolate and dry trifluoromethyl diazirine (**3.10**) by using column chromatography. This gave good yields of 78 and 67 % respectively (Table **3.6**, entry **7** and **8**). However, on larger scale (9.2 mmol) the trifluoromethyl imine (**3.32**) was also isolated, in 9 % yield as a by-product, potential formed through hydrolysis on the column (Table **3.6**, entry **7**). In the next two reactions, further scale-up reactions at 11.8 and 16 mmol was combined with rapid purification by silica plug resulting in excellent yields of up to 90 % (Table **3.6**, entry **9** and **10**). Finally, a further reaction on a 22 mmol scale was attempted. Unfortunately the ^{1}H NMR the crude material showed considerable quantities of contaminants, thus purified the reaction mixture by column chromatography to give a 44 % yield of trifluoromethyl diazirine (**3.10**) along with a 14 % yield of trifluoromethyl ketone (**3.9**) (Table **3.6**, entry **10**).

Entry	**Reaction Scale/mmol**	**Yield/%**	**Entry**	**Reaction Scale/mmol**	**Yield/%**
1	0.4	32 %[b]	7	5.5	78 %[a]
2	0.8	15 %[b]	8	9.2	67 %[a]
3	2.6	95 %[b]	9	11.8	90 %[c]
4	2.8	93 %[b]	10	16.0	84 %[c]
5	4.4	50 %[b]	11	22.0	44 %[a]
6	4.5	68 %[b]	-	-	-

Table 3.6: Scaling up the oxidation of trifluoromethyl diaziridine (**3.31**) to trifluoromethyl diazirine (**3.10**) [**a**] Isolated by column chromatography, [**b**] Taken forward without further purification, [**c**] Purified by silica plug.

After successful synthesis of trifluoromethyl diazirine (**3.10**) on large scale, I moved to examining the subsequent C-4 formylation.

3.2.4 Functionalisation of Trifluoromethyl Diazirine (3.10) *en route* to Diazirine Carboxycoumarin (3.2)

In order to access the target diazirine carboxycoumarin (**3.2**), for the next steps consideration of the involvement of a selective C-4 formylation of trifluoromethyl diazirine (**3.10**), followed by a selective C-5 demethylation and finally a Knoevenagel condensation with Meldrum's acid was planned (Figure **3.28**).

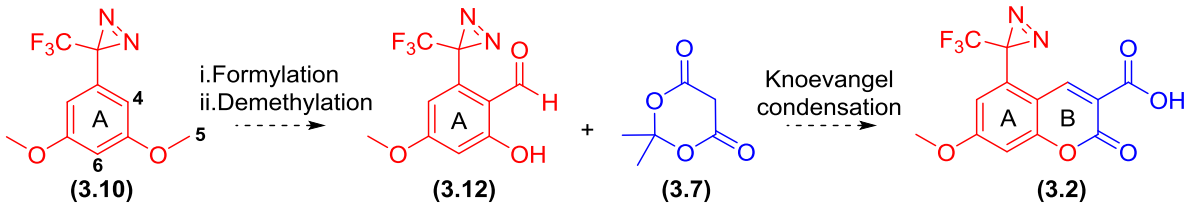

Figure 3.28: Planned synthesis of diazirine carboxycoumarin (**3.2**).

3.2.4.1 C-4 Formylation of trifluoromethyl diazirine (3.10) with $TiCl_4$

For our planned C-4 formylation the work of Tomohero *et al*. was adapted,[2] in which they reported the a Rieche-Gross formylation[19,20] of trifluoromethyl diazirine (**3.10**) via a $TiCl_4$ mediated reaction with dichloromethyl methyl ether to give both the C-4 and C-6 regioisomers of formyl trifluoromethyl diazirine (**3.11**) and (**3.33**) respectively (Figure **3.29**).

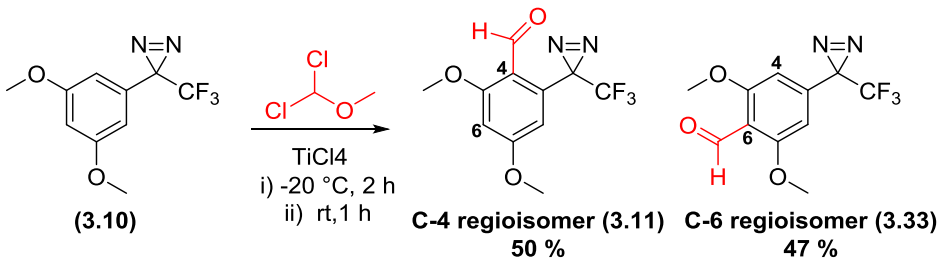

Figure 3.29: Tomohero's formylation of trifluoromethyl diazirine (**3.10**).

Therefore, in our first attempt at the formylation reaction, trifluoromethyl diazirine (**3.10**) was reacted with $TiCl_4$ (1.5 eq.) and dichloromethyl methyl ether (1 eq.) at -20 °C for 2 h, then allowed to warm up to rt for 1h. The reaction was quenched with the addition of water

and extracted into CH_2Cl_2. Following work-up, C-4 formyl trifluoromethyl diazirine (**3.11**) was isolated by column chromatography in a 20 % yield, along with 18 % of C-6 formyl trifluoromethyl diazirine (**3.33**) and 6 % of unreacted starting material (Table **3.7**, entry **1**).

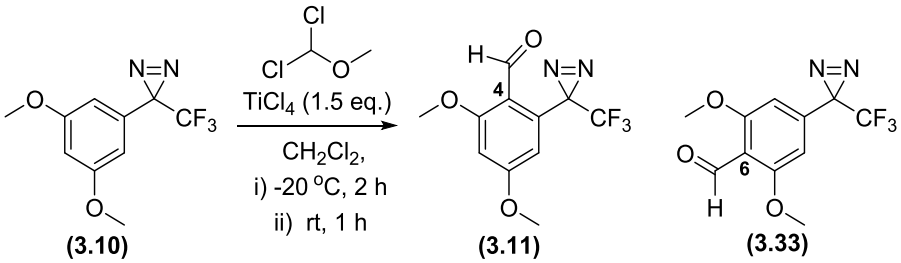

Entry	Reaction Scale/mmol	$CCl_2H(OCH_3)$ (eq.)	Isolated Yield of C-4 (3.11)/%	Isolated Yield of C-6 (3.33)/%	Notes
1	1.8	1	20 %	18 %	6% starting material recovered
2	2.5	1.5	6 %	4 %	27% starting material recovered

Table 3.7: Formylation of trifluoromethyl diazirine (**3.10**) with $TiCl_4$ and dichloromethyl methyl ether.

Repeating the formylation trifluoromethyl diazirine (**3.10**) with an increased number of equivalents of dichloromethyl methyl ether (1.5 eq.) unfortunately also gave poor yields of the desired formylated products (Table **3.7**, entry **2**).

The structures of C-4 formyl trifluoromethyl diazirine (**3.11**) and C-6 formyl trifluoromethyl diazirine (**3.33**) were confirmed by the analysis of ^1H and ^{13}C NMR spectra. The NMR spectra of C-4 formyl trifluoromethyl diazirine (**3.11**) showed signals in the ^1H NMR at 10.47 ppm (s, 1H) and the ^{13}C NMR at 187.9 ppm corresponding to the newly introduced aldehyde. The regiochemistry was assigned via the ^1H NMR spectrum, which showed two coupled doublets at 6.76 ppm (d, J = 2.3 Hz, 1H) and 6.55 ppm (d, J = 2.3 Hz, 1H) suggesting a *meta*-arrangement of the protons and thus C-4 formylation. On the other hand, the NMR analysis of C-6 formyl trifluoromethyl diazirine (**3.33**) again showed the presence of a new aldehyde group (^1H NMR 10.45 ppm (s, 1H); ^{13}C NMR 188.5 ppm),

whilst the aromatic protons appeared as a single peak at 6.31 ppm (s, 2H) corresponding to the two equivalent aromatic protons and thus a C-6 substitution.

In order to further confirm the molecular structure of C-4 formyl trifluoromethyl diazirine (**3.11**), crystals have been grown by the slow evaporation of ethyl acetate solution of compound (**3.11**). After which single suitable crystals were submitted to X-ray diffraction analysis which confirmed the molecular structure of C-4 formyl trifluoromethyl diazirine (**3.11**) (Figure **3.30**).

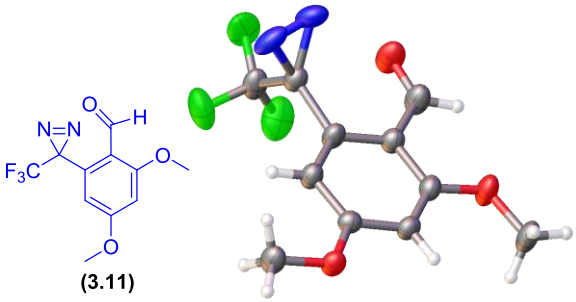

Figure (3.30): Crystal structure of trifluoromethyl ortho-benzaldehyde diazirine (**3.11**).

3.2.4.2 C-4 Formylation of Trifluoromethyl Diazirine (3.10) with $SnCl_4$

Due to the low yields obtained with $TiCl_4$ an alternative Lewis acid in the formylation of trifluoromethyl diazirine (**3.10**) was examined. $SnCl_4$ has also be used in Rieche-Gross formylations with a range of aromatic substrates, particularly in the synthesis of calixarenes.[20,21] Thus, a CH_2Cl_2 solution of trifluoromethyl diazirine (**3.10**) was reacted with $SnCl_4$ (1.5 eq.) and dichloromethyl methyl ether (1.5 eq.) at -20 °C for 2 h, after which the reaction mixture was allowed to warm up to rt for 1 h. Following work-up, the obtained crude reaction material was divided into two equal batches of approximately 100 mg each in order to test possible purification methods. The first batch was separated by column chromatography to give 52.5 mg of C-4 formyl trifluoromethyl diazirine (**3.11**) along with 48.9 mg of C-6 formyl trifluoromethyl diazirine (**3.33**) corresponding to a yield of 24 % and 21 % of the total reaction material. The second batch was recrystallised from EtOAc/hexane and washed with hexane to give 65.7 mg of C4-formyl trifluoromethyl diazirine (**3.11**) as a crystalline solid, corresponding a yield of 30 % of the total reaction material, the remaining C-6 formyl trifluoromethyl diazirine (**3.33**) not giving crystalline

material. Combining the C-4 formyl trifluoromethyl diazirine (**3.11**) obtained from both column chromatography and crystallisation gave a total recovered yield of 54 % for C-4 formyl trifluoromethyl diazirine (**3.11**), and a total yield of 75 % for the reaction to produce both the C-4 and C-6 regioisomer (Table **3.8**, entry **1**).

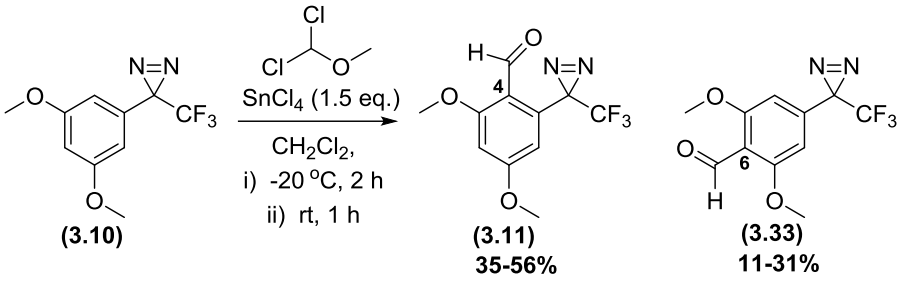

Entry	Reaction Scale/mmol	Isolated Yield of C-4 (3.11) /%	Isolated Yield of C-6 (3.33) /%	Notes
1	0.8	54 %[a]	21 % [b]	Purification in two batches (column and recrystallisation)
2	0.8	51 %[b]	30 %[b]	-
3	3.0	36 %[b]	18 %[b]	-
4	4.3	53 %[b]	31 %[b]	Trifluoromethyl diazirine (**3.10**) dried by silica plug
5	6.1	56 %[b]	26 %[b]	Trifluoromethyl diazirine (**3.10**) dried by silica plug
6	12.3	44 %[b]	13 %[b]	Trifluoromethyl diazirine (**3.10**) dried by silica plug
7	13.5	35 %[b]	11 %[b]	trifluoromethyl diazirine (**3.10**) dried by silica plug
8	24.6	52%	37%[b]	Trifluoromethyl diazirine (**3.10**) dried by silica plug

Table 3.8: Formylation of trifluoromethyl diazirine (**3.10**) with $SnCl_4$ and dichloromethyl methyl ether [**a**] Combined by column chromatography and recrystallisation, [**b**] Isolated by column chromatography.

With improved yields in the formylation of trifluoromethyl diazirine (**3.10**) with $SnCl_4$, I looked next to scale-up the formylation reaction. Due to the large difference in R_f between C-4 (R_f = 0.43; Petrol:Et_2O 3:2) and C-6 (R_f = 0.67; Petrol:Et_2O 3:2) regioisomers, it was decided to use column chromatography to isolate the products of our scale-up reactions. Thus repetition of the first reaction with $SnCl_4$ on a 0.8 mmol scale, with purification by column chromatography gave good isolated yields of 51 % (C-4) and 30 % (C-6) (Table **3.8**, entry **2**). However further scale-up to 3 mmol resulted in a decrease in yields 36 % (C-4) and 18 % (C-6), which was thought to be due to water in the starting material effecting the reaction (Table **3.8**, entry **3**). Therefore, in the next reaction the starting material trifluoromethyl diazirine (**3.10**) was dried by silica plug (as described previously) resulting in a return to good yields of the products, 53 % (C-4) and 31 % (C-6) (Table **3.8**, entry **4**). Next the reaction was scaled up in increments from 6.1 to 24.6 mmol (Table **3.8**, entry **5-8**). Although some lower yields were observed, C-4 formyl trifluoromethyl diazirine (**3.11)** was typically isolated in >50 % yields. Therefore, with sufficient C-4 formyl trifluoromethyl diazirine (**3.11**) available, I proceeded to the next synthetic step.

3.2.4.3 Demethylation of C-4 Formyl Trifluoromethyl Diazirine (3.11)

The next synthetic step was to to examine the regioselective C-5 demethylation of C-4 formyl trifluoromethyl diazirine (**3.11**), to give the desired C-5 hydroxy trifluoromethyl diazirine (**3.12**). Tomohero *et al*.,[2] has previously reported a regioselective McOmie-Watts-West demethylation[22] of C-4 formyl trifluoromethyl diazirine (**3.11**) using BBr_3.

Thus, a CH_2Cl_2 solution of C-4 formyl trifluoromethyl diazirine (**3.11**) (0.2 mmol, 1 eq.) was reacted with BBr_3 (1M in CH_2Cl_2, 1 eq.) at -20 °C for 10 min, then the reaction mixture warmed up to at 0 °C and stirred for 4 h. The reaction mixture was quenched with water (1 mL) and the product extracted into CH_2Cl_2. Following work-up, C-5 hydroxy trifluoromethyl diazirine (**3.12**) was isolated by column chromatography in a 9 % yield alongside 50 % of the starting material, C-4 formyl trifluoromethyl diazirine (**3.11**) (Table **3.9**, entry **1**).

The structure of C-5 hydroxy trifluoromethyl diazirine (**3.12**), including the regiochemistry of the demethylation was confirmed through comparison of the ^1H and ^{13}C NMR spectra to the literature.[2] The presence of a single methoxy group could be seen

in the ^{1}H and ^{13}C NMR with single peaks at 3.87 ppm (s, 3H) and 56.0 ppm, whilst new signal at 12.73 ppm (s, 1H) corresponded to an intramolecularly H-bonded hydroxyl group.

Since the low yields observed might have been due to hydrolysis of our BBr_3 reagent during storage, next the demethylation reaction was repeated on the same scale with 1 eq. of BBr_3 (1 M in CH_2Cl_2) from a new bottle of reagent. After a reaction time of -20 °C for 10 min and 2.5 h at 0 °C, TLC showed starting material remaining, thus a further 0.5 eq. of BBr_3 was added and the reaction mixture stirred for another 1.5 h at 0 °C, followed by rt overnight. After work-up and column chromatography, the desired C-5 hydroxy trifluoromethyl diazirine (**3.12**) was isolated in an improved 39 % yield, alongside 18 % of recovered starting material (**3.11**) (18 %) and 13 % yield the double demethylated trifluoromethyl diazirine (**3.34**) (Table **3.9**, entry **2**). To further check for the quality of BBr_3 used, the demethylation reaction was repeated using an ampule of neat BBr_3. After however after a reaction time of -20 °C for 10 min, and 2.75 h at 0 °C, only a 22 % yield of C-5 hydroxy trifluoromethyl diazirine (**3.12**) was recovered after column chromatography along with 51 % of the starting material, C-4 formyl trifluoromethyl diazirene (**3.11**) (Table **3.9**, entry **3**).

Due to the lack of conversion in our reactions so far, it was decided next to increase the initial reaction temperature, -20 to 0 °C. Therefore, to C-4 formyl trifluoromethyl diazirene (**3.11**) (0.4 mmol) in CH_2Cl_2 at 0 °C was added 1.5 eq. of BBr_3 (1 M in CH_2Cl_2) dropwise over 5 min. The reaction mixture was stirred at 0 °C for 2.25 h after which TLC showed no starting material remaining. Following an aqueous quench, work-up and column chromatography, C-5 hydroxy trifluoromethyl diazirine (**3.12**) was isolated in an excellent 90 % yield, alongside 9 % of the starting material, C-4 formyl trifluoromethyl diazirene (**3.11**) (Table **3.9**, entry **4**).

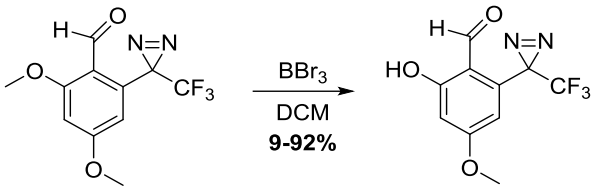

(3.11) **(3.12)**

Entry	Reaction Scale/mmol	BBr_3 eq.	Reaction time and temperature	Isolated Yield/%[a]	Recovered starting material C-4 (3.11)[a]	Note
1	0.2	1 (1M in DCM)	i. -20 °C, 10 min ii. 0 °C, 4 h	9 %	51 %	
2	0.8	1.5 (1M in DCM)	i. -20 °C, 10 min ii. 0 °C, 4 h iii. rt, o/n	39 %	18 %	Doubled demethylated product 13%
3	0.3	1 (neat BBr_3)	i. -20 °C, 10 min ii. 0 °C, 2.75 h	22 %	51 %	-
4	0.4	1.5 (1M in DCM)	0 °C, 2.25 h	90 %	10 %	-
5	0.9	1.5 (1M in DCM)	0 °C, 2 h	90 %	7 %	-
6	2.3	1.5 (1M in DCM)	0 °C, 2 h	92 %	6 %	-
7	4.7	1.5 (1M in DCM)	0 °C, 2 h	70 %	30 %	-
8	4.8	1.5 (1M in DCM)	0 °C, 2 h	56 %	3 %	-

Table 3.9: Demethylation of C-4 formyl trifluoromethyl diazirine (**3.11**) with BBr_3 [**a**] Isolated by column chromatography.

After optimising the demethylation of C-4 formyl trifluoromethyl diazirine (**3.11**), I next looked to scale-up the reaction. Reactions at 0.9 and 2.3 mmol scale gave reproducibly high yields of 90 % and 92 % of C-5 hydroxyl trifluoromethyl diazirine (**3.12**) respectively (Table **3.9**, entry **5** and **6**). Further attempts at scale-up to 4.7 and 4.8 mmol showed slightly decreasing yields of C-5 hydroxy trifluoromethyl diazirine (**3.12**) (70 % and 56 %), however I had sufficient material available to progress to the next step (Table **3.9**, entry **7** and **8**).

3.2.5 Synthesis of Diazirine Carboxycoumarin (3.2) via a Knoevenagel Condensation

Next the synthesis of diazirine carboxycoumarin (**3.2**) was examined, through a Knoevenagel condensation reaction, as a key intermediate on route to our final target methoxy coumarin trifluoromethyl diazirine D-alanine (**3.3**) (MCTDA) (Figure **3.31**).

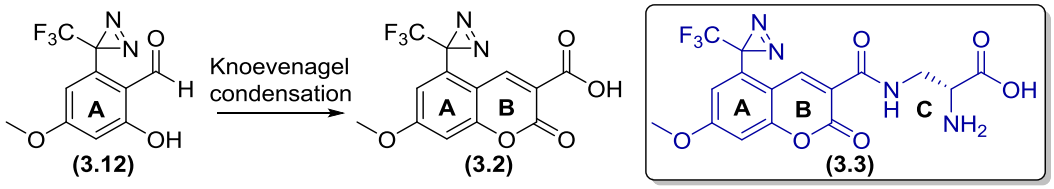

Figure 3.31: Planned Knoevenagel condensation to form diazirine carboxycoumarin (**3.2**) alongside the structure of target molecule MCTDA (**3.3**).

3.2.5.1 Synthesis of Diazirine Carboxycoumarin (3.2) via the Tomohero method

Recently, Tomohero *et al*., have demonstrated synthesis of diazirine carboxycoumarin (**3.2**) via a Knoevenagel condensation with Meldrum's acid in presence of DIPEA (Figure **3.32**)

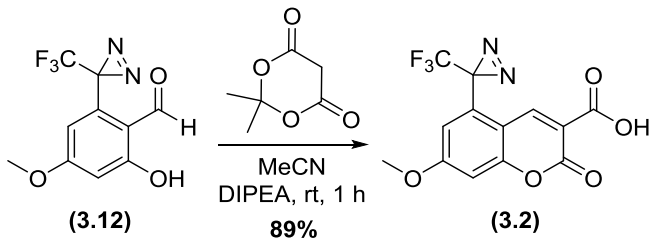

Figure 3.32: Tomohero's synthesis of diazirine carboxycoumarin (**3.2**) via a Knoevenagel condensation.

Thus, following Tomohero's approach C-5 hydroxy trifluoromethyl diazirine (**3.12**) (0.3 mmol, 1 eq.) in MeCN was reacted with Meldrum's acid (1.1 eq.) and DIPEA (2.5 eq.) at

rt for 2 h. Following work-up, ^{1}H NMR spectroscopic analysis of crude material showed traces of the desired product (**3.2**) alongside a number of other by-products, with isolation attempts by column chromatography proving unsuccessful with only Meldrum's acid recovered (Table **3.10** entry **1**).

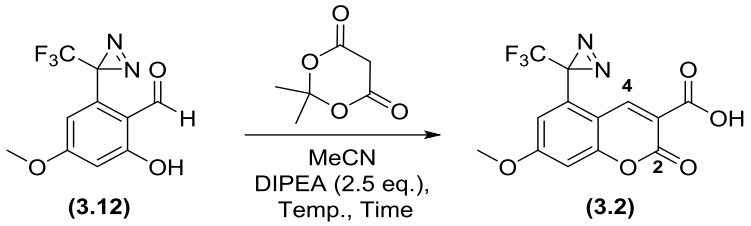

Entry	Reaction scale mmol	Meldrum's acid eq.	Reaction Time (h)	Reaction Temp.	Isolated yield %
1	0.3	1.1	2	rt	0 %
2	0.4	1.1	19	rt	40 %[a]
3	1.3	1.2	19	rt	-
4	2.1	1.1	2	rt for 1.5 h and then 50 °C for 2.25 h	15 %[b]

Table 3.10: Synthesis attempts of methoxy carboxycoumarin trifluoromethyl diazirine (**3.2**) via Tomohero's chemistry. [**a**] isolated by column chromatography, [**b**] isolated by three sequential recrystallisations.

Repeating the Knoevenagel condensation reaction with an extended reaction time of 19 h, followed by purification by column chromatography (buffered with acetic acid) afforded diazirine carboxycoumarin (**3.2**) in a 40 % yield (Table **3.10**, entry **2**).

The structure of diazirine carboxycoumarin (**3.2**) was confirmed through appearance in the ^{1}H NMR spectra of a signal at 9.46 ppm (s, 1H) corresponding to the 4-position of the coumarin and a peak in the ^{13}C NMR at 162.1 ppm corresponding to carbonyl carbon at the 2-position.

Unfortunately, attempts to scale-up the Knoevenagel condensation, proved unsuccessful due in part to difficulties in purification (Table **3.10**, entry **3**). A further attempt was made, increasing the reaction temperature, however complex mixture of products was obtained (Table **3.10**, entry **4**). Due to previous difficulties in column chromatography the

purification of diazirine carboxycoumarin (**3.2**) was attempted by recrystallisation from hexane and EtOAc. The first crystals obtained appeared to contain both the desired product and an additional molecule by ^{1}H NMR spectroscopy, and were submitted for further analysis by X-ray diffraction.

Single crystal X-ray diffraction analysis showed that the crystal contained two molecules a 1:1 ratio, the desired diazirine carboxycoumarin (**3.2**) and along with a by-product (**3.35**), in a triclinic space group P-1. By-product (**3.35**) appearing to be formed from diazirine carboxycoumarin (**3.2**) via a 1,4-addition of a second molecule of Meldrum's acid and a decarboxylation reaction (Figure **3.33**).

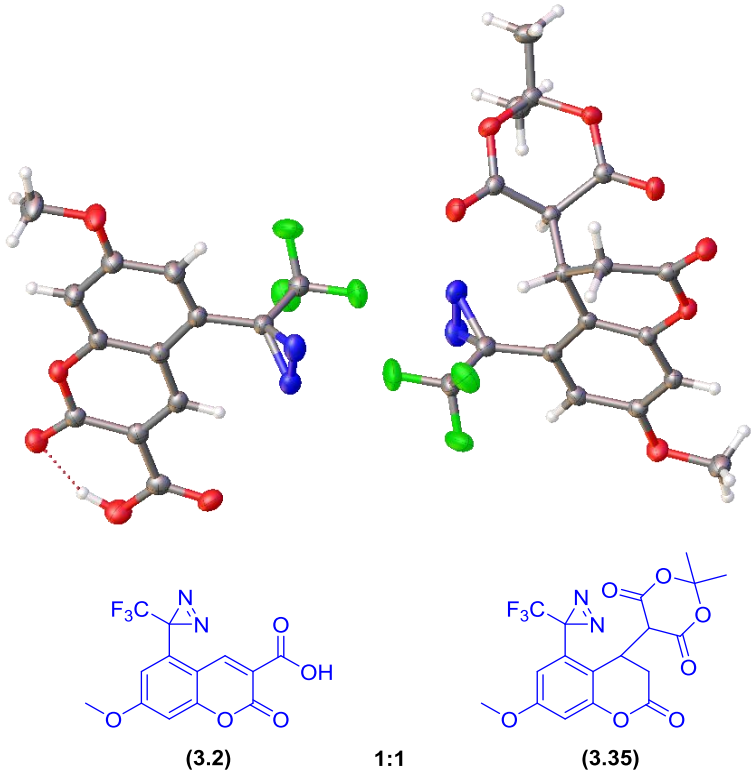

Figure 3.33: X-ray crystal structures of diazirine carboxycoumarin (**3.2**) and by-product (**3.35**).

With by-product (**3.35**) now removed from the sample through the first crystallisation, two further recrystallisations from hexane and EtOAc resulted in a 15 % isolated yield of diazirine carboxycoumarin (**3.2**).

In conclusion, diazirine carboxycoumarin (**3.2**) was successfully synthesised but with low yield and complex purifications required. Therefore, an alternative chemistry to synthesise our target molecule will be adopted.

3.2.5.2 Synthesis of Coumarin (3.2) as a Test Molecule to Evaluate the Tapia Method

In 1988, Tapia *et al*., reported[23] the synthesis of coumarin (**3.3**) via a Knoevenagel condensation of 2-methoxybenzyaldehyde (**3.36**) with Meldrum's acid (**3.7**) in DMF, followed by an acid catalysed acetal deprotection, demethylation and cyclisation to give the corresponding coumarin (**3.39**) (Figure. **3.34**).

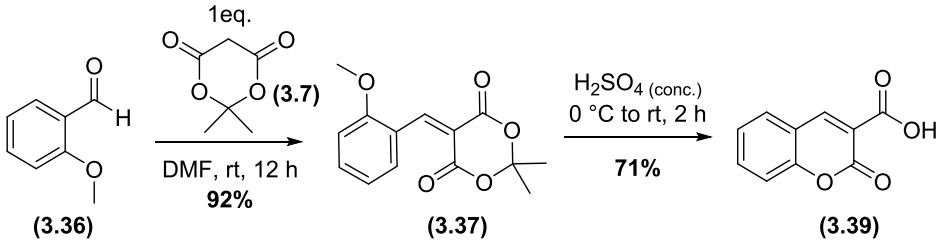

Figure 3.34: Tapia's synthesis of coumarin.

Therefore, Tapia's method was tested first with a simple model system to make coumarin (**3.39**), but using 2-hydroxybenzaldehyde (**3.38**) as the starting material in place of 2-methoxybenzyaldehyde (**3.36**). Thus, 2-hydroxybenzaldehyde (**3.38**) was reacted with 1 eq. of Meldrum's acid in DMF at rt overnight, followed by acidification with concentrated sulfuric acid at 0 °C to rt over 2 h. The reaction mixture was then poured over crushed ice and overnight in order to promote crystallisation of the product, which was collected by filtration to give a 30 % yield of coumarin (**3.39**) (Figure. **3.35**).

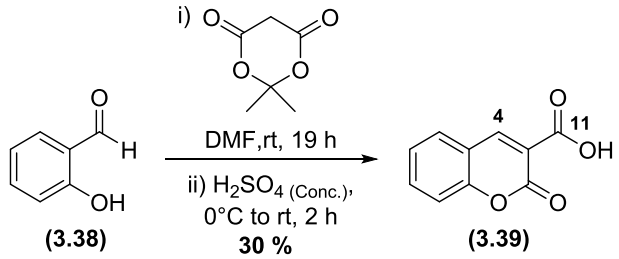

Figure 3.35: Synthesis of coumarin (**3.39**) via Tapia's method.

The ^{1}H and ^{13}C NMR spectroscopic analysis confirmed the structure of coumarin (**3.39**), including a ^{13}C NMR peak at 164.4 ppm corresponding to the carboxylic acid (C-11) and a ^{1}H NMR peak at 8.75 ppm (s, 1H) corresponding to the proton at C-4.

In order to improve the yields of coumarin (**3.39**) formation, following the chemistry of Tomohero *et al.*, and our previous work, it was decided upon to adapt the reaction conditions to include an amine base (DIPEA) to assist in the coumarin formation. Therefore, the reaction was repeated between 2-hydroxybenzaldehyde (**3.38**) and 1 eq. of Meldrum's acid (**3.7**) in presence of 20 mol % DIPEA, resulting in a much improved 77 % yield of coumarin (**3.39**) (Figure **3.36**).[2]

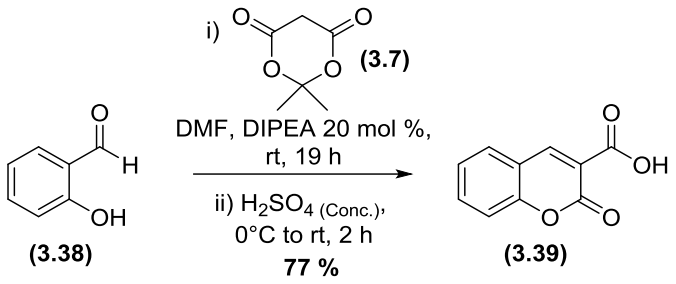

Figure 3.36: Improved synthesis of coumarin (**3.39**) with catalytic DIPEA.

3.2.5.3 Synthesis of Diazirine Carboxycoumarin (3.2) via the Tapia Method

Since the Tapia chemistry uses *ortho*-methoxy groups in place of *ortho*-hydroxyl groups on the benzaldehyde component, it was decided on to evaluate this approach in the synthesis of diazirine carboxycoumarin (**3.2**) directly from an *ortho*-methoxy containing precursor, thus potentially removing the need for a separate demethylation step. Due to the limited quantities of C-4 formyl trifluoromethyl diazirine (**3.11**) available, it was decided on to test this approach using the unwanted by-product C-6 formyl trifluoromethyl diazirine (**3.33**).

Thus, C-6 formyl trifluoromethyl diazirine (**3.33**) (0.8 mmol) was reacted with 1 eq. of Meldrum's acid in presence of catalytic amount of DIPEA (20 mol %) at rt overnight. Following treatment with concentrated sulfuric acid at 0 °C the reaction was poured over ice and allowed to warm to rt overnight and filtered to collect a single product in 66 % yield (Figure **3.37**).

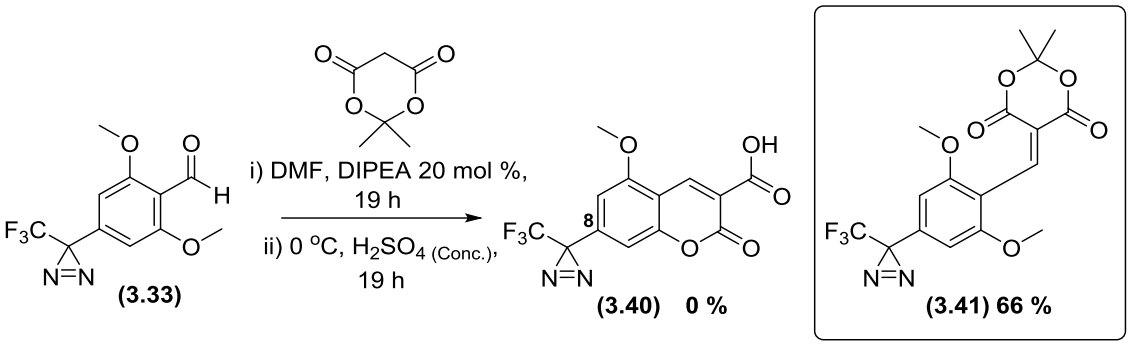

Figure 3.37: Synthesis of benzyldiene (**3.41**) via a Knoevenagel condensation.

^{1}H NMR spectroscopic analysis of the reaction product showed that the expected C-8 diazirine carboxycoumarin (**3.40**) had not been formed. Therefore to establish the molecular structure, crystals were grown by the slow evaporation of an ethyl acetate solution. A suitable crystal was submitted for X-ray diffraction analysis, revealing the product to be benzyldiene (**3.41**) arising from a Knoevenagel condensation reaction which had not continued on to form the desired C-8 diazirine carboxycoumarin (**3.40**) (Figure **3.38**).

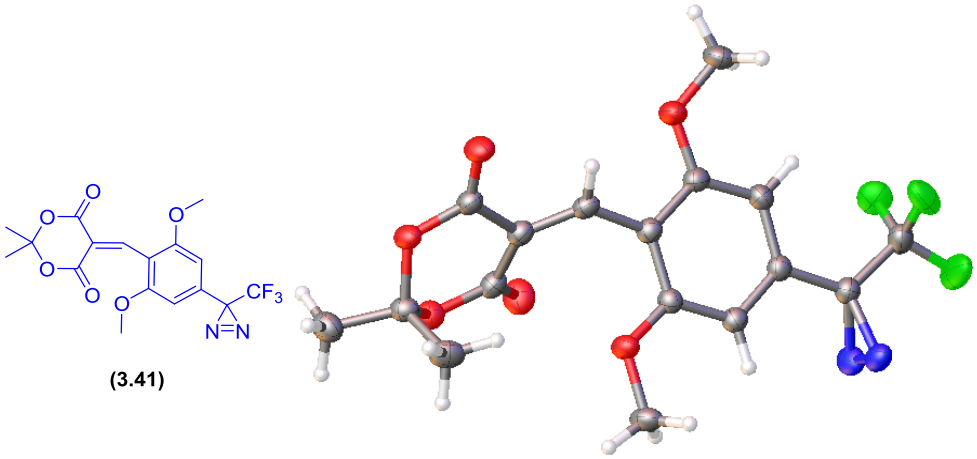

Figure 3.38: X-ray crystal structure of benzylidene (**3.41**).

Since the presence of an *ortho*-methoxy group in our starting material has prevented coumarin formation under these conditions, next the modified Tapia method with C-5 hydroxy trifluoromethyl diazirine (**3.12**) was evaluated. Therefore, C-5 hydroxy trifluoromethyl diazirine (**3.12**) was reacted with Meldrum's acid (**3.7**) (1 eq.) in DMF in

the presence of 20 mol % DIPEA at rt overnight. After which the reaction was acidified with sulfuric acid (0 °C to rt over 2 h) and poured over ice to crystallise. Pleasingly, the desired diazirine carboxycoumarin (**3.2**) was isolated by filtration in 74 % yield (Figure **3.39**).

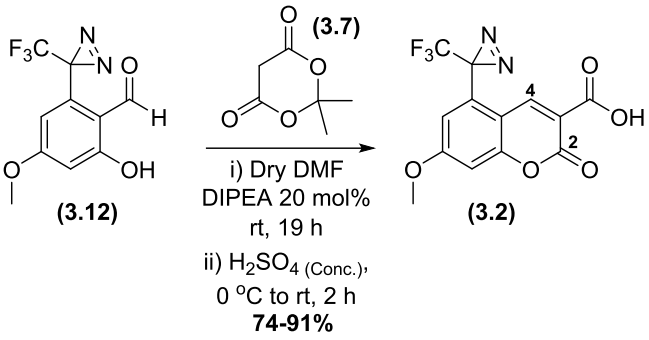

Figure 3.39: Synthesis of diazirine carboxycoumarin (**3.2**) via a modified Tapia method.

Crystals of diazirine carboxycoumarin (**3.2**) were grown by slow evaporation of an ethyl acetate solution. X-ray diffraction analysis showed that diazirine carboxycoumarin (**3.2**) had crystallised in the space group $Pca2_1$ with four molecules in the unit cell (Z = 4) (Figure **3.40**).

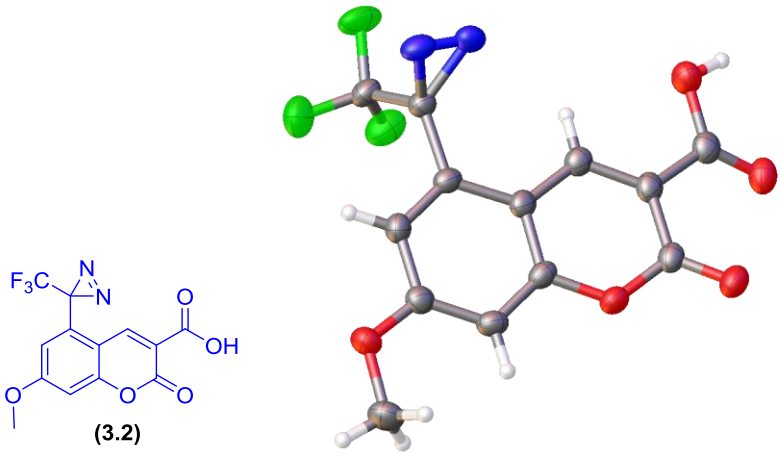

Figure 3.40: X-ray crystal structure of diazirine carboxycoumarin (**3.2**).

After confirming the structure of diazirine carboxycoumarin (**3.2**) I looked next to scale-up the synthesis of diazirine carboxycoumarin (**3.2**). This proved successful up to 4 mmol,

it should be noted that for the larger scale reaction an additional purification by silica plug or column chromatography was introduced to assist in drying the product for the next synthetic step, leading to some loss of yield (Table **3.11**).

Entry	Reaction Scale/mmol	Yield %	Entry	Reaction Scale/mmol	Yield %
1	0.76	74 %[a]	4	2.6	61%[a],[b]
2	1.0	90 %[a]	5	4.3	37%[a][c]
3	1.3	91 %[a]	-	-	-

Table 3.11: Synthesis of diazirine carboxycoumarin (3.2) via Tapia's method. [**a**] Purified by precipitation from ice water, [**b**] Purified by silica plug, [**c**] purified by column chromatography.

After synthesisng our desired diazirine carboxycoumarin (**3.2**) in gram quantities, our next task was to couple diazirine carboxycoumarin (**3.2**) to the amino acids of interest to complete the synthesis of our target probe molecule MCDTA (**3.3**).

3.2.6 Synthesis of Methoxy-coumarin Trifluoromethyl Diazirine D-Alanine (3.3) (MCTDA) through Amide Bond Forming Chemistry

Finally, I wished to investigate the last step in the synthesis of the target molecule, methoxy coumarin trifluoromethyl diazirine D-alanine (**3.3**) (MCTDA), via an amide bond forming reaction between our previously isolated diazirine carboxycoumarin (**3.2**) and 3-amino-D-alanine (**3.6**) (Figure **3.41**).

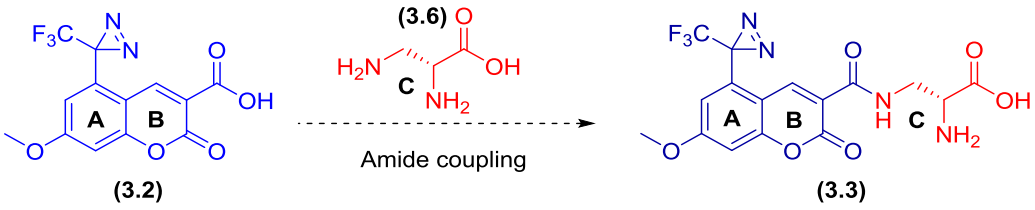

Figure 3.41: Planned synthesis of MCTDA via amide bond formation.

Our initial attempts focused on the conversion of diazirine carboxycoumarin (**3.2**) into the corresponding NHS ester, as a suitable coupling partner for 3-amino-D-alanine. Unfortunately test reactions, involving both the model substrate coumarin (**3.39**) (prepared previously) and diazirine carboxycoumarin (**3.2**) failed to provide clean

conversion to the corresponding NHS esters with the use of HATU or CDI as coupling agents. Next, direct coupling reactions was attempted between diazirine carboxycoumarin (**3.2**) and 3-amino-D-alanine (**3.6**) using HATU, however only complex product mixtures were observed.

3.2.6.1 Synthesis of Methoxy-coumarin Trifluoromethyl Diazirine D-Alanine (3.3) (MCTDA) through CDI Coupling with 3-Amino-D-Alanine (3.6)

Next CDI was investigated as an amide coupling reagent for the functionalisation of coumarins. Therefore, coumarin (**3.39**), as a model system, was activated with CDI in DMF for 2 h at rt, followed by overnight reaction with glycine methyl ester (**3.42**). After work up and column chromatography, coumarin glycinate methyl ester (**3.43**) was isolated in 92 % yield (Figure **3.42**).

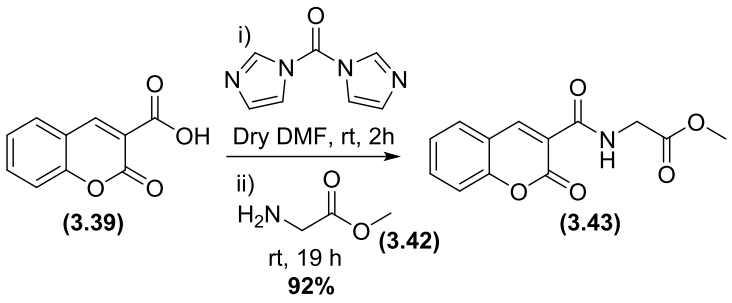

Figure 3.42: Synthesis of coumarin glycinate methyl ester (**3.43**).

As our test CDI coupling reaction had proven successful, next diazirine carboxycoumarin (**3.2**) was activated with CDI under the previous conditions, followed by reaction with 3-amino-D-alanine (**3.6**) (Figure **3.43**).

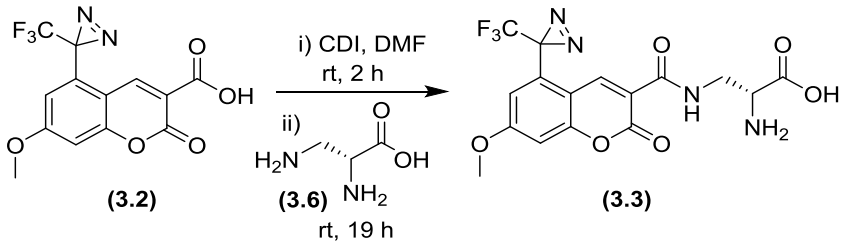

Figure 4.43: Planned synthetic route to investigate the CDI amide coupling between diazirine carboxycoumarin (**3.2**) and 3-amino-D-alanine (**3.6**).

Following work up the ^{1}H NMR spectrum of the crude reaction mixture showed the presence of several products and as such was further analysed by LC-MS (Lina Mardiana, Newcastle). Alongside unreacted starting material (22.9 min; *m/z* = 351.0223), a major (17.8 min; *m/z* = 415.0892) and minor peak (24.9 min; *m/z* = 415.0849) corresponding to two regioisomeric methoxy coumarin trifluoromethyl diazirine D-alanines (**3.3**) and (**3.44**), along with a further peak (27.9 min; *m/z* = 725.1055) corresponding to a 2:1 diazirine carboxycoumarin/3-amino-D-alanine adduct (**3.45**) (Figure **3.44**).

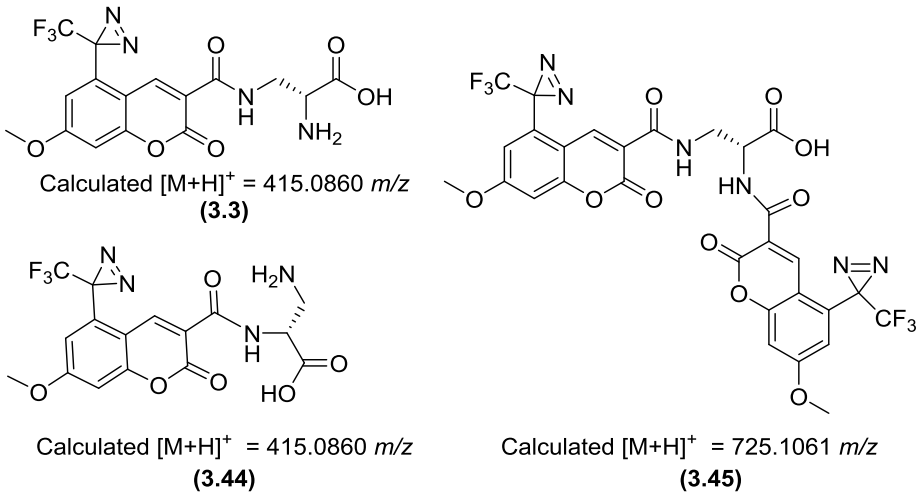

Figure 3.44: Products arising from the CDI coupling between diazirine carboxycoumarin (**3.2**) and 3-amino-D-alanine (**3.6**).

Due to the complex product mixture observed from CDI couplings with the bi-functional 3-amino-D-alanine (**3.6**), next it was decided to examine suitably protected versions of our amino acid to help to control the regioselectivity of this reaction.

3.2.6.2 Synthesis of Coumarin-D-alanine (3.48) through CDI Coupling with *α*-Boc Protected 3-Amino-D-Alanine (3.47) and Boc Deprotection

Next it was planned to test the CDI coupling of *α*-Boc protected 3-amino-D-alanine (**3.47**) with our model compound coumarin (**3.39**). Thus, coumarin (**3.39**) was activated with CDI and reacted with *α*-Boc protected 3-amino-D-alanine (**3.47**) under the previous reaction conditions. Following work up and column chromatography (buffered with 0.01% triethylamine) the desired coumarin-*α*-*N*-Boc-D-alanine (**3.46**) was isolated in a 19 % yield, assigned as the triethyl ammonium salt by integration analysis of the ^{1}H NMR spectrum (Figure **3.45**).

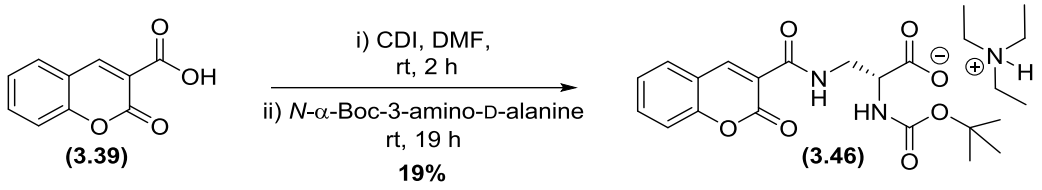

Figure 3.45: Synthesis of coumarin-*α*-*N*-Boc-D-alanine (**3.46**) via CDI coupling.

To confirm the molecular structure of coumarin-*α*-*N*-Boc-D-alanine (**3.46**), crystals were grown by slow evaporation of chloroform solution and a suitable crystal was subjected to X-ray diffraction analysis. Interestingly the crystal contained the free acid form of coumarin-*α*-*N*-Boc-D-alanine (**3.46**), possibly due to loss of trimethylamine during the crystallisation under slow evaporation conditions (Figure **3.46**).

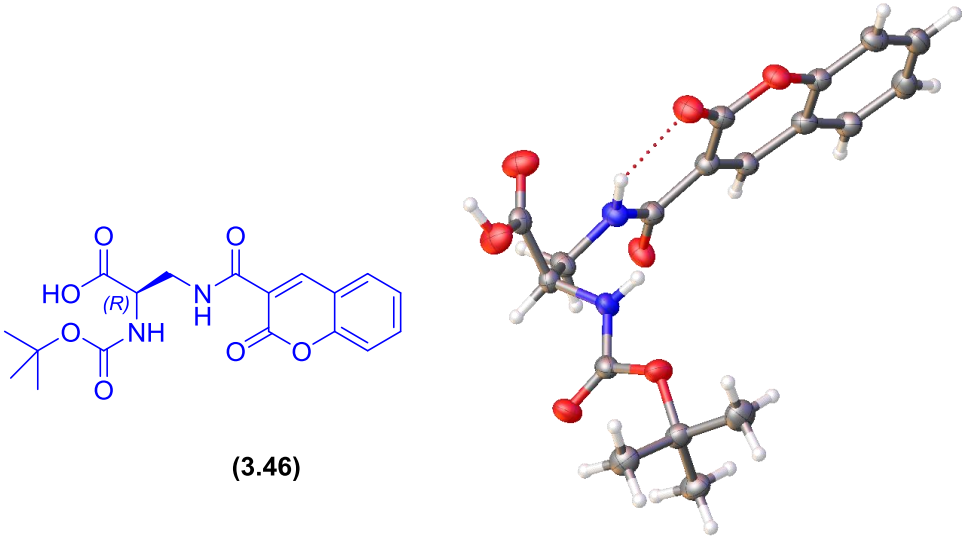

Figure 3.46: X-ray crystal structure of coumarin-*α*-*N*-Boc-D-alanine (**3.46**).

Next the removal of the Boc protecting group of coumarin-*α*-*N*-Boc-D-alanine (**3.46**) was examined, through treatment with TFA in DCM (1:1) for 30 min at rt. After work up and purification by reverse phase column chromatography (Biotage; C18 column, gradient elution in H_2O/MeCN) coumarin-D-alanine (**3.48**) was obtained in 37 % yield as the triethyl ammonium salt by integration analysis of the ^{1}H NMR spectra (Figure **3.47**).

.

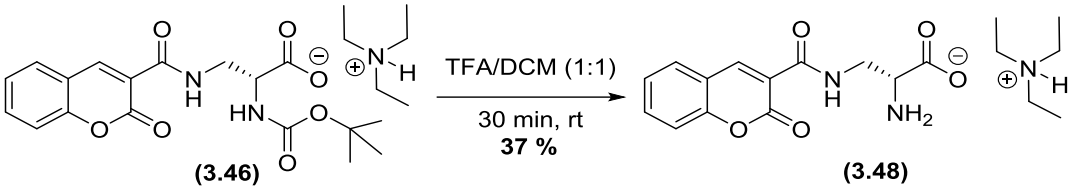

Figure 3.47: Synthesis of coumarin-D-alanine (**3.48**) via acid-mediated Boc deprotection.

The structure of our isolated amide (**3.48**) was confirmed by analysis of ^{1}H NMR spectrum (D_2O solvent), supported by COSY and HSQC experiments, showing the disappearance of the Boc group and the retention of two geminal coupled diastereotopic protons (H-2a/H-2b) at 3.96 (dd, *J* = 14.8, 4.5 Hz, 1H), and 3.88 (dd, *J* = 14.8, 6.3 Hz, 1H) (Figure **3.48**).

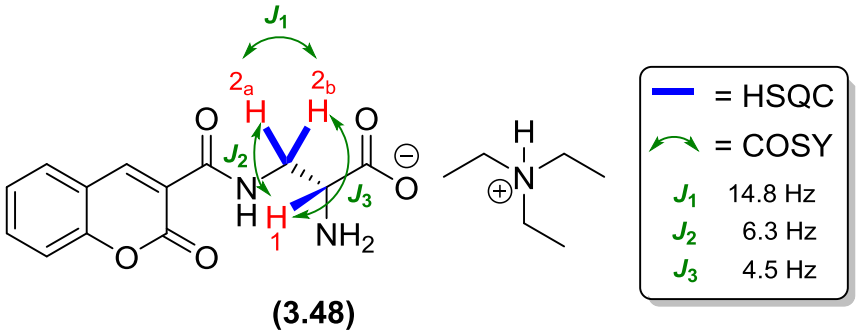

Figure 3.48: NMR analysis of coumarin D-alanine (**3.48**).

Following a successful two step CDI coupling/Boc deprotection to make coumarin D-alanine (**3.48**) I decided to use this chemistry in the synthesis of our target molecule MCTDA (**3.3**).

3.2.6.3 Synthesis of Methoxy-coumarin Trifluoromethyl Diazirine D-Alanine (3.3) (MCTDA) through CDI Coupling with *α*-Boc Protected 3-Amino-D-Alanine (3.47) and Boc Deprotection

Thus, in order to access methoxy coumarin trifluoromethyl diazirine D-alanine (**3.3**) (MCTDA) via a two step CDI coupling/Boc protection approach, first diazirine carboxycoumarin (**3.2**) was activated with CDI in DMF, followed reaction with *α*-Boc protected 3-amino-D-alanine (**3.47**) under the previous reaction conditions. Following work up, analysis of the crude reaction mixture by LC-MS analysis which showed a major peak with *m/z* = 515.1429 corresponding to diazirine coumarin-*α*-*N*-Boc-D-alanine (**3.49**) [Calculated: $C_{21}H_{22}F_3N_4O_8$ $[M+H]^+$: 515.1390].

Therefore, in our next step the Boc group of diazirine coumarin-*α*-*N*-Boc-D-alanine (**3.49**) was deprotected through treatment of the crude reaction material from the CDI coupling with TFA in CH_2Cl_2 (1:1) for 30 min at rt. Following work up and purification by reverse phase chromatography (Biotage; C18 column; gradient elution in H_2O/MeCN, 0.1 % FA) three separate fractions were identified which correlated closely with the desired product by ^{1}H NMR spectroscopy, this may be due to the formation of both the trifluoroacetate and formate salts alongside the free base of methoxy coumarin trifluoromethyl diazirine D-alanine (**3.3**) (MCTDA). The most promising fraction was therefore redissolved in methanol-d4 containing added TFA for further analysis as the trifluoroacetate salt, with ^{1}H and ^{13}C NMR spectroscopic analysis showed this to be the desired trifluoroacetate salt of MCTDA (**3.3**). The ^{1}H NMR spectrum showed a key signal at 4.32 (dd, *J* = 6.6, 4.0 Hz, 1H), suggesting an *α*-proton coupled to two inequivalent protons. Furthermore, two signals at 4.11 (dd, *J* = 14.6, 4.0 Hz, 1H) and 3.94 (dd, *J* = 14.6, 6.7 Hz, 1H) were observed suggesting two diastereotopic protons coupled to the *α*-proton at 4.32 ppm (Figure **3.48A**). Furthermore, the ^{1}H NMR spectrum showed two aromatic protons at 7.44 (d, *J* = 2.4 Hz, 1H), and 7.22 (d, *J* = 2.4 Hz, 1H), suggesting an aromatic system with 1,3 substitution. And the ^{1}H NMR spectrum showed a signal at 9.40 (s, 1H) which could be associated with an aromatic proton within an *α*-*β* unsaturated environment.

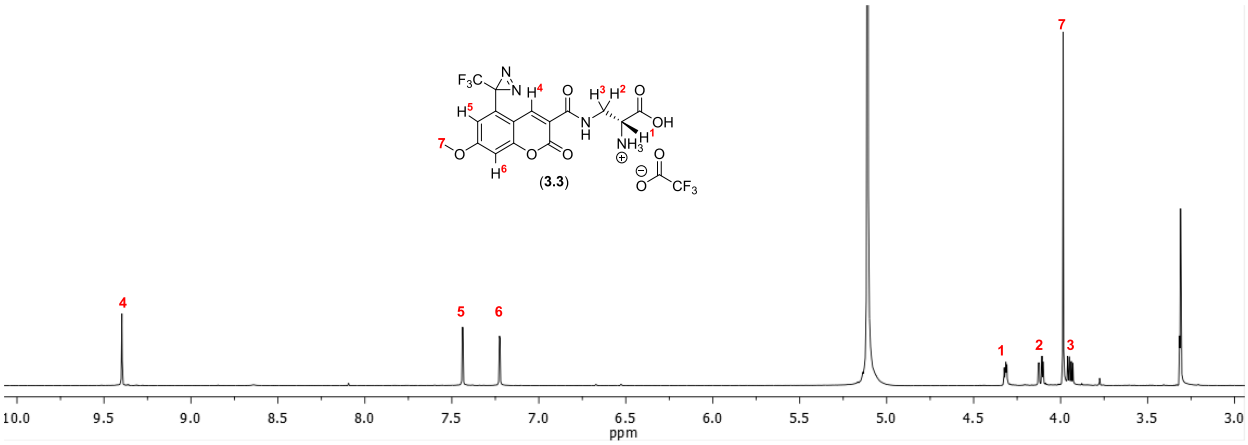

Figure 3.48A: ^{1}H NMR spectrum of MCTDA (**3.3**).

Finally, the presence of MCTDA (**3.3**) being supported by mass spectrometry, showing the expected molecular ion $[M+H]^{+}$ = 415.0338 *m/z* (Figure **3.49**).

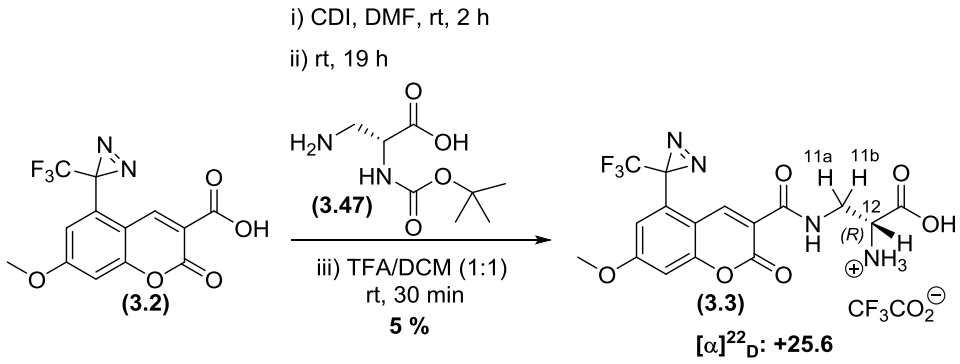

Figure 3.49: Synthesis of methoxy-coumarin trifluoromethyl diazirine-D-alanine (MCTDA).

The optical activity of MCTDA (**3.3**) was measured after recovery from methanol-d4/TFA in methanol (13 mg / 2.6 mL) at 22 °C to give $[\alpha]^{22}_{D}$: +25.6 (c 0.5, MeOH).

3.2.6.4 Synthesis of Methoxy-coumarin Trifluoromethyl Diazirine L-Alanine (3.4) (MCTLA) through CDI Coupling with *α*-Boc Protected 3-Amino-D-Alanine (3.47) and Boc Deprotection

Following the synthesis of our desired photoactivatable probe MCTDA (**3.3**), we next wished to synthesise its enantiomer the L-isomer MCTLA (**3.4**) to provide a control compound for later biological experiments. Thus, following a modification of our previous procedure, we activated diazirine carboxycoumarin (**3.2**) with CDI (1.5 eq.) followed by

reaction with *N*-α-Boc-3-amino-L-alanine (**3.47**) (1.5 eq.) for 19 h at rt. Following work up, the obtained crude reaction material was reacted with TFA in CH_2Cl_2 for 30 min at rt, concentrated and purified by reverse phase chromatography (Biotage; C18 column; gradient elution in H_2O/MeCN, 0.1 % FA). Analysis of the fractions by ^1H NMR spectroscopy in methanol-d4/TFA allowed the identification of the desired product MCTLA (**3.4**) as a trifluoroacetate salt, obtained in 20 % yield from the reaction (Figure **3.50**).

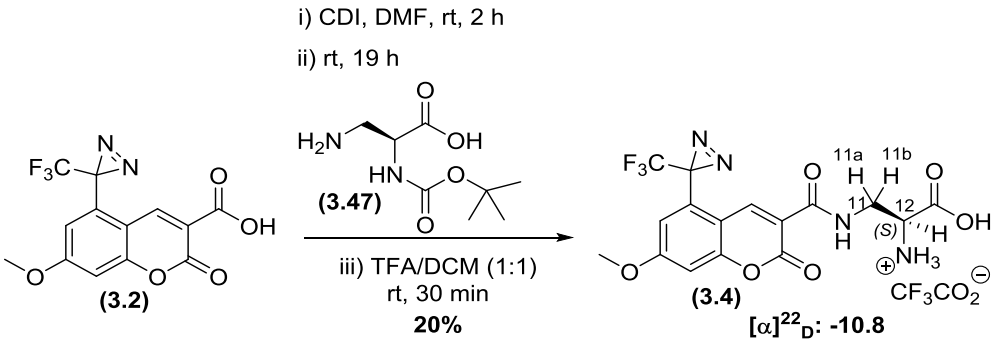

Figure 3.50: Synthesis of methoxy coumarin trifluoromethyl diazirine-L-alanine (MCTLA).

The optical activity of MCTLA (3.4) was measured after recovery from methanol-d4/TFA in methanol (13 mg / 2.6 mL) at 22 °C to give $[\alpha]^{22}_D$: -10.8 (c 0.5, MeOH), showing the opposite sign to that observed for MCTDA (3.3). Note that there is a significant difference in the magnitude of $[\alpha]^{22}_D$ values for MCTDA (+25.6) and MCTLA (-10.8), this maybe due to the prescence of small quantities of optically active impurities in the samples. Future work will involve verification of the enantiopurity by chiral HPLC.

3.3 Conclusion

The aim of this chapter was the synthesis of the fluorescent and photoactivatable amino acid, methoxy coumarin trifluoromethyl diazirine D-alanine (**3.3**) (MCTDA) and methoxy coumarin trifluoromethyl diazirine L-alanine (**3.4**) (MCTLA) as probes for the bacterial cell wall biosynthesis. A 10 step linear synthesis of MCTDA/MCTLA with overall yields of 2 % and 6 % respectively have been successfully developed (Figure **3.51**).

Although only a few 10's of milligrams of both MCTDA (**3.3**) and MCTLA (**3.4**) were prepared, however, this was sufficient to move forward to explore the enzymatic (LdtD) incorporation of these molecular probes into the bacterial cell wall (PG) of *E. coli* as described in the next chapter.

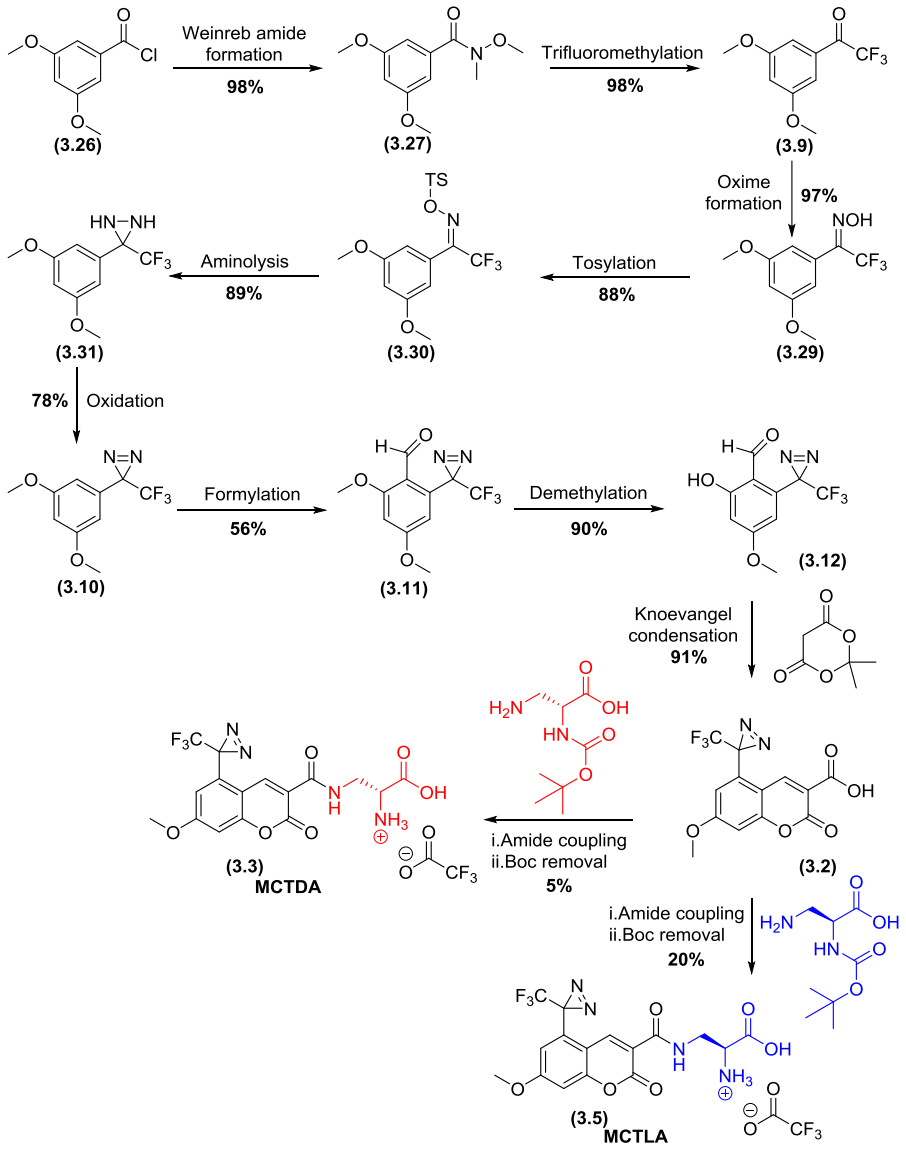

Figure 3.51: Synthesis of MCTDA (**3.3**) and MCTLA (**3.4**) starting from 3,5-dimethoxybenzoyl chloride (**3.26**).

3.4 References

1- E. Kuru, H. Hughes, P. Brown, E. Hall, S. Tekkam, F. Cava, M. de Pedro, V Brun, and M. VanNieuwenhze, *Angew. Chem., Int. Ed*., 2012, **51**, 12519-12523

2- T. Tomohiro, A. Yamamoto, Y. Tatsumi and Y. Hatanaka, *Chem. Commun.*, 2013, **49**, 11551.

3- R. Salvador, R., Saucier, *Tetrahedron.*, 1971, **27**, 1221-1226.

4- K. Korvinson, H. Akula, C. Malinchak, D. Sebastian, W. Wei, T. Khandaker, M. Andrzejewska, B. Zajc, and M. Lakshman, *Adv. Synth. Catal*., 2020, **362**, 166-176.

5- N. Kirai, and Y. Yamamoto, *Eur. J. Org*., 2009, **12**, 1864-1867.

6- J. Garst, M. Soriaga, *Coord. Chem. Rev*., 2004, **248**, 623-652.

7- S. Xia, L. Gan, K. Wang, Z. Li, and D. Ma, *J. Am. Chem. Soc*., 2016, **138**, 13493-13496.

8- M. Goebel and C. Marvel, *J. Am. Chem. Soc*., 1933, **55**, 1693-1696.

9- C. Walling and S. Buckler, *J. Am. Chem. Soc*., 1955, **77**, 6032-6038.

10- D. Rudzinski, C. Kelly and N. Leadbeater, *Chem. Commun*., 2012, **48**, 9610-9612.

11- R. Singh, G. Cao, R. Kirchmeier, and J. Shreeve., *J. Org. Chem.* 1999, **64**, 2873-2876.

12- J. Wiedemann, T. Heiner, G. Mloston, G. Prakash, and G. Olah, *Angew. Chem. Int. Ed*., 1998, **37**, 820-821.

13- S. Nahm and S. Weinreb, *Tetrahedron Lett*., 1981, **22**, 3815-3818.

14- A. Blencowe, N. Caiulo, K. Cosstick, W. Fagour, P. Heath, and W. Hayes, *Macromolecules*, 2007, **40**, 439-449.

15- J. Brunner, H. Senn and F. Richards, *J. Biol. Chem*., 1980, **255**, 3313-3317.

16- Y. Zeifman, E. Abduganiev, E. Rokhlin, and I. Knunyants, *Russ. Chem. Bull.*, 1972, **21**, 2667-2671.

17- A. Blencowe, K. Cosstick, and W. Hayes, *New. J. Chem.*, 2006, **30**, 53-58.

18- B. Raimer, P. Jones, and T. Lindel, *J. Fluor. Chem*., 2014, **166**, 8-14.

19- A. Rieche, H. Gross, and E. Höft, *Org. Synth*., 1967, **47**,1.

20- A. Rieche, H. Gross, and E. Hoft, *Chem. Ber*., 1960, **93**, 88.

21- O. Kundrat, H. Dvorakova, V. Eigner, and P. Lhotak, *J. Org. Chem*., 2010, **75**, 407-411.

22- J. McOmie, M. Watts, and D. West, *Tetrahedron*., 1968, **24**, 2289-2292.

23- V. Armstrong, O. Soto, J. Valderrama, and R. Tapia, *Synth. Commun*., 1988, **18**, 717-725.

Chapter 4. Incorporation of Methoxy Coumarin Trifluoromethyl Diazirine D-alanine into the peptidoglycan of *E. coli* by LdtD Enzyme

4.1 Introduction

In our previous chapter a key fluorescent photoactivatable D-amino acid (**3.3**), methoxy coumarin trifluoromethyl diazirine D-alanine (MCTDA) was successfully synthesised in 10 synthetic steps. In this chapter the plan is to incorporate this MCTDA probe (**3.3**) into *E. coli* peptidoglycan (PG) *in vitro* as a model system for future incorporation into live bacteria (Figure **4.1**).

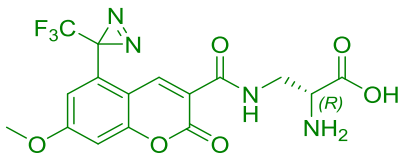

(3.3)

Figure 4.1: Methoxy coumarin trifluoromethyl diazirine D-alanine (MCTDA) (**3.3**).

In order to incorporate MCTDA into PG we plan to use a purified L,D-transpeptidase (Tpase) enzyme (LdtD), which is involved in the biosynthesis of PG including the exchange of terminal amino acids of the muropeptide subunit. Previous work[1,2] by VanNieuwenhze and Vollmer has shown that LdtD is a promiscuous enzyme which can accept many different amino acids including synthetic amino acid mimics, and can incorporate these synthetic amino acids into the muropeptide subunits. Thus our first challenge is to determine if LdtD will accept our photoactivatable probe (MCTDA) as a substrate and thus promote exchange of the native terminal amino acid (D-ala) with MCTDA for either the Tetra muropeptide or the Tetra-Tetra(4-3) muropeptide of the PG (Figure **4.2**).

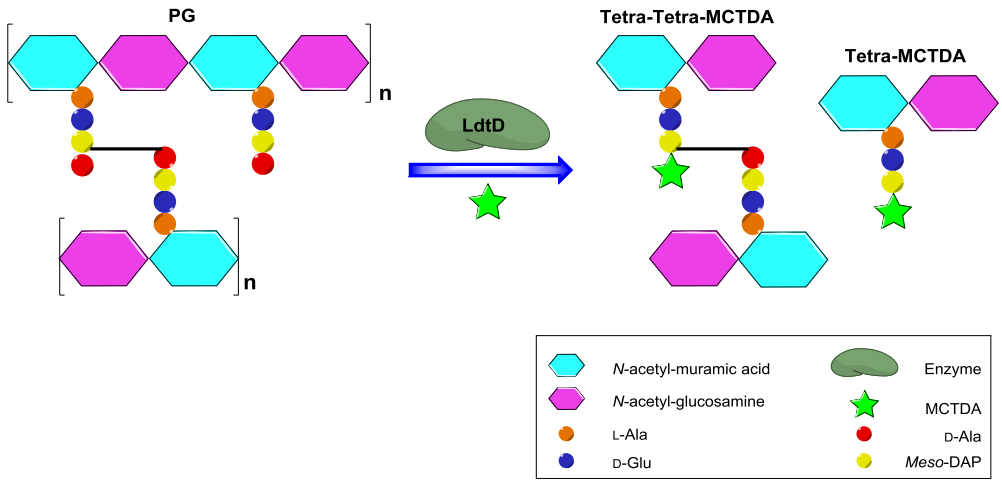

Figure 4.2: Planned *in vitro* enzymatic incorporation of MCTDA into PG by LdtD.

Therefore, the incorporation of our methoxy coumarin trifluoromethyl diazirine D-alanine probe (**3.3**) (MCTDA) into *E. coli* PG in the presence of LdtD was investigated first.

It should be noted that the enzymatic incorporation experiments (MP/LdtD/MCDTA) and associated analytical and semi-preparative HPLC discussed in this chapter were carried out in close collaboration with Matthais Winkle (Centre of Bacterial Cell Biology, Institute for Cell and Molecular Biosciences, Newcastle University). In addition, the LC-MS/MS experiments discussed in this chapter were carried out by Dr Joe Gray (Pinnacle Laboratories, Institute for Cell and Molecular Biosciences, Newcastle University).

4.2 Examination of the Incorporation of MCTDA into Isolated *E. coli* PG by LdtD

Herein, I planned to test the enzyme-mediated incorporation of our methoxy coumarin trifluoromethyl diazirine D-alanine probe (**3.3**) (MCTDA) into isolated PG from *E. coli* (Δ6PG). In addition, I will also examine the incorporation of our previously synthesised methoxy coumarin trifluoromethyl diazirine L-alanine probe (**3.4**) (MCTLA) by LdtD, as a potential negative control, and the incorporation of glycine (**4.1**) as a further positive control (Figure **4.3**).

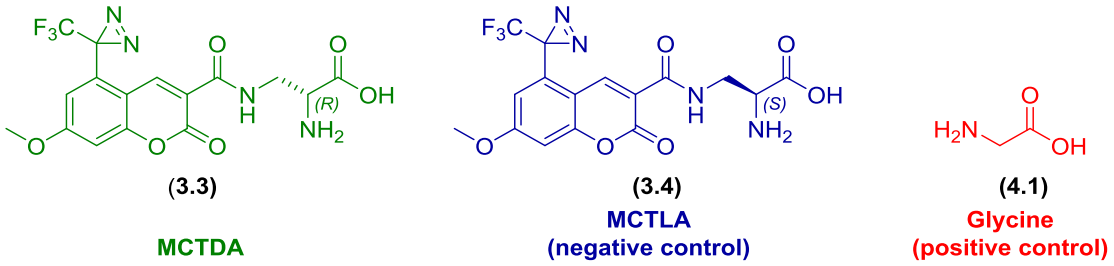

Figure 4.3: Molecular structures of MCTDA (3.3), MCTLA (**3.4**) and glycine (**4.1**).

Therefore, the incorporation of MCTDA (**3.3**) into the isolated PG (*E. coli* Δ6PG) was tested with LdtD. Our PG incorporation experiment involved the incubation of 5 µL of MCTDA (100 mM in DMSO) with 4.1 µL of LdtD (24.2 µM in aqueous buffer) and 4.1 µL of a buffer solution containing approximately 100 µg of PG (*E. coli* Δ6PG). The resulting mixture was incubated for 3 h at 37 °C, and then heated for 10 min at 100 °C to inactivate LdtD and to stop the experiment.

In order to facilitate subsequent HPLC analysis the modified PG must be digested into its constituent muropeptides. Thus, the glycan backbone was cleaved through incubation with 50 µL cellosyl buffer (muramidase also called *N*-acetyl-*β*-D-muramidase, final concentration 20 µg/ml in 20 mM sodium phosphate buffer, 0.02 % sodium azide) overnight at 37°C, heated for 10 min (100 °C) and centrifuged to remove precipitated denatured cellosyl. The resulting modified muropeptides were reduced with sodium borohydride in order to reduce the open chain form of *N*-acetylmuramic acid (NAM), and thus simplify later HPLC analysis. The excess sodium borohydride was then quenched with orthophosphoric acid and samples were submitted to HPLC analysis (Figure **4.4**).[3,4,5]

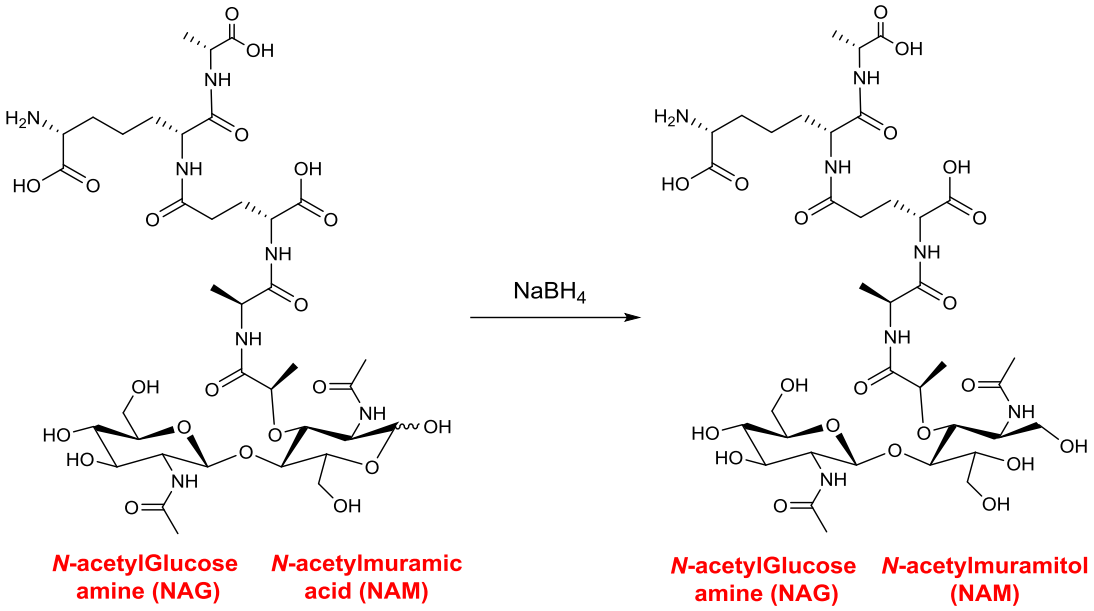

Figure 4.4: $NaBH_4$ reduction of the tetra muropeptide, a subunit of PG.

This enzymatic incorporation procedure was repeated with both MCTLA, as a negative control, and glycine, as a positive control, to check the specificity and activity of LdtD respectively. Further negative controls were prepared by the incubation of isolated PG (*E. coli* Δ6PG), MCTLA or MCTDA as individual components with buffer (HEPES, NaCl, TX-100), and isolated PG (*E. coli* Δ6PG) with LdtD and buffer. It should be noted that in control experiments containing no probe, 5 µL of DMSO was included to maintain the solvent mixture.

Analysis of the LtdD incorporation experiments was undertaken using the standard HPLC method developed by Glauner *et al.*.[5] HPLC analysis of native PG (*E. coli* Δ6PG) showed the presence of the expected Tetra and Tetra-Tetra (3-4) muropeptides at 27 and 42 min respectively (Figure **4.5,a**).[4] PG, following treatment with LdtD, showed a decrease Tetra (27 min) and a new peak at 38 min corresponding to a cross-linked product of LdtD, Tetra-Tri (3-3) (Figure **4.5,b**). Furthermore PG, with LdtD and glycine, showed two new signals at 22 and 42 min, corresponding to Tetra-glycine (Tetra Gly4) and Tetra-Tri-glycine (Tetra-Tri (3-3)) Gly4) respectively. This confirmed that the LdtD I had used in our experiments was capable of forming cross-linking products and of swapping the terminal D-ala of Tetra for added glycine (Figure **4.5, g**).

In our attempted probe incorporation experiments, the HPLC chromatogram of PG with LdtD and MCTDA appeared very similar to that of PG with LdtD, suggesting that no significant incorporation of MCTDA had occurred in this experiment (Figure **4.5, c**). In additional control experiments neither MCTDA (**3.3**) or MCTLA (**3.4**) as a single component could not be observed in the HPLC, suggesting that the HPLC method was not suitable for the analysis of MCTDA/MCTLA (Figure 4.5d, 4.5f). Furthermore PG, with LdtD and MCTDA, also showed no significant changes verses PG with LdtD, showing no incorporation.

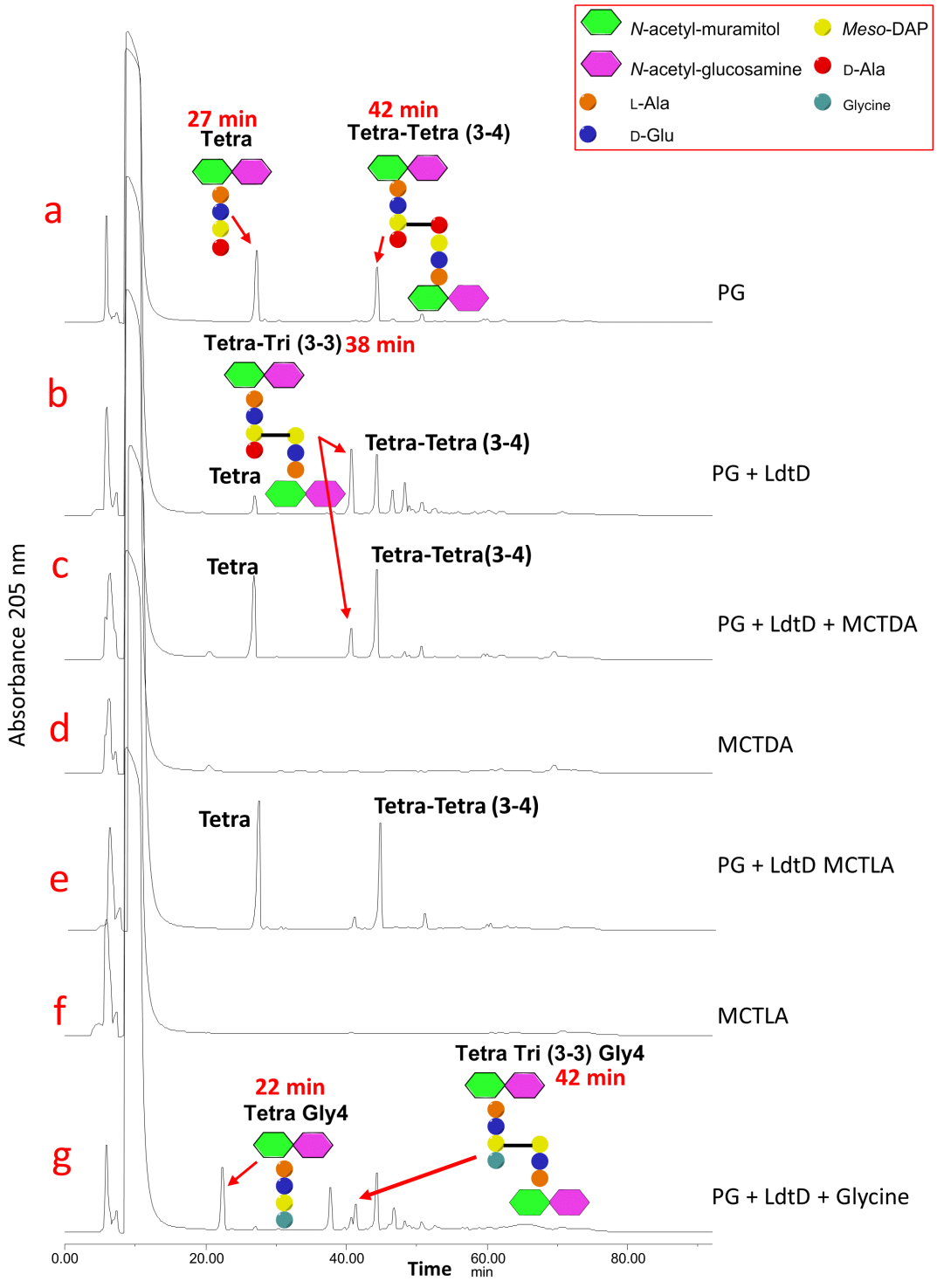

Figure 4.5: HPLC results of LtdD mediated incorporation experiments on PG isolated from *E. coli*. (**a**) PG only. (**b**) PG and LdtD. (**c**) PG, LdtD and 10 mM of MCTDA. (**d**) MCTDA only. (**e**) PG, LdtD and 10 mM of MCTLA. (**f**) MCTLA only. (**g**) PG, LdtD and 10 mM of glycine.

In conclusion our probe incorporation experiments have failed to show any uptake of either MCTDA or MCTLA. Assuming that LdtD is capable of accepting MCTDA as a substrate, the lack of incorporation of the probe is likely due to a number of experimental factors. These could include:

(i) PG (*E. coli* Δ6PG). The poor solubility and highly complex nature of native PG from *E. coli* Δ6PG is likely to complicate both probe incorporation and subsequent sample processing and HPLC analysis, thus for future experiments an isolated muropeptide (*E. coli* Δ6PG) will be used.

(ii) Probe concentration (10 mM final concentration in incorporation experiment). During our initial incorporation experiments we observed precipitation of MCTDA and MCTLA probes. Therefore, for future experiments we will employ lower concentrations following solubility testing in appropriate buffer solutions.

(iii) Thermal degradation of MCTDA/MCTLA. Due to the presence of a sensitive diazirine functional group in our probes, we were concerned that the chemical decomposition may have occurred during either the incubation (37 °C/3 h) or enzyme inactivation (100 °C/10 min x2) steps. Therefore, we planned to test the thermal stability of MCTDA/ MCTLA under these conditions.

(iv) HPLC conditions. The HPLC conditions used are design for standard muropeptide analysis, however MCTDA/MCTLA labelled muropetpides are likely to be significantly more lipophilic and thus may require extended HPLC run times.

4.3 Optimisation of MCTDA/MCTLA Probe Incorporation Conditions

Therefore, next we worked to examine conditions for the MCTDA/MCTLA probe incorporation in order to eliminate potential experimental problems.

4.3.1 Initial Testing of Maximum MCTDA/MCTLA Probe Concentration

Therefore, the solubilities of MCTDA and MCTLA in three different buffer solutions were tested, all of which could be employed in LdtD probe incorporation experiments (HEPES, TRIS and sodium phosphate buffer), to set maximum concentration limits for future experiments.

Solubility tests involved the preparation of solutions containing MCTDA or MCTLA (1 mM), NaCl (100 mM), TX-100 (0.05 %), and either HEPES (20 mM), Tris (20 mM) or sodium phosphate (20 mM) buffers.

Significant precipitation was observed for solutions based on Tris buffer containing 1 mM MCTDA or MCTLA. In the case of solutions containing HEPES or sodium phosphate buffer some precipitation was also observed, suggesting that the probes (MCTDA or MCTLA) were near their solubility limit under these conditions. Therefore it can be concluded that HEPES and sodium phosphate buffer (SPB) would be our buffers of choice and that 1 mM would be the maximum concentration possible for MCTDA and MCTLA in future experiments.

4.3.2 Thermal Stability of MCTDA/MCTLA Probes in Solution

As discussed above the potential thermal instability of the MCTDA and MCTLA probes during our incorporation experiments was a concerning matter. A typical experimental approach for enzymatic incorporation of a probe into PG/muropeptides by LdtD involves incubation at 37 °C for 3 h, followed by enzyme inactivation for 10 minutes at 100 °C. Thus, I next planned to evaluate the thermal stability of the MCTDA and MCTLA under comparable conditions.

To maximize the lifetime of MCTDA/MCTLA in solution, it was decided that for further LdtD incorporation experiments the incubation times would be reduced to 1 hour and enzyme inactivation to 3 minutes. Therefore, the stability of our probes were tested under these new proposed conditions.

Thus, solutions of MCTDA or MCTLA dissolved in HEPES, TRIS and sodium phosphate buffer (SPB) buffers (prepared as previously), were incubated for 1 h at 37 °C, heated to 100 °C for 3 min and centrifuged (10 min). The resulting supernatants analysed by reverse phase TLC against reference samples of MCTDA and MCTLA. Pleasingly, no significant degradation of MCTDA or MCTLA could be observed under the conditions tested (Figure **4.6**)

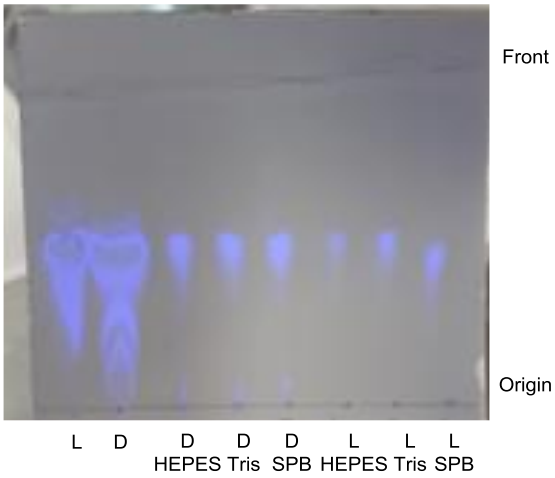

Figure 4.6: RP TLC (MeCN : H_2O (1:1)): (L) MCTLA in DMSO; (D) MCTDA in DMSO; (D HEPES) MCTDA incubated with HEPES; (D Tris) MCTDA incubated with Tris; (D SPB) MCTDA incubated with SPB; (L HEPES) MCTLA incubated with HEPES, (L Tris) MCTLA incubated with Tris, (L SPB) MCTLA incubated with SPB.

4.4 Incorporation of MCTDA into *E. coli* Muropeptide by LdtD

In our next experiments I planned to examine the incorporation of MCTDA into isolated muropeptide (*E. coli* Δ6PG) in different buffer systems. Due to their improved solubility and simplified HPLC analysis, it was decided to use isolated muropeptide in place of PG. I chose to evaluate both HEPES and sodium phosphate buffers, to restrict concentration of probe employed to 0.5 mM in order to maintain solubility, and to limit the incubation time to 1 h at 37 °C and LdtD inactivation to 3 min at 100 °C in order to prevent probe degradation.

4.4.1 Examination of the Incorporation of MCTDA into *E. coli* Muropeptide via LdtD in HEPES Buffer

First, the incorporation of MCTDA (**3.3**) into isolated muropeptide (*E. coli* 6ΔPG) by LdtD in HEPES buffer was investigated.

Therefore MCTDA was incubated with LdtD and muropeptide (*E. coli* 6ΔPG) in HEPES buffer for 1 h at 37 °C. Following which LdtD was inactivated by heating for 3 min at 100 °C. The resulting modified muropeptides were then reduced with sodium borohydride as before, in order to reduce the open chain form of *N*-acetylmuramic acid (NAM) and

simplify the HPLC analysis. The obtained supernatant was treated with 20% formic acid and submitted for HPLC analysis. In parallel, a negative control experiment using MCTLA (**3.3**) (0.5 mM as a final concentration) with LdtD and muropeptide was undertaken under the same conditions.

In previous HPLC analysis, using the method of Glauner *et al.,* (buffer A: 50 mM sodium phosphate buffer and 10 mM NaN_3 in H_2O and buffer B: methanol : 75 mM sodium phosphate buffer (15 : 85)) designed for muropeptides purification, there were no observed peaks associated to our probe molecules in the corresponding control experiments.[5] This may be due to the lipophilic nature of the probes, thus based on preliminary RP TLC results, we decided to change the HPLC method used to one in which a higher organic solvent percentage was employed at the end of the method.

HPLC analysis of the enzymatic incorporation of MCTDA/MCTLA into muropeptide, via LdtD followed by sodium borohydride reduction of the resulting reaction material, shows several peaks attributable to the muropeptides along with a number of new peaks. In both the MCTDA and MCTLA experiments I assigned the three peaks at 24, 27 and 28 min to the Tetra, Tetra-Tri (3-3) and Tetra-Tetra (3-4) muropeptide subunits, based on their order of elution. It should be noted that the Tetra-Tri (3-3) results from crosslinking two Tetra monomers by the LdtD enzyme, confirming that the LdtD is active in these experiments. Interestingly in the case of MCTDA, two new split peaks were observed at 45 and 48 min, it is possible that these peaks correspond to modified muropeptide-MCTDA adducts. In addition, another peak was observed at 55 min, for which a corresponding peak can also observed in the MCTLA control reaction, which we have therefore assigned as unreacted probe. Thus, our new HPLC method appears to allow observation of the lipophilic probe molecules.

It should also be noted that two new peaks at 43 and 44 min could be observed in the experiment with MCTLA. These may correspond to modified muropeptide-MCTLA adducts or unincorporated probe molecules which have undergone other reaction chemistry, such as reduction with sodium borohydride (Figure **4.7**).

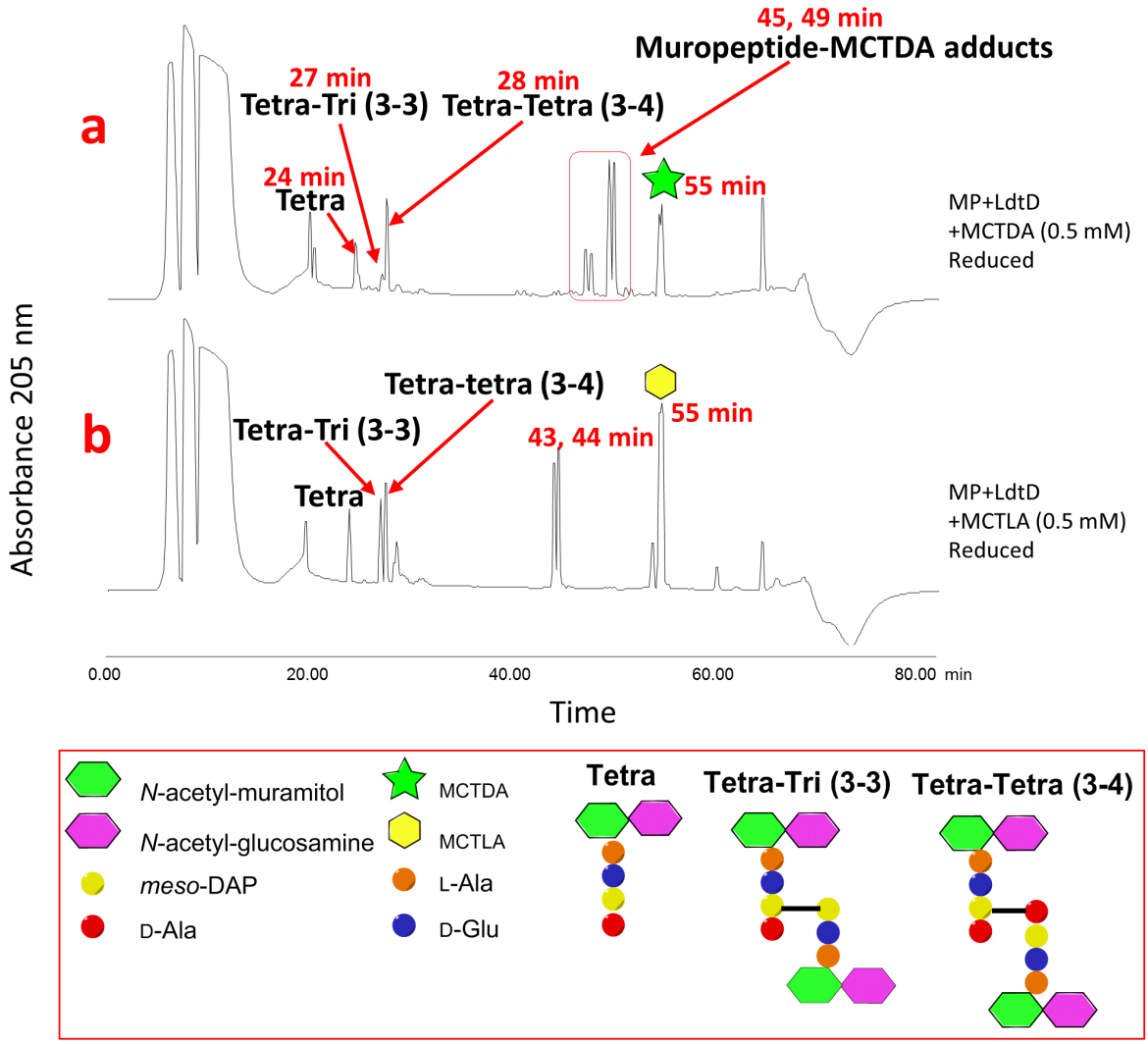

Figure 4.7: Overlay of HPLC results of $NaBH_4$ reduced reaction samples resulted after an enzymatic incorporation of MCTDA into *E. coli* muropeptide via LdtD (**a**) 0.5 mM MCTDA, LdtD, muropeptide (**b**) negative control of 0.5 mM MCTLA, LdtD, muropeptide. Samples were reduced with sodium borohydride before HPLC analysis.

In conclusion, our enzymatic incorporation experiment of MCTDA into *E. coli* muropeptide showed some promising HPLC results, since new peaks were observed not related to the native *E. coli* muropeptides (Tetra, Tetra-Tetra (3-4)), or simple LdtD derived muropeptide cross-linking products (Tetra-Tri (3-3)). However, the observation of splitting in these new peaks was concerning. I postulated that this might arise due to the formation of diastereomeric muropeptide-MCTDA adducts resulting from sodium borohydride

reduction of the probe moiety. Therefore, the next step was to examine the effect of sodium borohydride reduction on the products of the LdtD incorporation of MCTDA/MCTLA into muropeptides.

4.4.2 Examination of the Incorporation of MCTDA into *E. coli* Muropeptide via LdtD in HEPES Buffer without $NaBH_4$ Reduction

Therefore, we planned to repeat our previous MCTDA/MCTLA enzymatic incorporation experiment but without subjecting our obtained reaction mixture to sodium borohydride reduction, which is usually applied before HPLC analysis.

Thus, as before, the enzymatic incorporation experiment of both MCTDA/MCTLA into muropeptide were repeated in the presence of LdtD and HEPES (NaCl, TX-100), along with control experiments containing probe only. After incubation of the reaction mixture for 1 h at 37 °C, the sample was heated at 100 °C for 3 min, centrifuged and the reaction mixture treated with 20 % formic acid and submitted for HPLC analysis.

HPLC analysis of the non-reduced reaction material for both the MCTDA and MCTLA experiments showed the muropeptide subunits Tetra, Tetra-Tri (3-3), and Tetra-Tetra (3-4) at 26, 28, and 29 min respectively as before. Similar to our previous experiments, There was an observed peak at 57 min in the probes only and the MCTDA/MCTLA incorporation experiments which can be assigned to the unreacted probes (MCTDA/MCTLA). Excitingly, in the incorporation experiments with MCTDA I also observed two new peaks at 53 and 55 min, which were not present in the corresponding MCTLA experiment. I proposed that these new peaks might correspond to new muropeptide-MCTDA adducts formed by the action of LdtD (Figure **4.8, a**).

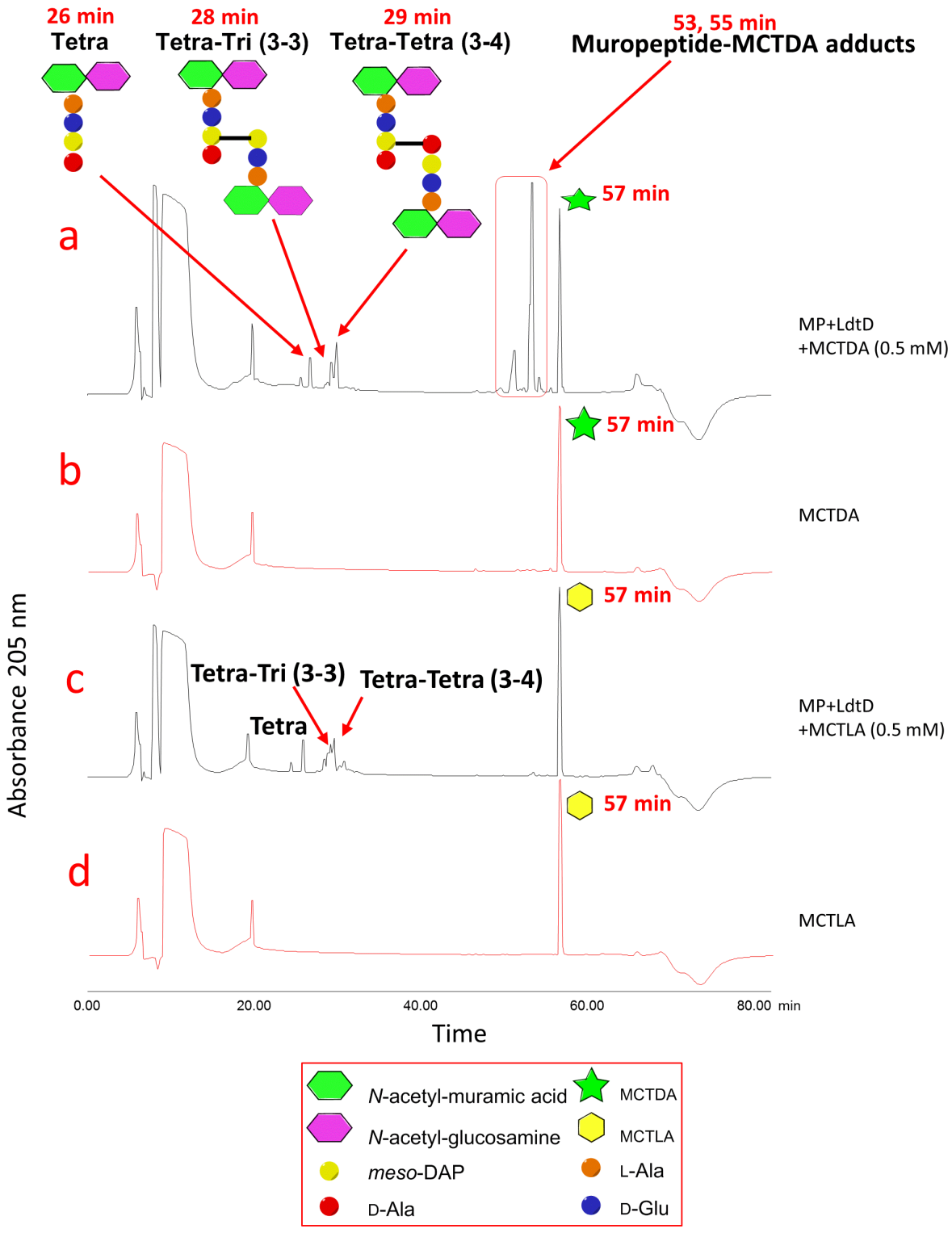

Figure 4.8: Overlay of HPLC results of non-reduced enzymatic incorporation of MCTDA into *E.coli* muropeptide, (**a**) 0.5 mM MCTDA, LdtD, muropeptide, non-reduced; (**b**) reference of MDTDA in DMSO, non-reduced; (**c**) negative control of MCTLA, LdtD, muropeptide, non-reduced; (**d**) reference of MDTLA in DMSO, non-reduced.

Based on our incorporation experiments with MCTDA/MCTLA into muropeptide, it appears that MCTDA is accepted as a substrate by the LdtD enzyme resulting in the formation of muropeptide-MCTDA adducts. However, the formation of muropeptide-MCTDA adducts will require further confirmation by mass spectrometry.

4.4.3 Examination of the Incorporation of MCTDA into *E. coli* Muropeptide via LdtD in Sodium Phosphate Buffer

Next, in order to extend the scope of the reaction conditions the incorporation of MCTDA/MCTLA into isolated muropeptide (*E. coli* 6ΔPG) by LdtD was investigated in the presence of sodium phosphate buffer in place of HEPES. For consistency with the literature, it was also decided to retain the $NaBH_4$ reduction step at this stage.

Therefore, the enzymatic incorporation experiment of both MCTDA/MCTLA into muropeptide was repeated as previously, in presence of LdtD and sodium phosphate buffer (NaCl, TX-100), along with control experiments including: probe (MCTDA/MCTLA) only, muropeptide only, muropeptide with LdtD, muropeptide with MCTDA/MCTLA but no LdtD. After incubation of each reaction mixture for 1 h at 37 °C, the samples were heated at 100 °C for 3 min, centrifuged, reduced with $NaBH_4$, centrifuged again and the resulting supernatants were treated with 20 % formic acid and submitted for HPLC analysis. The HPLC conditions were slightly modified to extend the elution time, particularly during the end of the run with high organic solvent content, to allow observation of nonpolar molecules related to our probes

Control experiments with muropeptide only, showed the expected peaks corresponding to the Tetra (27 min) and Tetra-Tetra (3-4) (32 min) muropeptide subunits (Figure **4.9, a**). Muropeptide and LdtD only, showed the presence of the cross-linked product Tetra-Tri (3-3) (31 min) showing that LdtD was active (Figure **4.9, b**). Experiments containing probe only, either MCTDA or MCTLA, both gave two split peaks (minor, 53 and 54 min and major, 67 and 68 min) and a further single peak (84 min). I suggest that these peaks are related directly to the probes themselves, the peak at 84 min corresponding to the chemically unchanged probes, whilst the split peaks may be due to diastereoisomers arising

from $NaBH_4$ reduction (Figure **4.9, c, f**). Our final control experiments, containing muropeptide and probe but no LdtD, showed only Tetra and Tetra-Tetra (3-4) muropeptide subunits (27 and 32 min), alongside native probes (84 min) and reduced probes (53, 54 min and 67, 68 min). This suggests that no incorporation of the probes occurs in the absence of LdtD (Figure **4.9, e, h**).

HLPC analysis of the muropeptide incorporation experiments with MCTDA/MCTLA, muropeptide and LdtD, showed a number of new peaks in the presence of MCTDA but not with MCTLA. These new split peaks, observed in the MCTDA incorporation experiment at 49 and 50, 60 and 61, 64 and 65 min, are likely due to the formation of new muropeptide subunits which have been labelled with MCTDA by action of LdtD. The lack of corresponding peaks in the MCTLA experiments suggests that LdtD is selective for the D-form of our probe molecules, as a mimic for the native D-amino acid substrates. Interestingly, in this muropeptide incorporation experiment with MCTDA, there was also an observed decrease in intensity of the peak corresponding to the cross-linked muropeptide Tetra-Tri (3-3), verses muropeptide and LdtD only control. This suggests that MCTDA may be in competition with the native substrates of the LdtD enzyme, reducing the rate of Tetra to Tetra-Tri (3-3) conversion (Figure **4.9, d**).

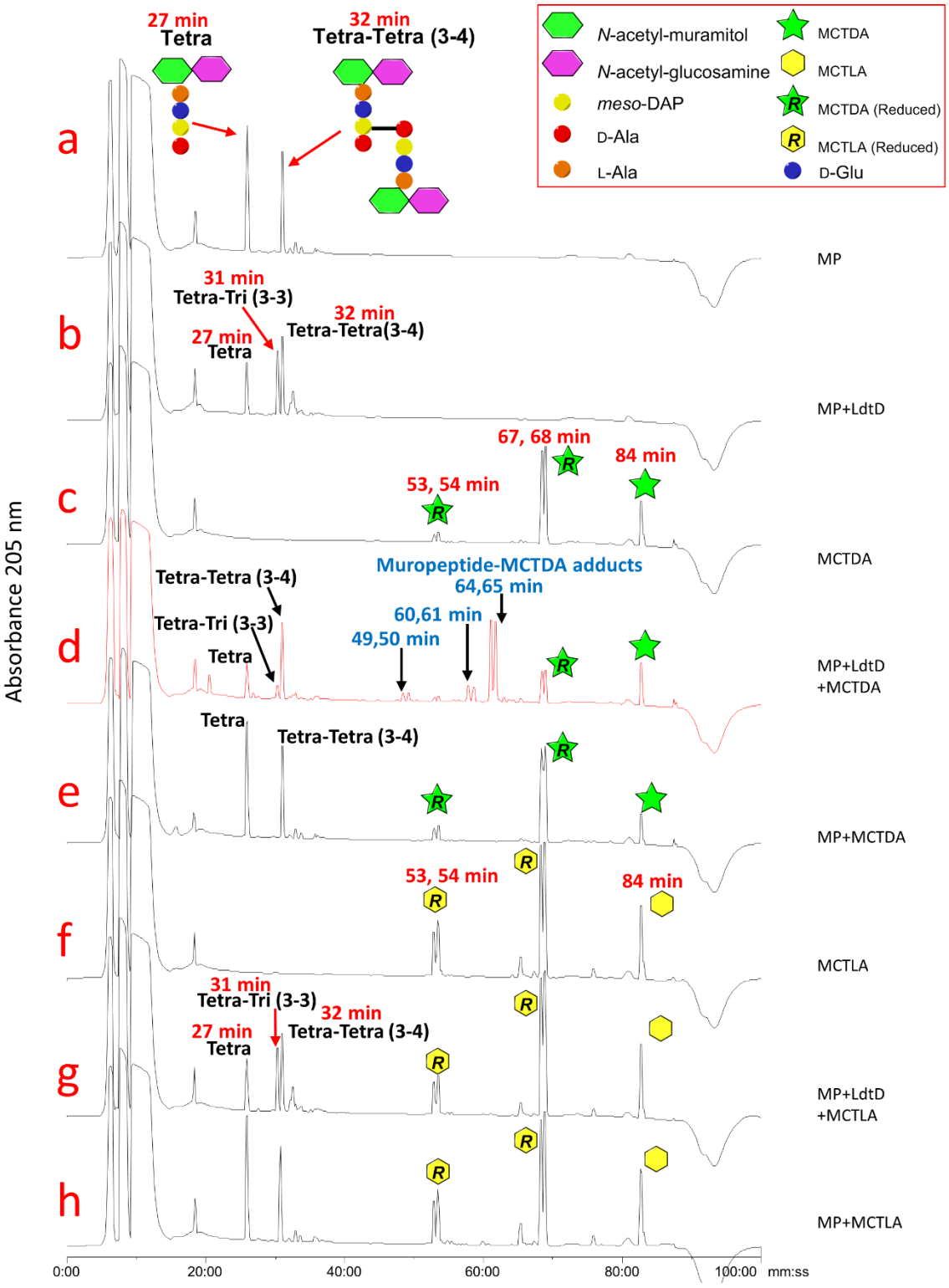

Figure 4.9: HPLC chromatograms proposed the formation of muropeptide-MCTDA adducts after MCTDA incubation with muropeptides isolated from *E. coli* and in presence of LdtD. All samples were reduced with sodium borohydride before HPLC analysis.

In conclusion, muropeptide incorporation experiments of MCTDA with LdtD in sodium phosphate has shown the formation of several postulated muropeptide-MCTDA adducts. Our next challenge being to establish the molecular structure of these molecules to understand both the biochemistry of incorporation of MCTDA into the muropeptide and the chemical impact of the use of $NaBH_4$ on the probes.

4.5 Isolation and Characterisation of Muropeptide-MCTDA Products

In order to determine the molecular structures of our postulated muropeptide-MCTDA adducts, formed through the LdtD mediated incorporation of MCTDA into muropeptide, our next challenge was to isolate postulated muropeptide-MCTDA adducts in sufficient quantities for LCMS analysis. To do this, it was first planned to repeat the previous successful LdtD incorporation experiment of MCTDA into muropeptide, in sodium phosphate buffer and with reduction with $NaBH_4$.

4.5.1 Incorporation of MCTDA into *E. coli* Muropeptide, via LdtD in Sodium Phosphate Buffer with Reduction, for LCMS Analysis

Therefore, the enzymatic incorporation of MCTDA into *E. coli* muropeptide was repeated in presence of LdtD in sodium phosphate buffer with reduction, to confirm our previous observations and to provide an analytic HPLC reference for subsequent semi-preparative HPLC. Following the previous incorporation protocol, two experiments were carried out. MCTDA was incubated with LdtD and *E. coli* muropeptide, alongside a control experiment involving MCTDA with muropeptide but without LdtD. After 1 h incubation at 37 °C and heating for 3 min at 100 °C, both experiments underwent $NaBH_4$ reduction, and the obtained reaction mixtures were subjected to analytical HPLC analysis, using the previous HPLC conditions.

HPLC analysis of the MCTDA incorporation into muropeptide via LdtD showed the expected three new split peaks as before (49 and 50 min, 60 and 61 min, 64 and 65 min) which I believe correspond to muropeptide-MCTDA adducts. In addition, three new peaks were also observed in both the incorporation and the control experiment, two split peaks at 53 and 54 min and 67 and 68 min as well as a peak at 84 min. I postulate that these peaks

are related to the unincorporated MCTDA probe, including reduced probe molecules (Figure **4.10**).

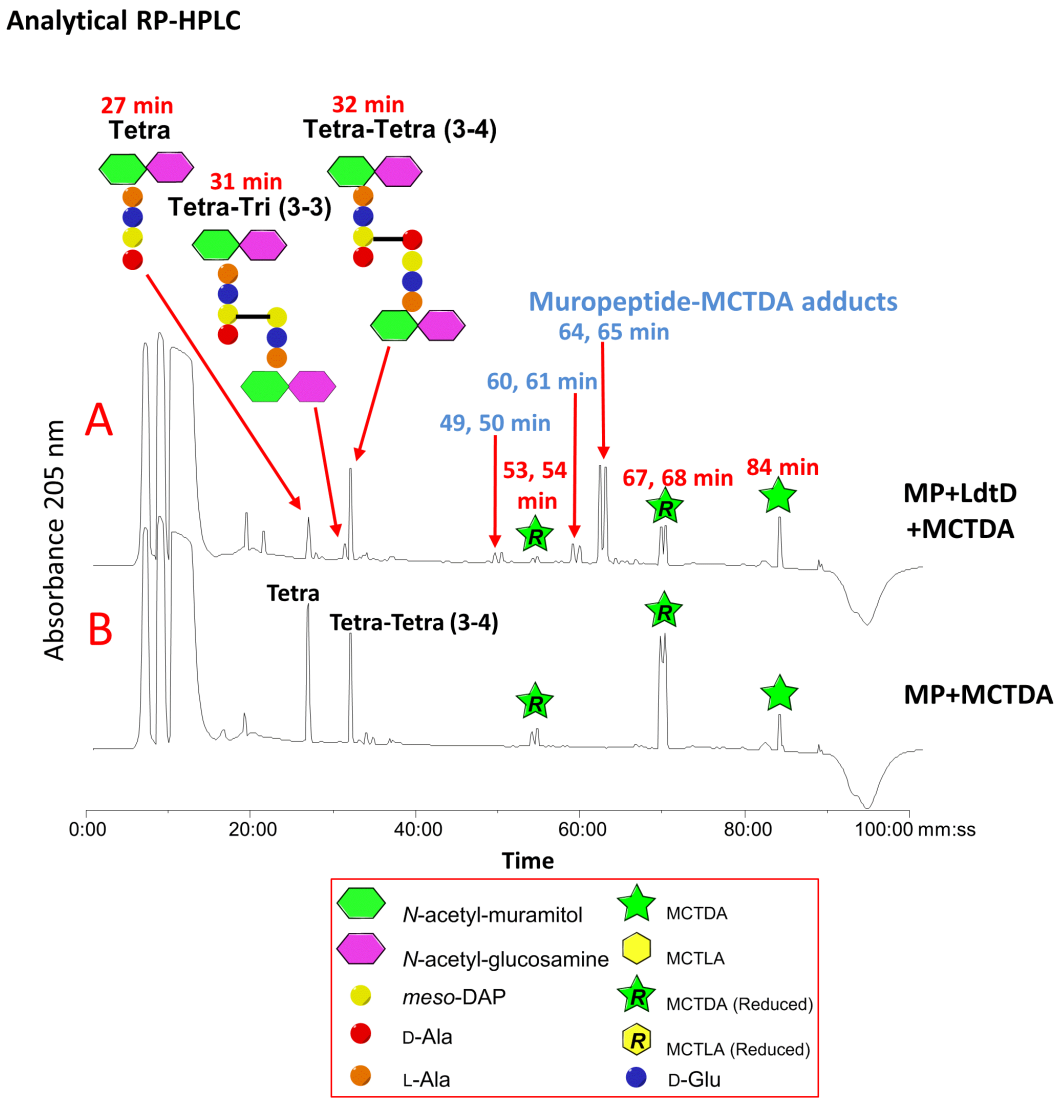

Figure 4.10: Results of analytical HPLC, (**A**) MCTDA enzymatic incorporation into *E. coli* muropeptide via LdtD in sodium phosphate buffer, (**B**) control experiment of MCTDA and muropeptide only. Both experiment reaction mixtures were reduced with sodium borohydride before HPLC analysis.

Since the analytical HPLC has shown that the peaks associated with both potential muropeptide-MCTDA adducts and with unincorporated MCTDA were separable, the enzymatic incorporation of MCTDA into *E. coli* muropeptide was repeated to allow isolation of these molecules via semi-preparative HPLC.

MCTDA incorporation experiment into muropeptide via LdtD was repeated as previously and then subjected to semi-preparative HPLC, using our previous HPLC conditions. Alongside the expected Tetra, Tetra-Tri (3-3), Tetra-Tetra (3-4) peaks, semi-preparative HPLC analysis of the MCTDA incorporation into muropeptide via LdtD showed the three new split peaks as before, at 49 and 50 min, 60 and 61 min, 64 and 65 min corresponding to potential muropeptide-MCTDA adducts. In addition, a major split peak at 67 and 68 min, corresponding to a potential unincorporated reduced MCTDA by-product, was also observed. The aforementioned four split peaks, corresponding to postulated muropeptide-MCTDA adducts and unincorporated reduced MCTDA by-products, were all collected from the semi-preparative HPLC experiment, were then dried by lyophilisation and submitted for LC-MS/MS (ESI-ITMS) analysis (Figure **4.11**).

Semi-preparative RP-HPLC - Peak Collection 49-68 min

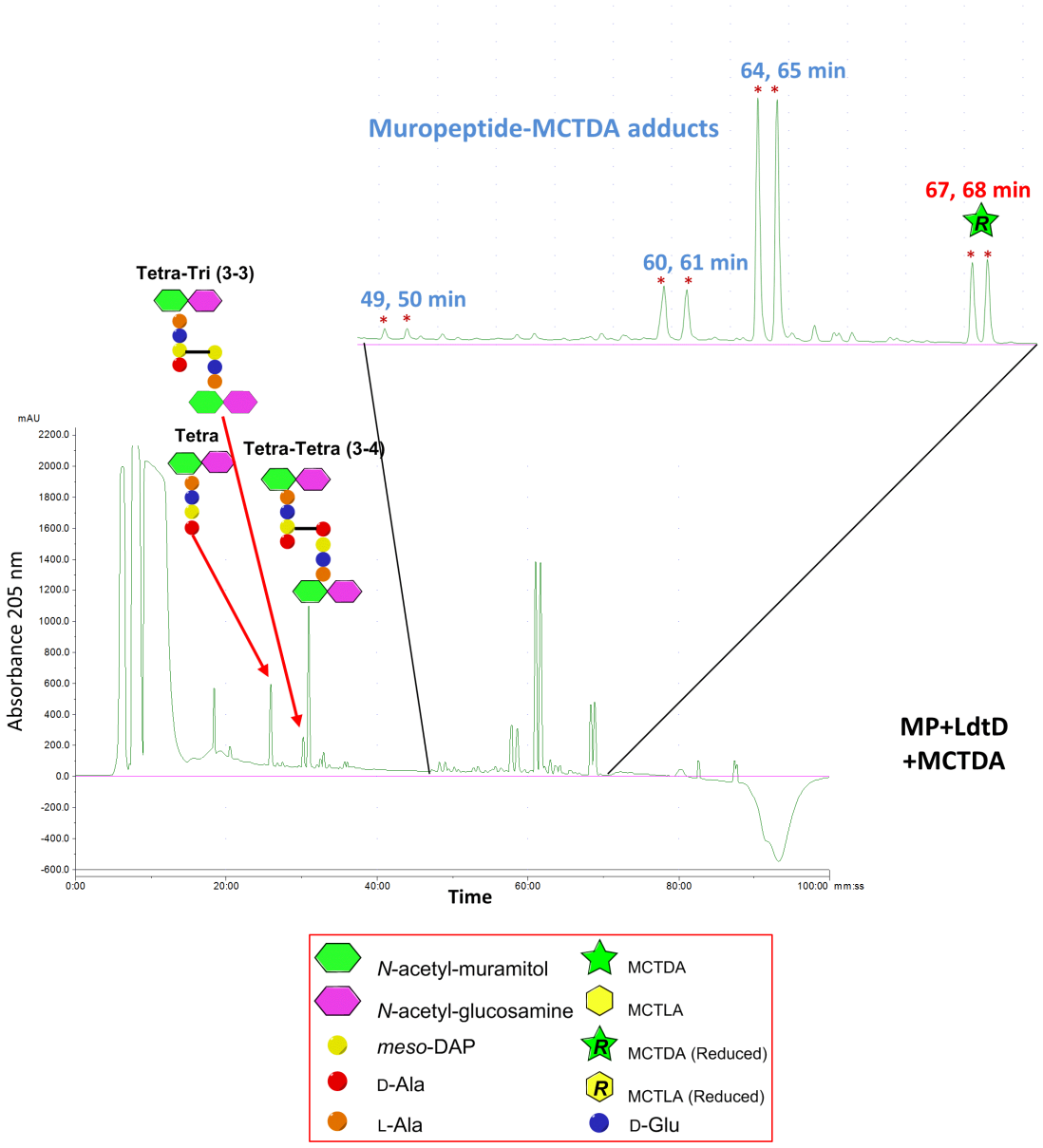

Figure 4.11: Semi-preparative RP-HPLC chromatogram of methoxy coumarin trifluoromethyl diazirine D-alanine probe (MCTDA) incorporation into *E. coli* muropeptide (MP) via LdtD.

4.5.2 LC-MS/MS Analysis of Muropeptide-MCTDA Adducts via LdtD Incorporation into Muropeptide with Reduction

In this section the LC-MS/MS analysis of each of the eight peaks (four split peaks) isolated by semi-preparative HPLC from the LdtD incorporation of MCTDA into muropeptide will be discussed. I anticipated that the four isolated split peaks maybe closely related molecules, therefore the data will be analysed in four groups based on similar retention times (Band A (49, 50 min); Band B (60, 61 min); Band C (64, 65 min); and Band D (67, 68 min)). The following MS and MS/MS experiments were carried out on an ion trap, therefore mass accuracy is +/- 0.3 Da.

4.5.2.1 Band D (67, 68 min)

First, I will discuss the LC-MS/MS analysis of band D products (67 and 68 min), which had previously been assigned as arising from the probe molecule MCTDA. Each of the samples corresponding to the 67 and 68 min peaks, were analysed independently by LC-MS and in each case the major ion in the MS spectra was subjected to fragmentation to aid in structural elucidation. The two samples corresponding to the 67 and 68 min peaks, gave major peaks with 25.14 and 25.24 min retention times respectively by LC-MS, as measured by the total ion chromatogram (TIC). For both peaks similar ions were observed at *m/z* = 840.4466, 420.9606 (67/25.14 min) and 840.3743, 420.9564 (68/25.24 min) which were assigned as $[M+H]^+$ and $[2M+H]^+$. Each major ion (420.9606, 67/25.14 min; 420.9564, 68/25.24 min) gave similar fragmentation ions with *m/z* = 393.1284, 376.1023 and 393.1098, 376.1330, corresponding to the loss of N_2 and CO_2 respectively (Figure **4.12, a, b**).

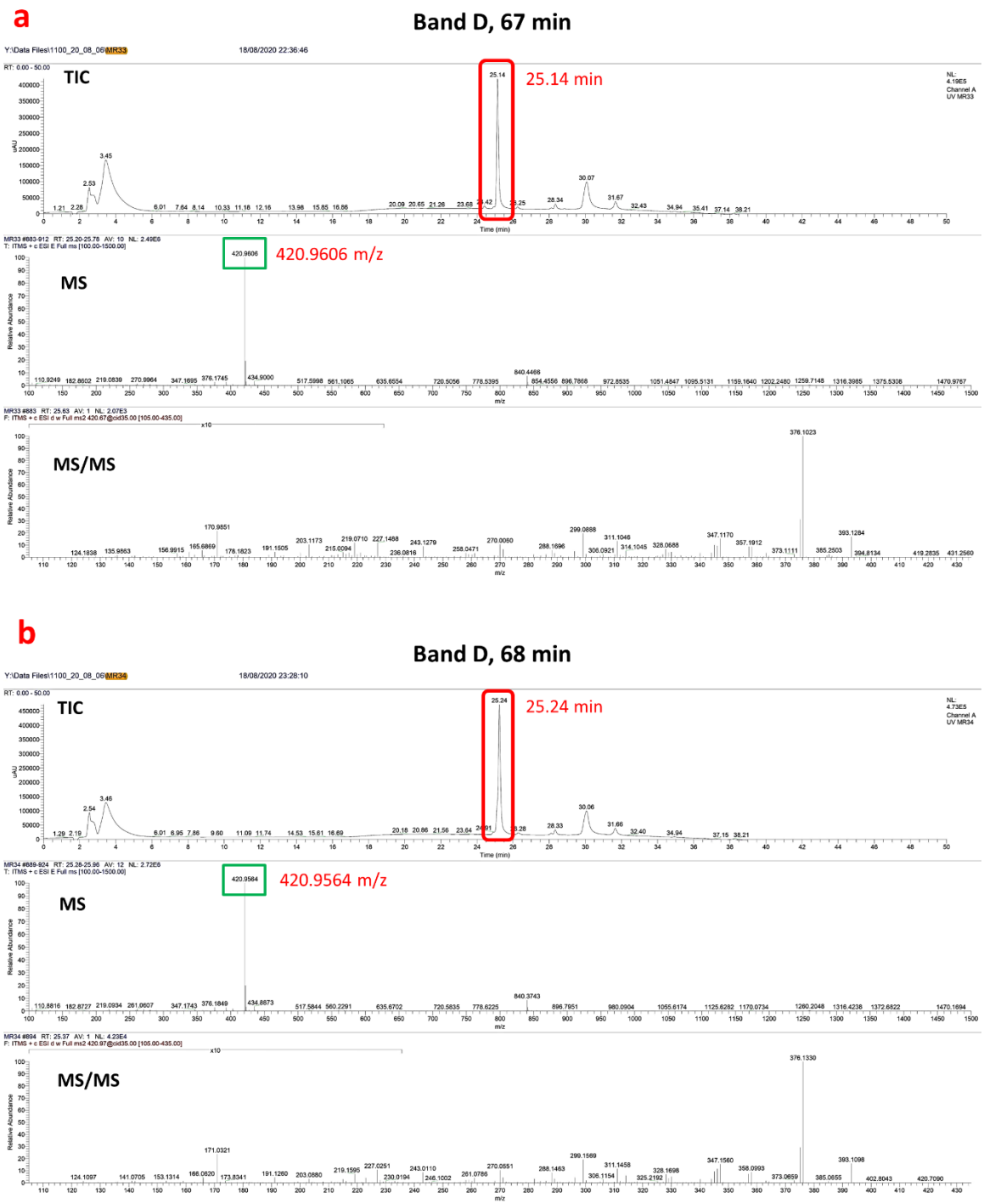

Figure 4.12: LC-MS/MS data of Band D products (67 and 68 min).

From this, it can be concluded that the two original peaks at 67 and 68 minutes show the same molecular masses (approx. 420 Da) and as such are likely correspond to two diastereomeric molecules related to MCTDA. In addition, the fragmentation mass spectrometry shows the loss of N_2, suggesting that the diazirine ring has remained intact and the loss of CO_2, suggesting a carboxylic acid. Since the molecular weight of MCTDA is 414 Da I postulated that the observed peaks might be correlated to unincorporated reduced MCTDA by-products, which contain an additional 6 hydrogen atoms resulting from the $NaBH_4$ reduction step.

The reduction of coumarins with sodium borohydride has been reported by Pitchumani *et. al.*, in which the α,β-unsaturated lactone (**4.2**) is reduced stepwise to give the corresponding carboxylic acid (**4.4**) (addition of 2 hydrogen atoms and hydrolysis) and the diol (**4.5**) (addition of 6 hydrogen atoms) (Figure **4.13**).[6]

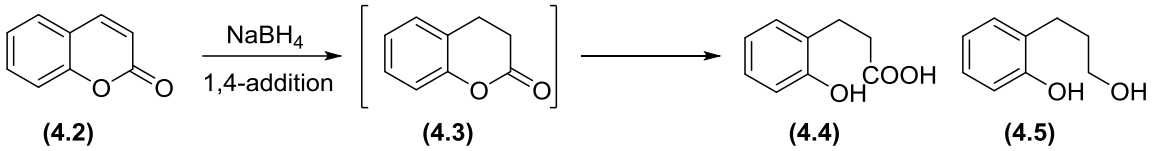

Figure 4.13: Pitchumani *et al.*, reduction of coumarin with $NaBH_4$.

Therefore, it was decided to carry out a direct sodium borohydride reduction of MCTDA under the reaction conditions, in an attempt to independently prepare a series of reduced MCTDAs for comparative analysis.

Thus, a 850 µL solution containing MCTDA (40 mM), along with sodium phosphate (20 mM), NaCl (100 mM) and TX-100 (0.05 %) was treated with sodium borate buffer 50 µL (0.5 M in H_2O) to adjust the pH of the solution to 9, then sodium borohydride ~ 65 mg was added to the reaction mixture.

The reaction mixture was then stirred at room temperature for 20 min, after which formic acid solution in acetonitrile (0.1%) was added to quench the remaining $NaBH_4$. The resulting sample was filtered (milipore HP filter, 45 µm) purified via automated RP flash chromatography (Biotage), and the peak at 16 min was collected and dried (5 mg). NMR

spectroscopic analysis of 16 min product showed the presence of multiple compounds, therefore the sample submitted for to LC-MS (ES-API) for high resolution mass analysis.

Analysis of the LC-MS spectra showed four peaks, the minor peaks at 9, 15 and 17 min and a major peak at 11 min. The two minor peaks at 15 and 17 minutes were not assignable, however the peaks at 9 and 11 minutes could be assigned as being associated with MCTDA

.

The MS spectra of the peak at 9 min showed two major ions 417.1 and 440.1 *m/z*. The mass difference of 22 Da between these peaks allowed assignment as the corresponding $[M+H]^+$ and $[M+Na]^+$ ions, suggesting a molecular weight for the parent molecule of 416.1 Da. The molecular weight of MCTDA is 414.1 Da, thus the molecule at 9 minutes has gained 2 Da corresponding to the addition of H_2. Therefore, it was concluded that our observed peak at 9 min is a reduced form of MCTDA probe in which H_2 has been added across the α,β-unsaturated lactone moiety of MCTDA to give the corresponding 2-chromanone (**4.6**) (Figure **4.14, B**).

The MS spectra of the major peak observed at 11 min, showed a major ion with *m/z* = 421.2 that was assigned as the $[M+H]^+$ ion, suggesting the presence of a parent compound with a molecular weight of 420.2 Da. Since MCTDA has a molecular weight 414 Da, I propose that the major peak at 11 min corresponds to a different reduced form of MCTDA in which 3 equivalents H_2 have been added to the molecule via $NaBH_4$. Following the previous work of Pitchumani *et. al.*, I postulate that this triply reduced form of MCTDA is a diol (**4.7**) resulting from the stepwise exhaustive reduction of the α,β-unsaturated lactone moiety (Figure **4.14, C**).

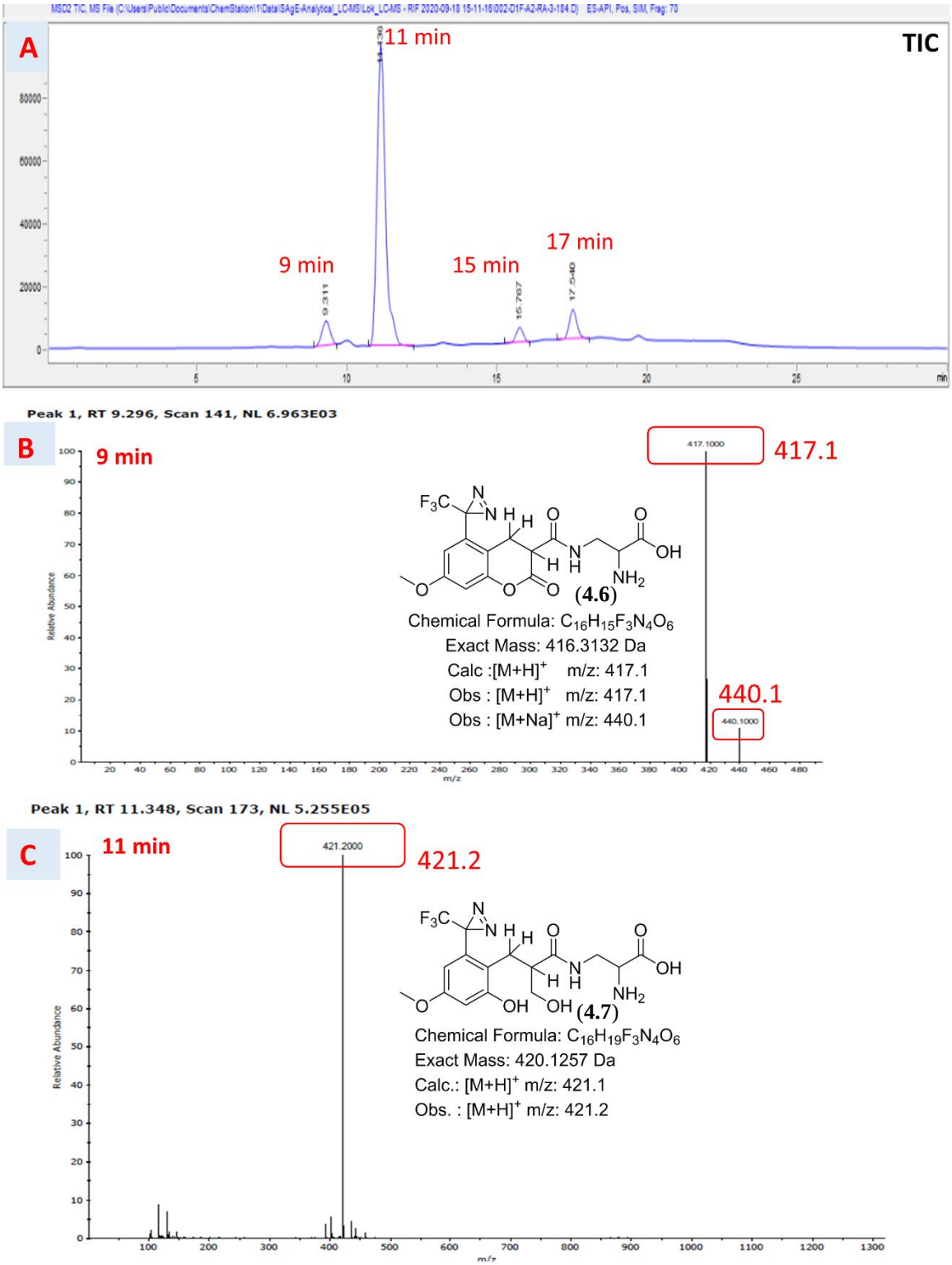

Figure 4.14: LC-MS result of MCTDA reduction test with sodium borohydride. (**A**) TIC chromatogram compromising 4 products (9 min, 11 min, 15 min, and 17 min), (**B**) MS (ES-API) spectra and proposed molecular structure of product eluted at 9 min (**C**) MS (ES-API) spectra and proposed molecular structure of product eluted at 11 min.

In conclusion, our test reaction of MCTDA (**3.3**) with sodium borohydride gave two main products resulting from the complete reduction of the *α,β*-unsaturated lactone to the corresponding diol (**4.7**), alongside the partial reduction of the *α,β*-unsaturated lactone to give 2-chromanone (**4.6**). Despite the likely formation of diastereomers only single peaks for the reduced forms of MCTDA, diol (**4.7**) and 2-chromanone (**4.6**), were observed in comparison to the split peaks observed in previous LC-MS experiments. This is likely due to improved separation in our previous analysis of MCTDA labelled muropeptide.

Thus, the LC-MS data obtained from MCTDA reduction with sodium borohydride test reactions are consistent with our previous results associated with MCTDA enzymatic incorporation into muropeptide (band D, 67 and 68 min). I therefore propose that the split peak seen for the D products arise due to the presence of diastereomeric diols formed via the reduction of unincorporated MCTDA ($MCTDA_{(reduced)}$), with separation of the diastereomers observed (Figure **4.15**).

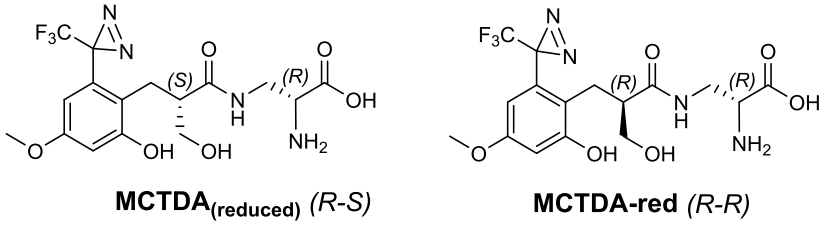

Figure 4.15: Molecular structures of band D products 67, and 68 min.

4.5.2.2 Band A (49, 50 min)

Two peaks from our LdtD incorporation of MCTDA into muropeptide, assigned as the band A products (49, 50 min), had been previously isolated by semi-preparative HPLC and subsequently analysed by LC-MS/MS. Unfortunately, LC-MS/MS analysis failed to identify any molecules that could be assigned as associated with muropeptides, MCTDA or muropeptide MCTDA adducts. This was in part due to the poor signal to noise ratio observed, likely due to the low mass of sample isolated. Future assignment will require the isolation of larger quantities of these band A products for further analysis.

4.5.2.3 Band C (64, 65 min)

In order to determine the molecular structure of isolated band C products, each sample associated with the 64 and 65 min peaks was individually analysed by LC-MS, including MS/MS fragmentation.

LC separation of the isolated peaks at 64 and 65 mins gave corresponding peaks with retention times at 23.63 and 23.80 min. MS of both peaks, 64/23.63 and 65/23.80 min, showed similar ionisation patterns and subsequently similar MS/MS fragmentation spectra. The MS spectra of both the 64/23.63 and 65/23.80 min peaks showed two major ions in each case 1273.0881, 637.2282 *m/z* (64/23.63), and 1273.0937, 637.2696 *m/z* (65/23.80 min) (Figure **4.16**, **a, b**).

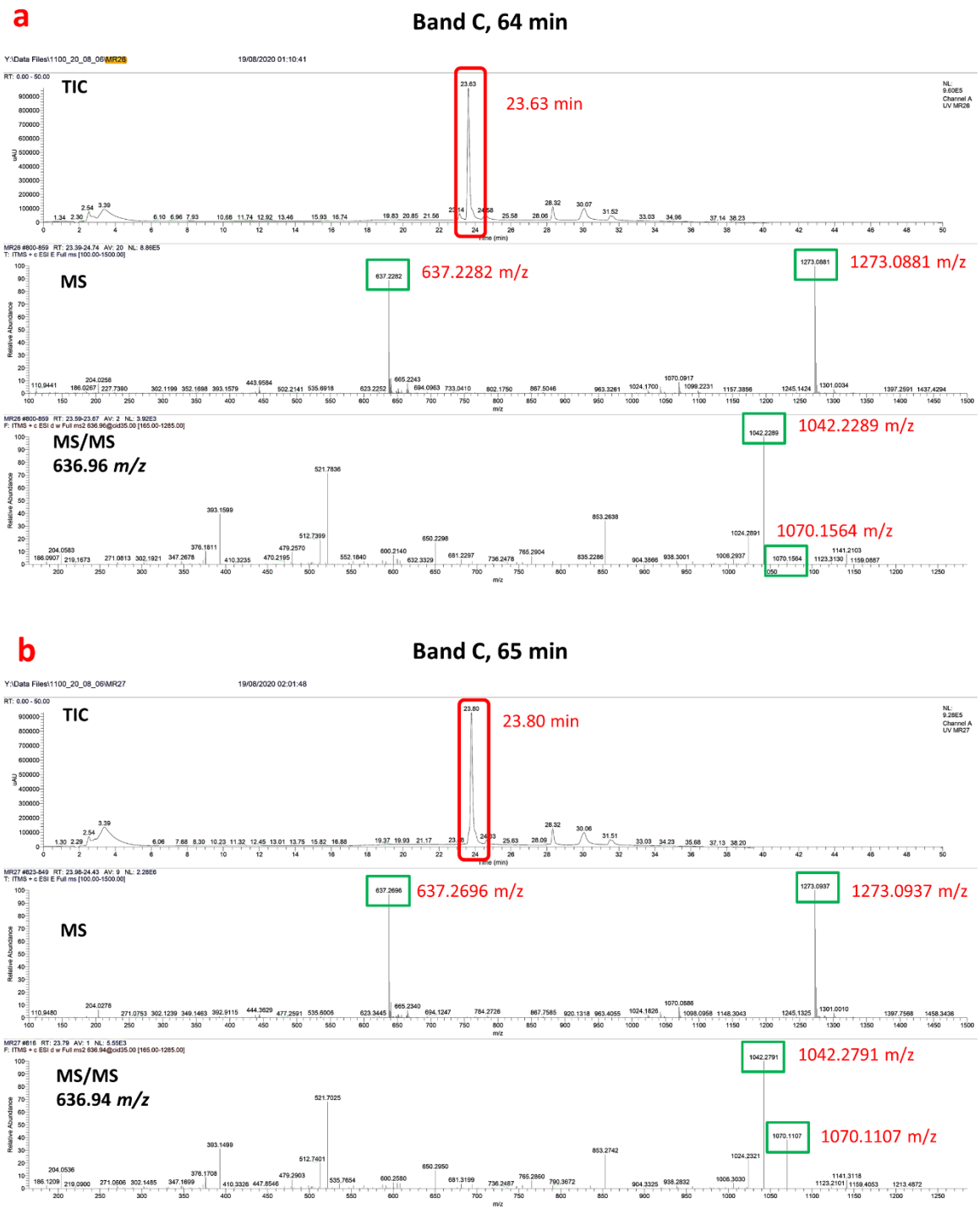

Figure 4.16: The LC-MS/MS spectrum of band C products. (a) 64 min product, first panel is LC/TIC, second panel ESI (ITMS) MS, third panel ESI (ITMS) MS/MS. (b) 65 min product, first panel is LC/TIC, second panel ESI (ITMS) MS, third panel ESI (ITMS) MS/MS.

In order to assign the major ions for the band C products (1273.0881, 637.2282 *m/z* (64/23.63 min); and 1273.0937, 637.2696 *m/z* (65/23.80 min)), their isotopic splitting patterns was examined. For the two ions 1273.0881 *m/z* (64/23.63 min) and 1273.0937 *m/z* (65/23.80 min), a standard separation of 1 *m/z* was observed in the isotopic splitting pattern, suggesting these ions are singly charged species. Thus, the two ions 1273.0881 *m/z* (64/23.63 min) and 1273.0937 *m/z* (65/23.80 min) was assigned as $[M+H]^+$, with corresponding molecular weights of approximately 1272 Da. In the case of the two ions 637.2282 *m/z* (64/23.63 min) and 637.2696 *m/z* (65/23.80 min) the observed isotopic spacing was approximately 0.5 *m/z*, suggesting these ions are doubly charged $[M+2H]^{2+}$ species corresponding to the same molecular weight of approximately 1272 Da (Figure **4.17, a, b**).

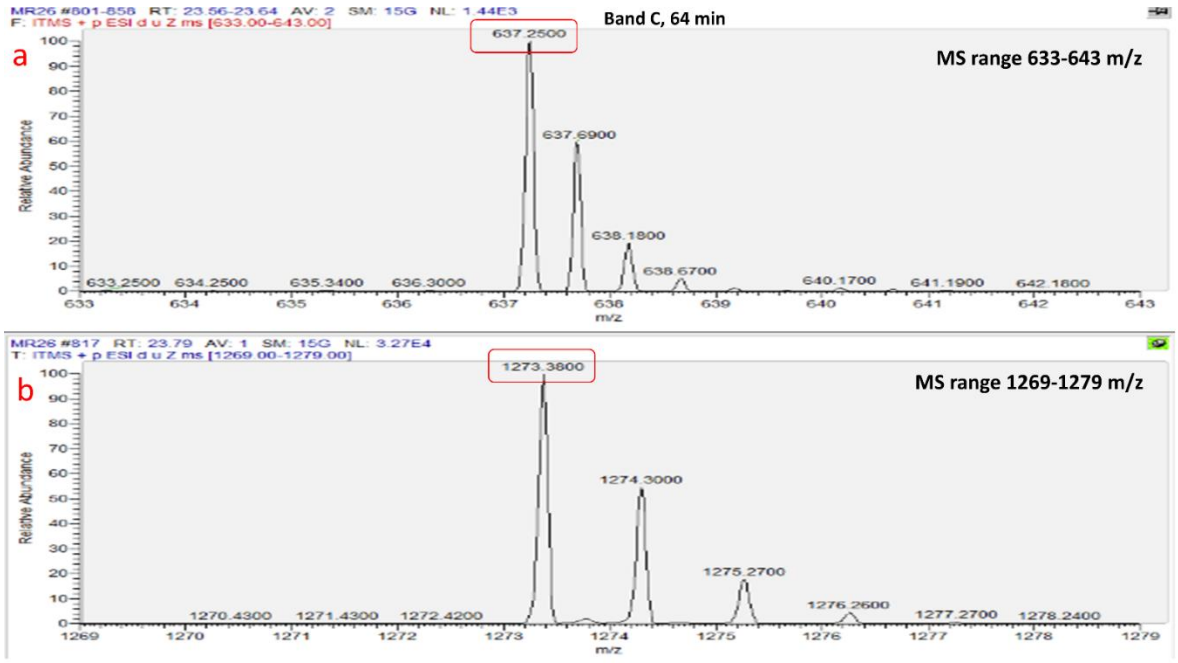

Figure 4.17: Expansions of the LC-MS spectra of the band C 64/23.63 min peak showing the isotopic splitting for the molecular ions at 1273.0881 and 637.2282 m/z.

MS/MS of the $[M+2H]^{2+}$ ions from both isolated peaks (637.2282, 64/23.63 min; 637.2696, 65/23.80 min) gave similar fragmentation patterns, 1070.1564, 1042.2289 *m/z* (64/23.63 min); and 1070.1107, 1042.2791 *m/z* (65/23.80 min), corresponding to singly protonated fragments. Therefore, based on a 1272 Da mass of the parent compound, this corresponds

to the loss of NAG (loss of 204 Da) and the loss of both NAG and N_2 (loss of 204 and 28, for a total loss of 232 Da) respectively.

Thus, I propose that the two isolated band C peaks at 64 and 65 minutes, have the same molecular formula (mass ≈ 1272 MW). In addition, the MS/MS shows both the loss of NAG and N_2, suggesting the presence of both the glycan (NAG and NAM) and the MCTDA diazirine ring. Based on the molecular weight of the native muropeptide Tetra (941 Da), the terminal D-Alanine fragment (88 Da) and the reduced MCTDA fragment (419 Da) I propose that the observed peaks correlate to the muropeptide Tetra-$MCTDA_{(reduced)}$ ($C_{50}H_{75}F_3N_{10}O_{25}$, 1272.4857 Da, calculated $[M+H]^+$ = 1272.48 *m/z*, $[M+2H]^{2+}$ = 637.2501 *m/z*). I further postulated that the two close running LC peaks, 64/23.63 min and 65/23.80 min, correspond to two diastereomeric muropeptide Tetra-$MCTDA_{(reduced)}$ molecules (Figure **4.18**).

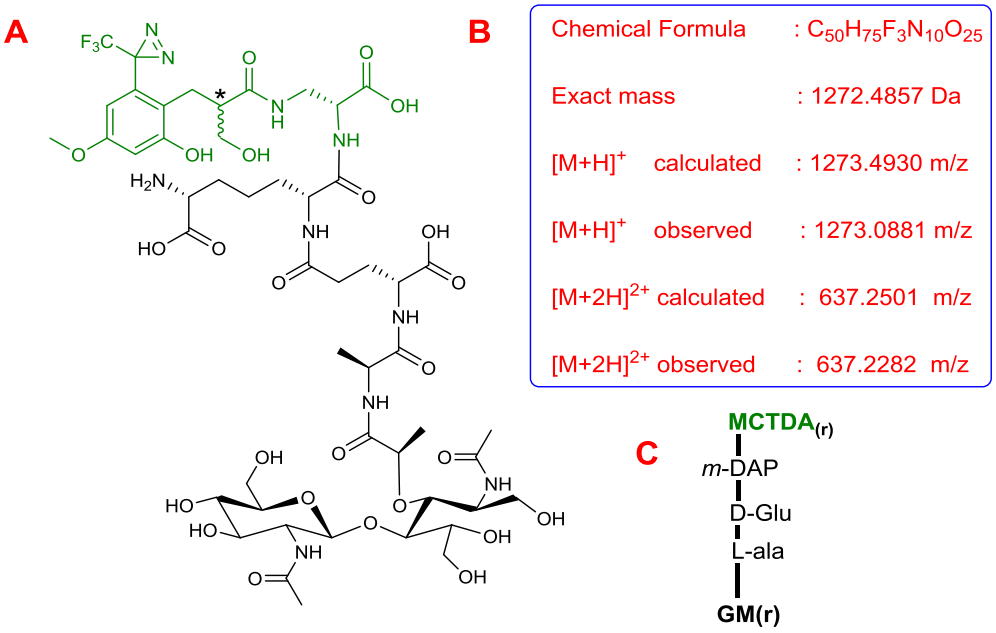

Figure 4.18: (**A**) Proposed molecular structure of band C products, muropeptide Tetra-$MCTDA_{(reduced)}$, (**B**) Observed and calculated HRMS data, (**C**) Abbreviated structure of muropeptide Tetra-$MCTDA_{(reduced)}$.

4.5.2.4 Band B (60, 61 min)

To elucidate the molecular structure of band B products (60, 61 min), isolated from the LdtD incorporation of MCTDA into muropeptide, the two samples corresponding to the 60 and 61 min peaks were analysed independently by LC-MS. In each case the major ion in the MS spectra was subjected to fragmentation to aid in structural elucidation.

The LC-MS/MS analysis of the two samples associated with band B products (60, 61 min) showed two major peaks with retention times of 23.10 and 23.22 min respectively as measured by the TIC. Both observed peaks showed very similar MS and MS/MS spectra therefore I will consider them together. In the MS spectra, major ions were observed at 1098.7642 and 1063. 3375 *m/z* for the 60/23.10 min peak, and 1098.8127 and 1063.3905 *m/z* for the 61/23.22 min peak (Figure **4.19, a, b**).

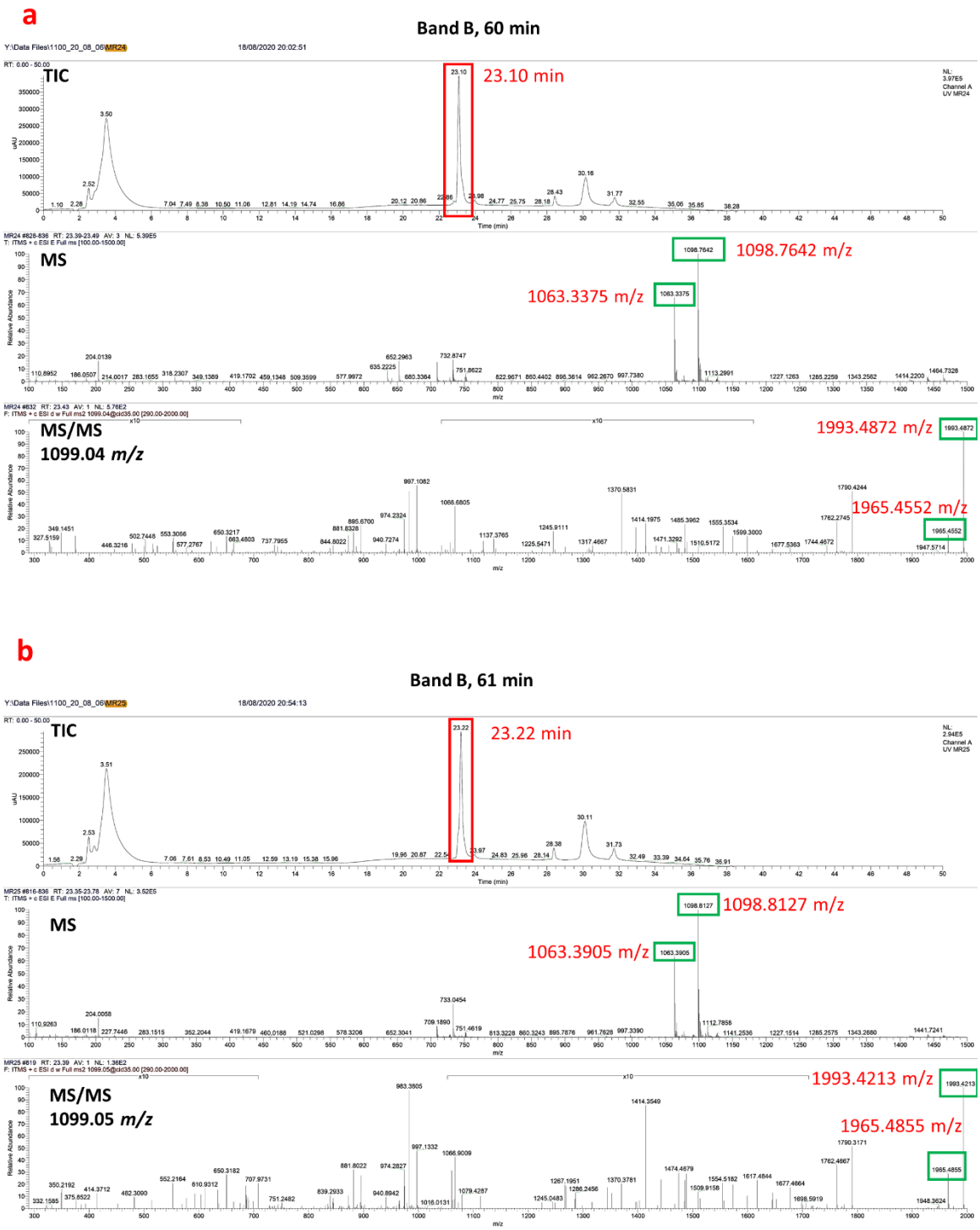

Figure 4.19: The LC-MS/MS spectrum of band B products. (**a**) 60 min product, first panel is LC/TIC, second panel ESI (ITMS) MS, third panel ESI (ITMS) MS/MS. (**b**) 61 min product, first panel is LC/TIC, second panel ESI (ITMS) MS, third panel ESI (ITMS) MS/MS.

In order to assist in the assignment of the LC-MS spectra for band B peaks, the isotopic splitting pattern for all four major ions (1098.7642, 1063.3375 *m/z*, 60/23.10 min; 1098.8127, 1063.3905 *m/z*, 61/23.22 min) were examined. In all cases, the observed isotopic spacing between each of peaks was approximately 0.5 *m/z*. Since standard isotopic splitting in MS would typically be an integer value of *m/z*, the observation of splitting of 0.5 *m/z* suggests the presence of a doubly charged ion. Therefore, all four major ions (1098.7642, 1063.3375 *m/z*, 60/23.10 min; 1098.8127, 1063.3905 *m/z*, 61/23.22 min) were assigned as doubly charged species. If these ions all contain two protons (e.g. $[M+2H]^{2+}$) this would suggest the presence of four compounds in total, two of which have molecular weights of approximately 2195.5 and two with molecular weights to approximately 2124.7 Da (Figure **4.20**).

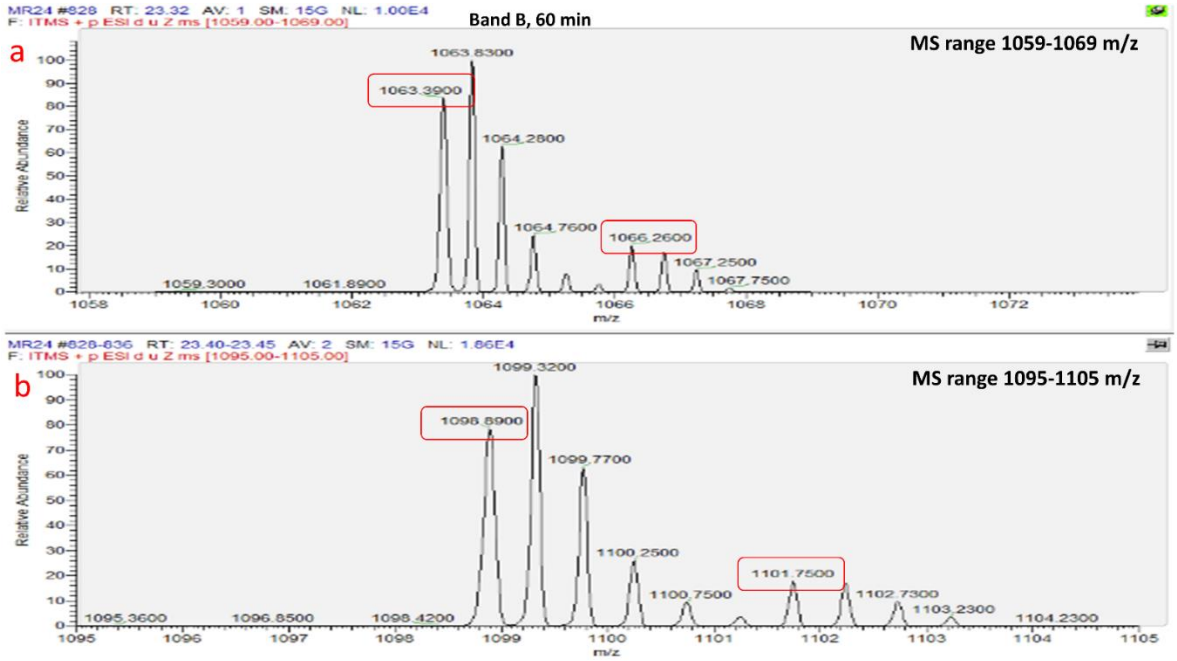

Figure 4.20: Expansions of the LC-MS spectra of the band B 60/23.1 min peak showing the molecular ions at 1063.3375 and 1098.7642 m/z.

For each peak, 60/23.10 min and 61/23.22 min, the major ions (*m/z* = 1098.7642 and 1098.8127) was subjected to MS/MS. Similar fragmentation was observed in each case with *m/z* ≈ 1993.5, 1965.5 corresponding to two singly charged species. Given a parent ion mass of 2195.5 Da, these two fragments correspond to the loss of the sugar NAG (1993.5)

and the loss of both NAG and N_2 (1965.5). This confirms the presence of both MCTDA (loss of N_2) and muropeptide (loss of NAG).

Based on our analysis so far, each of the two peaks of band C (60/23.10 and 61/23.22 min) contains two co-eluting compounds, making a total of four compounds in band C. From this set of four compounds, two (one from each peak 60/23.10 and 61/23.22 min) have a molecular weight of 2195.5 Da and two (one from each peak 60/23.10 and 61/23.22 min) have a molecular weight of 2124.7 Da. This suggests that band C contains two pairs of structural isomers, likely diastereomers arising from the reduction of MCTDA.

Considering the mass of reduced native (*E. coli*) dimeric muropeptide Tetra-Tetra (3-4) (1864 Da), the two 2195.5 Da diastereomers were assigned as modified Tetra-Tetra (3-4) muropeptides. Based on the loss of a terminal D-alanine fragment (88 Da) and the gain of a $MCTDA_{(reduced)}$ fragment (419 Da), this suggests that the two 2195.5 Da diastereomers observed correspond to two Tetra-Tetra (3-4)-$MCTDA_{(reduced)}$ molecules ($C_{87}H_{136}F_3N_{17}O_{45}$, 2195 Da, calculated $[M+2H]^{2+}$ = 1098.9487 *m/z*, observed = 1098.7642 *m/z* (60/23.10 min) and 1098.8127 *m/z* (61/23.22 min)).[7]

Considering the mass of reduced native (*E. coli*) dimeric muropeptide Tetra-Tri (3-3) (1793 Da), the two 2124.7 Da diastereomers were assigned as modified Tetra-Tri (3-3) muropeptides. Again, based on the loss of a D-alanine fragment (88 Da), and the gain of a $MCTDA_{(reduced)}$ fragment (419 Da), the two 2124.7 Da diastereomers were assigned as two Tetra-Tri (3-3)-$MCTDA_{(reduced)}$ molecules ($C_{84}H_{131}F_3N_{16}O_{44}$, 2124.8 Da, calculated $[M+2H]^{2+}$ = 1063.4301 *m/z*, observed = 1063.3375 *m/z* (60/23.10 min) and 1063.3905 *m/z* (61/23.22 min)) (Figure **4.21**).

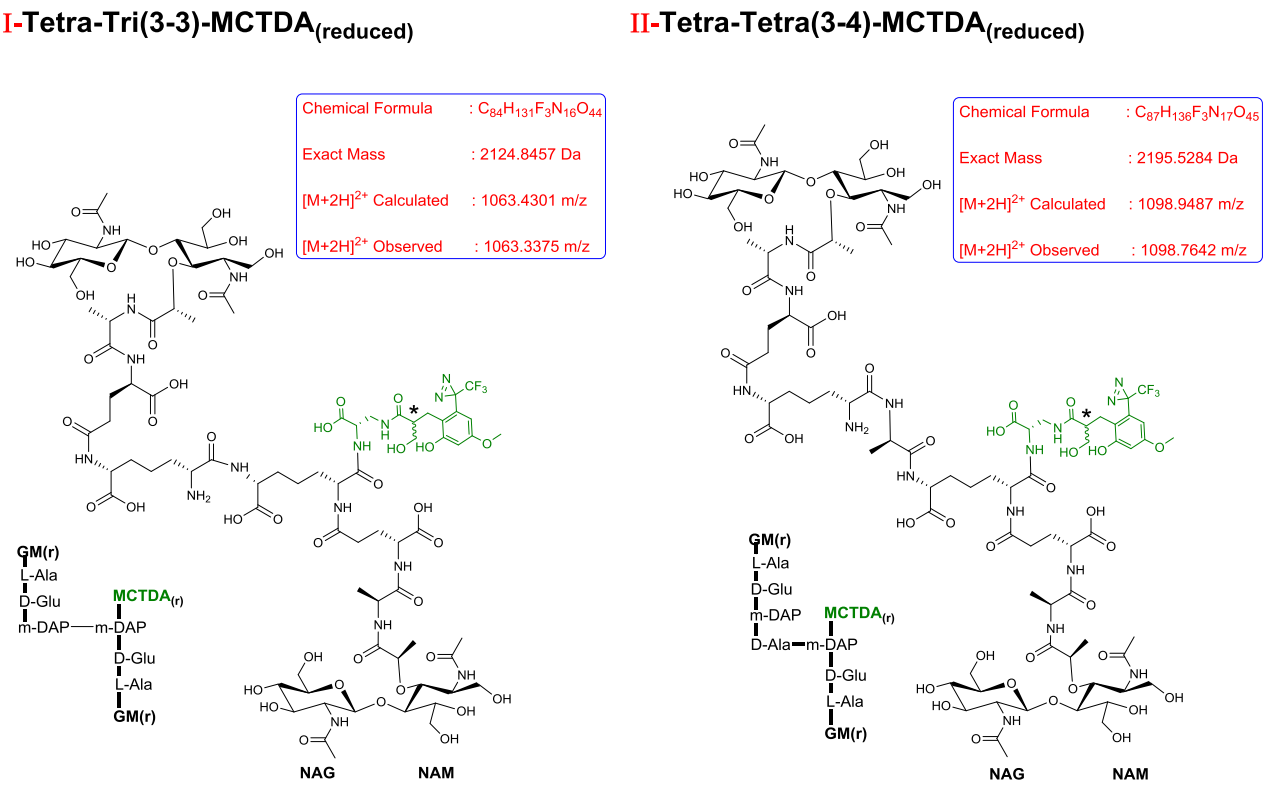

Figure 4.21: Proposed molecular structures of band B products (60 and 61 min). (**I**) Tetra-Tri(3-3) -MCTDA reduced labelled muropeptide, (**II**) Tetra-Tetra(3-4)-MCTDA reduced labelled muropeptide. Muropeptide samples in this experiment were isolated from *E. coli.*

4.5.3 Conclusion

To conclude, I have shown that MCTDA is incorporated into isolated muropeptide (*E. coli*) by the action of LdtD, under our optimized incorporation conditions (sodium phosphate buffer). The use of semi-preparative HPLC allowed the isolated of modified muropeptides, with subsequent LC-MS/MS analysis allowing identification and structural assignment. In our incorporation experimentsthe formation, by LdtD, of Tetra-MCTDA$_{(reduced)}$, Tetra-Tri (3-3)-MCTDA$_{(reduced)}$ and Tetra-Tetra (3-4)-MCTDA$_{(reduced)}$ muropeptides has been identified. In each case the MCTDA modified muropeptides were obtained as mixtures of diastereomers arising from the reduction of the MCTDA moiety.

Therefore, in the next experiments I wished to examine the MCTDA enzymatic incorporation experiment into *E. coli* muropeptide using LdtD, without the sodium borohydride reduction step. This will hopefully avoid the reduction of MCTDA probe moiety, allowing it to retain its fluorescent properties.

4.6 MCTDA Enzymatic Incorporation into Muropeptide via LdtD without $NaBH_4$ Reduction

Our previous MCTDA enzymatic incorporation protocol involved a standard step, namely $NaBH_4$ reduction of assay mixture before HPLC purification. The $NaBH_4$ reduces the terminal anomeric position of the glycan NAM unit and hence simplifies the subsequent HPLC analysis. Unfortunately, the addition of $NaBH_4$ also reduces the coumarin ring of any MCTDA probe, incorporated into the muropeptide, resulting in a non-fluorescent $MCTDA_{(reduced)}$ adduct. Therefore, I wished to repeat our previous successful enzymatic (LdtD) incorporation of our MCTDA probe into *E. coli* muropeptide, in sodium phosphate buffer and without $NaBH_4$ reduction. It was hoped that this would conserve the fluorescence of MCTDA, and to allow the isolation (HPLC) and characterization (LC-MS/MS) of fluorescent muropeptide-MCTDA adducts.

Therefore, four experiments were carried out following our previous incorporation protocol. MCTDA was incubated with LdtD and *E. coli* muropeptide alongside control experiments involving muropeptide only, MCTDA only, and muropeptide with LdtD only. All of the experiments were incubated for 1 h at 37 °C, 3 min at 100 °C, the pH was adjusted to pH 4, centrifuged, and the obtained supernatants were analysed by analytical HPLC using the previous conditions.

HPLC analysis of the unreduced *E. coli* muropeptide showed two peaks (25 and 27 min) corresponding to the anomers of Tetra and a further two peaks (31 and 33 min) for the anomers of Tetra-Tetra (3-4) (Figure **4.22, b**). Incubation of muropeptide with LdtD only resulted in the formation of Tetra-Tri (3-3), seen in the HPLC as two new peaks overlapping with the anomers of Tetra-Tetra (3-4) (Figure **4.22, c**). Whilst MCTDA only gave a peak at 73 min, corresponding to incorporated probe. Finally, MCTDA incorporation into muropeptide via LdtD showed a new peak at 67 min which was thought could be associated with a muropeptide-MCTDA adduct (Figure **4.22, a**).

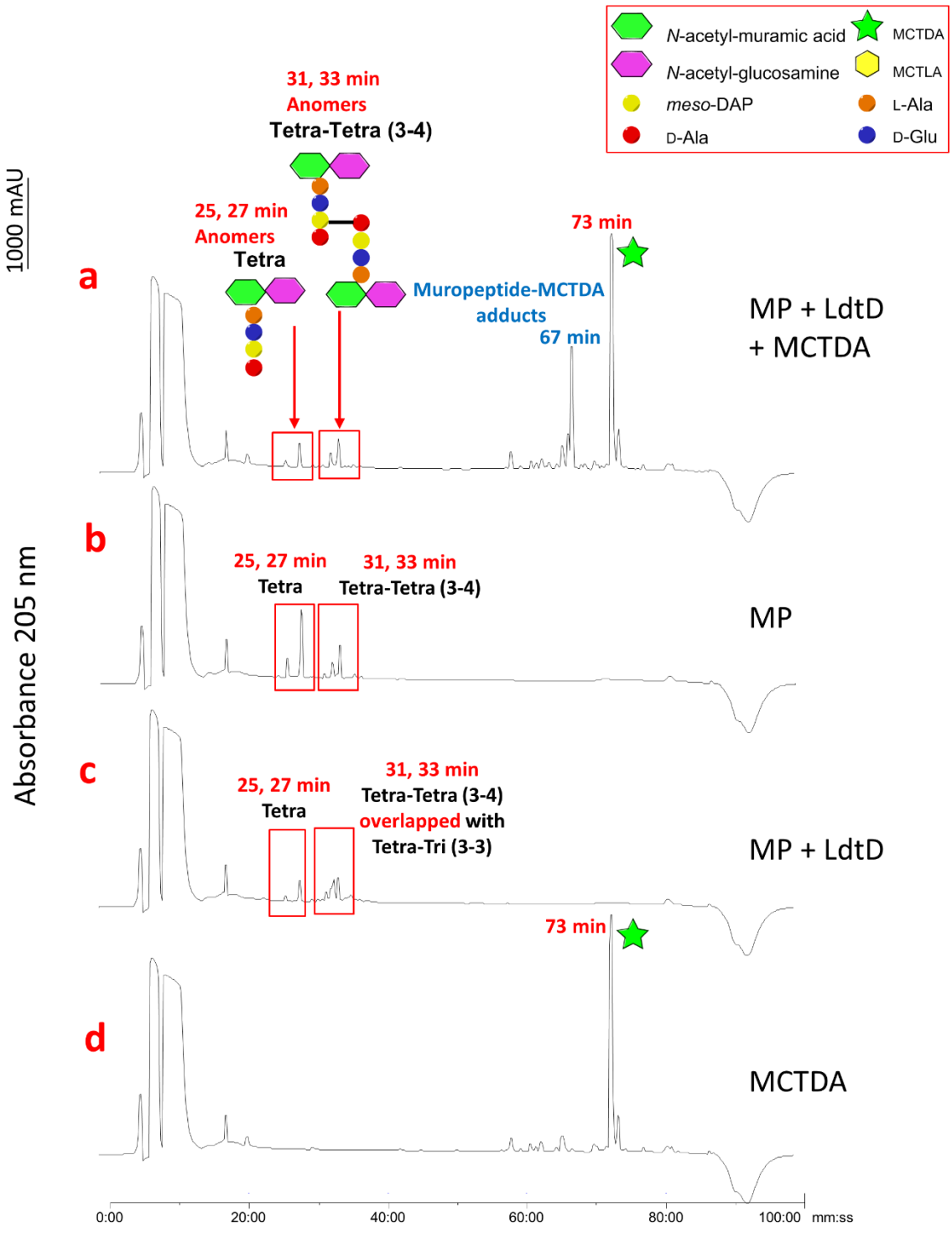

Figure 4.22: Results of analytical HPLC, (**A**) MCTDA enzymatic incorporation into *E. coli* muropeptide via LdtD in sodium phosphate buffer without reduction, (**B**) control experiment of muropeptide only, (**C**) control experiment of LdtD and muropeptide only. (**D**) control experiment of MCTDA only.

As our analytical HPLC results showed the formation of a potential muropeptide-MCTDA adduct (67 min) formed through the action of LdtD, I wished next to isolate sufficient material in order to investigate the molecular structure by LC-MS/MS.

Thus, the MCTDA incorporation into muropeptide via LdtD was repeated as previously and the resulting supernatant was separated by semi-preparative HPLC. The corresponding peaks with retention times at 67 min (putative muropeptide-MCTDA adduct) and 73 min (unincorporated MCDTA) were collected, dried and then analysed by LC-MS/MS.

4.6.1 LC-MS/MS Analysis of Muropeptide-MCTDA Adducts via LdtD Incorporation into Muropeptide without Reduction

LC-MS/MS analysis of the two peaks (67 and 73 min), isolated via semi-preparative HPLC of the non-reduced products of LdtD incorporation of MCTDA into muropeptide, was then carried out using an ion trap with mass spectrometer with MS/MS of the major ions observed.

4.6.1.1 Peak 73 min

LC-MS/MS analysis of the 73 min peak, gave a single peak at 13.23 min with a major ion with 415.00 *m/z*. MS/MS of the major ion showed a fragment ion at 387.09 *m/z*, corresponding to the loss of N_2, suggesting the presence of a diazirine moiety. Therefore this peak was assigned as the $[M+H]^+$ ion of unreacted MCTDA (calculated molecular weight = 415.09 *m/z*) (Figure **4.23**).

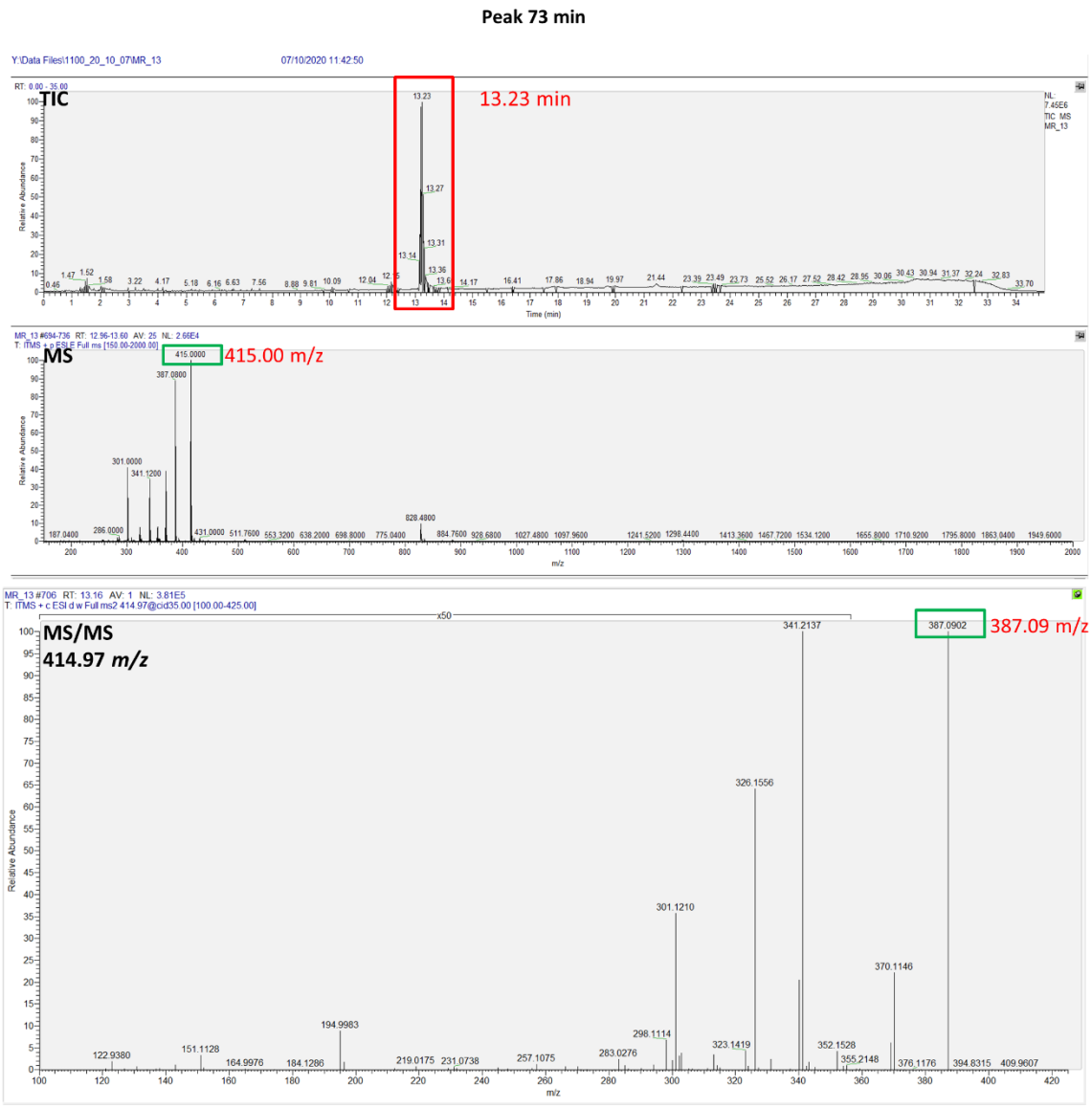

Figure 4.23: The LC-MS/MS spectrum of peak 73 min., first panel is LC/TIC, second panel ESI (ITMS) MS, third panel ESI (ITMS) MS/MS.

4.6.1.2 Peak 67 min

Analysis of the 67 min peak, have a new peak in the LC-MS at 12.20 min. The MS spectra showed a major ion at 1265.16 *m/z*. The fragmentation spectra of this ions showed two major components with 1219.2350 and 1016.2574 *m/z*, corresponding to the loss of CO_2 and the loss of both CO_2 and NAG from the parent ion. (Figure **4.24**).

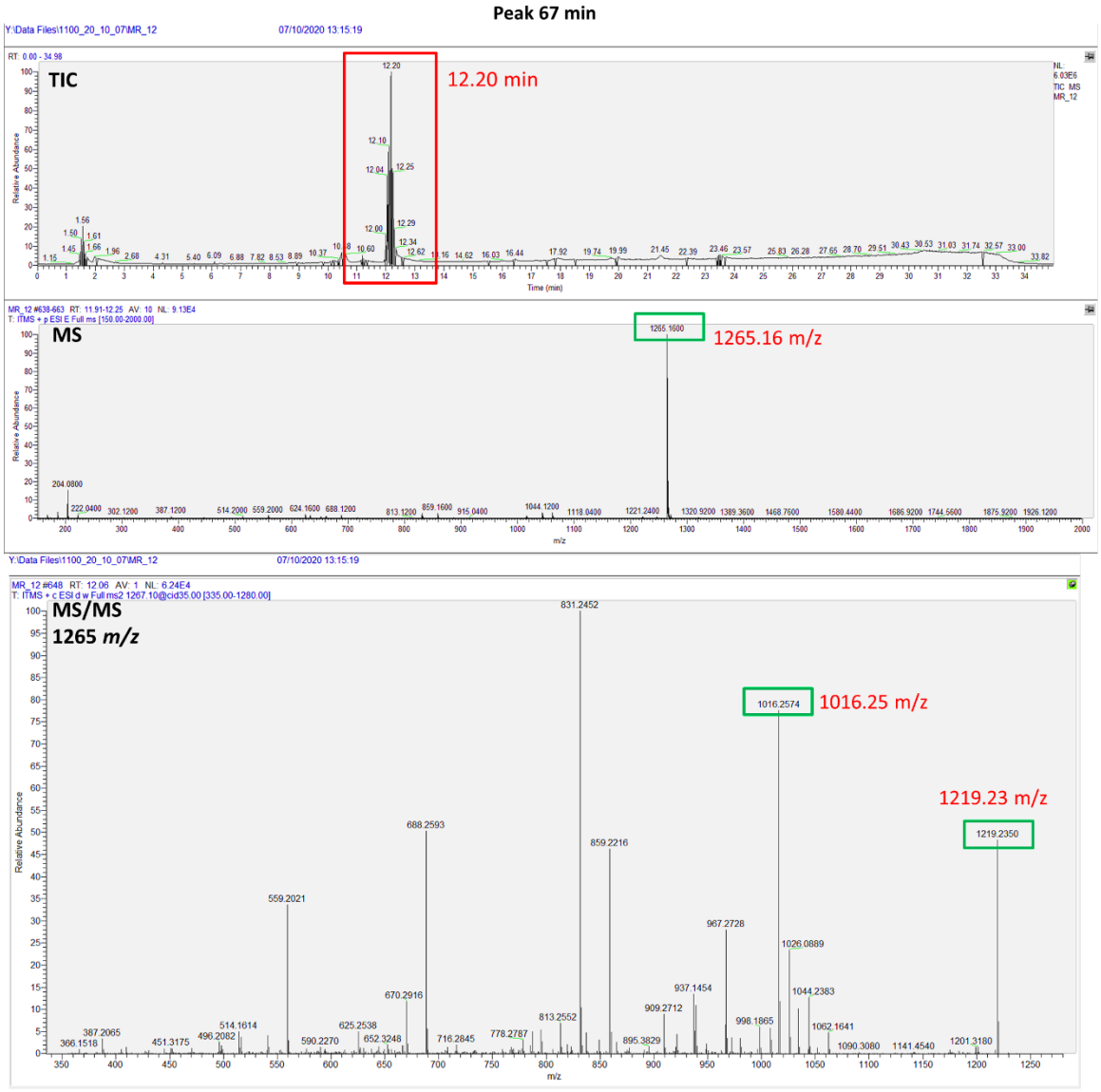

Figure 4.24: The LC-MS/MS spectrum of peak 67 min., first panel is LC/TIC, second panel ESI (ITMS) MS, third panel ESI (ITMS) MS/MS.

Based on an assignment as $[M+H]^+$ this suggests a compound with a molecular weight of 1264.42 Da. Since the molecular weight of native non-reduced Tetra muropeptide is 939 Da, the D-alanine fragment is 88 Da and the MCTDA fragment is 413 Da, it was proposed that the observed 67/12.20 min peak corresponds to modified muropeptide Tetra-MCTDA ($C_{50}H_{67}F_3N_{10}O_{25}$, 1264 Da) (Figure **4.25**).

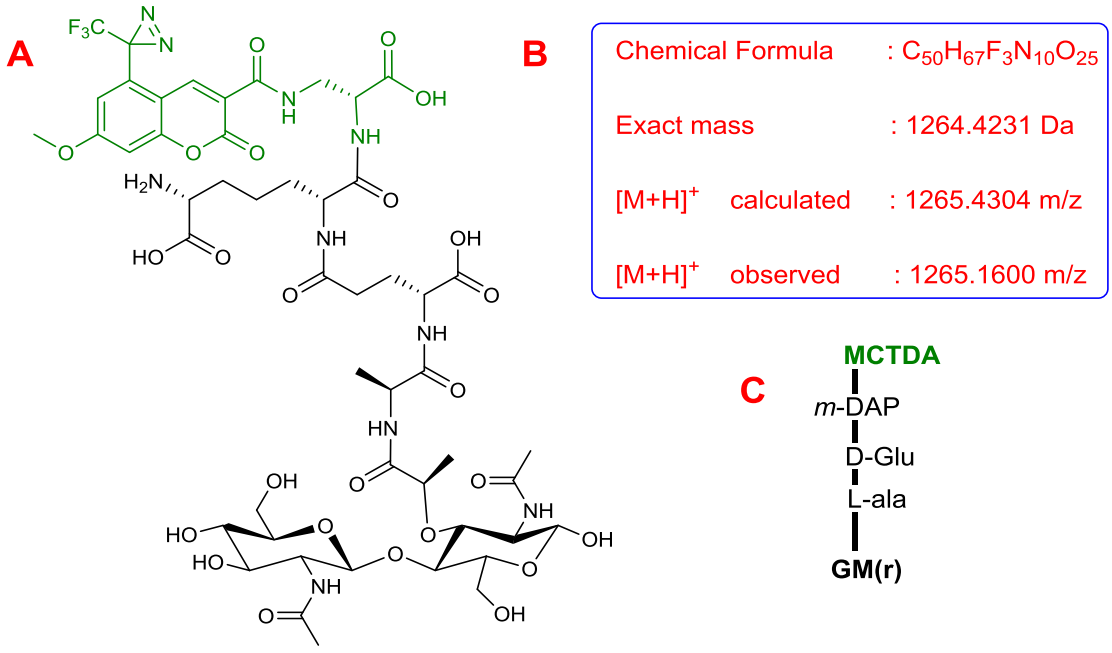

Figure 4.25: (**A**) Proposed molecular structure of Tetra-MCTDA, (**B**) Presentation of LC-MS/MS data observed and calculated of Tetra-MCTDA, (**C**) Abbreviated structure of panel A product.

In conclusion, after carrying out an LdtD incorporation experiment of MCTDA into *E. coli* muropeptide without $NaBH_4$ reduction. Despite the presence of anomeric muropeptide products, a new modified muropeptide, Tetra-MCTDA, via semi-preparative HPLC followed by LC-MS/MS analysis has been successfully isolated and characterised.

However, I surprisingly did not observe the formation of any dimeric muropeptide-MCTDA adducts (e.g. Tetra-Tetra (3-4)-MCTDA) as had been seen in previous experiments. Therefore, in the future the LdtD incorporation of MCTDA will be reinvestigated without reduction in order to search for these higher muropeptide adducts.

4.7 Examination of the Incorporation of MCTDA into *E. coli* Peptidoglycan via LdtD in Sodium phosphate Buffer

Finally, following our success in demonstrating MCDTA incorporation into isolated muropeptides it was proposed to return to the investigation of MCTDA incorporation into the more complex but biologically relevant *E. coli* peptidoglycan (PG).

Therefore, *E. coli* PG (Δ6PG) was treated with MCTDA, LdtD, TX-100, NaCl and sodium phosphate buffer as described before. In addition, control experiments were undertaken involving PG and LdtD only, PG and MCTDA only, and MCTDA only. Following overnight incubation at 37 ^{o}C, enzyme inactivation at 100 ^{o}C for 3 min, the obtained material was digested with muramidase at 37 ^{o}C overnight. The muramidase was then inactivated at 100 ^{o}C for 3 min, insoluble proteins were removed by centrifugation, the supernatant adjusted to pH 9, reduced with sodium borohydride, re-centrifuged, readjusted to pH 3 with formic acid and the sample analysed by HPLC.

HPLC showed a number of peaks that corresponded to those observed in our LdtD MCTDA incorporation experiments with muropeptides. Control experiments with PG and LdtD only, showed the successful isolation of both, Tetra-Tri (3-3) and Tetra-Tetra (3-4) due to the action of LdtD and digestion with muramidase. In the case of MCTDA only, a pair of split peaks at 67 and 68 min were observed corresponding to reduced unincorporated MCTDA with a further single peak at 83 min, corresponding to unincorporated MCTDA. Finally, in our incorporation experiment two new pairs of split peaks at 56 and 57 min and 59 and 60 min were observed. Through comparison with retention times observed in our previous incorporation experiments with muropeptide (Figure 4.9), which were analysed using the same HPLC conditions, the peaks at 59 and 60 min were assigned as the overlapping signals corresponding to Tetra-Tri (3-3)-MCTDA$_{(reduced)}$ and Tetra-Tetra (3-4)-MCTDA$_{(reduced)}$. Interestingly, the previously identified Tetra-MCTDA$_{(reduced)}$ could not be observed in this experiment. Furthermore, the split peak at 56 and 57 min does not correlated with any previously observed peaks, however the split nature would suggest the presence of two diastereomers associated with a reduced MCTDA. Thus, it was proposed that the split peaks at 56 and 57 min correspond

to a new unidentified muropeptide MCTDA adduct. However, these results would require further confirmation by subsequent LC-MS/MS analysis (Figure **4.26, b**).

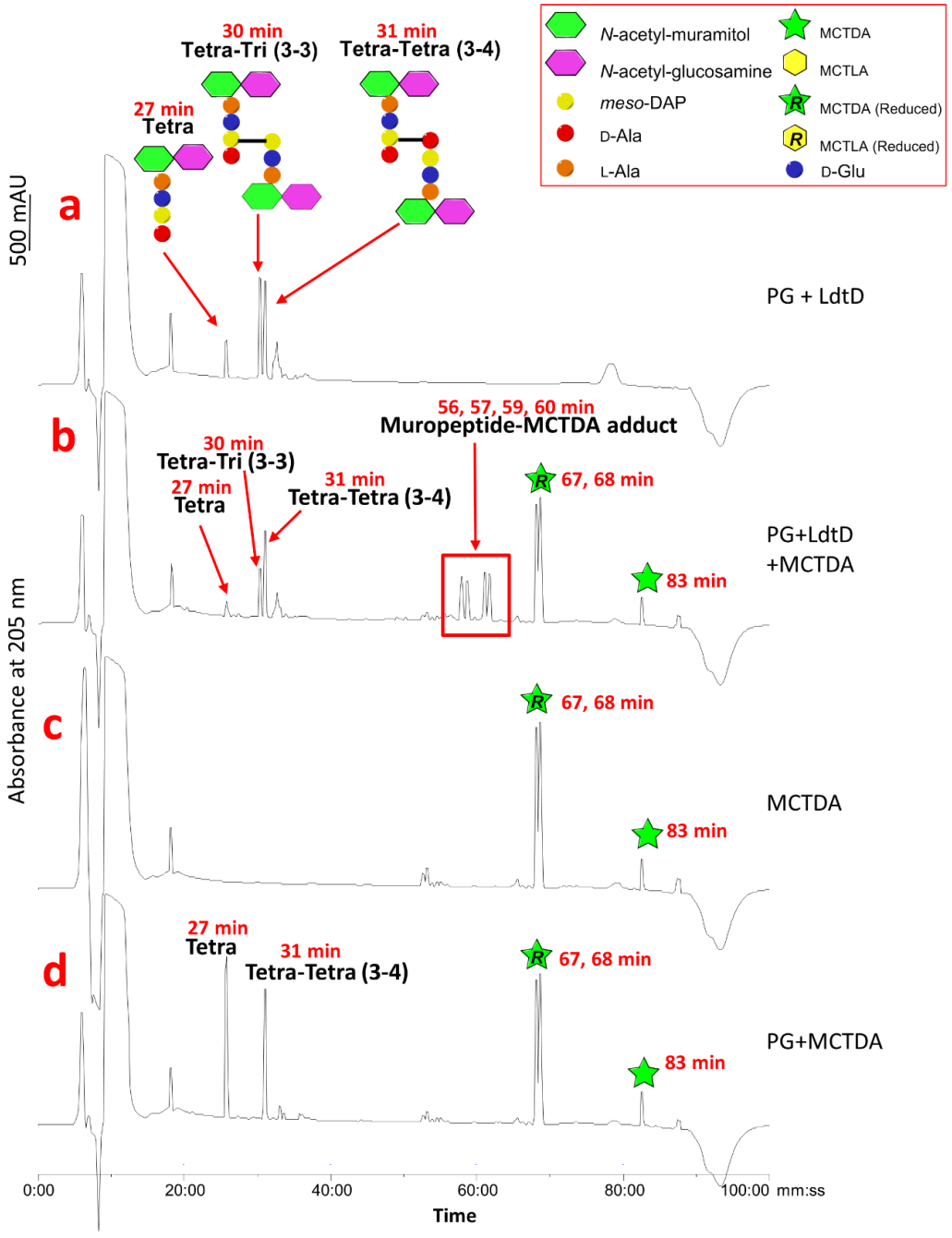

Figure 4.26: Overlay of HPLC results of reduced enzymatic incorporation of MCTDA into *E. coli* PG (Δ6PG), (**a**) PG with LdtD (**b**) 0.5 mM MCTDA, LdtD, PG (**c**) blank control of 0.5 mM MCTDA into DMSO only (**d**) Reference of 0.5 mM MCTDA and PG only. Samples were reduced with sodium borohydride before HPLC analysis.

To conclude, HPLC analysis the incorporation experiments of MCTDA into *E. coli* PG by LdtD showed the formation of both Tetra-Tri (3-3)-MCTDA$_{(reduced)}$ and Tetra-Tetra (3-4)-MCTDA$_{(reduced)}$ along with the formation of a new muropeptide MCTDA adduct. Future work will involve LC-MS/MS analysis of these muropeptide MCTDA adducts to confirm their molecular structure.

4.8 Conclusion

The aim of this chapter was to investigate the enzymatic incorporation of our fluorescent and photoactivatable amino acid probe MCTDA (**3.3**) into the peptidoglycan (PG) of the cell wall of *E. coli* via the L,D-transpeptidase, LdtD. The incorporation, via LdtD, of MCTDA (**3.3**) into isolated *E. coli* muropeptide as a test system for PG incorporation was examined. Furthermore, the impact of $NaBH_4$ reduction in the analysis of MCTDA (**3.3**) labelled muropeptides was also evaluated.

I have successfuly shown that MCTDA can be incorporated into *E. coli* muropeptide by LdtD through, following $NaBH_4$ reduction, and identification, by LC-MS/MS, of several muropeptide-MCTDA adducts, Tetra-Tri(3-3)-MCTDA$_{(reduced)}$, Tetra-Tetra(3-4)-MCTDA$_{(reduced)}$, and Tetra-MCTDA$_{(reduced)}$. It hasalso been shown that treatment with $NaBH_4$ of both MCTDA and muropeptide-MCTDA adducts results in reduction of the core fluorophore of MCTDA. Therefore to support future fluorescent labelling of bacterial PG with MCTDA, we have also shown that modified a *E. coli* muropeptide adduct (Tetra-MCTDA) can be isolated without the need of $NaBH_4$ reduction, avoiding unwanted reduction of the fluorophore core of MCTDA.

Finally, there is preliminary data to show that MCTDA can be incorporated into *E. coli* PG itself, through identification by HPLC of the muropeptide-MCTDA adducts, Tetra-Tri (3-3)-MCTDA$_{(reduced)}$ and Tetra-Tetra (3-4)-MCTDA$_{(reduced)}$.

In the future, the incorporation by L,D-transpeptidases and/or D,D-transpeptidases of MCTDA into the PG of live *E. coli*, combined with measurements the resulting fluorescence of the MCTDA modified PG will be tested. Furthermore, investigatation intothe photolysis of muropeptide-MCTDA and PG-MCTDA adducts in order identify

enzymes associated with PG biosynthesis, through cross-linking pull-down experiments will be done.

4.9 References

1- E. Kuru, H. Hughes, P. Brown, E. Hall, S. Tekkam, F. Cava, M. de Pedro, V Brun, and M. VanNieuwenhze, *Angew. Chem., Int. Ed*., 2012, **51**, 12519-12523.

2- A. Silva, C. Otten, J. Biboy, E. Breukink, M. VanNieuwenhze, W. Vollmer and T. Blaauwen, *Front. Microbiol*., 2018, **9**, 1-15.

3- E. Kuru, A. Radkov, X. Meng, A. Egan, L. Alvarez, A. Dowson, G. Booher, E. Breukink, D. Roper, F. Cava, W. Vollmer, Y. Brun, and M. VanNieuwenhze, *ACS. Chem. Bio*., 2019, **14**, 2745-2756.

4- A. Radkove, Y. Hsu, G. Booher, and M. VanNieuwenhze, *Ann. Rev. Biochem*., 2018, **87**, 991-1014.

5- B. Glauner, J. Holtje, and U. Schwarz, *J. Biol. Chem*., 1988, **263**, 10088-10095.

6- K. Pitchumani, P. Velusamy and C. Srinivasan, *Tetrahedron*, 1994, **50**, 12979-12988.

7- V. M. T. Mayer, I. Hottmann, R. Figl, F. Altmann, C. Mayer and C. Schäffer, *BMC. Microbiol*., 2019, **19**, 1-9.

Chapter 5. Conclusion and Future Work

The aim of this PhD project was to develop new photoactivatable D-amino acids to probe bacterial cell wall biosynthesis, based on a diazirine photoactivatable group. These photoactivatable D-amino acids would then be enzymatically introduced into the bacterial cell wall (peptidoglycan, PG), irradiated to form carbenes that can generally covalently capture any nearby cell wall-associated proteins.

Our initial work into the enantioselective synthesis of photoactivable unnatural amino acids (D-photoleucine and D-photomethionine) demonstrated O'Donnell enantioselective phase-transfer catalysis as the most promising route investigated. However, in order to speed up the development of photoactivatable D-amino acid probes I decided to use commercially available 3-amino-D-alanine as our source of chirality and focus on the synthesis of a new class of photoactivatable fluorescent D-amino acids.

Therefore I next looked to synthesise photoactivatable D-amino acid MCTDA (**3.3**), and its enantiomer MCTLA (**3.4**), as structural analogues to D-alanine (**3.5**). Both MCTDA (**3.3**) and MCTLA (**3.4**) were synthesised in 10 steps and 2 % and 5 % overall yield respectively, starting from 3,5-dimethoxylbenzyl chloride, providing 10's of milligrams for biological evaluation (Figure **5.1**).

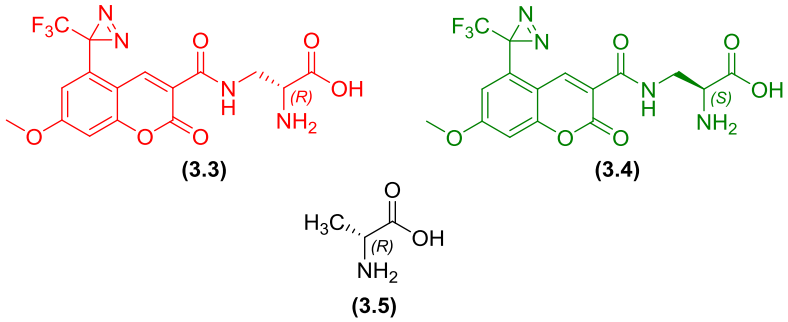

Figure 5.1: Molecular structures of photoactivatable D-amino acids, MCTDA and MCTLA along with naturally occurring D-alanine.

Next I looked next to investigate if MCTDA (**3.3**) and MCTLA (**3.4**) could be incorporated into the peptidoglycan (PG) of *E. coli* using the enzyme LdtD. I showed that MCTDA (**3.3**) was incorporated into both isolated muropeptides (*E. coli*.) and isolated PG (*E. coli*.),

whilst MCTLA (**3.4**) was not, demonstrating that MCTDA (**3.3**) is a substrate for LdtD (Figure **5.2**).

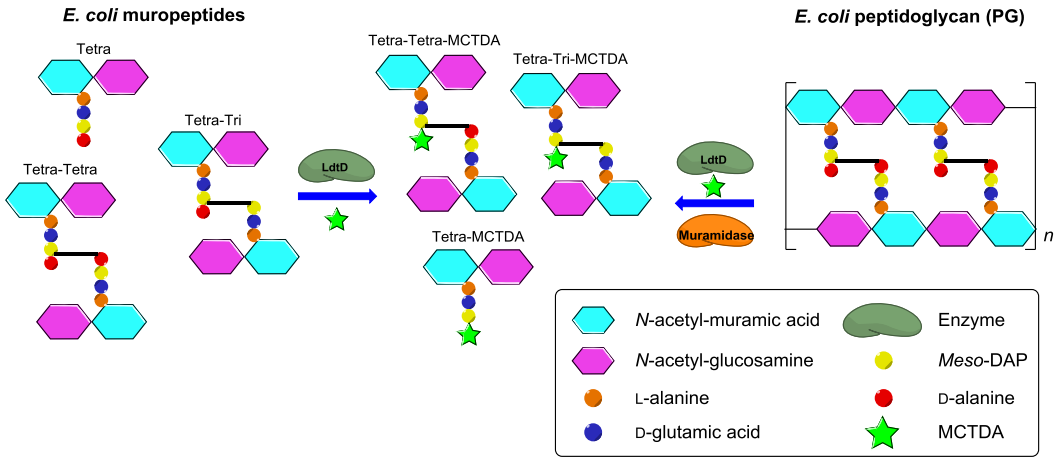

Figure 5.2: Results of MCTDA (**3.3**) LdtD enzymatic incorporation into both *E. coli*. PG and muropeptides.

In future, we would like to evaluate our MCTDA (**3.3**) probes for the identification of PG associated proteins through photoactivated covalent capture. This would involve incorporation of MCTDA (**3.3**) into the PG of live *E. coli* strains, followed by covalent cross-linking by UV irradiation, isolation and digestion of the PG and finally protein identification by LCMS. If successful this approach could also be applied to other bacterial species such as *B. subtilis*, to help to understand the PG biosynthesis in Gram-positive bacteria. Finally, we wish to extend our MCTDA (**3.3**) probes to include other D-amino acids, such as D-lysine (**5.1**), to study if such probes can also be incorporated into the PG of *E.coli* (and other bacteria) via LD-transpeptidase enzymes to provide further information into PG biosynthesis (Figure **5.3**).

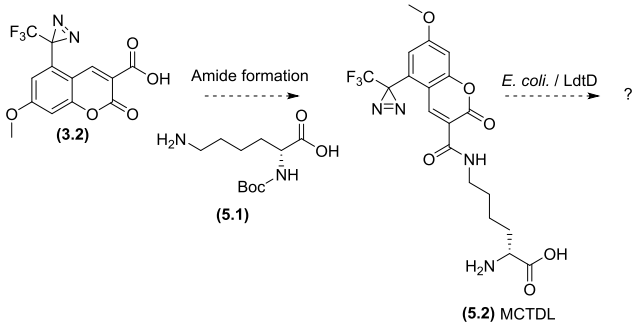

Figure 5.3: Planned synthesis of MCTDL (**5.2**) for enzymatic incorporation into *E. coli* PG.

Chapter 6. Experimental

6.1 General – Chemistry

Unless otherwise noted, ^{1}H NMR and ^{13}C NMR spectroscopic analysis were performed on a Bruker Avance III 300 MHz or Jeol Ec S-400 MHz, samples were dissolved in $CDCl_3$, d_6-DMSO, D_2O or CD_3OD. Infrared analysis carried out by Varian 800 FT-IR spectrophotometer as neat, all IR spectra characterized by cm^{-1} units. Melting points were recorded on Stewart variable temperature apparatus and all melting points were uncorrected. Reverse phase column chromatography purifications were carried out using Biotage automated flash system, models Isolera One and LS with SNAP ultra C18 column (12 and 30 g), with UV monitoring at 278 nm and collection at 254 nm, and 280 nm. High resolution mass analysis was accessed through the National Mass Spectrometry Service (Swansea University) and Science, Agriculture & Engineering (SAgE) mass spectrometry center (Newcastle University) performed by Dr Rachael Dack and Dr Alex Charlton. Optical rotation measurements were carried out with POLAAR 2001 polarimeter using cell path length of 0.5 dm at 25 °C, with a $\lambda = 589$ nm and all measurements were performed in spectrometric grade methanol. All chromatographic separation was performed by column chromatography with Geduran silicagel 60 (40-63 μm). Analytical thin layer chromatography (TLC) tests were performed by using aluminum plates coated with a 0.2 mm thickness of silica gel 60 F_{254} from Merck.

All air sensitive chemical reactions were performed using standard Schlenk techniques involving inert reaction atmosphere (nitrogen) and anhydrous solvents distilled under inert atmosphere and used directly. Anhydrous dichloromethane was distilled from calcium hydride, Anhydrous tetrahydrofuran and Anhydrous diethyl ether were distilled from sodium/benzophenone, and anhydrous toluene was distilled from sodium. All light sensitive diazirine formation reactions were carried out in dark.

6.1.1) 2,2'-((*1R,2R*)-1,2-bis(((*E*)-2,4,6-trimethylbenzylidene)amino)ethane-1,2-diyl)diphenol (2.21)[1]

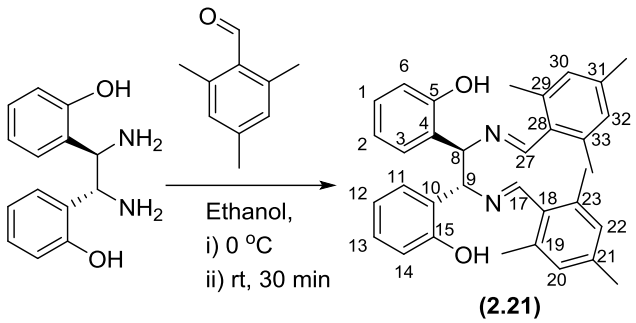

(2.21)

(*R,R*)-HPEN (0.2 g, 0.8186 mmol) was added to 100 mL round bottom flask, under air, then ethanol (1.64 mL) was added, the reaction mixture became cloudy after ethanol addition. The obtained cloudy solution was cooled to 0 ˚C, then mesitaldehyde (0.27 g, 1.842 mmol) was added, and after stirring for 5 minutes the reaction mixture solution became clear. The clear solution of reaction mixture was allowed to warm at room temperature. A white solid precipitated out within minutes. After 30 minutes the colour of the obtained precipitate was changed to yellow. The reaction mixture was then filtrated under vacuum to collect precipitated product. The collected yellow precipitate was washed with ethanol, and dried under vacuum then was redissolved in chloroform and solvent removed under reduced pressure to give (**2.21**) (0.3201 g, 0.63 mmol, 77 %) as a yellow solid. It should be noted that traces of the [3,3] diaza-Cope rearrangement product (**2.22**) were observed in the ^{1}H and ^{13}C NMR spectra.

^{1}H NMR (300 MHz, Chloroform-*d*) δ 10.30 (s, 2H, OH), 8.55 (s, 2H, H-17, H-27), 7.11 (qd, *J* = 8.1, 1.8 Hz, 2H, H-2, H-12), 6.88 (dd, *J* = 8.1 , 1.2 Hz, 2H, H-3, H-11), 6.81 (s, 4H, H-20, H-22, H-30, H-32), 6.55 (td, *J* = 7.4, 1.2 Hz, 2H, H-1, H-13), 6.46 (dd, *J* = 7.6, 1.7 Hz, 2H, H-6, H-14), 4.91 (s, 2H, H-8, H-9), 2.27 (s, 12H, H-24, H-25, H-34, H-36), 2.26 (s, 6H, H-26, H-35); ^{13}C NMR (75 MHz, $CDCl_3$) δ 163.8 (C- 17,27), 156.1 (C-5,15), 140.5 (C-21,31), 138.7 (C-19,23,29,33), 133.8 (C-20,22,30,32), 131.7 (C-18,28), 129.2 (C-4,10), 128.4 (C-2,12), 124.4 (C-1,13), 119.1 (C-6,14), 118.5(C-3,11), 81.0 (C-8,9), 21.1 (CH_3), 21.0 (CH_3).

Observed ^{1}H NMR and ^{13}C NMR spectra were consistent with those reported by Chin *et al.*[1]

6.1.2) 2,2s'-((*1E,1'E*)-(((*1S,2S*)-1,2-dimesitylethane-1,2-diyl)bis(azanylylidene))bis(methanylylidene))diphenol (2.22).[1]

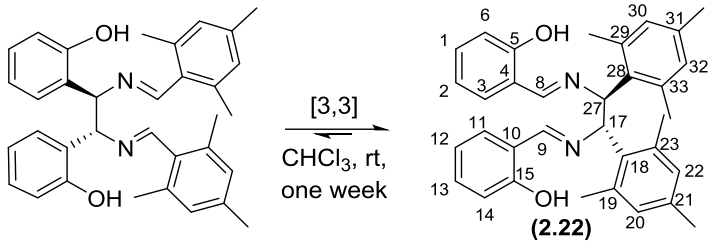

(*R,R*)-**7**a (0.289 g, 0.572 mmol) was placed in 100 mL round bottom flask, then chloroform (25 mL) was added under air, and the resulting solution was kept stirring at room temperature for 1 week. The solvent was removed under reduced pressure to give (**2.22**) (0.256 g, 0.50 mmol, 89 %) as a yellow oil and with no further purification required.

^{1}H NMR (300 MHz, Chloroform-*d*) δ 13.22 (s, OH), 8.44 (s, 2H, H-8,9), 7.30 – 7.19 (m, 8H), 6.93 – 6.80 (m, 4H), 5.68 (s, 2H), 2.69 (s, 6H, CH_3), 2.22 (s, 6H, CH_3), 1.87 (s, 6H,CH_3),

^{13}C NMR (75 MHz, $CDCl_3$) δ 165.8 (C-8,9), 161.3 (C-5,15), 137.5 (C-18,28), 137.2, 134.4 (C-4,10), 132.8 (C-20,22,30,32), 132.2 (C-6,14), 131.6 (C-21,31), 129.6 (C-19,23,29,33), 119.4 (C-3,11), 119.1 (C-1,13), 117.3 (C-2,12), 71.4 (C-17,27), 22.6 (CH_3), 21.2.(CH_3).
Observed ^{1}H NMR and ^{13}C NMR spectra were consistent with those reported by Chin *et al.*[1]

6.1.3) (*1S,2S*)-1,2-dimesitylethane-1,2-diamine (2.23).[1]

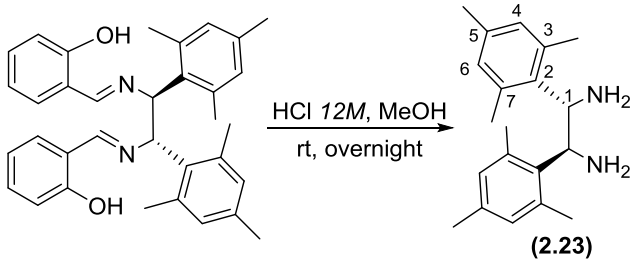

(2.23)

(*S,S*)-**7**b (0.7054 mmol, 0.356 g) was placed in 100 mL round bottom flask, followed by the addition of methanol (71 mL) under air. The obtained solution was acidified with HCl 12*M* (1.78 mL). The reaction mixture left to stir at room temperature overnight. The aqueous layer was washed with diethyl ether and then basified with NaOH 6*M* solution to pH 13.

The aqueous basic layer was extracted by diethyl ether, the organic layer was dried over anhydrous sodium sulphate, filtered, and solvent removed under reduced pressure to give (**2.23**) (0.123 g, 0.41 mmol, 59 %) as a yellow oil.

^{1}H NMR (300 MHz, Methanol-d_4) δ 6.79 (s, 2H, H-4), 6.48 (s, 2H, H-6), 4.57 (s, 2H, H-1), 2.58 (s, 6H, CH_3), 2.13 (s, 6H, CH_3), 1.62 (s, 6H, CH_3); ^{13}C NMR (75 MHz, Methanol-d_4) δ 137.9 (C-2), 137.6 (C-5), 137.1 (C-3,7), 132.0 (C-4), 129.9 (C-6), 55.4 (C-1), 21.7 (CH_3), 20.8 (CH_3), 20.6 (CH_3).

Observed ^{1}H NMR and ^{13}C NMR spectra were consistent with those reported by Chin *et al*.[1]

6.1.4) (*S*,*S*) 4,5-dimesityl-4,5-dihydro-1*H*-imidazol-2-amine [(*S*,*S*)-mesityl guanidine] (2.15).[1]

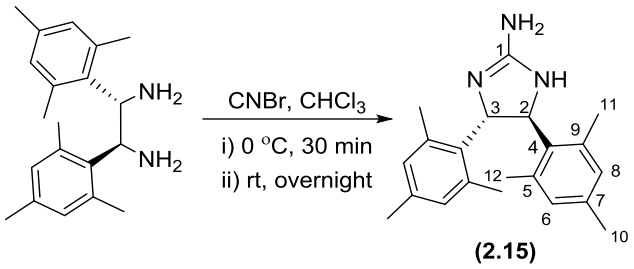

(2.15)

CNBr (0.1377 g, 1.3 mmol) was placed in 25 mL round bottom flask followed by the addition of $CHCl_3$ (1.5 mL) under air. The obtained solution was slowly added to a stirred solution of mesityl diamine (*S*,*S*)-TPEN (0.3 g, 1 mmol) in $CHCl_3$ (10 mL) at 0 °C.

The resulted mixture was stirred for 30 minutes at 0 °C, then the mixture was allowed to warm to room temperature overnight. After 19 h the reaction mixture was concentrated under reduced pressure, and the resulted guanidinium salt was partitioned between $CHCl_3$ (15 mL)/ H_2O (15 mL). The resulted mixture was basified with NaOH (0.03 g) and left to stir at room temperature for one hour and then concentrated under reduced pressure. The obtained aqueous residue was then filtered and the obtained precipitate was washed with H_2O and dried under vacuum to give (**2.15**) (0.198 g, 0.61 mmol, 62 %) as an olive powder.

^{1}H NMR (300 MHz, Methanol-d_4) δ 6.89 (s, 2H, H-8), 6.68 (s, 2H, H-6), 5.41 (s, 2H (H-2)), 2.51 (s, 6H, CH_3-12), 2.21 (s, 6H, CH_3-11), 1.75 (s, 6H, CH_3-10); ^{13}C NMR (75 MHz, Methanol-d_4) δ 161.7 (C-1), 138.3 (C-5), 138.0 (C-9), 137.4 (C-7), 135.2 (C-4), 132.5 (C-8), 129.9 (C-6), 65.1 (C-2,3), 20.8 (C-11), 20.3 (C-10,12). IR (neat): υ_{max}/cm^{-1}: 848, 1029, 1075, 1153, 1203, 1277, 1382, 1446, 1519, 1583, 1610, 1633, 1689, 2963, 3385, 3487.

Observed ^{1}H NMR and ^{13}C NMR spectra were consistent with those reported by Chin *et al*.[1]

6.1.5) 3-(3-Methyl-3-diazirinyl)propanoic acid (2.6).[2]

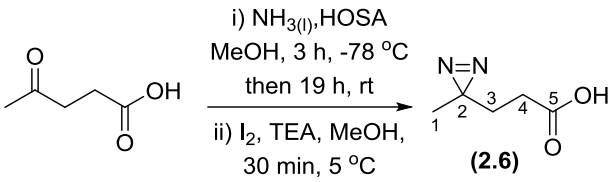

Levulinic acid (2.3224 g, 20 mmol), was placed in1-L, three-necked round-bottomed flask, then it was dissolved in methanol (152 mL) under air. The reaction flask was placed in ice bucket containing dry ice and acetone. Anhydrous ammonia (30 mL) was added to a conical flask via controlled rubber hose. The anhydrous ammonia (30 mL) was then added to the reaction mixture. The reaction vessel side necks were sealed by glass stoppers and the main middle one was closed by a cold figure filled with acetone and dry ice. Hydroxylamine-*O*-sulfonic acid (HOSA) (3.845 g, 34 mmol,) was dissolved in methanol (25 mL), and the resulted solution was added in 10 portions over 1 h to the reaction mixture. Ammonium sulfate salt formed upon the previous additions as a white precipitate. Liquid ammonia (30 mL) was added to compensate the loss of ammonia volume during (HOSA) addition. The reaction mixture left to stir at -78 ˚C for 3 h. After 3 hr the cold Finger was removed, the side stoppers were removed also, the reaction mixture was removed from the ice bath, and then the suspension was stirred for 19 h at room temperature to evaporate the excess amount of ammonia gas.

The reaction mixture was filtered by vacuum to remove the ammonium sulfate, and then was washed with methanol (25 mL). After which the solvent was removed under reduced pressure obtaining a green yellowish residue. The obtained residue was dissolved in methanol (11 mL) and cooled to 5 ˚C. The reaction mixture was then removed from the ice bath and triethylamine (3.911 mL, 28 mmol,) was added. The resulting reaction mixture was stirred for 15 min at room temperature. The solvent was again removed under reduced pressure. Then, the obtained residue was left to evaporate at room temperature overnight to remove any excess of ammonia.

After 19 h the reaction mixture was tested by litmus paper which gave green colour, therefore the obtained residue was left to stir under air for 2 hours to remove excess of

ammonia. The obtained green oil was dissolved in methanol (101 mL) and cooled to 5 ˚C. Then triethylamine (20.06 mL, 142.37 mmol) was added followed by the addition of solid iodine (5.0763 g, 20 mmol). The reaction mixture stirred at 5 ˚C for 30 min. The reaction mixture was then concentrated under reduced pressure. The obtained residue was partitioned between DCM (100) mL and 3 % Na_2CO_3 (50 mL). The two layers were separated, and the isolated aqueous layer was washed two times with DCM (50 mL). The organic layer was extracted two times with 3 % Na_2CO_3 (50 mL). Then the combined aqueous layers were acidified with concentrated HCl and extracted with three times with DCM (50 mL). The obtained organic layer was washed with brine, dried over magnesium sulfate, filtered and solvent removed under reduced pressure. The previous work-up procedure was repeated using diethyl ether as a replacement to DCM as an attempt to remove excess amount of iodine. However, following second work-up attempt (**2.6**) was obtained (0.849 g, 6.62 mmol, 34 %) as a red oil.

^{1}H NMR (300 MHz, Chloroform-*d*) δ 2.23 (t, *J* = 7.6 Hz, 2H, H-4), 1.72 (t, *J* = 7.8 Hz, 2H, H-3),1.04 (s, 3H, H-1); ^{13}C NMR (75 MHz, Chloroform-*d*) δ 178.8 (C-5), 30.3 (C-3), 29.4 (C-4), 26.0 (C-2), 20.7 (C-1); IR (neat): υ_{max}/cm^{-1}: 833, 917, 1068,1209, 1292, 1386, 1415, 1440, 1585 (diazirine), 1709, 2961 (broad).

Observed ^{1}H NMR and ^{13}C NMR spectra were consistent with those reported by Behrman *et al*.[2]

6.1.6) *Tert*-butyl-2-((diphenylmethylene)amino)-3-phenylpropanoate (2.37).[3]

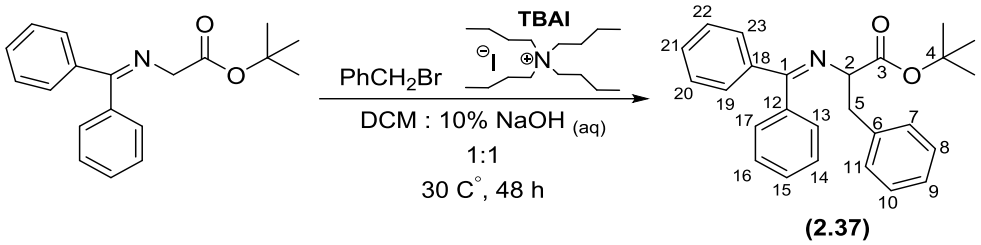

Schiff base (*N*-(diphenylmethylene) glycine *tert*-butyl ester) (0.14769 g, 0.5 mmol) and TBAI (221.6 g, 0.6 mmol) were placed in 100 mL round bottom flask under air, followed by the addition of DCM (10 mL). The obtained solution was basified with $NaOH_{(aq)}$ 10% (10 mL), then benzyl bromide (0.6 mmol, 0.0712 mL) was added and the reaction mixture was stirred at room temperature for 48 h. Then the reaction phases were separated and the organic layer was washed with brine (25 mL), dried over anhydrous sodium sulfate and filtered, then the solvent was removed under reduced pressure to produce a light-yellow crude residue. The obtained crude residue was dissolved in diethyl ether (20 mL) then filtrated to remove the quaternary bromide salt. The filtrate was then concentrated under reduced pressure to remove solvent. The obtained residue was chromatographed using a mixture of petroleum, ethyl acetate, and chloroform (10:1:0.5) as an eluent to give (**2.37**) (0.1576 g, 0.40 mmol, 68 %) as a colorless oil.

^{1}H NMR (300 MHz, Chloroform-*d*) δ 7.59 – 7.56 (m, 2H-H-13,23), 7.38 – 7.26 (m, 6H, H-9, 14,16,17,19,20,22), 7.20 – 7.15 (m, 2H, H-15,21), 7.07 – 7.04 (m, 2H, H-8,10), 6.60 (d, *J* = 6.8 Hz, 2H, H-7,11)), 4.11 (dd, *J* = 9.0, 4.4 Hz, 1H, H-2), 3.26 (dd, *J* = 13.5, 4.4 Hz, 1H, H-5), 3.16 (dd, *J* = 13.5, 9 Hz, 1H, H-5), 1.44 (s, 9H, CH_3); ^{13}C NMR (75 MHz, $CDCl_3$) δ 171.0 (C-3), 170.4 (C-1), 139.7 (C12), 138.5 (C-18), 136.8 (C-6), 130.2 (C-9), 130.0 (C-13,23), 128.8 (C-14,22), 128.3 (17,19), 128.2 (C-7,11), 128.1 (20,16), 128.0 (15,21), 127.8 (C-8,10), 126.3 (C-9), 81.2 (C-4), 68.0 (C-2), 39.7 (C-5), 28.2 (tertiary butyl).

Observed ^{1}H NMR and ^{13}C NMR spectra were consistent with those reported by Dudding *et al*.[14]

6.1.7) *Tert*-butyl -2-((diphenylmethylene)amino)-5-oxohexanoate (±)(2.32).[3]

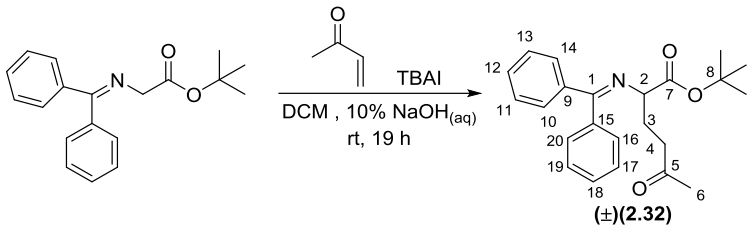

Schiff base (*N*-(Diphenylmethylene) glycine *tert*-butyl ester) (0.14769 g, 0.5 mmol) and TBAI (0.2314 g, 0.6267 mmol) were placed in 100 mL round bottom flask followed by the addition of DCM (10 mL) under air. The reaction vessel was closed with a rubber subta, then the reaction mixture was stirred on max speed for 10 minutes at room temperature. $NaOH_{(aq)}$ 10 % (10 mL) was added to the reaction mixture followed by the addition of methyl vinyl ketone (0.04205g, 0.6 mmol) in dropwise. The reaction mixture was left to stir at room temperature on max speed overnight.

After 19 hr the aqueous layer was removed and the organic layer was washed with brine, dried over anhydrous sodium sulphate, filtrated, and concentrated under reduced pressure to remove solvent. The obtained brown residue was dissolved in diethyl ether (25 mL) and filtered to remove iodine quaternary salt. The obtained filtrate solution was concentrated under reduced pressure to remove solvent to give the racemic (**2.32**) (0.2054 g, 0.56 mmol, 100 %) as a brown oil.

^{1}H NMR (300 MHz, Chloroform-*d*) δ 7.65-7.62 (m, 2H, H-14,16), 7.44 (dd, *J* = 5.0, 1.9 Hz, 3H, H-13,17,20), 7.40 – 7.29 (m, 3H, H-19,11,10), 7.16 (dd, *J* = 6.4, 3.2 Hz, 2H, H-18,12), 3.95 (t, *J* = 6.1 Hz, 1H, H-2), 2.52 (q, *J* = 7.1, 6.6 Hz, 2H, H-4), 2.12 (s, 3H, H-6), 2.17 (dd, , *J* = 13.9, 9 Hz, 1H, H-3), 1.43 (s, 9H, CH_3).

Observed ^{1}H NMR and ^{13}C NMR spectra were consistent with those reported by Belokon *et al*.[15]

6.1.8) *Tert*-butyl (*R*)-2-((diphenylmethylene)amino)-5-oxohexanoate (2.32).[4]

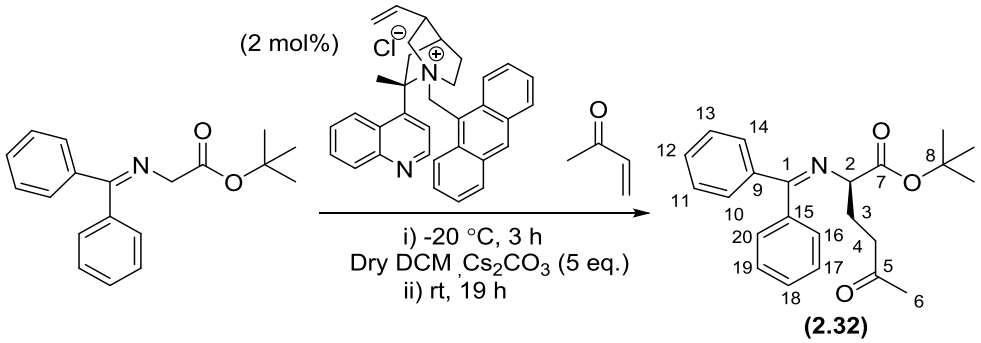

Schiff base (*N*-(Diphenylmethylene)glycine *tert*-butyl ester) (0.1476 g, 0.5 mmol), catalyst 2 mol% (0.52 mg, 0.0012 mmol) and CS_2CO_3 (0.81455 g, 2.5 mmol) were placed in 10 mL round bottom flask respectively followed by the addition of dry DCM (5 mL). The reaction mixture was stirred on max speed under nitrogen atmosphere at -20 ˚C for 10 min.

Methyl vinyl ketone (0.07 g, 1 mmol) was added to the reaction mixture in one portion, and then the reaction mixture was left to stir on max speed at -20 ˚C for 3 h under nitrogen atmosphere. The reaction mixture was warmed up to room temperature and stirred at that temperature overnight. The reaction phases were separated, then the organic layer was dried over anhydrous sodium sulphate, filtered and then solvent removed under reduced pressure to give (**2.32**) (0.17 g, 0.46 mmol, 93 %) as a red crude oil.

^{1}H NMR (300 MHz, $CDCl_3$) δ 7.68 – 7.59 (m, 2H, H-14,16), 7.49 – 7.28 (m, 6H, H-13,17,20,19,11,10), 7.21 – 7.12 (m, 2H, H-18,12), 3.95 (t, *J* = 6.4 Hz, 1H, H-2), 2.66 – 2.39 (m, 2H, H-4), 2.19 – 2.13 (m, 2H, H-3), 2.12 (s, 3H, H-6), 1.43 (s, 9H, CH_3).

^{13}C NMR (75 MHz, $CDCl_3$) δ 208.3 (C-5), 171.0 (C-7), 170.4 (C-1), 139.4 (C-9), 136.7 (C-15), 130.3 (C-14,16), 128.7 (C-13,17), 128.6 (C-11,19), 128.4 (C-10,20), 128.0 (C-12,18), 127.7 (C-Ar), 81.1 (C-8), 64.7 (C-2), 39.8 (C-4), 29.2 (C-6), 28.0 (C-3), 27.7 (tertiary butyl).

Observed ^{1}H NMR and ^{13}C NMR spectra were consistent with those reported by Belokon *et al*.[15]

6.1.9) *Tert*-butyl (*R*)-2-amino-5-oxohexanoate (2.33).[4]

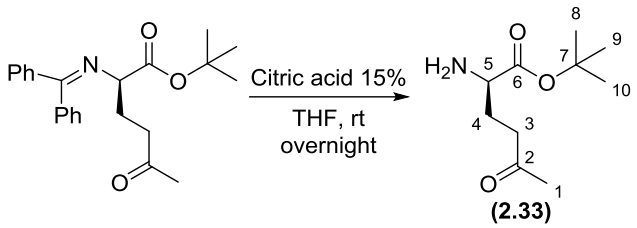

(2.33)

Tert-butyl (*R*)-2-((diphenylmethylene)amino)-5-oxohexanoate (0.7653 g, 2.094 mmol) was placed in 50 mL round bottom flask, followed by the addition of THF (20 mL) under air. Citric acid 15% (8 mL) was added to the reaction mixture. The reaction mixture was stirred on max speed at room temperature overnight. The reaction mixture was evaporated to remove the THF solvent, then the remaining aqueous layer was washed with DCM (20 mL X 3). The aqueous layer was basified with aqueous NaOH (10 %) (20 mL), then the obtained basic aqueous layer was extracted with DCM (5 mL) for three times. The combined organic layers were washed with brine, dried over anhydrous sodium sulphate, filtrated, and solvent removed under reduced pressure to give (**2.33**) (0.131 g,0.65 mmol, 33 %,) as a yellow oil.

^{1}H NMR (300 MHz, Chloroform-*d*) δ 4.56 – 4.50 (m, 1H, H-5), 2.69 – 2.58 (m, 1H, H-3), 2.54 – 2.43 (m, 1H, H-3), 2.21-2.10 (m, 1H, H-4), 2.04-1.92 (m, 1H, H-4), 2.08 (s, 3H, H-1), 1.47 (s, 9H, H-8, H-9, H-10). ^{13}C NMR (75 MHz, Chloroform-*d*) δ 178.1 (C-2), 172.5 (C-6), 80.9 (C-7), 75.0 (C-5), 39.1 (C-3), 28.0 (C-8,9,10), 26.9 (C-1), 19.7 (C-4). IR (neat): υ_{max}/cm^{-1} : 806, 846, 974, 1060, 1148, 1210, 1255, 1367, 1647, 1730, 2977.

6.1.10) *Tert*-butyl (*R*)-2-((*tert*-butoxycarbonyl)amino)-5-oxohexanoate (2.34).[4]

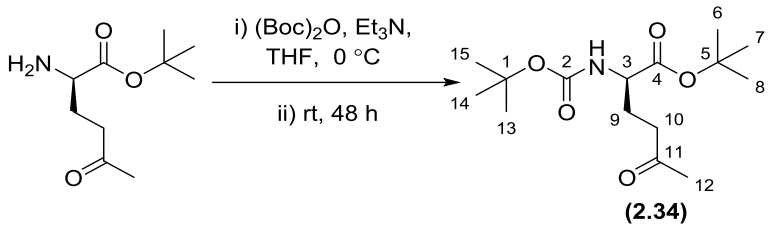

(2.34)

Tert-butyl (*R*)-2-amino-5-oxohexanoate (0.025 g, 0.12411 mmol) was placed in 25 mL round bottom flask, followed by the addition of THF (4 mL) under the air. $(Boc)_2O$ (0.0326 g, 0.161473 mmol) was added to the reaction mixture and then reaction mixture was cooled to 0 °C, followed by the addition of triethyl amine (0.01633 g, 0.161473 mmol). The reaction mixture was warmed up to room temperature and stirred overnight at that temperature. The reaction mixture was diluted with H_2O (20 mL), and the aqueous layer was extracted with ethyl acetate (20 mL) for three times. The combined organic layers were washed with brine, dried over anhydrous sodium sulfate, filtered and solvent removed under reduced pressure. The crude compound was chromatographed using a mixture of petroleum and ether (9:1) as an eluent to give (**2.34**) (0.007 g, 0.023 mmol, 19 %) as a yellow solid.

^{1}H NMR (300 MHz, $CDCl_3$) δ 5.06 (d, *J* = 7.2 Hz, 1H, NH), 4.21 – 4.06 (m, 1H, H-3), 2.65 – 2.39 (m, 2H, H-10), 2.15 (s, 3H, H-12), 1.93 – 1.73 (m, 1H, H-9), 1.46 (s, 9H, H-6,7,8), 1.44 (s, 9H, H-13,14,15), 1.32 – 1.08 (m, 1H, H-9).^{13}C NMR data was too weak to report. HRMS (pNSI) calcd for $C_{15}H_{27}NO_5Na$: 324.1781, found 324.1781.

6.1.11) *N*-3,5-trimethoxy-*N*-methyl benzamide (3.27)[5]

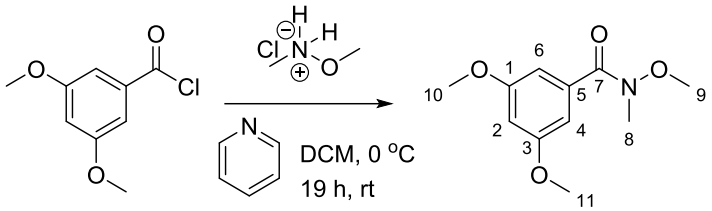

(3.27)

3,5-Dimethoxy benzoyl chloride (5 g, 25 mmol) was placed in 500 mL round bottom flask under inert atmosphere, followed by the addition of dry DCM (200 mL). Then *O*-*N*-dimethyl hydroxylamine (2.5 g, 26 mmol) was added to the reaction mixture. The reaction mixture was cooled to 0 °C for 10 min and pyridine (4.158 g, 52.5 mmol) was added dropwise over period of 10 min. The ice bath was then removed and the reaction mixture allowed to warm to room temperature and stirred overnight.

The reaction mixture washed with HCl 1M (300 mL) two times, $NaHCO_{3\,(sat.aq.)}$ (200 mL) two times, brine and then dried over sodium sulphide anhydrous, filtrated then the solvent removed under reduced pressure. The obtained residues chromatographed using petroleum ether and ethyl acetate mixture (5:5) as eluent to give (**3.27**) (5.5011 g, 24.423 mmol, 98 %) as a colourless oil.

^{1}H NMR (300 MHz, Chloroform-*d*) δ 6.78 (d, *J* = 2.3 Hz, 2H, H-6, H-4), 6.53 (t, *J* = 2.3 Hz, 1H, H-2), 3.80 (s, 6H, H-11, H-10), 3.59 (s, 3H, H-8), 3.33 (s, 3H, H-9); ^{13}C NMR (75 MHz, Chloroform-*d*) δ 169.7 (C-7), 160.4 (C1, C3), 136.1 (C-5), 106.0 (C-4, C-6), 102.9 (C-2), 61.2 (C-9), 55.6 (C-10, C-11), 34.1 (C-8); IR (neat): υ_{max}/cm^{-1} : 2997, 1916, 1733, 1683 (C=O), 1600, 1450, 1200, 1061; HRMS (pNSI) calcd for $C_{11}H_{15}NO_4Na$: 248.0899, found 248.0895.

Observed ^{1}H NMR and ^{13}C NMR spectra were consistent with those reported by Leadbeater *et al*.[5]

6.1.12) Trifluoro-1-(3,5-dimethoxyphenyl) ethanone (3.9)[5]

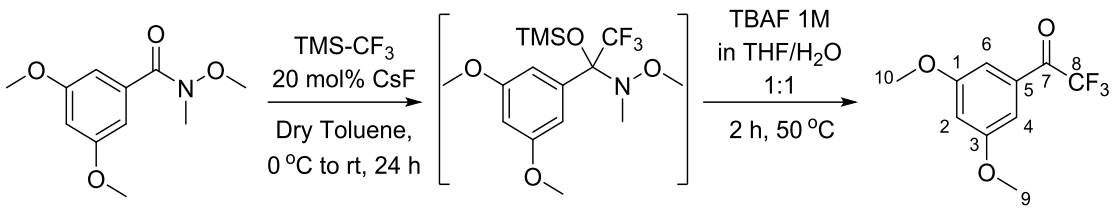

CsF (0.0137 g, 0.9 mmol) was placed in 25 mL round bottom flask under inert atmosphere followed by the addition of dry toluene 1 mL. Then *N*,3,5-dimethoxy-*O*-benzoyl amide solution (1.014 g, 4.50186 mmol) in toluene 1.3 mL was added to the reaction mixture. The reaction mixture placed in ice bath and stirred at 0 ^{o}C for 10 minutes, then TMS-CF_3 (1.28 g, 9 mmol) was added in dropwise at 0 ^{o}C over a period of 10 minutes. The reaction mixture stirred for another 10 minutes at 0 ^{o}C, then the ice bath was removed, and the reaction mixture was allowed to worm up to room temperature overnight. After 19 h, TBAF 1M in THF (4.5 mL-4.5 mmol) was added to the reaction mixture followed by the addition of H_2O 4.5 mL. The reaction mixture stirred at 50 ^{o}C for 2 hours. The reaction mixture then cooled to room temperature and diluted with ether 30 mL, then the organic layer was washed with H_2O (30 mL x 3), brine (30 mL x 3), dried over sodium sulphate anhydrous, filtered and solvent removed under reduced pressure. The obtained crude red oil was chromatographed using a mixture of petroleum ether, ethyl acetate and TFA 0.1% (6:4) as eluent to give (**3.9**) (1.0276 g, 4.388 mmol, 98 %) as a red residue.

^{1}H NMR (300 MHz, Chloroform-*d*) δ 3.85 (s, 6H, H-9, H-10), 6.77 (t, *J* = 2.2 Hz, 1H, H-2), 7.20 – 7.17 (m, 2H, H-4, H-6); ^{13}C NMR (75 MHz, Chloroform-*d*) δ 55.6 (C-9,10), 107.7 (C-2), 108.0 (C-6,4), 116.6 (q, J_{C-F} = 291.3 Hz, C-8), 131.4 (C-5), 161.0 (C-1,3), 180.2 (q, J_{C-F} = 35.0 Hz, C-7); ^{19}F NMR (75 MHz, Chloroform-*d*) δ -71.10 ppm; IR (neat): υ_{max}/cm^{-1} : 2943, 2844, 1715, 1593 (C=O), 1457, 1428, 1359, 1283, 1263, 1197, 1411, 1062, 1003; HMRS (pNSI) calcd for $C_{10}H_{10}F_3O_3$ $[M+H]^+$: 235.0580, found 235.0580.

Observed ^{1}H NMR and ^{13}C NMR spectra were consistent with those reported by Leadbeater *et al*.[5]

6.1.13) 2,2,2-Trifluoro-1-(3,5-dimethoxyphenyl) ethanone oxime (3.29)[6]

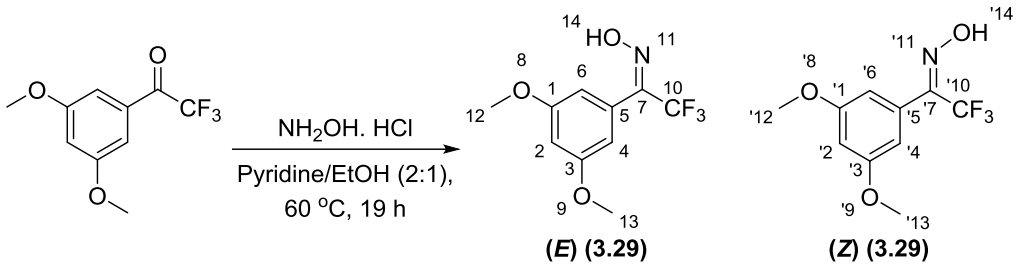

2,2,2-Trifluoro-1-(3,5-dimethoxyphenyl) ethanone (5 g, 22 mmol) was placed in 250 mL round bottom flask under inert atmosphere, followed by the addition of hydroxylamine hydrochloride (1.68 gm, 24 mmol) and ethanol (11 mL). The reaction mixture warmed up to 60 ^{0}C, then pyridine 1M (22 mL) was added to the reaction mixture. The reaction mixture then stirred at 60 ^{0}C for 19 h. The reaction mixture was evaporated to remove solvents. The resulted residue was dissolved in ether (200 mL) , washed with water (200 mLx2), 1M HCl (200 mL x 2), brine, and then the obtained organic layer was dried over anhydrous magnesium sulfate, filtrated and then the solvent was removed under reduced pressure. The crude compound was chromatographed using a mixture of petroleum ether and ethyl acetate (7:3) as an eluent to give (**3.29**) (5.26 g, 21.10 mmol , 97 %, mixture (1:3) of *Z* and *E* isomers) as an orange crystalline.

Mp = 68-71 ^{0}C, ^{1}H NMR (400 MHz, Chloroform-*d*) δ 8.79 (s, 1H, OH-14), 8.56 (s, 1H, OH-14`), 6.63 – 6.61 (m, 2H, H-4,6), 6.60 (m, 2H, H- 4`,6`), 6.58 – 6.55 (m, 2H, H-2, 2`), 3.81 (s, 12H, -H-12, H-13); ^{13}C NMR (75 MHz, $CDCl_3$) δ 161.3 (C-1,3), 148.2 (q, J_{C-F} = 32.6 Hz, C-7), 128.0 (C-5), 121.0 (q, J_{C-F} = 274.6 Hz, C-10), 107.1 (4-6), 103.1 (C-2), 56.0 (C-12,13- two methoxy peaks overlapped); ^{19}F NMR (282 MHz, Chloroform-*d*) δ -66.89, -62.35; IR (neat): υ_{max}/cm^{-1} : 3351, 2951, 1592, 1459; HRMS (ES-) calcd for $C_{10}H_9F_3O_3N$: 248.0535, found 248.0444.

Observed ^{1}H NMR and ^{13}C NMR spectra were consistent with those reported by Hayes *et al.*[6]

6.1.14) 2,2,2-Trifluoro-1-(3,5-dimethoxyphenyl)ethanone -*O*-*p*-toluenesulfonyloxime (3.30)[6]

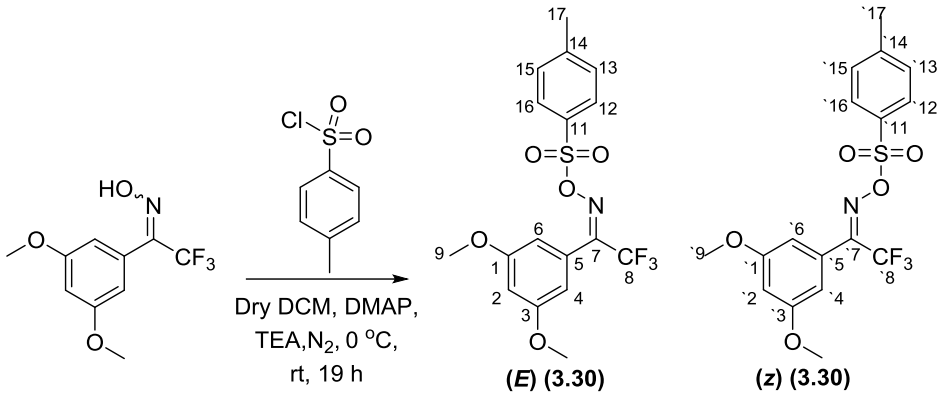

DMAP (0.05197 g, 0.4254 mmol) and *p*-toluene sulfonyl chloride (4.054 g, 21.268 mmol) were placed in 150 mL round bottom flask under inert atmosphere. Then 2,2,2-Trifluoro-1-(3,5-dimethoxyphenyl) ethanone oxime (5.3g, 21.268 mmol) dissolved in dry DCM (82 mL) and the resultant solution transferred to the reaction mixture via glass syringe. The reaction mixture stirred at room temperature under nitrogen in dark, then triethyl amine (3.29 g, 31.9 mmol) was added to reaction mixture. The reaction mixture left to stir at room temperature under nitrogen overnight.

The reaction mixture washed with 0.25 M HCl (100 mL x 2), $NaHCO_{3\ (sat.\ aq.)}$ (100 mL X 2) , water (100 mL X 3), brine, then dried over anhydrous $MgSO_4$, filtered and solvent removed under reduced pressure. The obtained residues recrystallized from hexane-ethyl acetate to give (**3.30**) (7.56 g, 18.74 mmol, 88 %) as colourless prism crystals of *E* and *Z* isomers (9:1).

Mp = 118-121 ˚C; ^{1}H NMR (300 MHz, Chloroform-*d*) δ 7.94 – 7.85 (m, 4H, H-16, H-12, E and Z), 7.42 – 7.33 (m, 4H, H-15, H-13, E and Z), 6.61 – 6.55 (m, 2H, H-2, E and Z), 6.55 – 6.50 (m, 2H), 6.45 (d, *J* = 2.3 Hz, 2H), 3.80 (s, 6H, H-9, H-10, Z), 3.79 (s, 6H, H-9, H-10, E), 2.48 (s, 3H, H-17, Z), 2.17 (s, 3H, H-17, E); ^{13}C NMR (75 MHz, Chloroform-*d*) δ 160.9 (C-1, 3), 160.7 (C-`1,`3), 154.3 (q, $J_{C\text{-}F}$= 37.5 Hz, C-7), 146.1 (C-11), 131.4 (C-5), 131.2 (C-`5), 129.88 (C-12,16), 129.86 (C-`12,`16), 129.28 (C-13,15), 129.20 (C-`13,`15), 126.0 (C-14), 121.3 (q, $J_{C\text{-}F}$ = 277.5 Hz, C-8), 107.9 (C-4,6), 106.3 (C-`4,`6), 103.6 (C-2), 103.3 (C-`2), 55.5 (9,10), 55.5 (C-`9,`10), 21.8 (C-17), 21.7 (C-`17). C-`7,`11,

`14 and `8 did not observed. Z isomer.^{19}F NMR (282 MHz, Chloroform-*d*) δ -61.53 (E), -67.07 (Z); IR (neat): υ_{max}/cm^{-1} : 2949, 1590. HRMS (TOF MS ESI +): calcd for $C_{17}H_{16}F_3NO_5SNa$ $[M+Na]^+$: 426.0599; observed: 426.0062.

Observed ^{1}H NMR and ^{13}C NMR spectra were consistent with those reported by Hayes *et al*.[6]

6.1.15) 3-(3,5-Dimethoxyphenyl)-3-(trifluoromethyl)-diaziridine (3.31)[6]

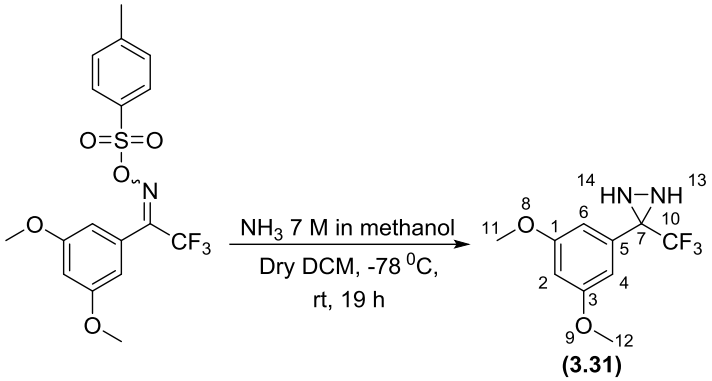

(3.31)

O-Tosyl-2,2,2-trifluoro-1-(3,5-dimethoxyphenyl)-ethanone oxime (2.01 g, 5 mmol) placed in 500 mL Schlenk flask under nitrogen atmosphere, followed by the addition of dry DCM (3 mL). The reaction mixture then cooled to -78 ˚C and methanolic ammonia 7 M (74 mmol, 10.71 mL) was added to the reaction mixture in dropwise behind blast shield.

The reaction mixture stirred at -78 ˚C for one hour and then allowed to warm up to room temperature over overnight.

The reaction mixture opened to air very carefully and diluted with DCM (100 mL), H_2O (100 mL), and stirred at room temperature for 2 h to safely evaporate ammonia gas.

The organic layer then washed with H_2O (100 mL x 3), brine and dried over magnesium sulfate, filtered and solvent removed under reduced pressure. The obtained residue was chromatographed using mixture of petroleum ether, ethyl acetate (4:1) as eluent to give (**3.31**) (01.0965 g, 4.417 mmol, 89 %) as colourless crystals.

Mp = 97-101 ^{o}C ; ^{1}H NMR (300 MHz, Chloroform-*d*) δ 6.75 (d, *J* = 2.3 Hz, 2H, H-4,6), 6.50 (t, *J* = 2.3 Hz, 1H, H-2), 3.79 (s, 6H, H-11,12), 2.79 (d, *J* = 8.3 Hz, 1H, H-13), 2.28 (d, *J* = 8.3 Hz, 1H, H-14);

^{13}C NMR (75 MHz, Chloroform-*d*) δ 160.9 (C-1,3), 133.5 (C-5), 117.9 (q, $J_{C\text{-}F}$= 270 Hz, C-10), 106.1(C-4,6), 102.1 (C-2), 57.4 (q, $J_{C\text{-}F}$ = 36 Hz, C-7), 55.4 (C-11,12); ^{19}F NMR (282 MHz, Chloroform-*d*) δ -75.43; IR (neat): υ_{max}/cm^{-1} : 3253, 2942, 2845, 1597. HRMS (TOF MS ESI +): calcd for $C_{10}H_{12}F_3N_2O_2$ $[M+H]^+$: 249.0851; observed: 249.0375.

Observed ^{1}H NMR and ^{13}C NMR spectra were consistent with those reported by Hayes *et al*.[6]

6.1.16) 3-Trifluoromethyl-3-(3,5-dimethoxyphenyl)-3*H*-diazirine (3.10)[6,8]

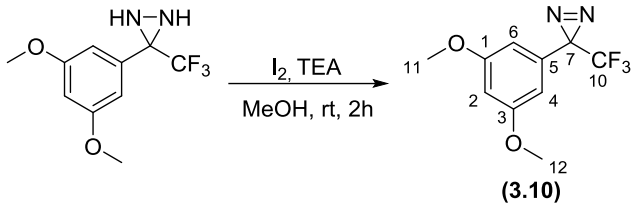

(3.10)

3-(3,5-Dimethoxyphenyl)-3-(trifluoromethyl)-diaziridine (1.3824 g, 5.5697 mmol) was placed in 500 mL round bottom flask, followed by the addition of methanol (10 mL) at room temperature under air. To the obtained solution, trimethylamine (1.127 g, 11.139 mmol, 1.5 mL) was added, followed by the addition of iodine (1.48g, 5.848 mmol), then the reaction mixture stirred at room temperature for 2 h.

The reaction mixture extracted by diethyl ether (50 mL x 3), then the combined etheric layers washed with water (50 mL x 3), brine, dried over magnesium sulfate, filtered, and slvent removed under reduced pressure to give (**3.10**) (1.0715 g, 4.352 mmol, 78 %) as a red oil.

^{1}H NMR (300 MHz, Chloroform-*d*) δ 6.48 (t, *J* = 2.2 Hz, 1H, H-2), 6.29-6.28 (m, 2H, H-4,6), 3.78 (s, 6H, H-11,12); ^{13}C NMR (62.5 MHz, CDCl3): 28.9 (q, J_{C-F} = 40 Hz, C-10), 55.4 (C-11,12), 101.5 (C-2), 104.7 (C-4,6), 123.8 (q, J_{C-F} = 275 Hz, C-10), 131.1 (C-5), 161.1 (C1,3) ppm; ^{19}F NMR (282 MHz, Chloroform-*d*) δ -65.08; IR (neat): υ_{max}/cm^{-1} : 2940, 2846, 1594. HRMS (pNSI) calcd for $C_{10}H_{10}F_3O_2N_2$: 247.0694, found 247.0825.

Observed ^{1}H NMR, ^{13}C NMR and ^{19}F NMR spectra were consistent with those reported by Hayes *et al*.[6]

6.1.17) 2-(3-Trifluoromethyl)-3*H*-diazirine-3-yl)-4,6-dimethoxybenzaldehyde and 4-(3-Trifluoromethyl)-3*H*-diazirin-3-yl)-2,6-dimethoxybenzaldehyde (3.11), (3.33)[7]

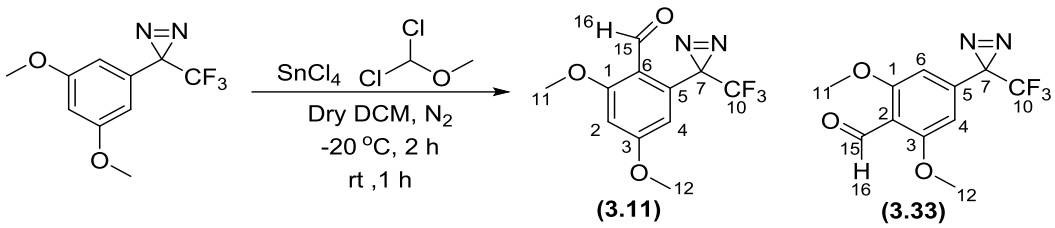

3-Trifluoromethyl-3-(3,5-dimethoxyphenyl)-3*H*-diazirine (1.5 g, 6.1415 mmol) was placed in 25 mL pear shape flask under nitrogen, followed by the addition of dry DCM (6 mL). The reaction mixture cooled to -20 °C then tin tetrachloride (2.39 g, 9.212 mmol) was added to the reaction mixture via syringe at -20 °C followed by the addition of dichloromethyl methyl ether (1.059 g, 9.212 mmol). The reaction mixture stirred at -20 °C for two hours then warned up to room temperature and stirred for one hour.

The reaction mixture quenched with water 10 mL and the product extracted by DCM three times, then the combined organic layers washed with water (200 mL), $NaHCO_{3(sat.aq)}$ (150 mL), brine, then dried over anhydrous magnesium sulfate, filtered and solvent removed under reduced pressure. The obtained crude residues chromatographed using petrol - ether (1:1) as eluent to give (**3.11**) (0.94 g, 3.428 mmol, 56 %) as colourless crystals; and the (**3.33**) (0.429 g, 1.564 mmol, 26 %) as yellow crystals.

2-(3-Trifluoromethyl)-3*H*-diazirine-3-yl)-4,6-dimethoxybenzaldehyde (3.11)

Mp: 145-150 °C; ^{1}H NMR (300 MHz**,** Chloroform-d) δ 10.48 (s, 1H, H-16), 6.76 (d, *J* = 2.0 Hz, 1H, H-4), 6.55 (d, *J* = 2.3 Hz, 1H, H-2), 3.91 (s, 3H, H-11), 3.90 (s, 3H, H-12); ^{13}C NMR (75 MHz, CDCl3) δ 187.9 (C-15), 166.2 (C-1), 165.4 (C-3), 131.4 (C-5), 124.0 (q, $J_{C\text{-}F}$ = 275 Hz, C-10), 118.8 (C-6), 108.8 (C-4), 100.7 (C-2), 56.6 (C-11), 56.4 (C-12), 30.0 (q, $J_{C\text{-}F}$= 42 Hz, C-7). ^{19}F NMR (282 MHz, Chloroform-d) δ -70.20; IR (neat): υ_{max}/cm-^{1}, 2955, 1673, 1595, 1457; HRMS (ES+) calcd for $C_{11}H_9F_3O_3N_2Na$: 297.0463, found 297.0597.

Observed ^{1}H NMR spectra were consistent with those reported by Tomohero *et al*.[8]

4-(3-Trifluoromethyl)-3*H*-diazirin-3-yl)-2,6-dimethoxybenzaldehyde (3.33)

Mp: 52-54 ^{o}C; ^{1}H NMR (400 MHz, Chloroform-*d*) δ 10.45 (s, 1H, H-16), 6.31 (s, 2H, H-4,6), 3.89 (s, 6H, H-11,12).^{13}C NMR (75 MHz, $CDCl_3$) δ 188.5 (C-15), 162.1 (C-1,3), 136.5 (C-5), 119.9 (C-10), 114.8 (C-2), 102.06 (C-6), 102.04 (C-4), 56.2 (C-11,12). ^{19}F NMR (282 MHz, $CDCl_3$) δ -64.55; IR (neat): υ_{max}/cm^{-1}: 1691, 1604, 1569, 1456.

Note: C-7 not observed in the ^{13}C NMR spectrum.

Observed ^{1}H NMR spectra were consistent with those reported by Tomohero *et al*.[8]

6.1.18) 6-Hydroxy-4-methoxy-2-(3-trifluoromethyl)-3*H*-diazirine-3-yl) benzaldehyde (3.12)[8]

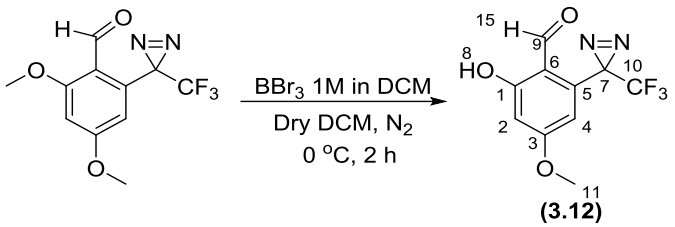

(3.12)

2-(3-Trifluoromethyl)-3*H*-diazirine-3-yl)-4,6-dimethoxybenzaldehyde (0.13g, 0.49mmol) was placed in 25mL pear shape flask under inert atmosphere, followed by the addition of dry DCM (1.4 mL). The reaction mixture cooled to 0 ^{o}C, followed by the addition of BBr_3 1M in DCM (0.74 mL, 0.73 mmol) slowly. The reaction mixture stirred at 0 ^{o}C for 2 h. Then the reaction mixture quenched with water (1mL) at 0 ^{o}C and left to stir at this temperature for 15 minutes.

The reaction mixture diluted with DCM (25 mL) and washed with water (30 mL X 2), dried over anhydrous $MgSO_4$, filtered and solvent removed under reduced pressure. The obtained crude was chromatographed using mixture of petroleum ether and ethyl acetate (5:1) as eluent to give (**3.12**) (0.1166 g, 90 %). as a purple oil.

^{1}H NMR (300 MHz, Chloroform-*d*) δ 12.37 (s, 1H, H-8), 10.55 (s, 1H, H-15), 6.79 (d, *J* = 2.4 Hz, 1H, H-4), 6.49 (d, *J* = 2.4 Hz, 1H, H-2), 3.87 (s, 3H, H-11);^{13}C NMR (75 MHz, Chloroform-d) δ 192.1 (C-9), 166.9 (C-3), 166.8 (C-1), 132.0 (C-5), 123.4 (C-10), 112.8 (C-6), 112.0 (C-4), 103.0 (C-2), 56.0 (C-11), 22.6 (C-7); ^{19}F NMR (282 MHz, Chloroform-*d*) δ -67.94; IR (neat): υ_{max}/cm^{-1} : 2924, 1651, 1608; HRMS (ES-) calcd for $C_{10}H_6F_3O_3N_2$: 259.0331, found 259.0235.

Observed ^{1}H NMR spectrum were consistent with those reported by Tomohero *et al.*[8]

6.1.19) 2-oxo-2*H*-chromene-3-carboxylic acid (3.39)[9]

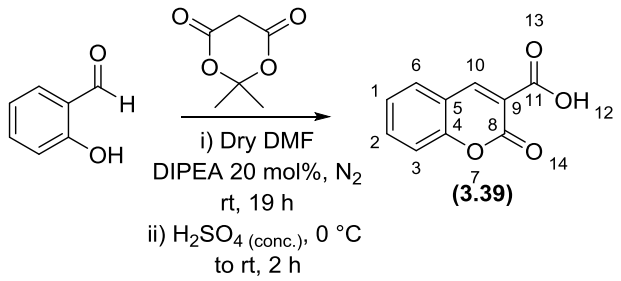

Meldrum's acid (0.735 g, 5 mmol) was placed in 25 ml round bottom flask under N_2 followed by the addition of dry DMF (8.3 mL). Then salicylaldehyde (0.6 g, 5 mmol) was added in dropwise. DIPEA (0.13 g,1 mmol) was added slowly via syringe to the reaction mixture at rt under a nitrogen atmosphere. The reaction mixture stirred at rt overnight.

The reaction mixture cooled to 0 ^oC and cold concentrated H_2SO_4 (5 mL) was added slowly and then stirred at rt for 2 h. The reaction mixture poured in crushed ice and left to crystalize overnight in a cool place. The retraction mixture was filtered under vacuum and the obtained powder was washed with cold water during the filtration process and dried to give (**3.39**) (0.7339g, 3.85 mmol, 77 %) as an olive powder.

Mp: 175-180 ^oC;^1H NMR (300 MHz, DMSO-d_6) δ 13.27 (s, 1H), 8.75 (s, 1H), 7.91 (dd, *J* = 7.7, 1.6 Hz, 1H), 7.74 (ddd, *J* = 8.5, 7.3, 1.7 Hz, 1H), 7.47 – 7.42 (m, 1H), 7.40 (dd, *J* = 7.5, 1.0 Hz, 1H); ^{13}C NMR (75 MHz, DMSO-d_6) δ 164.4 (C-11), 157.1 (C-8), 154.9 (C-4), 148.8 (C-10), 134.7 (C-1), 130.6 (C-6), 125.3 (C-3), 118.8 (C-9), 118.4 (C-5), 116.6 (C-2); IR (neat): υ_{max}/cm^{-1} : 3056 (Ar-CH), 2778 (OH carboxylic acid) 1735 (Ar-O-CO), 1670 (C=C-CO). HRMS (TOF MS ESI +): calcd for $C_{10}H_7O_4$ $[M+H]^+$: 191.0344; observed: 190.9918.

Observed ^1H NMR spectrum were consistent with those reported by Ghosh *et al*.[16]

6.1.20) Methyl (2-oxo-2*H*-chromene-3-carbonyl) glycinate (3.43)

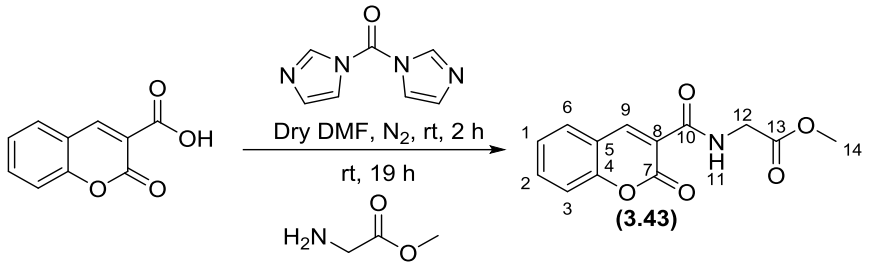

2-oxo-2*H*-chromene-3-carboxylic acid (201 mg, 1.058 mmol) was placed in 25 mL pear shape flask under N_2, followed by the addition of dry DMF 10.6 mL. *N*,*N*,carbonyldiimidazole (CDI) (172 mg, 1.058 mmol) was added to the reaction mixture in one portion. The reaction mixture then stirred at room temperature under nitrogen for 2 h. Glycine methyl ester hydrochloride (133 mg, 1.0586 mmol) was added in one portion to the reaction mixture. The reaction mixture allowed to stir at room temperature under nitrogen overnight. After a reaction time of 19 h, the reaction mixture was diluted with ethyl acetate (100 mL) and washed with 1M HCl (50 mL), H_2O (100 mL), the aqueous layer extracted with ethyl acetate (50 mL) to reduce any loss in product, then the combined organic layers were washed with brine, dried over anhydrous sodium sulfate, filtered and solvent removed under reduced pressure. The obtained crude material was chromatographed using DCM:MeOH (9:1) as eluent to give (**3.43**) (0.2526 g, 0.966 mmol, 92 %) as a white crystalline.

Mp: 186-189 ^{o}C; ^{1}H NMR (300 MHz, Chloroform-*d*) δ 9.24 (s, 1H, H-11), 8.90 (s, 1H, H-9), 7.76 (m, 1H, H-1), 7.62 (m, 1H, H-6), 7.47 (m, 1H, H-2), 7.32 (m, 1H, H-3), 4.25 (d, *J* = 5.6 Hz, 2H, H-12), 3.79 (s, 3H, H-14); ^{13}C NMR (75 MHz, Chloroform-*d*) δ 169.8 (C-13), 162.0 (C-10), 161.3 (C-7), 154.6 (C-4), 148.8 (C-9), 134.4 (C-1), 130.0 (C-6), 125.4 (C-3), 118.6 (C-8), 118.0 (C-5), 116.8 (C-2), 52.5 (C-14), 41.8 (C-12); IR (neat): υ_{max}/cm^{-1} : 3324 (NH amide), 3052 (Ar-CH), 2922 (OH carboxylic acid), 1746 (C=O ester), 1707 (C=O amide). HRMS (TOF MS ESI +): calcd for $C_{13}H_{11}NO_5Na$ $[M+Na]^+$: 284.0535; observed: 284.0074.

6.1.21) 7-Methoxy-5-(3-trifluoromethyl-3*H*-diazirine-3-yl) coumarin-3-cabroxylic acid-Tomohero's method (3.2)[8]

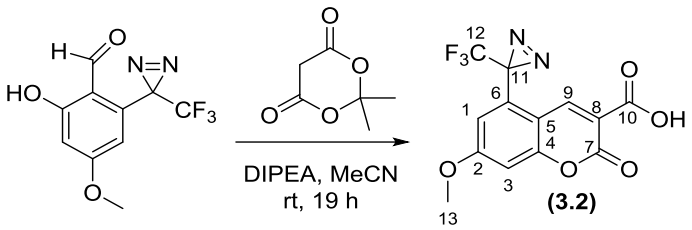

6-Hydroxy-4-methoxy-2-(3-Trifluoromethyl)-3H-diazirine-3-yl) benzaldehyde (0.1074g, 0.4 mmol) was placed in 25 mL pear shape flask under atmosphere, followed by the addition of MeCN (0.4 mL). Then DIPEA (0.13337g, 1.032 mmol) was added to the reaction mixture which left to stir at room temperature overnight. The reaction mixture was then concentrated under reduced pressure, and the obtained dark green oil diluted with water (10 mL), and acidified with HCl (5 M, 5 mL). Then the reaction mixture left to stir at room temperature for 15 min. Then, the reaction mixture was diluted with water (50 mL) and extracted with ethyl acetate (50 mL X 2). The obtained organic layer was then washed with water (100 mL X 3), brine, dried over anhydrous magnesium sulphate, filtered, and solvent removed under reduced pressure.

The obtained green crude solid was chromatographed over silica gel using dichloromethane, petroleum ether, methanol and acetic acid (10 %) (4:1:0.5: 5 drops) as eluent, which afforded (**3.2**) (0.053g, 0.162 mmol, 40 %) as a white solid.

Mp: 123-127 ^{o}C; ^{1}H NMR (300 MHz, Chloroform-*d*) δ 9.46 (s,1H), 7.33 (d, *J* = 2.4 Hz, 1H), 7.01 (d, *J* = 2.4 Hz, 1H), 3.99 (s, 3H). ^{13}C NMR (126 MHz, Chloroform-*d*) δ 165.8 (C10), 163.4 (C-2), 162.1(C7), 157.8 (C4), 156.3 (C12), 146.7 (C9), 129.3 (C6), 122.5 (C5), 120.3 (C-8), 118.5 (C1), 111.7 (C3), 103.1 (C11), 56.7 (C13); ^{19}F NMR (282 MHz, Chloroform-*d*) δ -67.41.

Observed ^{1}H NMR spectrum were consistent with those reported by Tomohero *et al*.[8]

6.1.22) 7-Methoxy-5-(3-trifluoromethyl-3*H*-diazirine-3-yl) coumarin-3-cabroxylic acid-Tapia's method (3.2)[9]

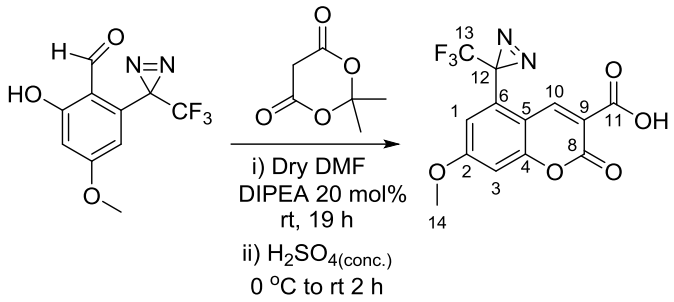

6-Hydroxy-4-methoxy-2-(3-Trifluoromethyl)-3H-diazirine-3-yl) benzaldehyde (0.35 g, 1.36 mmol) was placed in 100 mL pear shape flask under nitrogen. Then Meldrum's acid (0.197 g, 1.3629 mmol) was place in 10 ml pear shape flask under nitrogen followed by the addition dry DMF (5 mL). The resulted solution was added to 6-Hydroxy-4-methoxy-2-(3-Trifluoromethyl)-3H-diazirine-3-yl) benzaldehyde in dropwise via a syringe under nitrogen at room temperature. Then DIPEA (0.0193 g, 0.1499 mmol) was added to the reaction mixture slowly under nitrogen at room temperature. Then the reaction mixture left to stir at room temperature overnight. After 19 h the reaction mixture cooled to 0 ^{o}C and then cold concentrated H_2SO_4 (3.4 mL) was added slowly, after which the reaction mixture stirred at room temperature for 2 h. Then the reaction mixture was poured into a 250 mL beaker contained crushed ice and left overnight in a cool container.

After 19 h the resulted precipitate was filtered, then the obtained white powder was washed with water few times (total 800 mL), after which the white powder was dissolved in chloroform and evaporated to remove solvent. The resulting crude residue was chromatographed using a gradient of chloroform-acetonitrile (0 %-100 %) solvents which gave (**3.2**) in (0.4075 g, 1.241 mmol, 91%), as a beige solid.

Mp: 125-128 ^{o}C; ^{1}H NMR (700 MHz, Methanol-d_4) δ 9.17 (s, 1H, H-10), 7.37 (d, J = 2.4 Hz, 1H, H-1), 7.15 (d, J = 2.4 Hz, 1H, H-3), 3.98 (s, 3H, H-14), OH proton did not observed.

^{13}C NMR (176 MHz, Methanol-d_4) δ 167.1 (C-2), 166.3 (C-11), 160.04 (C-8), 160.00 (C-6), 145.3 (C-10), 129.3 (C-4), 124.2 (q, $J_{C\text{-}F}$ = 273.9 Hz, C-20), 118.5 (C-1), 117.5 (C-5),

112.7 (C-9), 104.6 (C-3), 57.6 (C-14), 27.6 (q, $J_{C\text{-}C\text{-}F}$ = 42.4 Hz, C-12); ^{19}F NMR (659 MHz, Methanol-d_4) δ -69.55; IR (neat): υ_{max}/cm^{-1} : 2980, 1779 (six membered lactone), 1682 (C=O carboxylic acid), 1592 (*α, β*-unsaturated). MS (ES+) calcd for $C_{13}H_7F_3O_5N_2Na$: 351.0171, found 351.0205.

6.1.23) 5-(2,6-dimethoxy-4-(3-(trifluoromethyl)-3*H*-diazirin-3-yl)benzylidene)-2,2-dimethyl-1,3-dioxane-4,6-dione (3.41)[9]

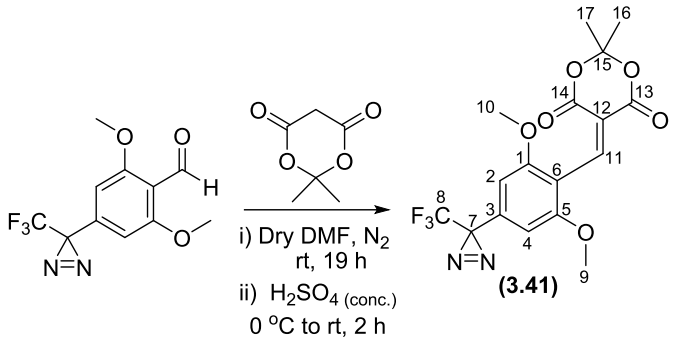

2,6-dimethoxy-4-(3-(trifluoromethyl)-3*H*-diazirin-3-yl)benzaldehyde (0.224 g, 0.816 mmol) was placed in 5mL round bottom flask under nitrogen and a solution of Meldrum's acid (0.24 g, 1.632 mmol) in dry DMF (1.4 mL) was added dropwise at room temperature.

The reaction mixture was stirred at room temperature overnight then cooled to 0 ^{o}C and $H_2SO_{4\ conc.}$ (1.3 mL) was added slowly, and the obtained reaction mixture stirred for 1 h at 0 ^{o}C. Then the reaction mixture poured in crushed ice and left in cool container overnight. The obtained yellow residue was filtered and washed few times with cold water (total 500 mL) which gave a yellow powder. The obtained yellow powder was recrystallized from water-acetone giving (**3.41**) (0.216 g, 0.559 mmol, 66 %) as a yellow solid.

^{1}H NMR (300 MHz, Chloroform-*d*) δ 8.33 (s, 1H, H-11), 6.30 (s, 2H, H-2, H-4), 3.84 (s, 6H, H-9, H-10), 1.84 (s, 6H, H-16, H-17). ^{19}F NMR (282 MHz, Chloroform-*d*) δ -64.57. ^{13}C NMR (75 MHz, Chloroform-*d*) δ 162.4 (C-13,14), 160.1 (C-3), 158.8 (C-1,5), 146.5 (C-11), 123.2 (q, $J_{C\text{-}F}$ =275 Hz, C8), 119.2 (C-12), 104.6 (C-2), 102.0 (C-4), 101.9 (C-6), 82.3 (C-7), 55.9 (C-9, 10), 29.0 (q, $J_{C\text{-}F}$ =40 Hz, C-7), 27.3 (C-16, 17). IR (neat): υ_{max}/cm^{-1} : 2990 (=C-H), 2948 (O-CH3), 1731 (C=O).

6.1.24) (*R*)-2-((*tert*-butoxycarbonyl)amino)-3-(2-oxo-2*H*-chromene-3-carboxamido)propanoic acid (3.46)[10]

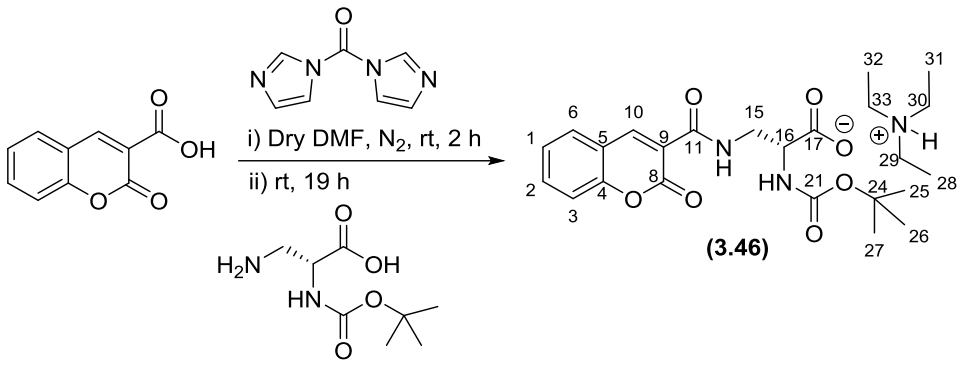

To a stirred 2 necks pear shape flask (10 mL) was added 2-oxo-2*H*-chromene-3-carboxylic acid (96 mg, 0.5 mmol), carbonyldiimidazole (CDI) (81.1 mg, 0.5 mmol), and dry DMF (5 mL) under nitrogen atmosphere in the dark. The reaction mixture was stirred at rt for 2 h. Boc-D-2,3-diaminopropanoic acid (112.4 mg, 0.55 mmol) was added to the reaction mixture in one portion and left to stir at room temperature overnight. After 19 h the reaction mixture diluted with ethyl acetate (50 mL), and washed with 1N HCl (25 mL), H_2O (50 mL). The aqueous layer was extracted again with ethyl acetate (25 mL) to minimise loss in product, then the combined organic layers washed with brine, dried over sodium sulphate, filtered and solvent removed under reduced pressure. The resulting crude product was chromatographed using a gradient of hexane : chloroform : MeOH 10 % : trimethylamine 1 %, which afforded (**3.46**) (46.4 mg, 0.097 mmol, 19 %) as the triethyl ammonium salt.

^{1}H NMR (400 MHz, Chloroform-*d*) δ 9.11 (broad m, 1H, NH), 8.85 (s, 1H, H-10), 7.70 – 7.55 (m, 2H, H-6, H-1), 7.41 – 7.21 (m, 2H, H-2, H-3), 5.68 (broad m, 1H, NH), 4.25 (m, 1H, H-16), 3.84 (m, 2H, H-15), 3.08 (q, *J* = 7.3 Hz, 6H, H-29, H-30, H-33), 1.40 (s, 9H, H-25, H-26, H-27), 1.29 (t, *J* = 7.3 Hz, 9H, H-28, H-31, H-32).

^{13}C NMR (101 MHz, Chloroform-*d*) δ 174.51(C-21), 161.95 (C-17), 160.95 (C-11), 155.65 (C-8), 154.41 (C-4), 148.26 (C-10), 133.84 (C-6), 129.81 (C-1), 125.13 (C-2), 118.65 (C-9), 118.62 (C-5)116.48 (C-3), 79.2 (C-24), 54.5 (C16) 45.3 (C-29, C-30, C-33), 42.4 (C-15), 28.36 (C-25, C-26, C-27), 8.51 (C-28, C-31, C-32).

6.1.25) (*R*)-2-amino-3-(2-oxo-*2H*-chromene-3-carboxamido) propanoic acid (3.48)[10]

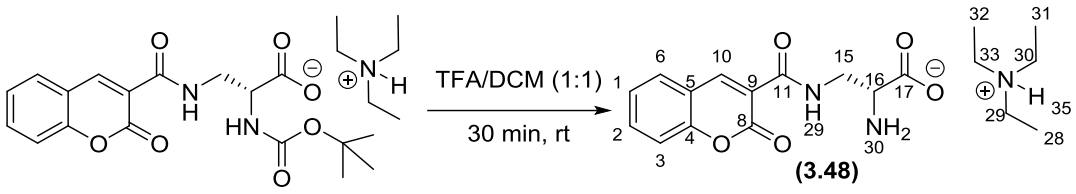

(*R*)-2-((*tert*-butoxycarbonyl)amino)-3-(2-oxo-*2H*-chromene-3-carboxamido) propanoic acid (40 mg, 0.0837 mmol) was placed in a pear shape flask (5 mL) under atmosphere, then a solution mixture of TFA in DCM (0.7 mL, 1:1) was added slowly. The reaction mixture stirred at room temperature for 30 min. Then the resulting crude material was concentrated under reduced pressure to remove solvent. The obtained brown residue was purified with Isolera^{TM} One (Biotage) equipped with C18 SNAP ultra 12 g column equilibrated with 3 CV of the starting solvent mixture. The flow rate was 12 mL/min, 254/280 nm wavelengths were monitored, and peaks that absorbed above 20 mAU were collected. The gradient was as follows: 2 % ACN/water for 8 CV, 20% MeCN/water for 5 CV, 75% MeCN/water for 5 CV, Note/ both solvents contains 0.1% (V/V) of FA. Reverse phase TLC was used to confirm pure fractions (MeCN: water: TFA, 2:8:5 drops). Isolated fractions were concentrated under reduced pressure. This yielded the triethyl ammonium salt of (**3.48** (15.3 mg, 0.0311 mmol, 37 %). as a white powder.

^{1}H NMR (300 MHz, D_2O) δ 8.70 (s, 1H, H-10), 8.60 (s, 1H, NH), 7.75 – 7.63 (m, 2H, H-2/H-6), 7.42 – 7.30 (m, 2H, H-1/H-3), 4.20 (dd, *J* = 6.3, 4.4 Hz, 1H, H-16), 3.96 (dd, *J* = 14.8, 4.5 Hz, 1H, H-15), 3.88 (dd, *J* = 14.8, 6.3 Hz, 1H, H-15), 3.11 (q, *J* = 7.3 Hz, 6H, H-29,30,33), 1.19 (t, *J* = 7.3 Hz, 9H, H-28,31,32); ^{13}C NMR (75 MHz, D2O) δ 170.5 (C-17), 165.0 (C-11),162.2 (C-8), 154.0 (C-4), 149.9 (C-10), 135.2 (C-2), 130.3 (C-6), 125.7 (C-1), 118.1 (C-5), 116.7 (C-3), 114.3 (C-9), 53.5 (C-16), 46.6 (C-29,30,33), 39.4 (C-15), 8.1 (C-28,31,32); ^{19}F NMR (282 MHz, D_2O) δ -75.60.

6.1.26) (*R*)-2-((*tert*-butoxycarbonyl)amino)-3-(7-methoxy-2-oxo-5-(3-(trifluoromethyl)-3*H*-diazirin-3-yl)-2*H*-chromene-3-carboxamido)propanoic acid[10]

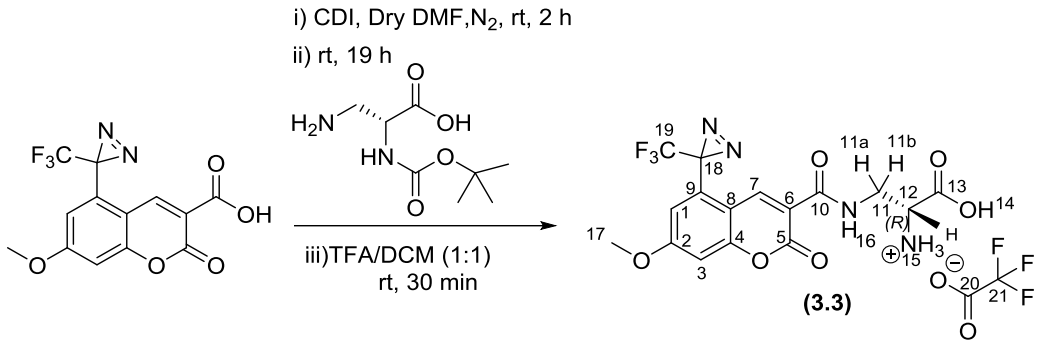

7-methoxy-2-oxo-5-(3-(trifluoromethyl)-3*H*-diazirin-3-yl)-2*H*-chromene-3-carboxylic acid (0.29 g, 0.9 mmol) was placed in 50 mL pear shape flask under high vacuum for 30 min followed by the addition of dry DMF (2 mL), under nitrogen atmosphere, at room temperature.

Carbonyldiimidazole (CDI) (0.147 g, 0.9 mmol) was placed in 25 mL pear shape flask under high vacuum for 30 min followed by the addition of dry DMF (3 mL) under nitrogen atmosphere, the resulted solution was transferred via glass syringe to the 7-methoxy-2-oxo-5-(3-(trifluoromethyl)-3*H*-diazirin-3-yl)-2*H*-chromene-3-carboxylic acid solution, and the resulting reaction mixture was stirred at room temperature for 2 h.

(*R*)-3-amino-2-((*tert*-butoxycarbonyl)amino)propanoic acid (0.203 g, 0.996 mmol) was placed in 25 mL pear shape flask under nitrogen followed by the addition of dry DMF (4.5 mL) and the resulted solution was transferred to the reaction mixture via a glass syringe.

The reaction mixture was stirred at rt under a nitrogen atmosphere in dark overnight.

After a reaction time of 19 h the reaction mixture was diluted with ethyl acetate (80 mL), washed with HCl 1N (40 mL), H_2O (40 mL X 3), then the combined organic layers were washed with brine, dried over anhydrous sodium sulphate, filtered and solvent removed under reduced pressure.

Without further purification, the crude compound (0.3917 g) was transferred to a 10 mL pear shape flask and then was treated with a (1:1) solution of TFA/dry DCM (5.2 mL). The resulting dark red solution was stirred at room temperature for 30 min in dark. Then the reaction mixture evaporated to remove the solvents.

The obtained red residue was purified on an Isolera^{TM} One (Biotage) equipped with C18 ultra SNAP 12 g column equilibrated with 3 CV of the starting solvent mixture. The flow rate was 12 mL/min, and peaks that absorbed above 20 mAU were collected. The gradient was as follows: 0% MeCN/water for 5 CV, 0-100 % MeCN/water for 35 CV, 100 MeCN for 3 CV, Note/ both solvents contains 0.1% (V/V) of FA. Pure fractions (R_f: 0.28) were confirmed by revers phase TLC (MeCN/water/TFA, 2:8:5drops), and concentrated under reduced pressure to give the TFA salt of (**3.3**) (14 mg, 0.0282 mmol, 5 %) as a white solid.

^{1}H NMR (700 MHz, Methanol-d_4 + TFA) δ 9.40 (s, 1H, H-7), 7.44 (d, J = 2.4 Hz, 1H, H-3), 7.22 (d, J = 2.4 Hz, 1H, H-1), 4.32 (dd, J = 6.6, 4.0 Hz, 1H, H-12), 4.11 (dd, J = 14.6, 4.0 Hz, 1H, H-11b), 3.99 (s, 3H, H-17), 3.94 (dd, J = 14.6, 6.7 Hz, 1H, H-11a).
Note: H-15, H-16, H-14 are not observed representing 5H; ^{13}C NMR (176 MHz, Methanol-d_4 + TFA) δ 169.9 (C-13), 166.8 (C-2), 165.1 (C-10), 161.7 (C-5), 160.7 (q, $J_{C\text{-}F}$ = 39.0 Hz, C-20), 159. 2 (C-4), 144.5 (C-7), 129.1 (C-6), 123.1 (q, $J_{C\text{-}F}$ = 274.2 Hz, C-19), 118.6 (C-1), 117.0 (C-8), 116.4 (q, J= 287.0, C-21), 112.5 (C-9), 104.1 (C-3), 57.3 (C-17), 54.5 (C-12), 40.5 (C-11), 27.3 (q, $J_{C\text{-}C\text{-}F}$ = 42.0 Hz, C-18); ^{19}F NMR (282 MHz, Methanol-d_4) δ -69.53 (F-19), -76.88 (F-21); HRMS (TOF MS ESI +): calcd for $C_{16}H_{15}F_3N_4O_6$ $[M+H]^+$: 415.0860 m/z; observed: 415.0338 *m/z*. $[\alpha]_{D}^{22}$: +25.6 (c 0.5, MeOH).

6.1.27) (*S*)-2-((*tert*-butoxycarbonyl)amino)-3-(7-methoxy-2-oxo-5-(3-(trifluoromethyl)-3*H*-diazirin-3-yl)-2*H*-chromene-3-carboxamido)propanoic acid (3.4)[10]

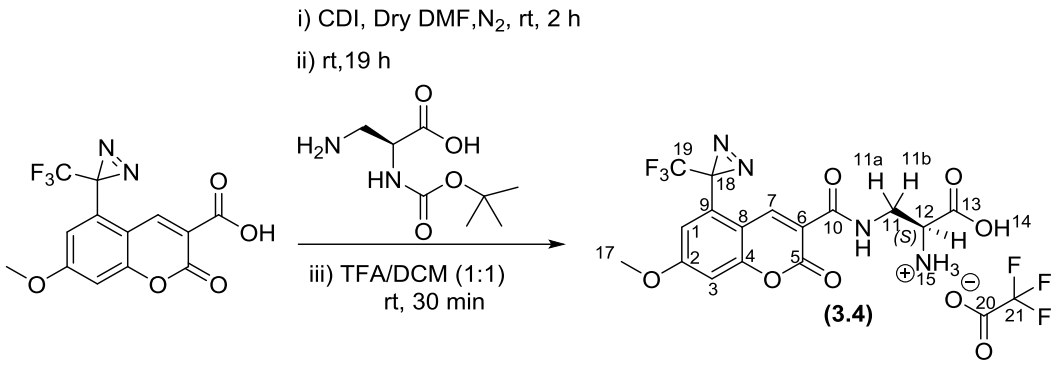

7-methoxy-2-oxo-5-(3-(trifluoromethyl)-3*H*-diazirin-3-yl)-2*H*-chromene-3-carboxylic acid (0.2 g, 0.6093 mmol) was placed in 50 mL pear shape flask under high vacuum for 30 min followed by the addition of dry DMF (3 mL), under nitrogen, at room temperature in dark. The resulting stirred solution was added to a stirred 25 mL pear shape flask contains anhydrous Carbonyldiimidazole (CDI) (0.147 g, 0.9 mmol) under a nitrogen atmosphere. The reaction mixture was stirred at rt for 2 h.

(*R*)-3-amino-2-((*tert*-butoxycarbonyl)amino)propanoic acid (0.203 g, 0.996 mmol) was placed in 25 mL pear shape flask under nitrogen followed by the addition of dry DMF (4.5 mL) and the resulted solution was transferred to the reaction mixture via a glass syringe.

The reaction mixture was stirred at rt under a nitrogen atmosphere in dark overnight.

After a reaction time of 19 h the reaction mixture was diluted with ethyl acetate (80 mL), washed with HCl 1N (40 mL), H_2O (40 mL X 3), then the combined organic layers were washed with brine, dried over anhydrous sodium sulphate, filtered and then evaporated to remove solvent.

Without further purification, the crude compound (0.3917 g) was transferred to a 10 mL pear shape flask and then was treated with a (1:1) solution of TFA/dry DCM (5.2 mL). The

resulting dark red solution was stirred at room temperature for 30 min in dark. Then the reaction mixture evaporated to remove the solvents.

The obtained red residue was purified on an Isolera^{TM} One (Biotage) equipped with C18 ultra SNAP 30 g column equilibrated with 3 CV of the starting solvent mixture. The flow rate was 20 mL/min, the 254/280 nm wavelengths were monitored, and peaks that absorbed above 20 mAU were collected. The gradient was as follows: 0% MeCN/water for 5 CV, 0-100 % MeCN/water for 35 CV, 100 MeCN for 3 CV, Note/ both solvents contains 0.1% (V/V) of FA. Pure fractions (R_f:: 0.56) were confirmed by revers phase TLC (MeCN/water/TFA, 1:1:5 drops), and concentrated under reduced pressure to give the TFA salt of (**3.4**) (63.25 mg, 0.11971 mmol, 20 %) as a white solid.

^{1}H NMR (700 MHz, Methanol-d_4 +TFA) δ 9.40 (s, 1H, H-7), 7.40 (d, J = 2.4 Hz, 1H, H-3), 7.19 (d, J = 2.4 Hz, 1H, H-1), 4.30 (dd, J = 6.6, 4.0 Hz, 1H, H-12), 4.11 (dd, J = 14.7, 4.0 Hz, 1H, H-11b), 3.98 (s, 3H, H-17), 3.94 (dd, J = 14.6, 6.6 Hz, 1H, H-11a).
Note: H-15, H-16, H-14, are not observed in ^{1}H NMR representing, 5H.

^{13}C NMR (176 MHz, Methanol-d_4 + TFA) δ 169.8 (C-13), 166.8 (C-2), 165.2 (C-10), 161.7 (C-5), 160.3 (q, J = 44.7 Hz, C-20), 159.3 (C-4), 144.6 (C-7), 129.2 (C-6), 123.1 (q, $J_{C\text{-}F}$ = 274.3 Hz, C-19), 118.6 (C-1), 117.4 (q, $J_{C\text{-}F}$ = 288.5 Hz, C-21), 116.9 (C-8), 112.6 (C-9), 104.2 (C-3), 57.3 (C-17), 54.5 (C-12), 40.6 (C-11), 27.4 (q, $J_{C\text{-}C\text{-}F}$ = 42.5 Hz, C-18); ^{19}F NMR (659 MHz, Methanol-d_4) δ -69.56 (F-19), -76.91 (F-21), -77.82 (TFA solvent). HRMS (TOF MS ESI +): calcd for $C_{16}H_{15}F_3N_4O_6$ $[M+H]^+$: 415.0860; observed: 415.1293. $[\alpha]_{D}^{22}$: -10.8 (c 0.5, MeOH).

6.2 General Experimental - Biology

Unless specified, all different compounds used for media composition were purchased from Sigma-Aldrich, Merck, VWR or Fisher Scientific.

Analytical and preparative Reversed-Phase High-Performance Liquid Chromatography (RP-HPLC) of muropeptides, employed an Agilent Technologies model 1220 Infinity LC with a PRONTOSIL 120-3-C18 AQ, 3 μm, 250 x 4.6 mm column, with monitoring at 205 nm.

High resolution mass spectrometry (HRMS) of muropeptides was performed on a Thermo LTQ (ion trap MS) equipped with an Agilent 1100 HPLC (ACE C18 column, 150 x 1 mm, Buffer A 0.1% formic acid (aq.) and buffer B acetonitrile 0.1% formic acid, 50 μl/min. HRMS analysis was performed by Dr. Joe Gray, Newcastle University.

6.2.1 Centrifugation and Shakers

AccuTherm Microtube Shaking Incubator (Labnet International).

Accuspin Micro 17 microcentrifuge (Fisher Scientific).

Shaker for flasks New Brunswick™ Innova® 2300.

6.2.2 Reagents

All stock solutions used in this study were prepared into dH_2O unless otherwise stated and stored at room temperature (15-25 °C).

1- Sodium phosphate buffer (SPB) (pH 7.4)

3.1 g of $NaH_2PO_4 \bullet H_2O$ and 10.9 g of Na_2HPO_4 (anhydrous) to distilled H_2O to make a volume of 1 L.

2- HEPES/NaOH stock solution (1 M, pH 7.5)

N-(2-hydroxyethyl)piperazine-*N*-(2-ethanesulfonic acid) (HEPES) (23.83) g in 90 ml of Milli-Q water. The pH was adjusted to 7.5 using 1 M sodium hydroxide solution. The final volume was adjusted to 100 ml.

3- Tris/HCl

4- TX-100

5- Cellosyl buffer (1 mg/mL *N*-acetyl-*β*-D-muramidase, 20 mM sodium phosphate, pH 4.8, and 0.02% sodium azide), the buffer recipe as follows:

25 µL of 20 mM sodium phosphate + 0.02% sodium azide
10 µL of 1 mg/mL *N*-acetyl-*β*-D-muramidase.
15 µL Milli-Q H_2O.

6.2.3 Isolation of PG from *E. coli* BW25113ΔLdtABCDEF[11]

The following PG isolation work form *E. coli* was performed by Matthias Winkle, Centre for Bacterial Cell Biology (CBCB) Newcastle University.
The PG was isolated from *E. coli* BW25113ΔLdtABCDEF strain as described by Datsenko *et al.*, following the isolation of PG pellets from cell growth media, the PG stored in Milli-Q water with 0.02% NaN_3.

6.2.4 Expression and Purification of LdtD Enzyme (YcbB)[13]

The following LdtD enzyme expression was performed by Matthias Winkle, Centre for Bacterial Cell Biology (CBCB) Newcastle University.
LdtD enzyme (YcbB) was overexpressed in *E. coli* LOBSTR-BL21(DE3) (Kerafast) using pETMM82 expression vector, plasmid encoding for LdtD carrying an *N*-terminal DsbC-His6-tag followed by a TEV-protease cleavage site. Following LdtD purification, the enzyme was stored in the following buffer: 25 mM HEPES pH 7.5 adjusted with NaOH, 300 mM NaCl, 10 % Glycerol.

6.2.5 Preparation of Muropeptide[12]

The following PG digestion was performed jointly with Matthias Winkle, Centre for Bacterial Cell Biology (CBCB) Newcastle University.

An exponential phase culture (OD_{600} ~ 0.4-06) of *E. coli* cells (BW25113ΔLdtABCDEF) was harvested by rapid suspending into NaCl/ice mixture for 15 min followed by centrifugation (12000g, 10 min, 4 °C). The resulted pellets were suspended in ice water then was added slowly to a boiling solution of 4% SDS. The solubilisation of bacteria membrane and removal of high molecular wight DNA were achieved by additional boiling

of pellets-SDS mixture for 30 min. The obtained solution was left to stand at room temperature overnight. After which, lipoproteins covalently bounded to sacculi, and high molecular weight glycogen were removed by enzymatic treatment with Pronase and α-amylase. The resulted murine was digested with 15 µL *N*-acetyl-*β*-D-muramidase buffer solution (20 µg/mL final concentration) to cleave the β1-4 glycosidic bonds between MurNAc and GlcNAc residues at 37 °C overnight. The enzyme reaction was stopped by heating at 100 °C (3 min), and the insoluble protein and other contaminants for media were removed by centrifugation. The recovered supernatant contained soluble muropeptide (monomeric, dimeric and trimeric) was lyophilised then redissolved in water, and 80 mM sodium phosphate (pH 4.8), then stored frozen at -18 °C with no further purification (for details see Glauner *et al.*).

6.2.6 Testing the Solubility of MCTDA/MCTLA

The solubility of MCTDA and MCTLA was tested in three different buffer solutions. A typical solubility test in buffer was performed as follows, into 72.1 or 73 µL of H_2O (Milli-Q) was added 1 µL of MCTDA or MCTLA (100 mM in DMSO), along with aqueous buffer reagents (2 µL of 1000 mM HEPES, 2 µL of 1000 mM Tris or 2.9 µL of 700 mM sodium phosphate buffer), 10 µL of NaCl (1000 mM in H2O) and 5 µL of TX-100 (1% in H_2O). This gave a 100 µL solution containing MCTDA or MCTLA (1 mM), NaCl (100 mM) and TX-100 (0.05 %), along with either HEPES (20 mM), Tris (20 mM) or sodium phosphate (20 mM) buffer (Table **6.1**).

Concentration			Chemical	MCTDA 1 mM			MCTLA 1 mM		
				1	2	3	4	5	6
Unit	Stock	Final		HEPES	Tris	SPB	HEPES	Tris	SPB
				V µL	V µL	V µL	V µL	V µL	V µL
mM	1000	20	HEPES	2.0	0.0	0.0	2.0	0.0	0.0
mM	1000	20	Tris	0.0	2.0	0.0	0.0	2.0	0.0
mM	700	20	SPB	0.0	0.0	2.9	0.0	0.0	2.9
mM	100	1	Probe	1.0	1.0	1.0	1.0	1.0	1.0
mM	1000	100	NaCl	10.0	10.0	10.0	10.0	10.0	10.0
%	1	0.05	TX-100	5.0	5.0	5.0	5.0	5.0	5.0
%	100	10	DMSO	9.0	9.0	9.0	9.0	9.0	9.0
			Milli-Q	73.0	73.0	72.1	73.0	73.0	72.1

Table 6.1: Solubility testing of MCTDA and MCTLA in 3 different buffers.

6.2.7 Evaluating the Thermal Stability of MCTDA/MCTLA Probes in Solution

In order to test the thermostabilities of our probes MCTDA and MCTLA under LdtD enzymatic incorporation conditions, samples were taken from the solution of previous solubility experiments (Table **6.1**, entries **1-6**) and analysed by reverse phase TLC against reference samples of MCTDA and MCTLA solutions in DMSO only.

6.2.8 Incorporation of MCTDA into *E. coli* Muropeptide via LdtD in HEPES Buffer[13]

Experiment of enzymatic incorporation of MCTDA into *E. coli* muropeptide using LdtD in HEPES was prepared as follows, into 1.5 mL Eppendorf vial contained 18.6 µL of H_2O (Milli-Q), was added 4.1 µL of LdtD (24.2 µM in aqueous buffer), 2.5 µL of MCTDA (100 mM in DMSO) and 15 µL of a buffer solution containing approximately 100 µg of muropeptide (*E. coli* BW25113ΔLdtABCDEF), along with a number of buffer reagents 1 µL of HEPES (1000 mM in H_2O), 3.8 µL of NaCl (1000 mM in H_2O) and 2.5 µL of TX-100 (1% in H_2O). This gave a 54.1 µL solution containing MCTDA (0.5 mM), LdtD (2 µM) and approximately 100 µg of muropeptide, along with HEPES (20 mM), NaCl (100 mM) and TX-100 (0.05 %) (Table **6.2**, entry**1**).

The sample was incubated at 37 °C shaking for 1 h and the reaction was stopped by boiling for 3 min. The resulted aliquot was centrifuged (12000 g) for 15 min at 4 °C. The recovered supernatant was treated with 50 µL of 0.5 M sodium borate, pH 9. The pH of the sample was tested by pH paper and adjusted to 9 if necessary, followed by the addition of solid sodium borohydride 1-2 mg and the sample was centrifuged at room temperature for 30 min (note: The lid of the Eppendorf vial was pierced to allow gas releasing). After recovering the obtained supernatant, excess borohydride was destroyed with 20% formic acid (20 µL) and the sample was adjusted to pH 3-4. The volume of the obtained sample was diluted to a final volume of 200 µL (2.5 % DMSO) before it injected to RP-HPLC without any further purification.

In parallel, a negative control experiment using MCTLA (0.5 mM as a final concentration) with LdtD and muropeptide was undertaken under the same previous conditions (Table **6.2**, entry **3**).

Our previous MCTDA/MCTLA enzymatic incorporation experiment into *E. coli* muropeptide was repeated but without subjecting our obtained reaction mixture to sodium borohydride reduction, which is usually applied before HPLC analysis. (Table **6.2**, entries **2** and **4**)

Thus, as before, we repeated the enzymatic incorporation experiment of both MCTDA/MCTLA into muropeptide in presence of LdtD and HEPES (NaCl, TX-100) (Table **6.2**, entries **2** and **4**), along with control experiments containing probes only (2.5 µL of each probe (10 mM in DMSO) with buffers (HEPES, NaCl, and TX-100) (Table **6.2**, entry **5** and **6**). It should be noted that in control experiments containing no probe, 5 µL of DMSO was included to maintain the solvent mixture. After incubation of the reaction mixture for 1 h at 37 °C, all samples were heated at 100 °C for 3 min, centrifuged and the reaction mixtures treated with 20 % formic acid and submitted for HPLC analysis. (**Table 6.2**)

Concentration			Experiment name	Reduce	-	Reduce	-	Reference	Reference
				1[a]	2[b]	3[a]	4[b]	5[b]	6[b]
				MP+LdtD	MP+LdtD	MP+LdtD	MP+LdtD	Probe (D)	Probe (L)
				Probe (D)	Probe (D)	Probe (L)	Probe (L)		
Unit	Stock	Final	**Reagents**	0.5 mM	0.5 mM	0.5 mM	0.5 mM	0.5 mM	0.5 mM
				V.µL	V.µL	V.µL	V.µL	V.µL	V.µL
uM	24.2	2	LdtD	4.1	4.1	4.1	4.1	0.0	0.0
mM	1000	20	HEPES (7.5)	1.0	1.0	1.0	1.0	1.0	1.0
mM	700	20	Na Phosphate	0.0	0.0	0.0	0.0	0.0	0.0
mM	10	x	Probe	2.5	2.5	2.5	2.5	2.5	2.5
mM	1000	100	NaCl	3.8	3.8	3.8	3.8	5.0	5.0
%	1	0.05	TX-100	2.5	2.5	2.5	2.5	2.5	2.5
			MP	15.0	15.0	15.0	15.0	0.0	0.0
			DMSO	2.5	2.5	2.5	2.5	2.5	2.5
			MilliQ	18.6	18.6	18.6	18.6	36.5	36.5
			DMSO	5	5	5	5	5	5
			Soduim borate	50	0	50	-	-	-
			$NaBH_4$	1 mg	-	1mg	-	-	-

Table 6.2: Enzymatic testing of MCTDA (0.5 mM) and MCTLA (0.5 mM) incorporation into *E. coli* muropeptide via LdtD in HEPES. [a]Assay mixture was reduced by $NaBH_4$ before submission to HPLC, [b]Assay mixture submitted to HPLC without reduction.

An aliquot (0.5 µL) from each experiment (1-6) was submitted to RP-HPLC analysis without further purification.

RP-HPLC conditions was as follows:

Buffer A: H_2O with 0.1 % formic acid and buffer B: acetonitrile with 0.1 % formic acid; 0-2 min (100 % A : 0 % B), 2-40 min (from 100 % A : 0 % B to 70 % A : 30 % B), 40-60 min (from 70 % A : 30 % B to 40 % A : 60 % B), 60-80 min (100 % A : 0 % B).

•

6.2.9 Examination of the Incorporation of MCTDA into *E. coli* Muropeptide via LdtD in Sodium Phosphate Buffer[13]

Experiment of enzymatic incorporation of MCTDA into *E. coli* muropeptide using LdtD in sodium phosphate buffer was prepared as follows, into 1.5 mL Eppendorf vial contained 18.2 µL of H_2O (Milli-Q), was added 4.1 µL of LdtD (24.2 µM in aqueous buffer), 2.5 µL of MCTDA (100 mM in DMSO) and 15 µL of a buffer solution containing approximately 100 µg of muropeptide (*E. coli* BW25113ΔLdtABCDEF), along with a number of buffer reagents 1.4 µL of sodium phosphate buffer (700 mM in H_2O), 3.8 µL of NaCl (1000 mM in H_2O) and 2.5 µL of TX-100 (1% in H_2O). This gave a 54.1 µL solution containing MCTDA (0.5 mM), LdtD (2 µM) and approximately 100 µg of muropeptide, along with sodium phosphate buffer (20 mM), NaCl (100 mM) and TX-100 (0.05 %) (Table **6.3**, entry **3**).

The sample was incubated at 37 °C shaking for 1 h and the reaction was stopped by boiling for 3 min. The resulted aliquot was centrifuged (12000 g) for 15 min at 4 °C. The recovered supernatant was treated with 50 µL of 0.5 M sodium borate, pH 9. The pH of the sample was tested by pH paper and adjusted to 9 if necessary, followed by the addition of solid sodium borohydride 1-2 mg and the sample was centrifuged at room temperature for 30 min (note: The lid of the Eppendorf vial was pierced to allow gas releasing). After recovering the obtained supernatant, excess borohydride was destroyed with 20% formic acid (20 µL) and the sample was adjusted to pH 3-4. The volume of the obtained sample was diluted to a final volume of 200 µL (2.5 % DMSO) before it injected to RP-HPLC without any further purification.

Concentration			Experiment name→	1	2	3	4	5	6	7	8
				MP	MP+LdtD	MP+LdtD Probe MCTDA	Probe MCTDA	MP+Probe MCTDA	MP+LdtD Probe MCTLA	Probe MCTLA	MP+ probe MCTLA
			Reagents								
Unit	Stock	Final		V µL	V µL	V µL	V µL	V µL	V µL	V µL	V µL
uM	24.2	2	LdtD	0.0	4.1	4.1	0.0	0.0	4.1	0.0	0.0
mM	700	20	Na Phosphate	1.4	1.4	1.4	1.4	1.4	1.4	1.4	1.4
mM	10	0.5	Probe	0.0	0.0	2.5	2.5	2.5	2.5	2.5	2.5
mM	1000	100	NaCl	5.0	3.8	3.8	5.0	5.0	3.8	5.0	5.0
%	1	0.05	TX-100	2.5	2.5	2.5	2.5	2.5	2.5	2.5	2.5
			MP	15.0	15.0	15.0	0.0	15.0	15.0	0.0	15.0
%		10	DMSO	5.0	5.0	2.5	2.5	2.5	2.5	2.5	2.5
			Milli-Q	21.1	18.2	18.2	36.1	21.1	18.2	36.1	21.1

Table 6.3: Enzymatic testing of MCTDA (0.5 mM) and MCTLA (0.5 mM) incorporation into *E. coli* muropeptide via LdtD in sodium phosphate buffer.

In parallel, a negative control experiment using MCTLA (**3.4**) (0.5 mM as a final concentration) with LdtD and muropeptide was undertaken under the same conditions (Table **6.3**, entry **6**). In addition, further control experiments involved probe (MCTDA/MCTLA) only, muropeptide only, muropeptide with LdtD, muropeptide with MCTDA/MCTLA but no LdtD were performed basing on our previous protocol (Table **6.3**, entry **4, 7, 1, 2, 5, 8** respectively).

An aliquot (0.5 µL) of each assay mixture (1-8) was analysed by RP-HPLC without further purification.

RP-HPLC conditions was as follows:

buffer A: H_2O with 0.1 % formic acid and buffer B: acetonitrile with 0.1 % formic acid; 0-2 min (100 % A : 0 % B), 2-60 min (from 100 % A : 0 % B to 55 % A : 45 % B), 60-180 min (from 55 % A : 45 % B to 14 % A : 86 % B), 180-200 min (100 % A : 0 % B).

6.2.10 Incorporation of MCTDA into *E. coli* Muropeptide, via LdtD in Sodium Phosphate Buffer with Reduction, for LC-MS Analysis[13]

The experiment of MCTDA enzymatic incorporation into muropeptide using sodium phosphate buffer was prepared as follows, into 1.5 mL Eppendorf vial contained 18.2 µL of H_2O (Milli-Q), was added 4.1 µL of LdtD (24.2 µM in aqueous buffer), 2.5 µL of MCTDA (100 mM in DMSO) and 15 µL of a buffer solution containing approximately 100 µg of muropeptide (*E. coli* BW25113ΔLdtABCDEF), along with a number of buffer reagents 1.4 µL of sodium phosphate buffer (700 mM in H_2O), 3.8 µL of NaCl (1000 mM in H_2O) and 2.5 µL of TX-100 (1% in H_2O). This gave a 50 µL solution containing MCTDA (0.5 mM), LdtD (2 µM) and approximately 100 µg of muropeptide, along with Sodium phosphate buffer (20 mM), NaCl (100 mM) and TX-100 (0.05 %)
(Table **6.4**, entry **1**).

Concentration			Buffers and enzyme	1	2
				MP+LdtD Probe MCTDA	MP+Probe MCTDA
Unit	Stock	Final		V µL	V µL
uM	24.2	5	LdtD	4.1	0.0
mM	700	20	Na Phosphate	1.4	1.4
mM	10	0.5	Probe	2.5	2.5
mM	1000	100	NaCl	3.8	5.0
%	1	0.05	TX-100	2.5	2.5
			MP	15.0	15.0
%		10	DMSO	2.5	2.5
			Milli-Q	18.2	21.1

Table 6.4: Enzymatic testing of MCTDA (0.5 mM) and MCTLA (0.5 mM) incorporation into *E. coli* muropeptide via LdtD for LC-MS analysis.

The assay mixture was incubated at 37 °C shaking for 1 h and the reaction was stopped by boiling for 3 min. The resulted aliquot was centrifuged (12000 g) for 15 min at 4 °C. The recovered supernatant was treated with 50 µL of 0.5 M sodium borate, pH 9. The pH of the sample was tested by pH paper and adjusted to 9 if necessary, followed by the addition of

solid sodium borohydride 1-2 mg and the sample was centrifuged at room temperature for 30 min (note: The lid of the Eppendorf vial was pierced to allow gas releasing). After recovering the obtained supernatant, excess borohydride was destroyed with 20 % formic acid (20 µL) and the sample was adjusted to pH 3-4. The volume of the obtained sample was diluted to a final volume of 200 µL (2.5 % DMSO). Then the resulting crude solution was submitted to an analytical RP-HPLC without any further purification and using our previous HPLC conditions.

In addition, a blank sample of MCTDA and muropeptide isolated from BW25113ΔLdtABCDEF was treated according to our previous enzymatic incorporation protocol (Table **6.4**, entry **2**) and was submitted to an analytical RP-HPLC without further purification. And then experiments 1 and 2 (Table 6.4, entries 1, and 2) was repeated and the resulting assay mixtures were submitted to semi-preparative HPLC, and following peak collections, pure isolated fractions were lyophilized and subjected to LC-MS/MS (ESI-ITMS) analysis.

6.2.11 MCTDA Enzymatic Incorporation into Muropeptide via LdtD without $NaBH_4$ Reduction[13]

Experiment of MCTDA enzymatic incorporation into muropeptide without reduction was prepared as follows, into 1.5 mL Eppendorf vial contained 18.2 µL of H_2O (Milli-Q), was added 4.1 µL of LdtD (24.2 µM in aqueous buffer), 2.5 µL of MCTDA (100 mM in DMSO) and 15 µL of a buffer solution containing approximately 100 µg of muropeptide (*E. coli* BW25113ΔLdtABCDEF), along with a number of buffer reagents 1.4 µL of Sodium phosphate buffer (700 mM in H_2O), 3.8 µL of NaCl (1000 mM in H_2O) and 2.5 µL of TX-100 (1% in H_2O). This gave a 57.6 µL solution containing MCTDA (0.5 mM), LdtD (2 µM) and approximately 100 µg of muropeptide, along with sodium phosphate buffer (20 mM), NaCl (100 mM) and TX-100 (0.05 %) (Table **6.5** entry **3**):

Concentration			Experiment name→	1	2	3	4
				MP	MP+LdtD	MP+LdtD Probe MCTDA	Probe MCTDA
			Buffers and enzyme ↓				
Unit	Stock	Final		V µL	V µL	V µL	V µL
uM	24.2	2	LdtD	0	4.1	4.1	0.0
mM	700	20	Na Phosphate	1.4	1.4	1.4	1.4
mM	10	0.5	Probe	0.0	0.0	2.5	2.5
mM	1000	100	NaCl	3.8	3.8	3.8	5.0
%	1	0.05	TX-100	2.5	2.5	2.5	2.5
			MP	15	15	15	0.0
%		10	DMSO	7.5	5.0	2.5	7.5
			Milli-Q	28.6	25.7	25.7	28.6

Table **6.5:** Enzymatic testing of MCTDA (0.5 mM) and MCTLA (0.5 mM) incorporation into *E. coli* muropeptide via LdtD without $NaBH_4$ reduction for LC-MS analysis.

The incoporation reaction was stopped by boiling the reaction mixture for 3 min. The resulted aliquot was centrifuged (12000 g) for 15 min at 4 °C. The recovered supernatant was treated with 20% formic acid (20 µL) and the sample was adjusted to pH 3-4. The volume of the obtained sample was diluted to a final volume of 200 µL (2.5 % DMSO). Then the resulting crude solution was submitted to an analytical RP-HPLC without any further purification.

In addition, few experiments including a reference sample of muropeptide (MP) with buffer solutions (Table X, entry1), muropeptide, LdtD with buffer solutions (Table X, entry 2), and MCTDA with buffer solutions (Table **6.5**, entry 4), were treated according to our previous chemoenzymatic incorporation protocol. After reaction times of 1 h, an aliquot sample of each experiment (1,2,4) was subjected to an analytical RP-HPLC without any further purification.

6.2.12 LC-MS/MS Analysis of Muropeptide-MCTDA Adducts via LdtD Incorporation into Muropeptide without Reduction

The experiment of MCTDA incorporation into muropeptide via LdtD was repeated as previously and the resulting supernatant was separated by semi-preparative HPLC. The corresponding peaks with retention times at 67 min (putative muropeptide-MCTDA adduct) and 73 min (unincorporated MCDTA) were collected, dried and then analysed by LC-MS/MS.

6.2.13 Examination of the Incorporation of MCTDA into *E. coli* Peptidoglycan via LdtD in Sodium Phosphate Buffer

Experiment of MCTDA enzymatic incorporation into PG was prepared as follows, into 1.5 mL Eppendorf vial contained 27.7 µL of H_2O (Milli-Q), was added 4.1 µL of LdtD (24.2 µM in aqueous buffer), 2.5 µL of MCTDA (100 mM in DMSO) and 7.5 µL of a buffer solution containing approximately 100 µg of PG (*E. coli* BW25113ΔLdtABCDEF), along with a number of buffer reagents 1.4 µL of sodium phosphate buffer (700 mM in H_2O), 3.8 µL of NaCl (1000 mM in H_2O) and 2.5 µL of TX-100 (1% in H_2O). This gave a 57.9 µL solution containing MCTDA (0.5 mM), LdtD (2 µM) and approximately 100 µg of muropeptide, along with sodium phosphate buffer (20 mM), NaCl (100 mM) and TX-100 (0.05 %) (Table **6.6**, entry **2**).

Concentration			Experiment name→	1	2	3	4
				PG+LdtD	PG+LdtD Probe MCTDA	Probe MCTDA	PG+Probe MCTDA
			Buffers and enzyme ↓				
Unit	Stock	Final		V µL	V µL	V µL	V µL
uM	24.2	2	LdtD	4.1	4.1	0.0	0.0
mM	700	20	Na Phosphate	1.4	1.4	1.4	1.4
mM	10	0.5	Probe	0.0	2.5	2.5	2.5
mM	1000	100	NaCl	3.8	3.8	5.0	5.0
%	1	0.05	TX-100	2.5	2.5	2.5	2.5
			PG	7.5	7.5	0.0	7.5
%		10	DMSO	5.0	2.5	7.5	7.5
			Milli-Q	25.7	25.7	28.6	28.6

Table 6.6: Enzymatic testing of MCTDA (0.5 mM) incorporation into *E. coli* PG via LdtD.

The sample was incubated for 1 h at 37 °C shaking overnight. After 19h the reaction was stopped by boiling for 3 min. The resulted aliquot was centrifuged (12000 g) for 15 min at 4 °C. The recovered murine supernatant was completely degraded to the corresponding muropeptides by the addition of muramidase (cellosyl) 10 µL, followed by the addition of cellosyl buffer (20 mM sodium phosphate, pH 4.8, and 0.02% sodium azide) (25 µL) and Milli-Q water (15 µL). The resulted aliquot was incubated at 37 °C shaking overnight. After 19 h, the enzymatic reaction was stopped by boiling for 3 min followed by centrifugation for 15 min to remove insoluble contaminants. The recovered supernatant was treated with 50 µL of sodium borate (0.5 M, pH 9) The pH of the sample was tested by pH paper and adjusted to 9 if necessary, followed by the addition of solid sodium borohydride 1-2 mg and the sample was centrifuged at room temperature for 30 min (note: The lid of the Eppendorf vial was pierced to allow gas releasing). After recovering the obtained supernatant, excess borohydride was destroyed with 20% formic acid (20 µL) and the sample was adjusted to pH 3-4. The volume of the obtained sample was diluted to a final volume of 200 µL (2.5 % DMSO) before it injected to RP-HPLC without any further purification.

In addition, another 3 experiments included, MCTDA as a single component (reference); PG-LdtD (positive control); PG-MCTDA. All these experiments were treated with similar

previous protocol (Table **6.6**, entries **1,3,4**) and.an aliquot (0.5 μL) from each reaction mixture was analysed by RP-HPLC without prior purification.

6.3 X-Ray Crystallography Data

2,2,2-Trifluoro-1-(3,5-dimethoxyphenyl) ethanone oxime (3.29)

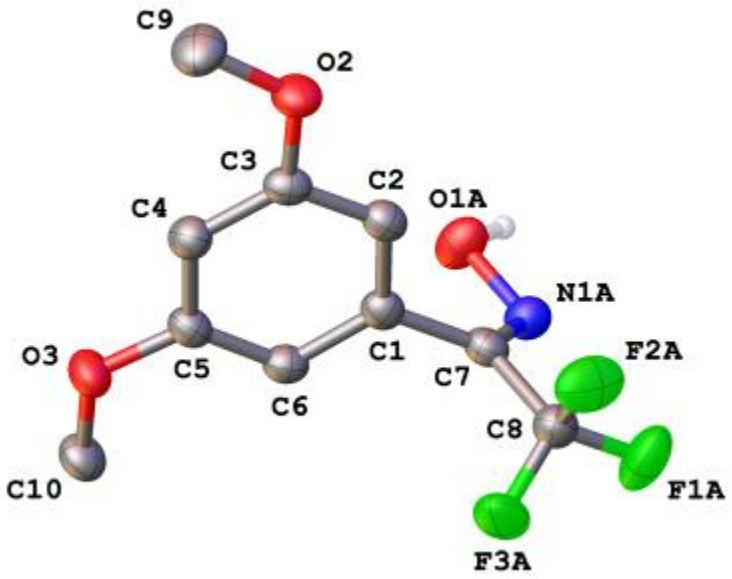

Identification code	mjh180023_fa
Empirical formula	$C_{10}H_{10}F_3NO_3$
Formula weight	249.19
Temperature/K	150.0(2)
Crystal system	monoclinic
Space group	$P2_1/c$
a/Å	5.1484(2)
b/Å	11.2035(4)
c/Å	18.8987(11)

α/°	90
β/°	91.809(5)
γ/°	90
Volume/Å^3	1089.54(9)
Z	4
ρ_{calc}g/cm^3	1.519
μ/mm^{-1}	1.279
F(000)	512.0
Crystal size/mm^3	0.24 × 0.07 × 0.01
Radiation	CuKα (λ = 1.54184)
2Θ range for data collection/°	9.178 to 133.512
Index ranges	-5 ≤ h ≤ 5, -13 ≤ k ≤ 13, -22 ≤ l ≤ 21
Reflections collected	7845
Independent reflections	1903 [R_{int} = 0.0445, R_{sigma} = 0.0354]
Data/restraints/parameters	1903/204/193
Goodness-of-fit on F^2	1.053
Final R indexes [I>=2σ (I)]	R_1 = 0.0402, wR_2 = 0.0912
Final R indexes [all data]	R_1 = 0.0562, wR_2 = 0.1003
Largest diff. peak/hole / e Å^{-3}	0.16/-0.19

2,2,2-Trifluoro-1-(3,5-dimethoxyphenyl)ethanone -*O*-*p*-toluenesulfonyloxime (*E*) (3.30)

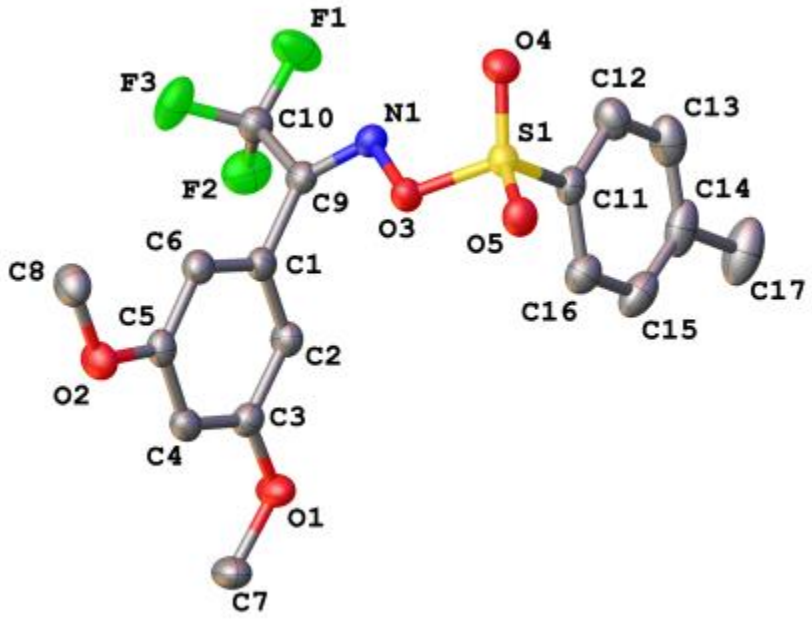

Identification code	mjh180044
Empirical formula	$C_{17}H_{16}F_3NO_5S$
Formula weight	403.37
Temperature/K	150.0(2)
Crystal system	monoclinic
Space group	C2/c
a/Å	17.5069(5)
b/Å	10.4249(4)
c/Å	19.4907(6)
α/°	90
β/°	92.820(3)

γ/°	90
Volume/Å^3	3552.91(19)
Z	8
ρ_{calc}g/cm^3	1.508
μ/mm^{-1}	2.183
F(000)	1664.0
Crystal size/mm^3	0.22 × 0.18 × 0.13
Radiation	CuKα (λ = 1.54184)
2Θ range for data collection/°	9.086 to 133.638
Index ranges	-20 ≤ h ≤ 20, -12 ≤ k ≤ 12, -23 ≤ l ≤ 18
Reflections collected	12982
Independent reflections	3146 [R_{int} = 0.0321, R_{sigma} = 0.0233]
Data/restraints/parameters	3146/0/247
Goodness-of-fit on F^2	1.043
Final R indexes [I>=2σ (I)]	R_1 = 0.0330, wR_2 = 0.0795
Final R indexes [all data]	R_1 = 0.0404, wR_2 = 0.0845
Largest diff. peak/hole / e Å^{-3}	0.24/-0.35

2,2,2-Trifluoro-1-(3,5-dimethoxyphenyl)ethanone -*O*-*p*-toluenesulfonyloxime (*Z*) (3.30)

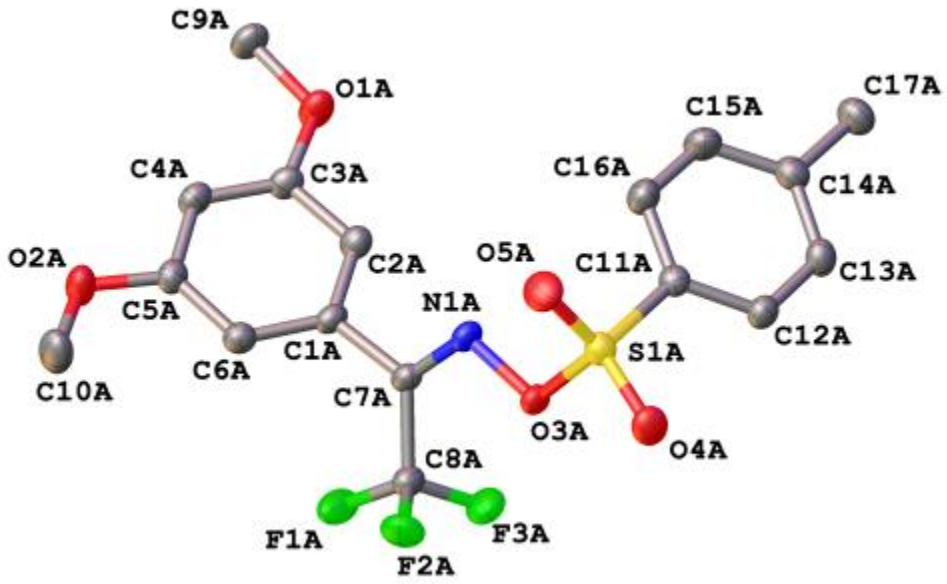

Identification code	mjh180050
Empirical formula	$C_{17}H_{16}F_3NO_5S$
Formula weight	403.37
Temperature/K	150.0(2)
Crystal system	triclinic
Space group	P-1
a/Å	7.7243(3)
b/Å	10.7713(4)
c/Å	11.0461(3)
α/°	88.790(3)

β/°	86.743(3)
γ/°	72.489(3)
Volume/Å^3	875.03(6)
Z	2
ρ_{calc}g/cm^3	1.531
μ/mm^{-1}	2.216
F(000)	416.0
Crystal size/mm^3	0.32 × 0.16 × 0.09
Radiation	CuKα (λ = 1.54184)
2Θ range for data collection/°	8.018 to 133.468
Index ranges	$-9 \leq h \leq 8$, $-12 \leq k \leq 12$, $-13 \leq l \leq 13$
Reflections collected	23761
Independent reflections	3080 [R_{int} = 0.0375, R_{sigma} = 0.0180]
Data/restraints/parameters	3080/1214/478
Goodness-of-fit on F^2	1.076
Final R indexes [I>=2σ (I)]	R_1 = 0.0307, wR_2 = 0.0739
Final R indexes [all data]	R_1 = 0.0360, wR_2 = 0.0775
Largest diff. peak/hole / e Å^{-3}	0.20/-0.24

3-(3,5-Dimethoxyphenyl)-3-(trifluoromethyl)-diaziridine (3.31)

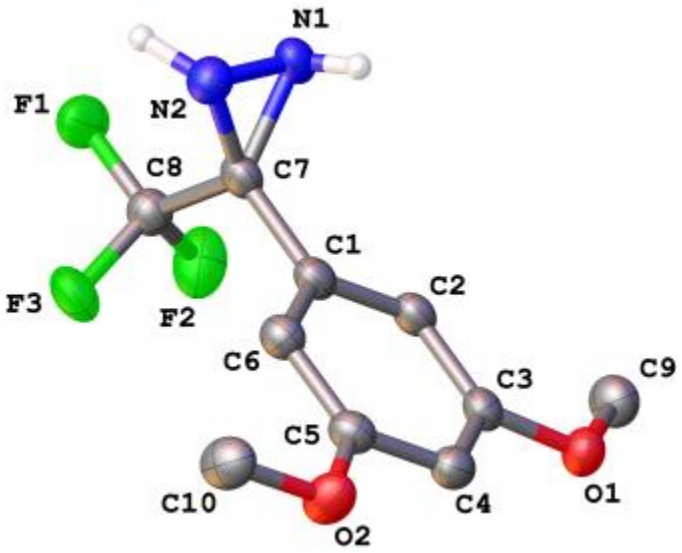

Identification code	mjh180056_fa
Empirical formula	$C_{10}H_{11}F_3N_2O_2$
Formula weight	248.21
Temperature/K	150.0(2)
Crystal system	monoclinic
Space group	$P2_1/c$
a/Å	10.8296(7)
b/Å	12.0545(7)
c/Å	8.4489(6)
α/°	90
β/°	104.671(7)
γ/°	90
Volume/Å^3	1067.00(12)

Z	4
ρ_{calc}g/cm^3	1.545
μ/mm^{-1}	1.257
F(000)	512.0
Crystal size/mm^3	0.15 × 0.13 × 0.07
Radiation	CuKα (λ = 1.54184)
2Θ range for data collection/°	8.44 to 135.582
Index ranges	$-12 \leq h \leq 10$, $-14 \leq k \leq 14$, $-10 \leq l \leq 10$
Reflections collected	14384
Independent reflections	1902 [R_{int} = 0.0880, R_{sigma} = 0.0469]
Data/restraints/parameters	1902/0/162
Goodness-of-fit on F^2	1.042
Final R indexes [I>=2σ (I)]	R_1 = 0.0577, wR_2 = 0.1622
Final R indexes [all data]	R_1 = 0.0678, wR_2 = 0.1791
Largest diff. peak/hole / e Å^{-3}	0.48/-0.48

2-(3-Trifluoromethyl)-*3H*-diazirine-3-yl)-4,6-dimethoxybenzaldehyde (3.11)

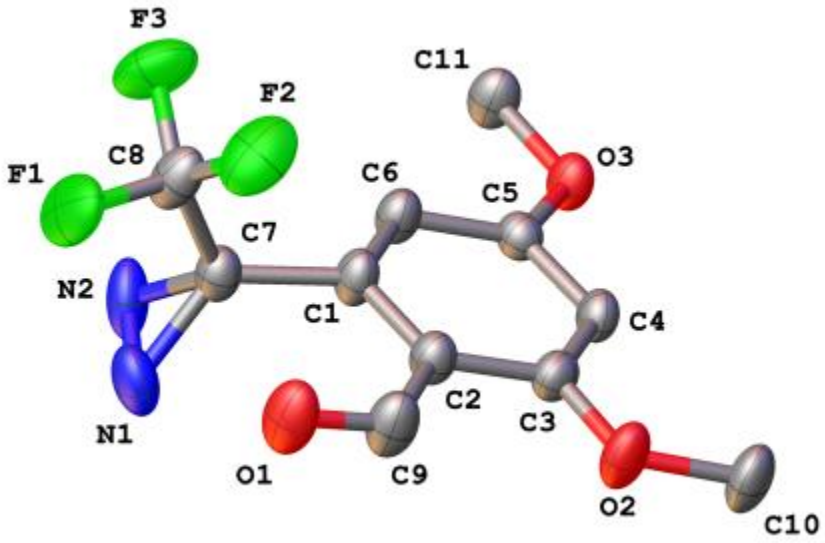

Identification code	mjh180060
Empirical formula	$C_{11}H_9F_3N_2O_3$
Formula weight	274.20
Temperature/K	150.0(2)
Crystal system	orthorhombic
Space group	Pnma
a/Å	13.5386(3)
b/Å	6.8957(2)
c/Å	12.2585(2)
α/°	90
β/°	90
γ/°	90
Volume/Å^3	1144.43(5)

Z	4
ρ_{calc}g/cm^3	1.591
μ/mm^{-1}	1.310
F(000)	560.0
Crystal size/mm^3	0.31 × 0.15 × 0.04
Radiation	CuKα (λ = 1.54184)
2Θ range for data collection/°	9.734 to 133.92
Index ranges	$-16 \leq h \leq 16$, $-8 \leq k \leq 8$, $-14 \leq l \leq 13$
Reflections collected	15605
Independent reflections	1115 [R_{int} = 0.0303, R_{sigma} = 0.0103]
Data/restraints/parameters	1115/0/137
Goodness-of-fit on F^2	1.059
Final R indexes [I>=2σ (I)]	R_1 = 0.0324, wR_2 = 0.0909
Final R indexes [all data]	R_1 = 0.0362, wR_2 = 0.0951
Largest diff. peak/hole / e Å^{-3}	0.18/-0.14

7-Methoxy-5-(3-trifluoromethyl-*3H*-diazirine-3-yl) coumarin-3-cabroxylic acid (3.2)

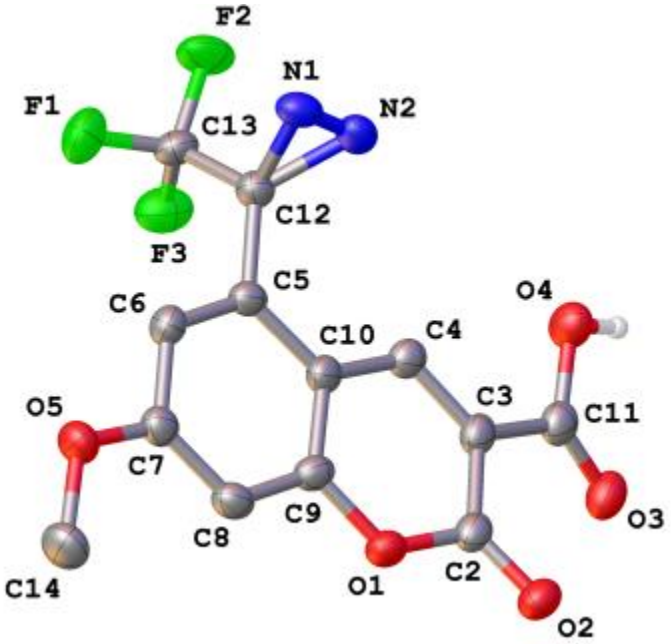

Identification code	mjh190023_fa
Empirical formula	$C_{13}H_7F_3N_2O_5$
Formula weight	328.21
Temperature/K	150.0(2)
Crystal system	orthorhombic
Space group	$Pca2_1$
a/Å	27.0115(15)
b/Å	4.9396(4)
c/Å	9.4076(5)
α/°	90
β/°	90

γ/°	90
Volume/Å^3	1255.22(14)
Z	4
ρ_{calc}g/cm^3	1.737
μ/mm^{-1}	1.445
F(000)	664.0
Crystal size/mm^3	0.17 × 0.08 × 0.02
Radiation	CuKα (λ = 1.54184)
2Θ range for data collection/°	11.464 to 133.524
Index ranges	-32 ≤ h ≤ 25, -5 ≤ k ≤ 4, -11 ≤ l ≤ 11
Reflections collected	4917
Independent reflections	1979 [R_{int} = 0.0495, R_{sigma} = 0.0557]
Data/restraints/parameters	1979/1/212
Goodness-of-fit on F^2	1.072
Final R indexes [I>=2σ (I)]	R_1 = 0.0432, wR_2 = 0.0989
Final R indexes [all data]	R_1 = 0.0557, wR_2 = 0.1076
Largest diff. peak/hole / e Å^{-3}	0.27/-0.25
Flack parameter	0.10(19)

5-(2,6-dimethoxy-4-(3-(trifluoromethyl)-*3H*-diazirin-3-yl)benzylidene)-2,2-dimethyl-1,3-dioxane-4,6-dione (3.41)

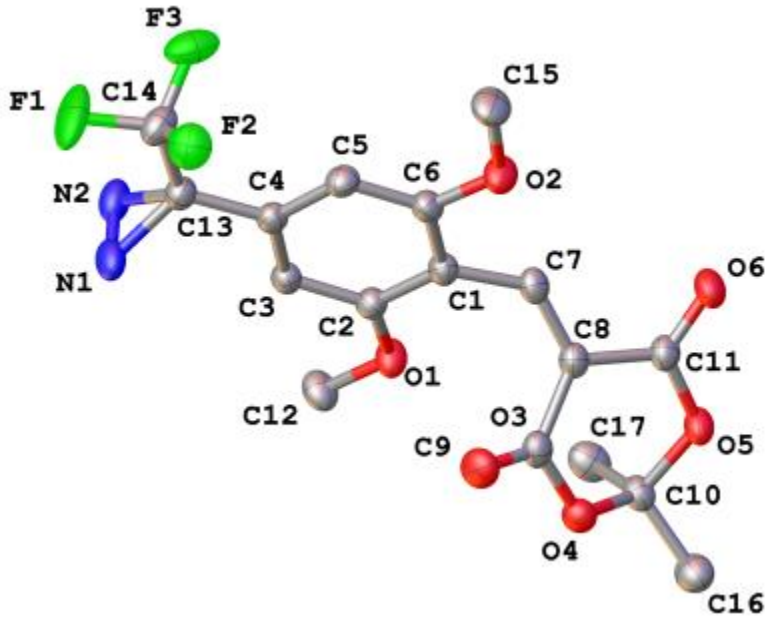

Identification code	mjh190021
Empirical formula	$C_{17}H_{15}F_3N_2O_6$
Formula weight	400.31
Temperature/K	150.0(2)
Crystal system	monoclinic
Space group	Cc
a/Å	26.8070(5)
b/Å	7.61139(14)
c/Å	18.0324(4)
α/°	90
β/°	104.572(2)

γ/°	90
Volume/Å^3	3560.94(12)
Z	8
ρ_{calc}g/cm^3	1.493
μ/mm^{-1}	1.169
F(000)	1648.0
Crystal size/mm^3	0.3 × 0.12 × 0.08
Radiation	CuKα (λ = 1.54184)
2Θ range for data collection/°	6.814 to 135.292
Index ranges	-32 ≤ h ≤ 26, -9 ≤ k ≤ 9, -21 ≤ l ≤ 21
Reflections collected	8215
Independent reflections	8215 [R_{int} = ?, R_{sigma} = 0.0240]
Data/restraints/parameters	8215/1163/626
Goodness-of-fit on F^2	0.993
Final R indexes [I>=2σ (I)]	R_1 = 0.0289, wR_2 = 0.0717
Final R indexes [all data]	R_1 = 0.0318, wR_2 = 0.0731
Largest diff. peak/hole / e Å^{-3}	0.12/-0.15
Flack parameter	0.00(6)

(*R*)-2-((*tert*-butoxycarbonyl)amino)-3-(2-oxo-*2H*-chromene-3-carboxamido)propanoic acid (3.46)

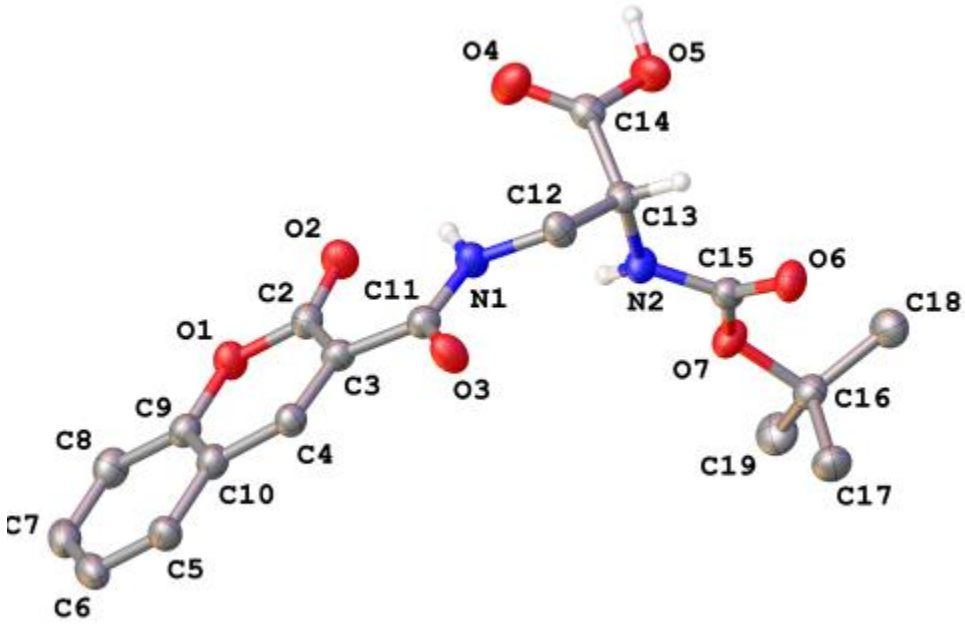

Identification code	mjh190050_fa
Empirical formula	$C_{18}H_{20}N_2O_7$
Formula weight	376.36
Temperature/K	150.0(2)
Crystal system	tetragonal
Space group	$P4_1$
a/Å	5.9238(2)
b/Å	5.9238(2)
c/Å	50.191(2)
α/°	90
β/°	90

γ/°	90
Volume/Å^3	1761.28(14)
Z	4
ρ_{calc}g/cm^3	1.419
μ/mm^{-1}	0.932
F(000)	792.0
Crystal size/mm^3	0.12 × 0.1 × 0.09
Radiation	CuKα (λ = 1.54184)
2Θ range for data collection/°	14.116 to 133.132
Index ranges	-6 ≤ h ≤ 5, -7 ≤ k ≤ 6, -53 ≤ l ≤ 59
Reflections collected	6426
Independent reflections	2475 [R_{int} = 0.0488, R_{sigma} = 0.0518]
Data/restraints/parameters	2475/2/257
Goodness-of-fit on F^2	1.049
Final R indexes [I>=2σ (I)]	R_1 = 0.0403, wR_2 = 0.0864
Final R indexes [all data]	R_1 = 0.0500, wR_2 = 0.0921
Largest diff. peak/hole / e Å^{-3}	0.16/-0.17
Flack parameter	-0.1(3)

Diazirine carboxycoumarin (3.2) and by-product (3.35)

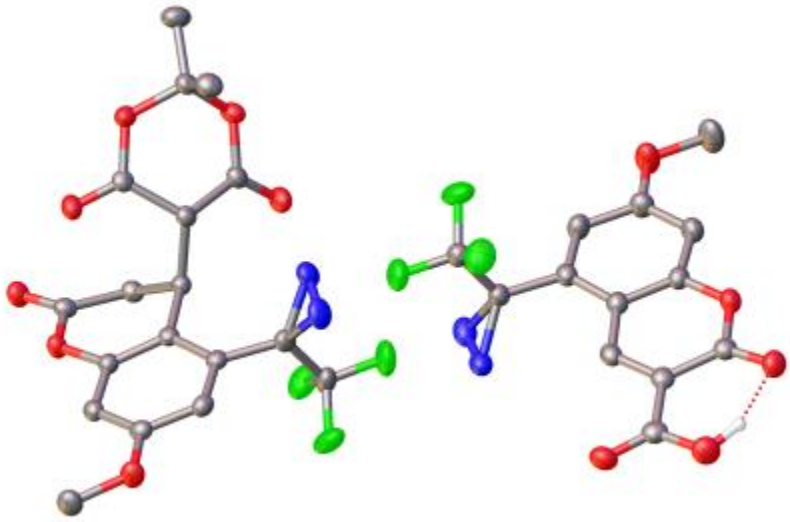

Identification code	mjh190010_fa
Empirical formula	$C_{31}H_{22}F_6N_4O_{12}$
Formula weight	756.52
Temperature/K	150.0(2)
Crystal system	triclinic
Space group	P-1
a/Å	8.2992(3)
b/Å	12.2276(6)
c/Å	16.7205(8)
α/°	70.632(4)
β/°	80.621(4)
γ/°	79.557(4)

Volume/$Å^3$	1564.54(13)
Z	2
$\rho_{calc}g/cm^3$	1.606
μ/mm^{-1}	1.295
F(000)	772.0
Crystal size/mm^3	0.19 × 0.09 × 0.02
Radiation	CuKα (λ = 1.54184)
2Θ range for data collection/°	7.736 to 133.936
Index ranges	$-9 \leq h \leq 8$, $-14 \leq k \leq 14$, $-19 \leq l \leq 19$
Reflections collected	21906
Independent reflections	5522 [R_{int} = 0.0417, R_{sigma} = 0.0332]
Data/restraints/parameters	5522/0/485
Goodness-of-fit on F^2	1.011
Final R indexes [I>=2σ (I)]	R_1 = 0.0347, wR_2 = 0.0824
Final R indexes [all data]	R_1 = 0.0501, wR_2 = 0.0914
Largest diff. peak/hole / e $Å^{-3}$	0.21/-0.21

6.4 References

1- K. Moozeh, S. So, and J. Chin, *Angew. Chem. Int. Ed*., 2015, **127**, 9513-9517.

2- Y. Ikeda and E. J. Behrman, *Synth. Commun*., 2008, **38**, 2276–2284.

3- M. O'Donnell, J. Boniece and S. Earp, *Tetrahedron Lett*., 1978, **30**, 2641-2644.

4- T. Ma, X. Fu, C. Kee, L. Zong, Y.Pan, K. Huang and C. Tan, *J. Am. Chem. Soc*., 2011, **133**, 2828–2831.

5- D. Rudzinski, C. Kelly and N. Leadbeater, *Chem. Commun*., 2012, **48**, 9610-9612.

6- A. Blencowe, N. Caiulo, K. Cosstick, W. Fagour, P. Heath, and W. Hayes, *Macromolecules*., 2007, **40**, 439-449.

7- A. Rieche, H. Gross, and E. Hoft, *Chem. Ber*., 1960, **93**, 88.

8- T. Tomohiro, A. Yamamoto, Y. Tatsumi and Y. Hatanaka, *Chem. Commun.*, 2013, **49**, 11551.

9- V. Armstrong, O. Soto, J. Valderrama, and R. Tapia, *Synth. Commun*., 1988, **18**, 717-725.

10- E. Kuru, S. Tekkam, E. Hall, Y. Brun, and M. VanNieuwenhze, *Nat Protoc*., 2015, 10, 33-52.

11- K. Datsenko and B. Wanner, *PANS*., 2000, **97**, 6640-6645.

12- B. Glauner, J. Holtje, and U. Schwarz, *J. Biol. Chem*., 1988, **263**, 10088-10095.

13- A. Silva, C. Otten, J. Biboy, E. Breukink,, M. VanNieuwenhze, W. Vollmer and T. Blaauwen, *Front. Microbiol*., 2018, **9**, 1-15.

14- L. Belding, P. Stoyanov, and T. Dudding, *J. Org. Chem*., 2016, **81**, 553-558.

15- V. Maleev, M. North, V. Larionov, I. Fedyanin, T. Savelyeva, M. Moscalenko, A. Smolyakov, and Y. Belokon, *Adv. Synth. Catal*. 2014, **356**, 1803-1810.

16- S. Ghosh, J. Das, and S. Chattopadhyay, *Tetrahedron Lett*., 2011, **52**, 2869-2872.